THE PHYSICO-CHEMICAL PROPERTIES OF ORGANIC INCLUSION COMPOUNDS

by

Tanya le Roex

B.Sc. (Hons.) University of Cape Town

Thesis presented to the

UNIVERSITY OF CAPE TOWN

for the degree of

DOCTOR OF PHILOSOPHY

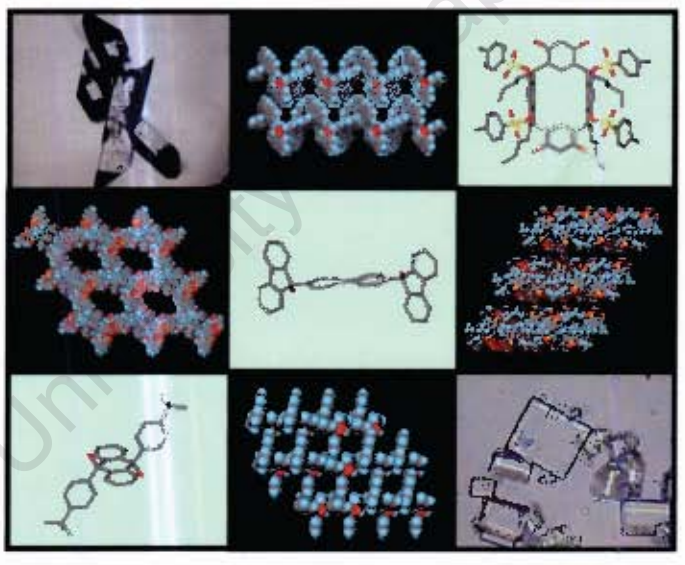

Department of Chemistry, University of Cape Town

Rondebosch, 7701, South Africa

December 2004

ACKNOWLEDGEMENTS

I would like to thank:

- My supervisors, Prof. Luigi R. Nassimbeni and Prof. Mino R. Caira, for their excellent advice, guidance and willingness to help, their ability to inspire and their constant dedication and enthusiasm, as well as their expertise and everything they have taught me about supramolecular chemistry and crystallography.

- Prof. Susan Bourne for her willing help and advice, as well as all the members of the Supramolecular chemistry research group for their friendship and support and making it such a pleasant place to work, and particularly Vincent Smith for his help.

- Dr. Hong Su for single crystal X-ray diffraction data collections.

- Dr. John Ripmeester for giving me the opportunity to spend some time in his research group at the Steacie Institute for Molecular Sciences in Ottawa and for his help with the solid-state NMR.

- Prof. Roger Davey for giving me the opportunity to spend some time in the Colloids, Crystals and Interfaces group at UMIST in Manchester, learning about nucleation and crystal growth, and for his great enthusiasm and willingness to help.

- My family and friends, and especially Warren, for their support and encouragement.

- The National Research Foundation and GOOT for financial support.

PUBLICATIONS AND CONFERENCES

Parts of this thesis have been published:

- 'Tunable Clathrates', M.R. Caira, T. le Roex, and L.R. Nassimbeni, *Chem. Comm.*, 2001, 2128.
- 'Inclusion compounds with mixed guests: controlled stoichiometries and kinetics of enclathration', L.J. Barbour, M.R. Caira, T. le Roex and L.R. Nassimbeni, *J. Chem. Soc., Perkin Trans. 2*, 2002, 1973.
- 'Inclusion by a fluorenyl host with volatile guests: structures, thermal stability and kinetics', M.R. Caira, T. le Roex, L.R. Nassimbeni, J.A. Ripmeester and E. Weber, *Org. Biomol. Chem.*, 2004, **16**, 2299.
- 'Selectivity of a resorcinarene host for pentanol isomers', M.R. Caira, T. le Roex and L.R. Nassimbeni, *Supramol. Chem.*, accepted.

Parts of this thesis have been presented at the following conferences:

- Presentation entitled 'Tunable Clathrates', South African Crystallographic Society, Annual meeting, Stellenbosch, 4 & 5 April, 2002.
- Poster entitled 'Tunable Clathrates', XIX Congress and General assembly of the IUCr, Geneva, Switzerland, August 6-15, 2002.
- Poster entitled 'Structure and kinetic reactivity of a diol host compound', Indaba IV: Patterns in Nature, Kruger National Park, South Africa, August 17-22, 2003.
- Presentation entitled 'Tunable Clathrates' and poster entitled 'Structure and kinetic reactivity of a diol host compound', 21st European Crystallographic Meeting, Durban, South Africa, August 24-29, 2003.
- Poster entitled 'Structure and kinetic reactivity of a diol host compound', Erice 35th Crystallographic Course, Erice, Italy, June 9-20, 2004.

ABSTRACT

In this thesis the inclusion properties of the host compounds *trans*-9,10-dihydroxy-9,10-bis(p-*tert*-butylphenyl)-9,10-dihydroanthracene (**TBDDDA**), 9,9'-(Biphenyl-4,4'-diyl)difluoren-9-ol (**WEB24**) and $1^4,1^6,5^4,5^6$-tetrahydroxy-2,4,6,8-tetrapentyl-$3^4,3^6$, $7^4,7^6$-tetra(p-toluenesulfonyl-oxy)-1,3,5,7(1,3)-tetrabenzenacyclooctaphane (**TTRSC**) were investigated. Each of these host compounds is bulky and rigid and in addition contains high-affinity functional groups which can engage in specific host···guest interactions, such as hydrogen bonding.

These host compounds readily form complexes with small organic guest molecules. The host **TBDDDA** was found to form inclusion compounds with DMF, DMSO and acetone of the type $H.nG_1.(4\text{-}n)G_2$, with n varying integrally from 0 to 4. Inclusion compounds of the host **WEB24** with N,N-dimethylacetamide, 1,4-dioxane, methyl ethyl ketone, ethylamine and propylamine were formed, while the host **TTRSC** was found to form host-guest compounds with seven pentanol isomers as well as pyridine and the three picoline isomers.

The structures of these complexes have been elucidated using single crystal X-ray diffraction methods, as were the structures of the unsolvated host α-phases of **TBDDDA** and **WEB24**. Thermogravimetry, differential scanning calorimetry and hot stage microscopy were used to analyse the thermal behaviour of the complexes. The kinetics of enclathration of certain guests in the vapour phase by two of the host compounds were investigated using an automated magnetic suspension balance designed for this purpose. The kinetics of desorption of selected inclusion compounds were studied using isothermal thermogravimetry, yielding estimates of the activation energies of decomposition. ^{13}C solid state CP/MAS NMR was used to analyse some of the inclusion compounds of **WEB24** and to monitor the desorption of the guest from each of these clathrates. A brief investigation of nucleation and crystal growth was carried out, during which the solubility and crystallisation of two of the inclusion compounds were investigated.

ABBREVIATIONS AND SYMBOLS

α	Angle between b and c unit cell vectors or extent of reaction
β	Angle between a and c unit cell vectors
γ	Angle between a and b unit cell vectors
τ	Torsion angle
A	Arrhenius pre-exponential factor
bp	Boiling point
CP/MAS	Cross-polarisation magic angle spinning
CSD	Cambridge Structural Database
DSC	Differential scanning calorimetry
E	Normalised structure factor
E_a	Activation energy
endo	endothermic
F	Structure factor
G	Guest
GC	Gas chromatography
H	Host
H:G	Host to guest ratio
HSM	Hot stage microscopy
k	Rate constant
mp	Melting point
M_r	Molecular mass
NMR	Nuclear magnetic resonance
R	Gas constant = 8.314 $J.K^{-1}.mol^{-1}$
s.o.f.	Site occupancy factor
T_{on}	Onset temperature
T_b	Boiling point
TG	Thermogravimetry
U	Isotropic or anisotropic displacement parameter
V	Unit cell volume
Z	Number of formula units in the unit cell

ATOMIC COLOUR SCHEME

The following colour scheme was used for the representation of atoms in the molecular diagrams

Carbon

Hydrogen

Oxygen

Nitrogen

Sulphur

TABLE OF CONTENTS

Chapter 1

INTRODUCTION

'There is no more basic enterprise in chemistry than the determination of the geometrical structure of a molecule. Such a determination, when it is well done, ends all speculation as to the structure and provides us with the starting point for the understanding of every physical, chemical and biological property of the molecule.'

- R. Hoffmann in *Determination of the Geometrical Structure of Free Molecules*, MIR Publishers, Moscow, 1983.

SUPRAMOLECULAR CHEMISTRY

Supramolecular chemistry is a young and rapidly developing science based on weak intermolecular interactions between molecules, resulting in the formation of supramolecular assemblies with unique properties.

The concept and term 'supramolecular chemistry' were introduced by Jean-Marie Lehn in 1978 who described it as being '*concerned with the entities of higher molecular complexity than molecules themselves – supramolecular species and assemblies held together and organised by means of intermolecular, binding interactions* ' or more informally as '*chemistry beyond the molecule*'.[1] In 1987 the Nobel prize in chemistry was awarded to D.J. Cram, J.-M. Lehn and C.J. Pedersen for their respective work in the field of supramolecular chemistry.

A number of excellent books have been written on this subject including a ten volume series entitled 'Comprehensive Supramolecular Chemistry' which was published in 1996[2] and the two volume 'Encyclopedia of Supramolecular Chemistry' published in 2004.[3] Much recent work in this field has focused on crystal engineering, the aim of which is to produce desired crystalline supramolecular assemblies with specific properties. The formation of a crystal is a process of self-assembly of molecules from solution or the vapour and relies on molecular recognition, a fundamental process which lies at the heart of supramolecular chemistry. The crystal of an organic molecule is the perfect supermolecule, "*a supermolecule par excellence*" in the words of Dunitz.[4] Crystallography is an invaluable tool in supramolecular chemistry as unique information on intermolecular interactions is given by a thorough understanding of crystal structures and crystal growth.

The field of inclusion chemistry or host-guest chemistry is a subfield of supramolecular chemistry which has seen rapid growth in the past ten years. Inclusion compounds are compounds in which one type of molecule is able to enclose another molecule within its structure with no covalent bonding between the two species. The molecular framework is termed the 'host' and the enclosed species the 'guest'.

Inclusion compounds can be broadly classified into two categories.[5] The first category is molecular complexes where the host is a single molecule within which the guest molecule is located. Typical examples are cyclodextrins,[6] calixarenes,[7] carcerands,[8] crown ethers and cryptands.[9] The second category is lattice* clathrates in which the host molecules pack to form a framework containing voids in which the guest molecules can be accommodated. These clathrates comprise a wide range of host molecules. A schematic diagram of molecular complexes and lattice clathrates is given in Figure 1.1.

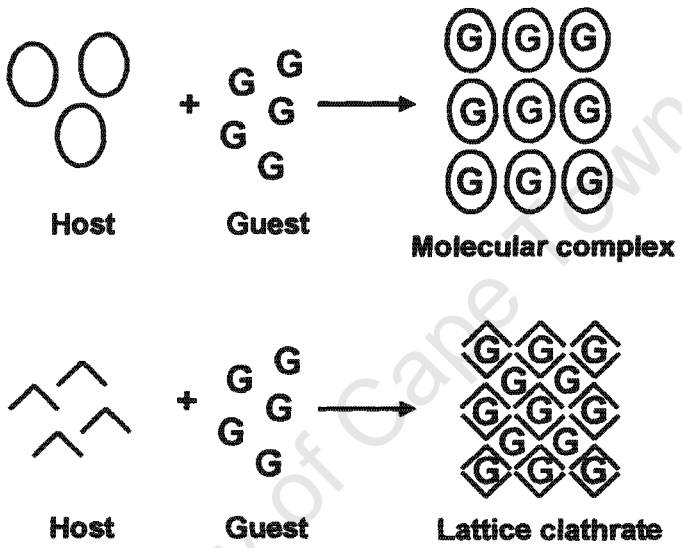

Figure 1.1 Schematic diagram showing molecular complexes and lattice clathrates.

The voids formed in lattice clathrates, in which the guests are situated, have a number of typical geometries which are illustrated in Figure 1.2 and include cages, channels, interconnected cages, intersecting channels and layers.[10] Weber has given a general classification[11] based on intermolecular interactions between the host and guest molecules, while Weber and Josel[12] have given a more detailed nomenclature which, in addition to host-guest interactions, takes into account host-guest types, topology and the number of components forming the host-guest aggregate.

** The author is aware that the term 'lattice' has a specific meaning in crystallography. It is a set of points which have identical surroundings and is therefore a mathematical abstraction. However chemists often use it to mean "a structural array of atoms" or "the structure", and it is used here in the latter sense.*

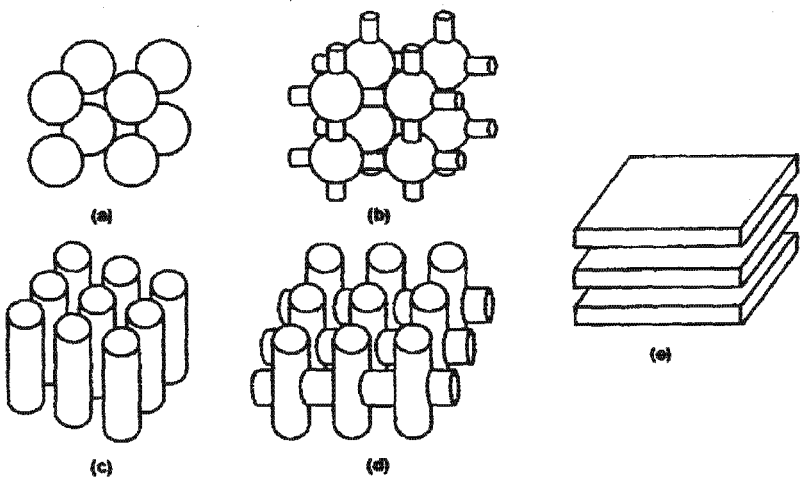

Figure 1.2 Typical topologies found in lattice clathrates: **(a)** cages or cavities, **(b)** interconnected cavities, **(c)** non-intersecting channels or tunnels, **(d)** intersecting channels or tunnels and **(e)** 2-dimensional layers.

Many of the compounds found to act as hosts in inclusion compounds were discovered by chance, but the rapid growth of host-guest chemistry has led to the development of rational design and synthesis of new host compounds. Volume 4 of the series 'Inclusion Compounds', entitled 'Key Organic Host systems', explores this subject and in this volume Weber has suggested some principles for host design.[13] These show that a successful host molecule should be bulky and rigid, have appropriately placed, high affinity functional groups for host-guest interactions such as hydrogen bonding and have a balanced shape to stabilise the overall crystal packing. Bulkiness provides low-density packing in the crystal, allowing the formation of cavities for inclusion of guest molecules and rigidity helps to maintain the cavity structure.

Based on these principles F. Toda,[14] E. Weber,[15] R. Bishop[16] and D.D. MacNicol[17] have designed and synthesised a diverse range of host compounds which have been found to include a wide variety of guest molecules, with the inclusion typically mediated by host-guest hydrogen bonding.

F. Toda has designed and synthesised numerous diol, bisphenol and diamide host compounds and obtained chiral hosts by introduction of a chiral moiety.[18] E. Weber has synthesised a range of diol host compounds designed using structural building elements (such as planes, rods, bridging, spacing and branching units and anchor

groups) to have particular overall shapes, for example, shapes which resemble a pair of scissors, a roof, a dumb-bell or a propeller.[19]

R. Bishop has designed and synthesised a series of alicyclic diol hosts,[20] based on the host *exo*-2-*exo*-6-dihydroxy-2,6-dimethylbicyclo[3.3.1]nonane, which include common solvents to form inclusion compounds which exhibit a helical tubuland structure. D.D. MacNicol introduced the hexa-host analogy and has thus designed and synthesised a vast range of compounds, based on host symmetry, called 'hexa-hosts' (hexa-substituted benzene molecules).[21,22]

Supramolecular chemistry is a field which is expanding rapidly in many directions and spans the fields of chemistry, biology, physics and materials science. The breadth of this field makes it impossible to write a comprehensive review in this introductory chapter, and so instead a brief introduction to a number of topics which we feel represent some of the highlights or areas of significant development in solid state supramolecular chemistry over the past twenty years will be given. These include the following:

- the concept of supramolecular synthons in crystal engineering
- solid-solid reactions
- separation by selective enclathration
- coordination polymers and porous solids as functional materials
- thermodynamic and kinetic studies of host-guest compounds
- covalent and non-covalent capsules
- gas sensing, storage and separation
- the study of nucleation processes and crystal growth
- catenanes and rotaxanes
- supramolecular systems as models for biological processes

In cases where the topic described relates directly to the work carried out in the thesis, greater background detail to the subject is given.

SUPRAMOLECULAR SYNTHONS IN CRYSTAL ENGINEERING

"Reason and imagination come into play simultaneously in the quest for new functionalised solids, while experiment and computation are of equal significance in the prediction and design of crystal structures."

- D. Braga, F. Grepioni and G.R. Desiraju, *Chem. Rev.*, 1998, **98**, 1375.

Crystal engineering is solid state supramolecular synthesis and has been defined as "*the understanding of intermolecular interactions in the context of crystal packing and in the utilisation of such understanding in the design of new solids with desired physical and chemical properties*".[23] G.R. Desiraju has developed the concept of 'supramolecular synthons' which he defines as "*structural units within supermolecules which can be formed and/or assembled by known or conceivable synthetic operations involving intermolecular interactions*".[24]

Designed combinations of intermolecular interactions are used to derive synthons which incorporate chemical as well as geometrical recognition features of molecular fragments.[24] Supramolecular synthons should ideally be robust and therefore likely to be found in many crystal structures.[25] The relationship between a molecule, a functional group and the derived supramolecular synthon is illustrated in Figure 1.3.[26]

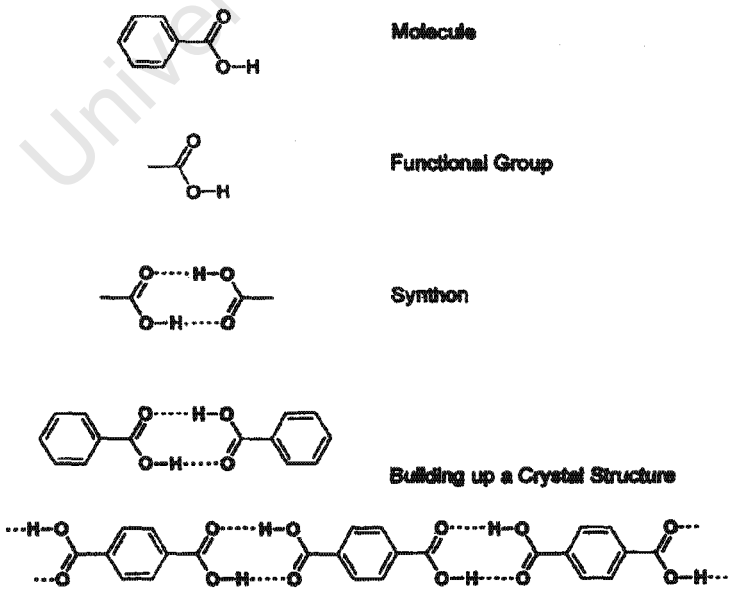

Figure 1.3 Self-assembly from molecule to crystal via supramolecular synthons.[26]

Supramolecular retrosynthesis in crystal engineering depends on a detailed knowledge and understanding of intermolecular interactions occurring in crystals. The Cambridge Structural Database (CSD) provides the essential tool for such retrosynthetic analysis and can be used to search for patterns of intermolecular interactions and the identification of supramolecular synthons.[27]

Conventional O-H···O and N-H···O hydrogen bonds as well as weaker interactions such as C-H···O, C-H···N, I···I, O···I, N···Cl, C···H and C···C are all directional and can be combined with functional groups in the molecular skeleton to generate supramolecular synthons. For crystal engineering purposes, intermolecular forces are classified in terms of distance dependence and directionality. Medium-range forces (typically C···C, C···H and H···H interactions) are generally isotropic and determine size, shape and close-packing of molecules. Long-range forces are electrostatic and anisotropic and involve interactions among heteroatoms or between heteroatoms and C or H.

Hydrogen bonding combines strength with directionality and is the most important interaction in supramolecular construction. A vast amount of research has been carried out on different aspects of hydrogen bonding and a review on hydrogen bonding in crystal engineering has been given by G.R. Desiraju.[28] The hydrogen bond is described as D-H···A where D is the donor atom and A is the acceptor atom. 'Strong' hydrogen bonds of the type O-H···O and N-H···O, where the donor and acceptor atoms are of medium to high electronegativity, are distinguished from 'weak' hydrogen bonds of the type C-H···O and O-H···π, where one or both of the two atoms involved are of moderate to low electronegativity.

The distance between the donor and acceptor atoms can vary from 2.2 Å to 4.0 Å, with typical hydrogen bonded O···O distances being 2.50 - 2.80 Å.[29] Weak hydrogen bonds have a significant influence on crystal packing and this was gradually realised with the work of Sutor,[30] Leiserowitz[31] and Kennard.[32] Another important interaction is that between halogen atoms, which form short non-bonded contacts.[23]

The use of supramolecular synthons in crystal engineering has been demonstrated by a number of studies[33,34,35] and the robustness of such synthons explored.[36,37] Supramolecular synthons of inorganic crystal engineering combine metal-ligand coordination bonding with other non-covalent bonds of organic crystal engineering

and a review has been given by Braga *et al*[38] discussing additional types of interactions which are characteristic of inorganic and organometallic systems due to the presence of metal atoms. Hydrogen bonded synthons are being utilised in inorganic crystal engineering to combine coordination chemistry with hydrogen bonding.[39, 40, 41] Interesting hydrogen bonded networks have been formed by Brammer *et al*[42] using Cr-coordinated arene ligands and N-ligands bound to Pt metals. M-X···H-N^+ hydrogen bond synthons have been employed by Orpen *et al*[43] in the preparation of crystalline salts [4,4'-H_2bipy][MX_4] (X = Cl, M = Pd, Pt, Co, Zn, Hg, Mn, Cd and Pb; X = Br, M = Pd, Co, Zn and Mn).

This supramolecular synthon approach gives a systematic strategy to the field of crystal engineering and promises to result in the discovery of numerous solid-state structures with fundamental and practical importance.

SOLID-SOLID REACTIONS

Solid-solid reactions are reactions carried out between reactants in the solid state without the presence of a solvent and many reactions have been found to proceed efficiently in the solid state, and in many cases more efficiently and selectively than in solution.

Solid state reactions have been classified by Rastogi[44] who carried out significant early work in this field. In the solid state the reactant molecules cannot move freely, as in solution, which results in solid-solid reactions usually being diffusion controlled. Diffusion in solids is fairly complex and can occur by many mechanisms, but occurs predominantly by the mechanism which requires the lowest activation energy. Disadvantages of solid state reactions are that the reaction does not easily go to completion and the mechanisms of these reactions are not well understood. The occurrence of solid-solid reactions is largely due to favourable geometry of the reactants and products.

F. Toda and co-workers have carried out numerous well-known organic reactions in the solid state with great success.[45] Some examples include Baeyer-Villiger oxidation reactions,[46] Michael addition reactions,[47] reduction of ketones with $NaBH_4$,[48] pinacol rearrangements[49] and dehydration, rearrangement and substitution reactions of alcohols.[50] F. Toda has also demonstrated that achiral molecules which are not arranged in a chiral form when crystalline, can be arranged in a chiral form in crystals of an inclusion complex with a chiral host compound. This technique was applied to carry out thermochemical and photochemical reactions in the solid state which were found to proceed both efficiently and selectively.[51] These reactions are successful due to the packing in inclusion compound crystals, which results in the guest molecules being arranged regularly in definite positions and in a definite form, allowing considerable control of the reactions of these organic species.[51] This has significant application to both organic synthesis as well as physical organic chemistry.

The field of solid-solid reactions was initiated by Schmidt[52] who formulated the geometric rules for photocycloaddition. L. MacGillivray and co-workers have explored supramolecular control of reactivity in the solid state using rigid bifunctional molecules as assemblers in the form of reaction templates.[53] The synthetic behaviour of a linear template is depicted in Figure 1.4. The assembler is essentially

a molecule which positions two molecules linearly by way of molecular recognition and self-assembly, and the ability of these assemblers to allow molecular synthesis by design has been demonstrated.

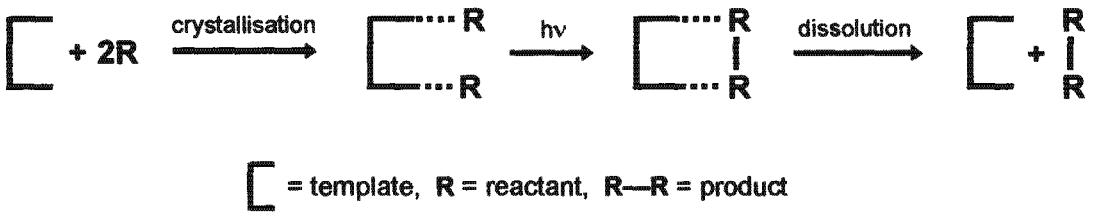

Figure 1.4 Synthetic behaviour of a linear template.[53]

Bis(resorcinol)anthracene was employed to position two *trans*-1,2-bis(4-pyridyl)ethylene molecules, through hydrogen bonding, in a 4-component molecular assembly held together by four O-H···N hydrogen bonds[54] and UV-irradiation of the solid was found to stereospecifically produce *rctt*-tetrakis(4-pyridyl)cyclobutane.

The assembly process of these templates was found to be tolerant to structural and chemical modification of the template[55] as well as to modification of the reactants by changing the number[56] and position[57,58] of the hydrogen bond acceptor sites, as well as by adding or removing functional groups.[59] Such tolerance shows that linear templates could serve as reliable tools for the formation of covalent bonds. These linear templates provide a method of controlling reactivity in the solid state and allow the design of molecular synthesis by applying the principles of molecular recognition and self-assembly. Further investigation of this approach will make the designed synthesis of molecules of increasing complexity possible.[60]

Trask *et al* have recently introduced the 'solvent-drop grinding' technique in which a very small amount of solvent is present and which was demonstrated to be successful in obtaining a particular cocrystal polymorph.[61] Solid state reactions have many applications in metallurgy, geochemical processes, ceramics and the manufacture of artificial gems. Carrying out reactions without solvents is important from an environmental point of view and has many other advantages including reduced costs and simpler processes and handling. There remains a large scope for research in this area in order to understand the mechanisms of the processes involved.

SEPARATION BY SELECTIVE ENCLATHRATION

One of the most important aspects of inclusion chemistry is its use in molecular separation processes and the host-guest complexation method is very effective for the separation of isomers. Selective enclathration of a particular guest from a mixture depends on molecular recognition which occurs between the host and guest compounds, as is shown in the schematic diagram given in Figure 1.5. Essentially a host compound placed in contact with a mixture of guests A and B selects A to form a crystalline inclusion compound $H{\cdot}A_n$ and excludes guest B. The inclusion compound is filtered and the guest released by gentle warming, allowing the host to be recycled.

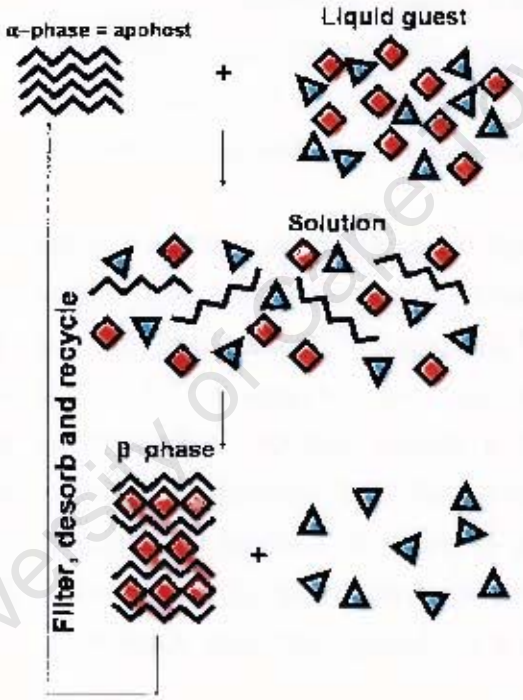

Figure 1.5 Schematic diagram showing selective inclusion.[62]

This method has considerable industrial application and can be employed to separate isomers with similar boiling points. Guanidium organosulfonates have been employed to separate isomeric mixtures of xylenes and dimethylnaphthalenes[63] and a number of host-guest systems have been studied with various host molecules and isomers such as cresols,[64] benzenediols,[65] picolines,[66] lutidines[67,68] and xylidines.[69] A review on the subject of separation of isomers by bulky diol hosts has been given by F. Toda.[70]

Competition experiments are used to determine the selectivity of a given host compound for a particular guest in a mixture. These experiments are carried out by dissolving the host compound in a mixture of guests of varying mole fractions. The resulting crystals are then analysed using a suitable analytical technique, such as gas chromatography or thermal gravimetry, in order to determine the relative quantities of the enclathrated guests. Three types of selectivity curves are typically obtained and these are illustrated in Figure 1.6. In each of the graphs shown, X_A is the mole fraction of guest A in the liquid mixture and Z_A that of guest A which has been enclathrated in the host-guest crystals. The red diagonal line is a reference line which represents zero selectivity.

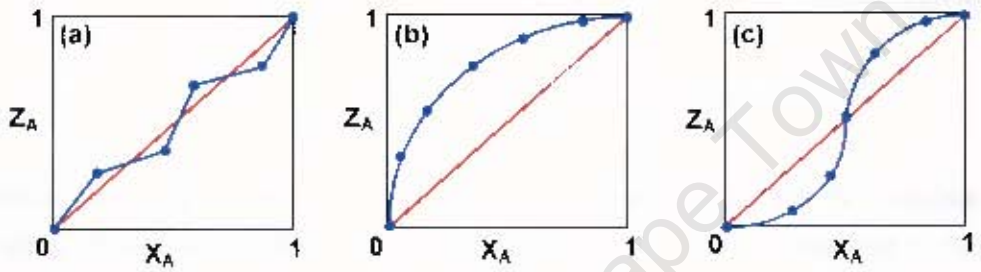

Figure 1.6 Typical selectivity curves obtained from competition experiments showing **(a)** poor selectivity, **(b)** good selectivity and **(c)** concentration dependent selectivity.

The graph displayed in Figure 1.6(a) results when the host displays poor selectivity, ie. the host does not discriminate between the two guests, and in this case the experimental curve follows the diagonal reference line closely. Figure 1.6(b) is the result obtained when guest A is strongly selected over guest B for the whole concentration range and Figure 1.6(c) shows the curve obtained when the selectivity is concentration dependent and the host preferentially includes the guest which has a higher concentration in the initial solution.

This methodology can be extended to the investigation of the selectivity for three guests simultaneously and such experiments have been carried out with the host 1,1-bis(4-hydroxyphenyl)cyclohexane with isomers of picoline,[66] lutidine[67] and benzenediol.[65] Competition experiments have also been carried out in the solid state by grinding appropriate mixtures of solid guests with the solid host. Using this method the selectivity of a diol host for isomers of aminobenzonitrile was determined.[71]

Inclusion compounds which contain mixed guests are of interest and if inclusion compounds of the type $H{\cdot}n_1G_1{\cdot}n_2G_2$ could be synthesised, where G_1 and G_2 differ in size, polarity and symmetry, then inclusion compounds with different properties would be obtained by varying the relative site occupancies of G_1 and G_2.[62] Some work has been carried out in this area,[72,73] which is an interesting one for further investigation.

An important aspect of separation using inclusion chemistry is the resolution of a racemic mixture of chiral guests. This has important implications for the pharmaceutical industry where it is essential to produce enantiomerically pure drugs. Separation of enantiomers can be carried out by preparing inclusion compounds with a chiral host as follows:[62]

(R)-Host + (R,S)-Guest → (R)-Host·(R)-Guest + (S)-Guest

The success of the above separation requires a higher degree of molecular recognition between the host and (R)-guest than between the host and (S)-guest. F. Toda has employed a number of techniques to carry out efficient separation of enantiomers and has reviewed the subject of designing host compounds for this purpose.[70,74]

R. Bishop has investigated the chirality of both the host and guest components and the resulting molecular assembly of inclusion compounds and has demonstrated that crystallisation of chiral molecules often results in considerable separation or ordering of the two enantiomers, although both are still contained in the compound.[75] Examples are shown by the crystallisation of a racemic dibromide host,[76] a racemic diol host[77] and helical tubuland diols[78] with small guest molecules. Enantiomeric self-resolution can occur on crystallisation or through guest complexation and resolution of enantiomeric crystals containing both enantiomeric molecules is also possible.[75]

It is thus evident that inclusion chemistry can be utilised for separation of isomers as well as enantiomeric resolution and there is a continuing need to design new host compounds capable of resolving isomeric and enantiomeric mixtures of compounds with increasing molecular weights.

COORDINATION POLYMERS AND POROUS SOLIDS

Recent work in inorganic crystal engineering has included the production of robust crystalline architectures based on strong, highly directional metal-ligand coordination interactions. Constructing extended solids from molecular building blocks is of interest as it offers advantages for the design of new materials including porous solids which are of commercial interest as they have application in separation, storage and heterogeneous catalysis. In the past, microporous silicas and aluminosilicates, such as zeolites, have been utilised for such applications, but recent work has shown that more versatile host frameworks can be prepared using inorganic coordination polymers.

The principal framework of coordination polymers consists of two central components, namely connectors and linkers, as well as auxiliary components including blocking ligands, counteranions and non-bonding guests or template molecules.[79] Transition metal ions are often used as versatile connectors as the metal can have a range of coordination numbers resulting in a variety of geometries. Various combinations of connectors and linkers result in a range of structural motifs and a review of the structural topologies of the frameworks of coordination polymers and interpenetration in these structures has been given by R. Robson *et al.*[80]

R. Robson and co-workers have very recently demonstrated the enormous scope for new engineered sodalite-related compounds in a publication in which the deliberate engineering of a series of guanidinium-templated metal carbonate networks with sodalite-type structures is reported.[81] These structures display a square arrangement of four carbonate oxygen centres into which it may be possible to introduce divalent metal ions and this could result in interesting magnetic or electronic behaviour.

Brammer and co-workers[82] have prepared a series of coordination polymers consisting of secondary building units (SBU's) made up of silver (I) ions and carboxylate anions, linked by ditopic nitrogen ligands into [4,4] layer nets. This was achieved by studying the structural chemistry relationship between carboxylate complexes of Ag^+ and H^+ and this analogy may undoubtedly be useful in design strategies.

Up until the mid 1990's there were essentially two types of porous materials including inorganic and carbon-based materials. Recently however, porous coordination polymers have been developed which are completely regular and have high porosity and highly designable frameworks.[79] Copper isonicotinate polymers have been reported by Williams *et al* which retain their structure to above 200°C and which can reversibly absorb and desorb water molecules.[83]

Figure 1.7 illustrates a selection of porous functions displayed by porous coordination polymers.[79] A typical property of porous materials is the ability to store desired compounds such as gases. The adsorption of gases at ambient temperature is important for storage and transport, and stable frameworks without guest molecules could provide suitable adsorbents. This, however, will be discussed in the section addressing sensing, storage and separation of gases.

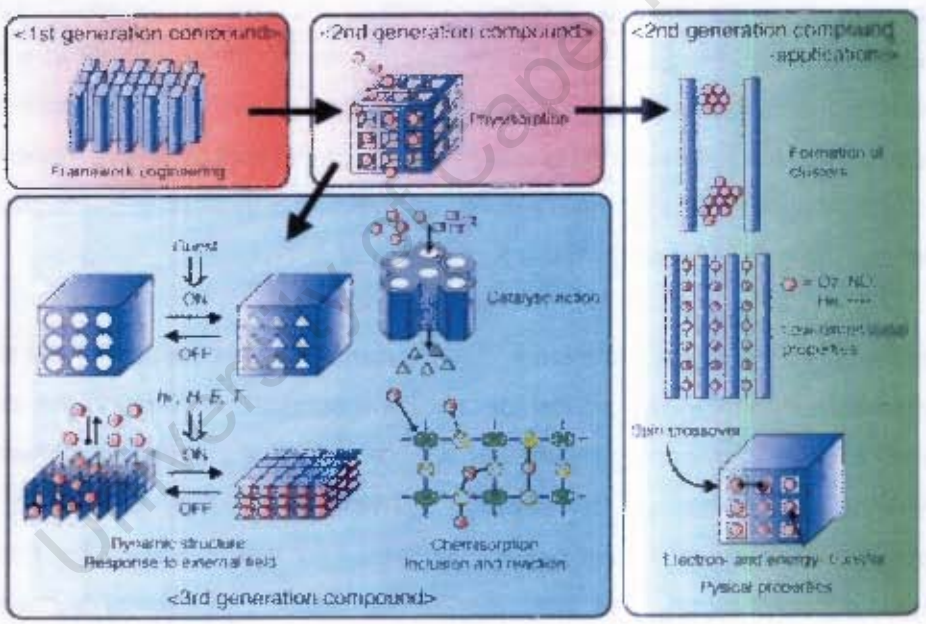

Figure 1.7 Selection of functions displayed by porous coordination polymers.[79]

O. Yaghi and co-workers have made important advances in the research of metal-organic frameworks, which are differentiated from any solid containing metal ions linked by molecular species, as one which must also display "*strong bonding providing robustness, linking units that are available for modification by organic synthesis, and a geometrically well-defined structure*" and a review on this new class of porous materials has been given.[84]

Yaghi and co-workers have synthesised such frameworks, with desired properties, using the strategy of linking together molecular or secondary building units (SBU's) exhibiting the desired property.[85] The properties of the framework are largely determined by the network connectivity of the building units and may include magnetic exchange, acentricity for non-linear optical (NLO) applications and possession of large channels available for the passage of molecules. They have successfully prepared highly porous materials which can withstand exchange of the guests and have also adapted the network functionality by synthesising a number of structures with the same metal-organic framework topology, using the same synthetic parameters but by varying the type and size of the spacers (Figure 1.8).[86]

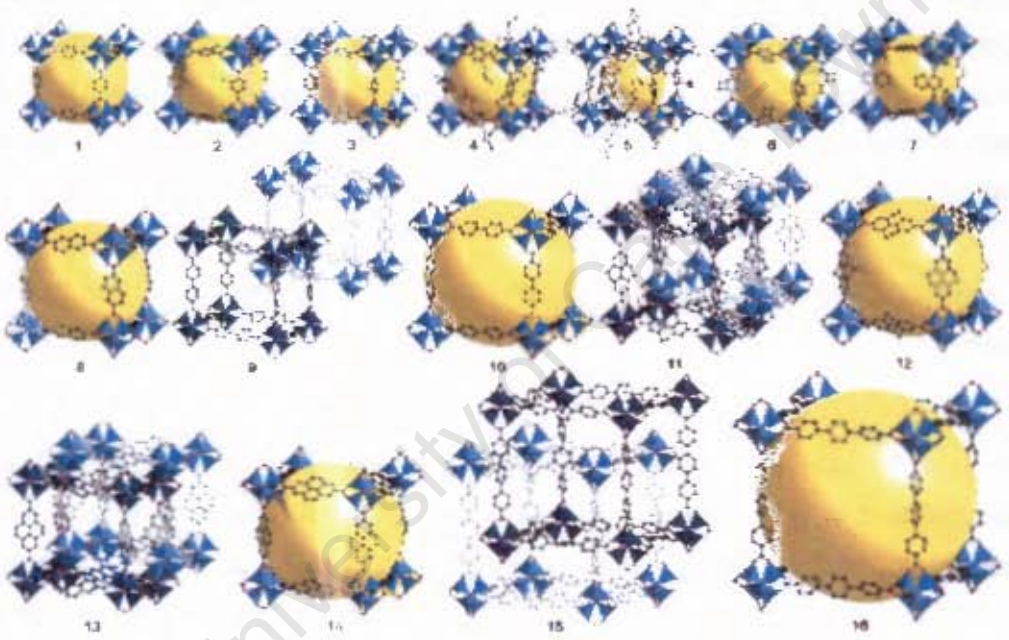

Figure 1.8 Series of 16 metal-organic frameworks produced by Yaghi *et al.*[86]

The construction of extended solids from molecular building blocks offers considerable advantages for the design of materials with desired properties such as high porosity. These materials are of great importance as they have many applications in catalysis, gas and liquid separations, methane and hydrogen storage and luminescence-based sensors.

THERMODYNAMIC AND KINETIC STUDIES OF HOST-GUEST COMPOUNDS

The formation and stability of inclusion compounds depend on the strengths and directions of the intermolecular forces found in the host-guest assembly. Structure determination by single crystal X-ray diffraction is an invaluable tool in the study of inclusion compounds as geometries and strengths of intermolecular interactions can be easily obtained, as can information about the topology and packing, which in turn affects thermal stability, guest selectivity, ability for guest exchange and kinetics of formation and decomposition.

Although design, synthesis and structures of a large number of host-guest compounds have been studied, their physical properties such as thermal stability and kinetics of enclathration and desorption have not received much attention. The subject of physico-chemical aspects of inclusion compounds has been reviewed recently.[87,88]

The formation of an inclusion compound can be represented by the following equation:

$$H_{(s,\alpha)} + nG_{(l)\ or\ (g)} \rightarrow H{\bullet}G_{n(s,\beta)}$$

where α is the non-porous phase of the host H, β is the phase of the host-guest compound and n is the guest:host ratio. A schematic diagram illustrating the formation and decomposition of an inclusion compound is given in Figure 1.9.[88] From this diagram it can be seen that host-guest compounds can decompose in a number of ways to either revert to the original non-porous α-phase, or to form a metastable intermediate γ-phase if only partial guest loss occurs, or thirdly the host framework or β_0–phase may be retained despite complete guest loss.

Thermal analysis is an important tool in the quantitative study of the thermal stability of host-guest compounds. Thermogravimetry (TG) measures the mass loss, due to guest release, upon heating and is suitable for determining accurate host:guest ratios of inclusion compounds. Differential scanning calorimetry (DSC) measures change in enthalpy as a function of temperature and idealised TG and DSC curves of an inclusion compound are illustrated in Figure 1.10.[82]

The DSC trace yields the onset temperature of guest release (T_{on}). It has been shown that the difference between this value and the normal boiling point of the guest (T_b) gives an indication of the stability of an inclusion compound where the more positive the value of (T_{on}-T_b), the more stable the inclusion compound. A value as high as +370°C was found for a clathrate of CF_4 in calix[4]arene reported by Atwood and Barbour.[89]

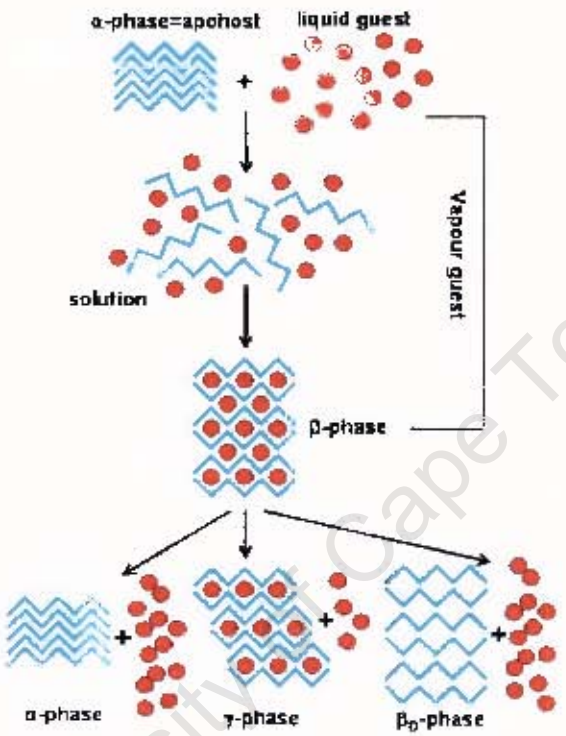

Figure 1.9 Formation and decomposition of an inclusion compound.[88]

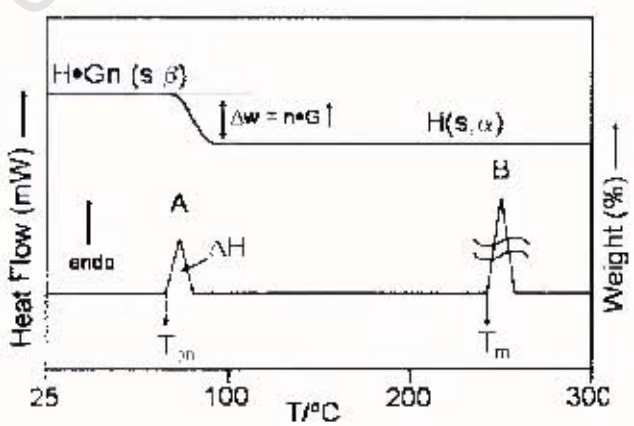

Figure 1.10 TG and DSC traces of an inclusion compound which decomposes in one step.[62]

A quantitative measure of thermal stability is the lattice energy of the compound which can be evaluated using the method of atom-atom potentials. Force fields of the type $V(r) = a \exp(-br) - c/r^6$ can be employed, where r is the interaction distance and coefficients a, b and c are those given by Gavezzotti.[90] A suitable hydrogen-bonding potential is incorporated, such as that of Vedani and Dunitz,[91] which is formulated as $V(H\text{-bond}) = (A/R^{12} - C/R^{10})\cos^2\theta$, where A and C are constants, R is the distance between the donor hydrogen and acceptor atom and θ is the donor-H···acceptor angle.

Kinetics of enclathration as well as desorption are important in inclusion chemistry. The theory of kinetics of decomposition of solids has been comprehensively reviewed by Brown[92] and is well established, while Byrn has explored the solid-state kinetics of decomposition of pharmaceuticals.[93]

For homogeneous reactions, the change in concentration of reactants or products can be measured with time at a constant temperature. The rate of the reaction can be expressed as

$$\text{rate} = k_T f(\text{concentration of reactants or products})$$

where k_T is the temperature dependent rate constant, related to the temperature by the Arrehnius equation

$$k_T = Ae^{-E_a/RT} \quad \text{or} \quad \ln k_T = -E_a/RT + \ln A$$

The activation energy E_a and the pre-exponential factor A can thus be calculated for a particular reaction by conducting a series of experiments at various temperatures.

For a heterogeneous reaction of the form

$$A_{(s)} + nB_{(g)} \rightarrow AB_{n\,(s)}$$

the change in concentration of reactants or products cannot be used to follow the reaction, and instead the reaction is monitored by the extent of reaction, α, defined as

$$\alpha = (m_i - m_t) / (m_i - m_f)$$

where m_i is the initial mass of the compound, m_f is the final mass of the compound and m_t is the mass of the compound at any time t.[92]

α can be measured as a function of time at constant temperature for kinetic studies of both formation and decomposition reactions. A generalised α–time curve is shown in Figure 1.11, which comprises surface adsorption or desorption, shown by step A, followed by an induction period, step B, during which nucleation takes place. Step C is an acceleration period, followed by D which is a deceleration period until completion of the reaction, step E.

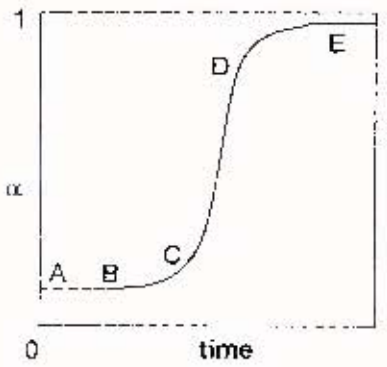

Figure 1.11 Generalised α-time curve for solid state reactions.

Analysis of the kinetics of these reactions involves correlating the experimentally observed α and t values with values predicted for a limited set of models based on nucleation and growth processes, diffusion processes or simpler geometrical progress of the reactant/product interface. The expressions derived from these models can all be written in their integral forms $f(\alpha) = kt$ as displayed in Table 1.1.

To obtain the activation energy of a desorption reaction, a series of isothermal experiments can be carried out at selected temperatures. The appropriate rate law is determined and the rate constants derived which can then be employed in the Arrhenius equation. Galwey and Brown have given theoretical justification for the application of this equation to heterogeneous reactions.[94]

The kinetics of enclathration of guest molecules in the vapour phase by a solid organic host has received little attention as such studies are experimentally difficult and the inclusion compounds formed are often unstable under ambient conditions. A suitable automated magnetic suspension balance has, however, been constructed for this purpose,[95] allowing such studies to be carried out.

Table 1.1 Broad classification of solid-state rate expressions[32]

		Kinetic model	$f(\alpha) = kt$
Sigmoid α-time curves		**B1** Prout-Tompkins	$\ln[\alpha/(1-\alpha)]$
		A2 Avrami-Erofeev	$[-\ln(1-\alpha)]^{1/2}$
		A3 Avrami-Erofeev	$[-\ln(1-\alpha)]^{1/3}$
		A4 Avrami-Erofeev	$[-\ln(1-\alpha)]^{1/4}$
Acceleratory α-time curves		**P1** power law	$\alpha^{1/n}$
		E1 exponential law	$\ln\alpha$
Deceleratory α-time curves	**based on geometrical models**	**R2** contracting area	$1-(1-\alpha)^{1/2}$
		R3 contracting volume	$1-(1-\alpha)^{1/3}$
	based on diffusion mechanisms	**D1** one-dimensional	α^2
		D2 two-dimensional	$(1-\alpha)\ln(1-\alpha)+\alpha$
		D3 three-dimensional	$[1-(1-\alpha)^{1/3}]^2$
		D4 Ginstling-Brounshtein	$(1-2\alpha/3)-(1-\alpha)^{2/3}$
	based on "order of reaction"	**F1** first order	$-\ln(1-\alpha)$
		F2 second order	$1/(1-\alpha)$
		F3 third order	$[1/(1-\alpha)]^2$

Applying various physico-chemical techniques to inclusion compounds allows accurate thermodynamic and kinetic parameters relating to their stability and modes of formation and decomposition to be established. Many macroproperties of inclusion compounds can be correlated with their crystal structures leading to a greater understanding of the intermolecular interactions occurring in the host-guest assemblies, which is of fundamental importance in supramolecular chemistry.

COVALENT AND NON-COVALENT CAPSULES

The design of discrete spherical molecular hosts began with the introduction of cryptands by Sauvage *et al.*[96] These hosts possess cavities in which guests can be completely enclosed and demonstrate a wide range of applications.

Carcerands have been defined as '*closed-surface sphere-like organic host compounds with structures rigid enough to contain enforced interiors of sufficient volume to incarcerate guest atoms, molecules or ions*' and carceplexes as '*carcerands containing guests in their inner phases which are unable to depart without breaking bonds in the host*'.[8] Hemicarcerands differ from carcerands in that it is possible for guests to enter and exit with an activation barrier, eg. cryptophanes which are able to reversibly entrap relatively small guests, and hemicarcerands containing guests form hemicarceplexes.

Cram and co-workers coupled the upper rims of two resorcinarene molecules to form the first example of a carcerand[97] and following this Cram and others have prepared a vast range of carcerand and hemicarcerand species based on [4]resorcinarenes and calix[n]arenes (n = 4,5) which have interesting binding behaviour and reactivity.[8,98]

The cavity of hemicarcerands allows the use of these host molecules as micro-reaction vessels which have the ability to protect reactive species by isolating them from the outside medium and may also have an effect on the reactivity of the guest.[26] Examples include the use of a hemicarcerand by Cram *et al* for the intracavity preparation of the highly unstable molecule cyclobutadiene,[99] as well as the stabilisation of highly reactive *o*-benzyne by Warmuth within a four-bridged hemicarceplex.[100]

A thorough understanding of the structure and thermodynamic stability of these systems is important and Sherman and co-workers have reported the formation of a variety of carceplexes and hemicarceplexes[101] and have also investigated the guest-selectivity, guest exchange rates, relative host selectivities and relative thermodynamic stabilities of molecular capsules which reversibly encapsulate small guest molecules.[102]

Rebek and co-workers pioneered the use of self-assembly to form a variety of capsules held together by hydrogen bonds and have reported the synthesis and characterisation of such capsules as well as their assembly with guest species.[103,104] J.L. Atwood and co-workers have also utilised non-covalent forces such as hydrogen bonds to construct large-volume molecular capsules by self-assembly including an enormous molecular capsule which has the geometry of a snub cube and is held together by 60 hydrogen bonds.[105] This capsule is made up of six calix[4]arenes and eight water molecules and is illustrated in Figure 1.12.

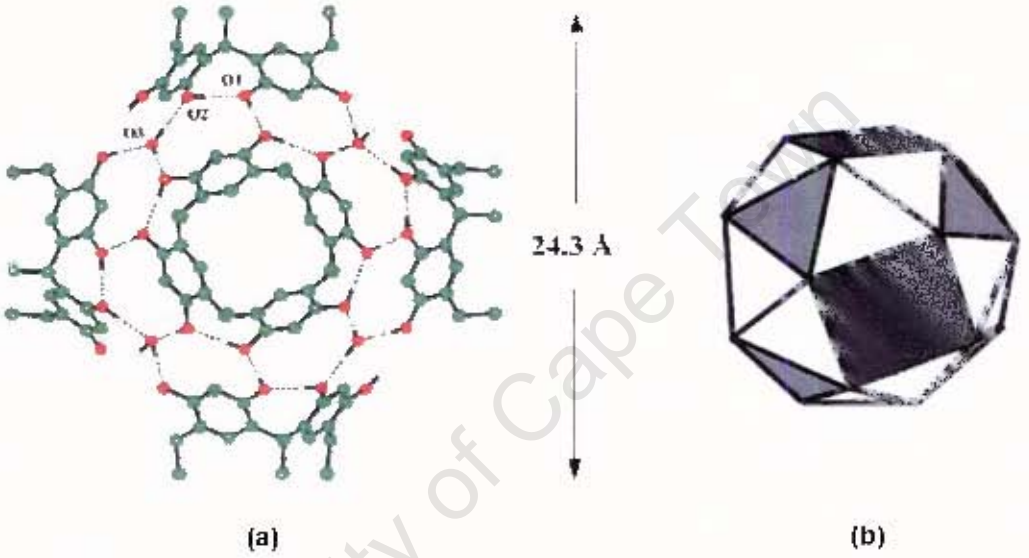

Figure 1.12 **(a)** cross-section of capsule and **(b)** the snub cube (one of the 13 Archimedean solids) with squares corresponding to calix[4]arenes and shaded triangles to water molecules.[105]

A review has been given by Atwood and MacGillivray which presents general principles of a design strategy for constructing these spherical molecular hosts and suggests the five Platonic and thirteen Archimedean solids as appropriate models for host design.[106] Formation of such capsules often involves replacing covalent bonds of monomolecular species such as carcerands with supramolecular synthons and the resulting frameworks can display properties such as reversible formation which are not found in the monomolecular species.[107] Atwood, Barbour and Raston have recently reported the formation of a spherical nanostructure made up of twelve calixarene building blocks which can assemble in two vastly different arrangements and provides insight into methods of designing self-assembled structures which may mimic features of biological systems.[108]

The mechanism of guest encapsulation and exchange in reversibly formed capsules has recently been investigated by Rebek *et al* using various spectroscopic methods.[109] This study showed that in various systems the guests generally enter and exit the capsules through the opening and closing of host "flaps". An example is illustrated in Figure 1.13. Guest exchange in capsules consisting of calixarene dimers has been investigated by Böhmer and co-workers.[110,111]

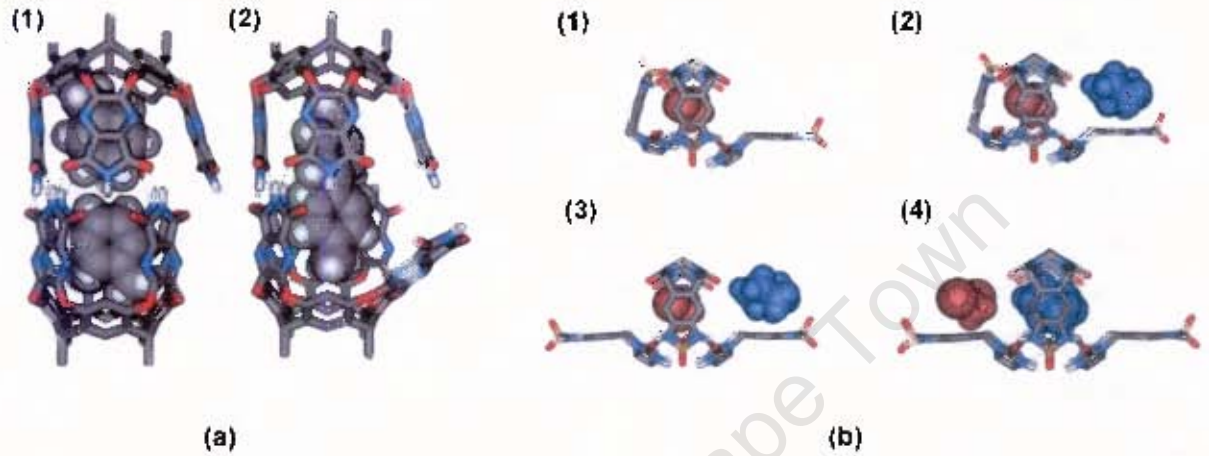

Figure 1.13 **(a)** guest exchange mechanism in a cylindrical capsule for (1) small guests and (2) larger guests and **(b)** proposed mechanism for guest exchange in the "football" capsule.

The design, formation and study of such capsules are significant and will undoubtedly move towards the formation of ever larger cavity systems as those of nanoscale dimensions are still rare. These structures have a wide range of applications in chemistry, biology and materials science as they can be used to stabilise reactive species within the host cavity, to transfer biologically active molecules to target cells and to construct molecular scale devices.[106]

GAS SENSING, STORAGE AND SEPARATION

Molecular recognition of gases is still at an early stage and a review on this subject has been given recently by D.M. Rudkevich.[112] A number of important receptor/sensing systems have however been developed, which function through Lewis acid-base, dipole-dipole interactions, hydrogen bonding, van der Waals forces and encapsulation within closed spaces. Electronic and geometrical complementarity can be used to rationalise kinetics, thermodynamics and selectivity of molecular hosts for gases.[112]

As previously mentioned, porous coordination polymers have the ability to provide suitable adsorbents for gases at ambient temperature. In 1997 the reversible adsorption of CH_4, N_2 and O_2 by a bilayer framework structure at ambient temperature was reported[113] and since then many similar coordination polymers have been synthesised which are capable of adsorbing gases.[114,115,116,117,118] Figure 1.14 displays a 1-dimensional array of O_2 adsorbed into the nanochannels of a microporous copper coordination polymer reported by S. Kitagawa *et al.*[119]

Utilising adsorbents for the storage of methane has been investigated as an alternative to compressed gas storage at high pressure, but none of the conventional adsorbents have been found to be commercially viable. Micropores of suitable size for methane molecules and which are abundant and uniformly distributed in the solid are necessary to achieve a high adsorption capacity. Porous coordination polymers thus show strong potential as adsorbents for CH_4 storage and the compounds $\{[Cu(AF_6)(4,4'\text{-bpy})_2].8H_2O\}_n$ (A = Si and Ge) show high CH_4 adsorption at room temperature and relatively low pressure.[117]

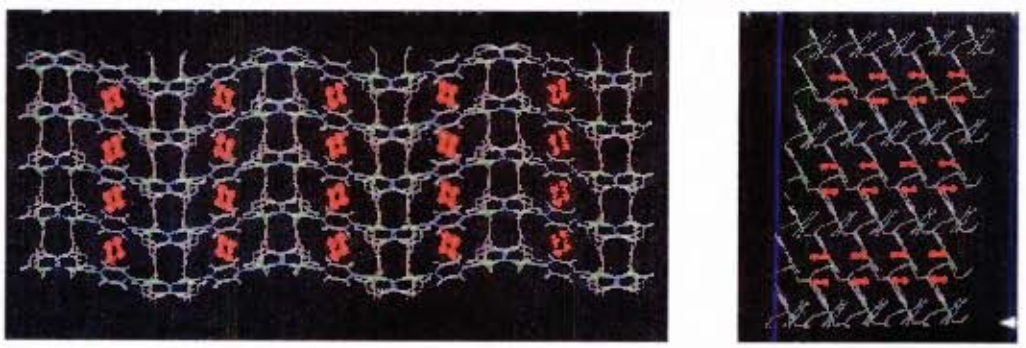

Figure 1.14 Representation of coordination polymer with adsorbed O_2 at 90K, viewed **(a)** down c-axis and **(b)** down b-axis.[119]

Molecular container compounds or capsules have been found to entrap and release guest species by using subtle chemical or physical control. Cram *et al* have encapsulated O_2, N_2, CO_2 and Xe in a hemicarcerand[120] and recently Atwood and co-workers have reported that CH_4, as well as a range of freons, can be encapsulated and retained within the lattice voids of a calix[4]arene framework (Figure 1.15),[89] thus demonstrating the use of solids held together by van der Waals forces in encapsulation of gases.

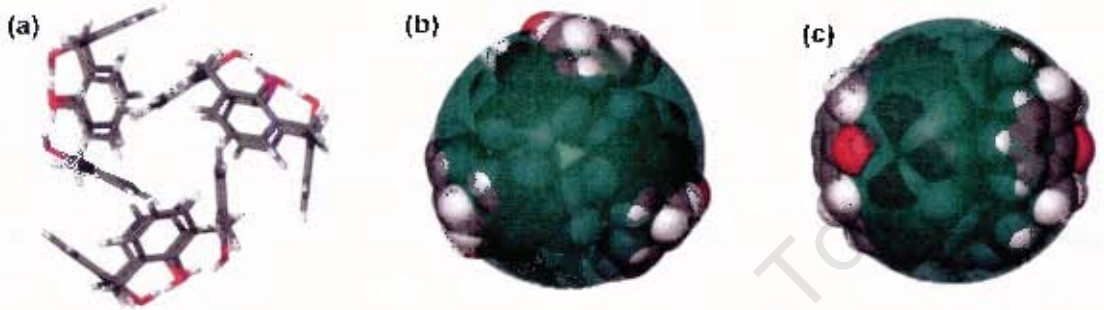

Figure 1.15 Cyclic, tetrameric arrangement of calix[4]arene in framework **(a)** in stick representation along 3-fold axis, **(b)** in space-filling representation along 3-fold axis and **(c)** in space-filling representation viewed perpendicular to 3-fold axis, with green sphere included for emphasis of small deviation from true spherical geometry.[89]

A practical means for H_2 storage and transportation has not yet been developed, but is desirable as the use of H_2 as a fuel does not create CO, CO_2, N_2O, NO or NO_2 emissions. H_2 adsorption has been carried out very recently with microporous Zn^{II}-cluster-dicarboxylate metal organic frameworks,[121] as well as with nickel(II) phosphates.[122] The use of H_2 as a fuel also relies on purification of H_2 by separation from impurities such as CH_4, CO, H_2O and CO_2. Atwood and Barbour have recently shown that a non-porous organic molecular crystal can be exploited for the purification of H_2 gas.[123] They found that a close-packed structure of p-*tert*-butylcalix[4]arene with vinyl bromide molecules located in enclosed cavities selectively absorbs gases CO_2, N_2 and O_2 into its structure and not H_2 gas.

Application of supramolecular chemistry and molecular recognition principles and techniques to the processes of gas sensing, storage and separation is only just beginning and as further research is carried out, will undoubtedly result in development of new materials for these important purposes.[112]

STUDY OF NUCLEATION AND CRYSTAL GROWTH

The nucleation process is of great importance in the field of crystal engineering as the nature of solvent-solute interactions can have a strong influence on the structural outcome of a crystallisation. A comprehensive introduction to nucleation and crystallisation has been given by R. Davey and J. Garside[124] and the structural aspects of the nucleation process in a number of small molecule systems have been investigated.[125,126,127,128,129]

Solution phases must be brought to a supersaturated state in order for crystals to nucleate and grow, as supersaturation, which is expressed by comparing the actual to the equilibrium composition, drives the nucleation process.[124] Nucleation is an activated process with a transition state, where the transition state is a cluster of molecules packed in a regular way and held together by weak intermolecular forces. The supersaturation determines the critical size, which is the size below which the clusters are unstable and above which further growth of the clusters leads to a decrease in free energy.[130]

In a supersaturated environment the flux of growth units to a crystal surface is greater than the equilibrium flux and so a greater number of growth units join the surface than leave. Solid state structural effects are important including the number of interactions that can form between the surface and the growth unit, as well as the strength of these interactions.[124] Faces which have more intermolecular interactions available at the surface will cause the system to gain more energy when molecules join that surface and will grow faster. Crystal morphology is determined by both the symmetry of the internal crystal structure and the relative growth rates of the crystal faces as well as external factors such as supersaturation, temperature and solvent.[124]

Davey *et al* have combined thermodynamics, structural and modelling approaches in order to understand the link between the kinetic processes of molecular assembly in solution and the structure of the resultant crystals.[130] Crystallisation can be brought about by a number of procedures including salting out reactions, evaporation of common organic solvents and drowning out, and the manner in which it occurs can often determine the final outcome of the process.[130]

Polymorphism is the property of a substance to exist in different crystalline phases resulting from different arrangements of the molecules in the solid state[131] and the subject of nucleation and crystal growth is of great significance in the formation of different polymorphs. There are many publications on organic polymorphism in the literature and a recent review has been given by Dunitz and Bernstein,[132] while the topic of concomitant polymorphs (polymorphs obtained from the same crystallisation process) has been discussed by Bernstein *et al.*[133] A review of organometallic polymorphism has been given by Braga and Grepioni [134]

Polymorphism can be used to investigate self-assembly in solution. Whether clusters corresponding to all possible polymorphs in a system exist in solution is not known, but the nature of the solvent-solute interactions can play an important role in determining whether or not an aggregate in solution will evolve to a crystal.[130] Evidence that molecular assembly in solution can mirror packing of potential polymorphs obtained by crystallisation is given by investigations of nucleation in polymorphic systems such as sulfathiozole[127] and dihydroxybenzoic acid[128] as well as the templated nucleation of glycine.[129] The concept of solute assembly as a prerequisite to nucleation has also been supported by molecular dynamics calculations.[135]

Whether the molecular clusters in solution are 'crystalline or 'amorphous' is not known and nor is the relationship between crystal growth units (the essential building blocks that transfer structural information from the solution to the crystal surface) and the intermolecular interactions in the resultant crystals. The cases investigated however, suggest that molecular dimers are often common building blocks between the solution and the crystal. It has been shown that tailor-made additives can be used to control nucleation and growth of crystals as well as for crystallisation of a desired polymorph.[136,126] Controlling the preparation of polymorphs is a major issue of modern crystal engineering[137] and it has been shown that this is possible to some extent.[134]

There is a large scope for further research in the area of nucleation and crystal growth in order to gain further understanding of the relationship between liquid phase molecular assemblies and solid-state molecular packing which is of enormous importance in crystal engineering.

CATENANES AND ROTAXANES

Catenanes are compounds consisting of two or more rings which are mechanically interlocked without any chemical interactions between the two, where the rings cannot be separated without breaking a covalent bond. Rotaxanes are compounds consisting of a dumbbell-shaped component, which includes a rod and two bulky stopper groups, encircled by a macrocyclic ring. The stoppers are too large to fit through the ring and like catananes, the components cannot be separated without breaking covalent bonds. Rotaxanes in which the stopper groups are absent or small enough to fit through the ring are termed *pseudorotaxanes* and these are often precursors to catenanes and rotaxanes in typical synthetic procedures. Schematic representations of some interlocked molecules and intertwined supermolecules are given in Figure 1.16.

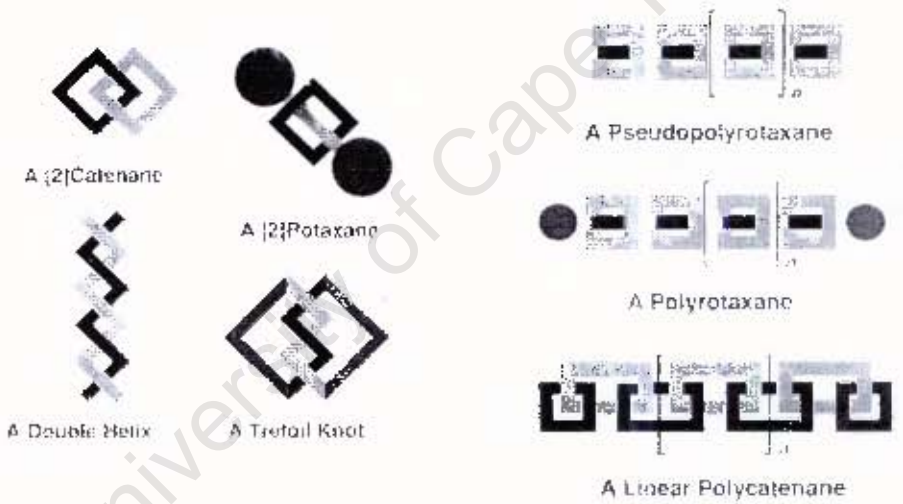

Figure 1.16 Schematic representation of catenanes, rotaxanes and larger inlocked supermolecules. (adapted from D.B. Amabilino and J.F. Stoddart, *Chem. Rev.*, 1995, **5**, 2725.)[138]

The first evidence for the formation of a catenane was reported by Wasserman[139] in 1960, while Harrison and Harrison reported the first synthesis of a [2]rotaxane in 1967.[140] For directed rotaxane and catenane synthesis, there is a greater probability of associating these molecules in the desired manner if the reactants are already associated as a self-assembled host-guest complex in solution, before the final cyclisation or stoppering reaction occurs. The final reaction which then covalently fixes the array together can take place by a number of mechanisms.[29]

J.F. Stoddart and co-workers have utilised such a self-assembly approach, making use of charge-assisted π–π stacking interactions, to construct a large variety of interlocked macromolecules including rotaxanes and catenanes as well as their macromolecular counterparts, polyrotaxanes and polycatenanes.[138,141] Sauvage and co-workers have used chelation of metal ions by coordinating ligands to synthesise trefoil knots.[142] There has been remarkable progress in the designed synthesis of these interlocked systems based on molecular recognition phenomena and increasingly intricate structures continue to be produced. The progression from simple recognition processes to complex structures and superstructures is illustrated schematically in Figure 1.17.[138]

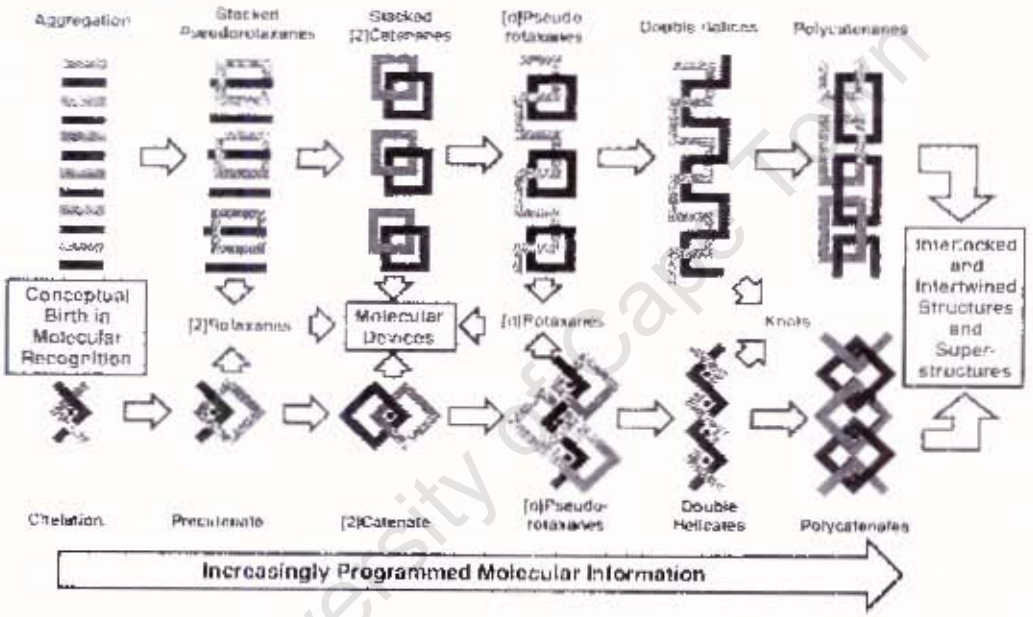

Figure 1.17 Progression from simple recognition processes to complex structures and superstructures based on donor-acceptor stacks (top) and metal ion chelation (bottom).[138]

Studies have been carried out in this field with the aim of understanding, at a fundamental level, how simple components assemble to form these complex arrays with an ultimate aim to generate systems with particular functions.[138] Possibilities for the application of these species include development of materials with new physical properties and the formation of sophisticated switchable molecular devices. Stoddart *et al* have given a review entitled 'Molecular Machines' where the reversible formation of pseudorotaxanes, rotaxanes and catenanes is investigated as a type of molecular switch and they have also recently reported an operational supramolecular nanovalve which is an example of a functioning molecular machine.[143]

SUPRAMOLECULAR SYSTEMS AS MODELS FOR BIOLOGICAL PROCESSES

"Few scientists aquainted with the chemistry of biological systems at the molecular level can avoid being inspired. Evolution has produced chemical compounds exquisitely organised to accomplish the most complicated and delicate of tasks. Many organic chemists viewing the crystal structures of enzyme systems or nucleic acids and knowing the marvels of specificity of the immune system must dream of designing and synthesising simpler organic compounds that imitate working features of these naturally occurring compounds."

- D.J. Cram, 'The design of molecular hosts, guests and their complexes (Nobel Lecture)'[144]

The development of supramolecular chemistry has been inspired by biological systems to a great extent and the beginnings of supramolecular chemistry, a field based on molecular recognition, can be traced back to Fischer's lock and key model of enzymatic catalysis.[145] Man-made materials can be used to construct artificial enzymes which simulate catalytic functions of enzyme proteins and today many supramolecular systems have been designed to mimic the structure or function of more complex biological processes.[29]

Receptor-substrate binding, which is governed by molecular recognition and is of great importance in biochemistry, is a reversible process governed by thermodynamics. The binding energy of the substrate is often used to bring about a conformational change in the receptor, which is referred to as the 'induced fit model'.[29] This model is compared to the lock and key model in a schematic representation in Figure 1.18.

In addition to a number of characteristic features of enzymes, an effective enzyme mimic should ideally have a low molecular weight, few chiral elements, stability to handling even at high temperatures and should be soluble in a variety of solvents.[29] An account of the supramolecular aspects of enzymes has been given by D.H. Kim.[146] Two types of artificial enzymes, namely macrocyclic compounds and molecular assemblies, are distinguished in a review given by Y. Murakami *et al.*[147] Cyclodextrins[148] and cyclophanes[149] are examples of macrocyclic compounds which

have been developed as enzyme mimics, while examples of molecular assemblies include micelles and bilayer membranes.[147]

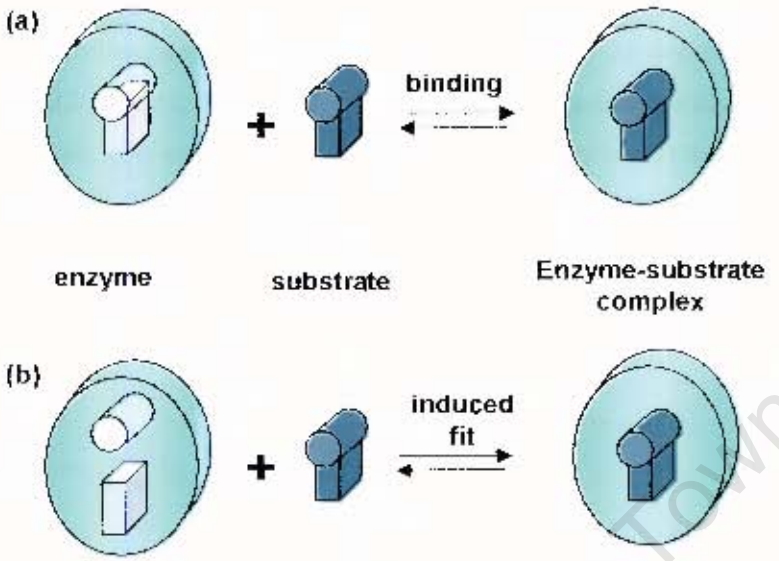

Figure 1.18 **(a)** rigid lock and key and **(b)** induced fit models for enzyme-substrate binding. (adapted from J.W. Steed, and J.L. Atwood, *Supramolecular Chemistry*, John Wiley & Sons, Chichester, 2000, page 643) [29]

Many biological proteins and enzymes have a metal ion at the core of their active site and coordination compound models of such sites (termed metallobiosites) can be developed through simulation of the immediate coordination sphere around the metal ion.[150] These are typically structural models which mimic the structure of the site, but not its function or catalytic activity.

The goals of studying systems which may mimic structure or function of biological systems include increasing understanding of natural enzymes, development of industrial catalysts and artificial regulation of biochemical reactions.[29] Biomacromolecules including enzymes, pharmacological receptors, ion carriers and ion channels perform their tasks with incredible efficiency as well as selectivity, and supramolecular chemistry can greatly assist our understanding of complex biochemical processes in living systems.[146]

ASPECTS OF THIS STUDY

This study explores the structural, thermodynamic and kinetic properties of a number of inclusion compounds formed with the following three organic host compounds: *trans*-9,10-dihydroxy-9,10-bis(p-*tert*-butylphenyl)-9,10-dihydroanthracene, 9,9'-(Biphenyl-4,4'-diyl)difluoren-9-ol and $1^4,1^6,5^4,5^6$-tetrahydroxy-2,4,6,8-tetrapentyl-3^4,3^6,7^4,7^6-tetra(p-toluenesulfonyl-oxy)-1,3,5,7(1,3)-tetrabenzenacyclooctaphane. The chemical structure of each of these molecules is displayed in Figure 1.19. In each case the included guests are small organic molecules which have the potential for participation in hydrogen bonding.

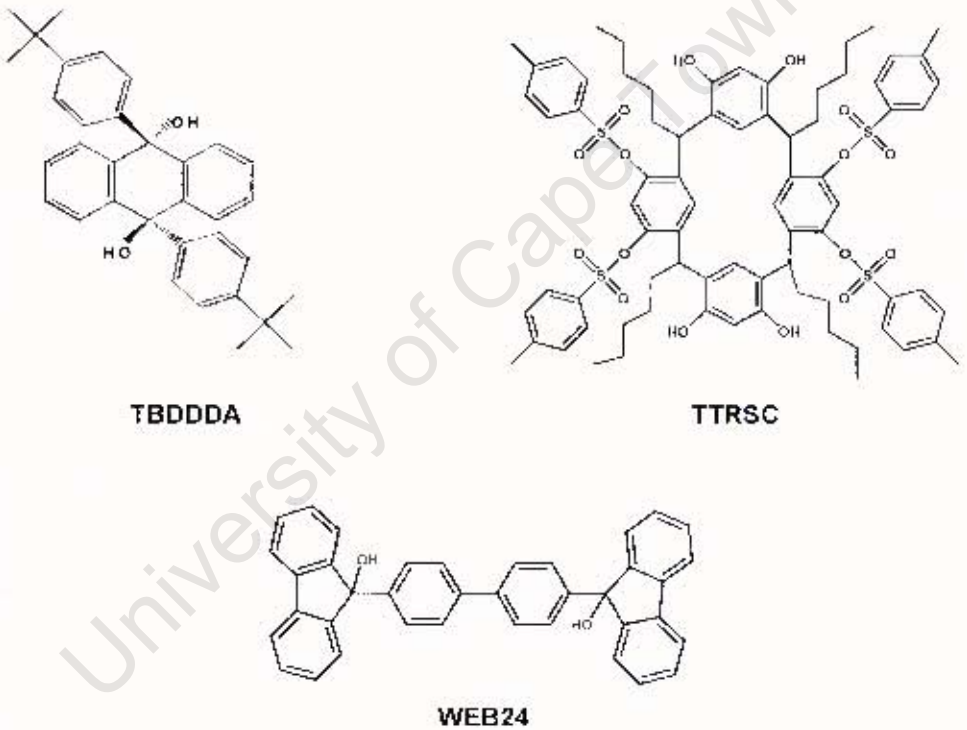

Figure 1.19 Molecular structures of **TBDDDA**, **WEB24** and **TTRSC**.

The diol host *trans*-9,10-dihydroxy-9,10-bis(p-*tert*-butylphenyl)-9,10-dihydroanthracene is a structurally modified analogue of the well known host compound *trans*-9,10-dihydroxy-9,10-diphenyl-9,10-dihydroanthracene.[15] This host has bulky *tert*-butylphenyl groups and two hydroxyl groups in a trans conformation which can act as hydrogen bond donors, and has previously been found to form host-guest compounds with methanol, diethyl ether, benzene and acetone.

The second host compound investigated was the fluorenyl host 9,9'-(Biphenyl-4,4'-diyl)difluoren-9-ol. Host compounds containing the fluorenyl moiety have been studied extensively, as they have the capacity to enclathrate a variety of guest molecules.[19] They conform to Weber's host design specifications in that they are rigid, bulky and contain the hydroxyl moiety, which facilitates the formation of coordinato-clathrates via hydrogen bonding.[13] A series of such host compounds, in which the fluorenyl moieties are separated by spacers of different lengths, have been synthesised, and their crystalline inclusion compounds with a large number of guests have been reported.[152] This particular host compound has previously been found to form inclusion compounds with a number of guest molecules, although the crystal structures of these compounds have not been elucidated.

The third host investigated in this study was the resorcinarene host $1^4,1^5,5^4,5^5$-tetrahydroxy-2,4,6,8-tetrapentyl-$3^4,3^6,7^4,7^5$-tetra(p-toluenesulfonyl-oxy)-1,3,5,7(1,3)-tetrabenzenacyclooctaphane with four substituted tosylate groups on the upper rim and with pentyl groups on the lower rim. The chemistry of resorcinarenes, including synthesis, conformational behaviour and complexation properties, has been studied extensively and is well established.[153]

The use of resorcinarenes in supramolecular host-guest chemistry is developing rapidly and C-methylcalix[4]resorcinarene has been found to act as a suitable building block for a wide variety of supramolecular complexes. Many inclusion compounds have been formed with this host, including host-guest compounds containing small organic guests only,[154,155,156,157,158] as well as inclusion compounds with additional spacers linking the resorcinarene host molecules together,[159,160,161,162] sometimes resulting in the formation of capsules in which the guest molecule is completely enclosed.[105,163,164,165,166,167] C-methylcalix[4]resorcinarene can be modified by substitution at the upper and lower rim or by extending the upper rim using various pillars[168,169] in order to increase the size of the cavity in which guests can be situated or even by covalently linking neighbouring hydroxyl groups in order to form cavitands.[170]

The crystal structures of each of the inclusion compounds formed in this study were elucidated using single crystal X-ray diffraction methods, while thermogravimetry, differential scanning calorimetry and hot stage microscopy were used to analyse the thermal behaviour of the complexes. The kinetics of formation as well as decomposition of selected inclusion compounds were investigated and selectivity of

two of the hosts for various guests was studied in order to explore the possibility of separation by selective enclathration. An attempt is made to relate the macroproperties of the inclusion compounds to their structures.

During this study a three month period was spent at the Steacie Institute of Molecular Sciences, National Research Council of Canada in Ottawa in the laboratory of Dr. John Ripmeester. ^{13}C solid state CP/MAS NMR was used to analyse some of the inclusion compounds of 9,9'-(Biphenyl-4,4'-diyl)difluoren-9-ol and to monitor the desorption of the guest from each of these clathrates. A two month period was also spent at UMIST in Manchester in the Crystals, Colloids and Interfaces group under Prof. Roger Davey learning various techniques for the study of nucleation and crystal growth. Various experiments were carried out, including investigating the solubility and crystallisation of two of the inclusion compounds, which is reported on briefly in this thesis.

REFERENCES

[1] J.-M. Lehn, *Pure Appl. Chem.*, 1978, **50**, 871.

[2] *Comprehensive Supramolecular Chemistry*, Vol. 1-10, eds. J.L. Atwood, J.E.D. Davies, D.D. MacNicol and F. Vögtle, Pergamon, Oxford, 1996.

[3] *Encyclopedia of Supramolecular Chemistry*, Vol. 1-2, eds. J.L. Atwood and J.W. Steed, Marcel Dekker, Inc., New York, 2004.

[4] J.D. Dunitz, *Pure Appl. Chem.*, 1991, **63**, 177.

[5] F. Vögtle, *Supramolecular Chemistry*, John Wiley & Sons, Ltd., Chichester, 1991, Chapter 5.

[6] *Comprehensive Supramolecular Chemistry*, Vol. 3, eds. J. Szejtli and T. Osa, Pergamon, Oxford, 1996.

[7] C.D. Gutsche, *Calixarenes*, The Royal Society of Chemistry, Cambridge, 1989.

[8] E. Maverick and D.J. Cram in *Comprehensive Supramolecular Chemistry*, Vol. 2, ed. F. Vögtle, Pergamon, Oxford, 1996, Chapter 12.

[9] G. Gokel, *Crown ethers and Cryptands*, The Royal Society of Chemistry, Cambridge, 1991.

[10] K.D.M. Harris, *Chemistry in Britain*, 1992, 132.

[11] E. Weber, *Top Curr. Chem.*, 1987, **140**, 17.

[12] E. Weber and H.-P. Josel, *J. Inclusion Phenom.*, 1983, **1**, 79.

[13] E. Weber in *Inclusion Compounds*, Vol 4, eds. J.L. Atwood, J.E.D. Davies and D.D. MacNicol, Oxford University Press, Oxford, 1991, Chapter 5.

[14] F. Toda, K. Tanaka, G. Ulibarri Daumas and M.C. Sanchez, *Chem. Lett.*, 1983, 1521.

[15] E. Weber, N. Dörpinghaus, C. Wimmer, Z. Stein, H. Krupitsky and I. Goldberg, *J. Org. Chem.*, 1992, **57**, 6825.

[16] R. Bishop and I.G. Dance in *Inclusion Compounds*, Vol. 4, eds. J.L. Atwood, J.E.D. Davies and D.D. MacNicol, Oxford University Press, Oxford, 1991, Chapter 6.

[17] D.D. MacNicol in *Inclusion Compounds*, Vol. 2, eds. J.L. Atwood, J.E.D. Davies and D.D. MacNicol, Academic Press, London, 1984, Chapter 5.

[18] F. Toda in *Comprehensive Supramolecular Chemistry*, Vol. 6, eds. D.D. MacNicol, F. Toda and R. Bishop, Pergamon, Oxford, 1996, Chapter 15.

[19] E. Weber in *Comprehensive Supramolecular Chemistry*, Vol. 6, eds. D.D. MacNicol, F. Toda and R. Bishop, Pergamon, Oxford, 1996, Chapter 17.

[20] R. Bishop in *Comprehensive Supramolecular Chemistry*, Vol. 6, eds. D.D. MacNicol, F. Toda and R. Bishop, Pergamon, Oxford, 1996, Chapter 4.

[21] D.D. MacNicol and D.R. Wilson, *Chem. Comm.*, 1976, 494.

[22] A.D.U. Hardy, D.D. MacNicol and D.R. Wilson, *J. Chem. Soc., Perkin Trans. 2*, 1979, 1011.

[23] G.R. Desiraju, *Crystal engineering: The Design of Organic Solids*, Elsevier, Amsterdam, 1989.

[24] G.R. Desiraju, *Angew. Chem., Int. Ed. Engl.*, 1995, **34**, 2311.

[25] A. Nangia, G.R. Desiraju, *Top Curr. Chem.*, 1998, **198**, 57.

[26] G.R. Desiraju, *J. Mol. Struct.*, 2003, **656**, 5.

[27] F.H. Allen in *Crystallography of Supramolecular Compounds*, NATO ASI Series, Series C: Mathematical and Physical Sciences, Vol. 480, eds. G. Tsoucaris, J.L. Atwood and J. Lipkowski, Kluwer Academic Publishers, Dordrecht, 1996, Chapter 5.

[28] G.R. Desiraju, *Acc. Chem. Res.*, 2002, **35**, 565.

[29] J.W. Steed and J.L. Atwood, *Supramolecular Chemistry*, John Wiley & Sons, Ltd., Chichester, 2000.

[30] D. Sutor, *J. Chem. Soc.*, 1963, 1105.

[31] L. Leiserowitz, *Acta Cryst.*, 1976, B**32**, 775.

[32] R. Taylor and O. Kennard, *J. Am. Chem. Soc.*, 1982, **104**, 5063.

[33] C.M. Reddy, A. Nangia, C.-K. Lam and T.C.W. Mak, *CrystEngComm*, 2002, **4**, 323.

[34] P. Coppens, B. Ma, O. Gerlits, Y. Zhang and P. Kulshrestha, *CrystEngComm*, 2002, **4**, 302.

[35] S.F. Alshahateet, R. Bishop, D.C. Craig and M.L. Scudder, *CrystEngComm*, 2001, **48**, 1.

[36] T.J. Podestra and A.G. Orpen, *CrystEngComm*, 2002, **4**, 336.

[37] C.B. Aakeröy, A.M. Beatty and D.S. Leinen, *CrystEngComm*, 2002, **4**, 310.

[38] D. Braga, F. Grepioni and G.R. Desiraju, *Chem. Rev.*, 1998, **98**, 1375.

[39] D. Braga, *J. Chem. Soc., Dalton Trans.*, 2000, 3705.

[40] A.D. Burrows, R.W. Harrington, M.F. Mahon and C.E. Price, *J. Chem. Soc., Dalton Trans.*, 2000, 3845.

[41] H.A. Miller, N. Laing, S. Parsons, A. Parkin, P.A. Tasker and D.J. White, *J. Chem. Soc., Dalton Trans.*, 2000, 3773.

[42] L. Brammer, J.C.M. Rivas, R. Atencio, S. Fang and F.C. Pigge, *J. Chem. Soc., Dalton Trans.*, 2000, 3855.

[43] A.L. Gillon, G.R. Lewis, A.G. Orpen, S. Rotter, J. Starbuck, X.-M. Wang, Y. Rodriguez-Martin and C. Ruiz-Pérez, *J. Chem. Soc., Dalton Trans.*, 2000, 3897.

[44] R.P. Rastogi, *J. Scient. Ind. Res.*, 1970, **29**, 177.

[45] K. Tanaka and F. Toda, *Chem. Rev.*, 2000, **100**, 1025.

[46] F. Toda, M. Yagi and K. Kiyoshige, *Chem. Comm.*, 1988, 958.

[47] F. Toda, K. Tanaka and J. Sato, *Tetrahedron Asymm.*, 1993, **4**, 1771.

[48] F. Toda, K. Kiyoshige and M. Yagi, *Angew. Chem., Int. Ed. Engl.*, 1989, **28**, 320.

[49] F. Toda and T. Shigemasa, *J. Chem. Soc., Perkin Trans. 1*, 1989, 209.

[50] F. Toda, H. Takumi and M. Akehi, *Chem. Comm.*, 1990, 1270.

[51] F. Toda, *CrystEngComm*, 2002, **4**, 215.

[52] G.M.J. Schmidt, *Pure Appl. Chem.*, 1971. **27**, 647.

[53] L.R. MacGillivray in *Perspectives in Supramolecular Chemistry, Vol. 8: Separations and Reactions in Organic Supramolecular Chemistry*, eds. F. Toda and R. Bishop, John Wiley & Sons, Ltd., Chichester, 2004, Chapter 8.

[54] L.R. MacGillivray, J.L. Reid and J.A. Ripmeester, *J. Am. Chem. Soc.*, 2000, **122**, 7817.

[55] G.S. Papaefstathiou, A.J. Kipp and L.R. MacGillivray, *Chem. Comm.*, 2001, 2462.

[56] L.R. MacGillivray, J.L. Reid, J.A. Ripmeester and G.S. Papaefstathiou, *Indust. Eng. Chem. Res.*, 2002, **41**, 4494

[57] T.D. Hamilton, G.S. Papaefstathiou and L.R. MacGillivray, *J. Am. Chem. Soc.*, 2002, **124**, 11606.

[58] D.B. Varshney, G.S. Papaefstathiou and L.R. MacGillivray, *Chem. Comm.*, 2002. 1964.

[59] G.S. Papaefstathiou and L.R. MacGillivray, *Org. Lett.*, 2001, **3**, 3835.

[60] L.R. MacGillivray, *CrystEngComm*, 2002, **4**, 37.

[61] A.V. Trask, W.D.S. Motherwell and W. Jones, *Chem. Comm.*, 2004, 890.

[62] L.R. Nassimbeni in *Perspectives in Supramolecular Chemistry, Vol. 8: Separations and Reactions in Organic Supramolecular Chemistry*, eds. F. Toda and R. Bishop, John Wiley & Sons, Ltd., Chichester, 2004, Chapter 5.

[63] A.M. Pivovar, K.T. Holman and M.D. Ward, *Chem. Mater.*, 2001, **13**, 3018.

[64] I. Goldberg, Z. Stein, K. Tanaka and F. Toda, *J. Inclusion Phenom.*, 1988, **6**, 15.

[65] M.R. Caira, A. Horne, L.R. Nassimbeni and F. Toda, *J. Chem. Soc., Perkin Trans. 2*, 1997, 1717.

[66] M.R. Caira, A. Horne, L.R. Nassimbeni and F. Toda, *J. Mater. Chem.*, 1997, **7**, 2145.

[67] M.R. Caira, A. Horne, L.R. Nassimbeni and F. Toda, *Supramol. Chem.*, 1998, **9**, 231.

[68] M.R. Caira, L.R. Nassimbeni, F. Toda and D. Vujovic, *J. Chem. Soc., Perkin Trans. 2*, 1999, 2681.

[69] L.R. Nassimbeni and H. Su, *J. Chem. Soc., Perkin Trans. 2*, 2002, 1246.

[70] F. Toda, *Top Curr. Chem.*, 1987, **140**, 43.

[71] M.R. Caira, L.R. Nassimbeni, F. Toda and D. Vujovic, *J. Am. Chem. Soc.*, 2000, **122**, 9367.

[72] R. Thaimattam, F. Xue, J.A.R.P. Sarma, T.C.W. Mak and G.R. Desiraju, *J. Am. Chem. Soc.*, 2001, **123**, 4432.

[73] N. Hayashi, K. Kuruma, Y. Mazaki, T. Imakubo and K. Kobayashi, *J. Am. Chem. Soc.*, 1998, **120**, 3799.

[74] F. Toda in *Inclusion Compounds*, Vol 4, eds. J.L. Atwood, J.E.D. Davies and D.D. MacNicol, Oxford University Press, Oxford, 1991, Chapter 4.

[75] R. Bishop in *Perspectives in Supramolecular Chemistry, Vol. 8: Separations and Reactions in Organic Supramolecular Chemistry*, eds. F. Toda and R. Bishop, John Wiley & Sons, Ltd., Chichester. 2004, Chapter 2.

[76] A.N.M.M. Rahman, R. Bishop, D.C. Craig and M.L. Scudder, *Eur. J. Org. Chem.*, 2003, 72.

[77] R. Bishop in *Comprehensive Supramolecular Chemistry*, Vol. 6, eds. D.D. MacNicol, F. Toda and R. Bishop, Pergamon, Oxford, 1996, Chapter 4.

[78] A.T. Ung, R. Bishop, D.C. Craig, I.G. Dance and M.L. Scudder. *Chem. Mater.*, 1994, **6**, 1269.

[79] S. Kitagawa, R. Kitaura and S.-I. Noro, *Angew. Chem., Int. Ed. Engl.*, 2004, **43**, 2334.

[80] S.R. Batten and R. Robson, *Angew. Chem., Int. Ed. Engl.*, 1998, **37**, 1460.

[81] B. F. Abrahams, A. Hawley, M.G. Haywood, T.A. Hudson. R. Robson and D.A. Slizys, *J. Am. Chem. Soc.*, 2004, **126**, 2894.

[82] L. Brammer, M.D. Burgard, M.D. Eddleston, C.S. Rodger, N.P. Rath and H. Adams, *CrystEngComm*, 2002, **4**, 239.

[83] C.Z.-J. Lin, S.S.-Y. Chui, S.M.-F. Lo, F.L.-Y. Shek, M. Wu, K. Suwinska, J. Lipkowski and I.D. Williams, *Chem. Comm.*, 2002, 1642.

[84] J.L.C. Rowsell and O.M. Yaghi, *Microporous and Mesoporous Materials*, 2004, **73**, 3.

[85] M. Eddaoudi, D.B. Moler, H. Li, B. Chen, T.M. Reineke, M. O'Keeffe and O.M. Yaghi, *Acc. Chem. Res.*, 2001, **34**, 319.

[86] M. Eddaoudi, J. Kim, N.L. Rosi, D. Vodak, J. Wachter, M. O'Keeffe and O.M. Yaghi, *Science*, 2002, **295**, 469.

[87] M.R. Caira and L.R. Nassimbeni *in Comprehensive Supramolecular Chemistry*, Vol. 6, eds. D.D. MacNicol, F. Toda and R. Bishop, Pergamon, Oxford, 1996, Chapter 25.

[88] L.R. Nassimbeni, *Acc. Chem. Res.*, 2003, **36**, 631.

[89] J.L. Atwood, L.J. Barbour and A. Jerga, *Science*, 2002, **296**, 2367.

[90] A. Gavezzotti, *Crystallogr. Rev.*, 1998, **7**, 5.

[91] A. Venadi and J.D. Dunitz, *J. Am. Chem. Soc.*, 1985, **107**, 7653.

[92] M.E. Brown, *Introduction to Thermal Analysis*, Chapman & Hall, London, 1988.

[93] S.R. Byrn, *Solid-state Chemistry of Drugs*, Academic Press, New York, 1982.

[94] M.E. Brown and A.K. Galwey, *Anal. Chem.*, 1989, **61**, 1136.

[95] L.J. Barbour, K. Achleitner and J.R. Greene, *Thermochim. Acta*, 1992, **205**, 171.

[96] B. Dietrich, J.-M. Lehn, J.P. Sauvage, *Tetrahedron Lett.*, 1969, **34**, 2889.

[97] D.J. Cram, S. Karbach, Y.H. Kim, L. Baczynskyj and G.W. Kallemeyn, *J. Am. Chem. Soc.*, 1985, **107**, 2575.

[98] J.C. Sherman and D.J. Cram, *J. Am. Chem. Soc.*, 1989, **111**, 4527.

[99] D.J. Cram, M.E. Tanner, and R. Thomas, *Angew. Chem., Int. Ed. Engl.*, 1991, **30**, 1024.

[100] R. Warmuth, *Angew. Chem., Int. Ed. Engl.*, 1997, **36**, 1347.

[101] A. Jasat and J.C. Sherman, *Chem. Rev.*, 1999, **99**, 931.

[102] R.G. Chapman and J.C. Sherman, *J. Am. Chem. Soc.*, 1998, **120**, 9818.

[103] M.M. Conn and J. Rebek, Jr., *Chem. Rev.*, 1997, **97**, 1647.

[104] J. Rebek, Jr., *Chem. Comm.*, 2000, 637.

[105] L.R. MacGillivray and J.L. Atwood, *Nature*, 1997, **389**, 469.

[106] L.R. MacGillivray and J.L. Atwood, *Angew. Chem., Int. Ed. Engl.*, 1999, **38**, 1018.

[107] L.R. MacGillivray and J.L. Atwood in *Crystal Engineering: From molecules and Crystals to Materials*, NATO Science Series, Series C: Mathematical and Physical Sciences, Vol. 538, eds. D. Braga, F. Grepioni and A.G. Orpen, Kluwer Academic Publishers, Dordrecht, 1999, Chapter 23.

[108] J.L. Atwood, L.J. Barbour, S.J. Dalgarno, M.J. Hardie, C.L. Raston and H.R. Webb, *J. Am. Chem. Soc.*, 2004, **126**, 13170.

[109] L.C. Palmer and J. Rebek, Jr., *Org. Biomol. Chem.*, 2004, **2**, 3051.

[110] O. Mogck, M. Pons, V. Böhmer and W. Vogt, *J. Am. Chem. Soc.*, 1997, **119**, 5706.

[111] A. Shivanyuk, T.P. Spaniol, K. Rissanen, E. Kolehmainen and V. Böhmer, *Angew. Chem., Int. Ed. Engl.*, 2000, **39**, 3497.

[112] D.M. Rudkevich, *Angew. Chem., Int. Ed. Engl.*, 2004, **43**, 558.

[113] M. Kondo, T. Yoshitomi, K. Seki, H. Matsuzaka and S. Kitagawa, *Angew. Chem., Int. Ed. Engl.*, 1997, **36**, 1725.

[114] H. Li, M. Eddaoudi, M. O'Keeffe and O.M. Yaghi, *Nature*, 1999, **402**, 276.

[115] S.S.-Y. Chui, S.M.-F. Low, J.P.H. Charmant, A.G. Orpen and I.D. Williams, *Science*, 1999, **283**, 1148.

[116] K. Seki, *Chem. Comm.*, 2001, 1496.

[117] S. Noro, R. Kitaura, M. Kondo, S. Kitagawa, T. Ishii, H. Matsuzaka and M. Yamashita, *J. Am. Chem. Soc*, 2002, **124**, 2568.

[118] K. Barthelet, J. Marrot, D. Riou and G. Férey, *Angew. Chem., Int. Ed. Engl.*, 2002, **41**, 281.

[119] R. Kitaura, S. Kitagawa, Y. Kubota, T.C. Kobayashi, K. Kindo, Y. Mita, A. Matsuo, M. Kobayashi, H.-C. Chang, T.C. Ozawa, M. Suzuki, M.Sakata and M. Takata, *Science*, 2002, **298**, 2358.

[120] D.J. Cram, M.E. Tanner and C.B. Knobler, *J. Am. Chem. Soc.*, 1991, **113**, 7717.

[121] N.L. Rosi, J. Eckert, M. Eddaoudi, D.T. Vodak, J. Kim, M. O'Keeffe and O.M. Yaghi, *Science*, 2003, **300**, 1127.

[122] P.M. Forster, J. Eckert, J.-S. Chang, S.-E. Park, G. Férey and A.K. Cheetham, *J. Am. Chem. Soc.*, 2003, **125**, 1309.

[123] J.L. Atwood, L.J. Barbour and A. Jerga, *Angew. Chem. Int. Ed. Engl.*, 2004, **43**, 2948.

[124] R.J. Davey and J. Garside, *From molecules to crystallizers - an introduction to crystallization*, Oxford University Press, Oxford, 2000.

[125] L. Williams-Seton, R.J. Davey and H.F. Lieberman, *J. Am. Chem. Soc.*, 1999, **121**, 4563.

[126] R.J. Davey, L. Williams-Seton, H.F. Lieberman and N. Blagden, *Nature*, 1999, **402**, 797.

[127] N. Blagden, R.J. Davey, H.F. Lieberman, L. Williams, R. Payne, R. Roberts, R. Rowe and R. Docherty, *J. Chem. Soc., Faraday Trans.*, 1998, **94**, 1035.

[128] R.J. Davey, N. Blagden, S. Righini, H. Alison, M.J. Quayle and S. Fuller, *Cryst. Growth Des.*, 2001, **1**, 59.

[129] K. Allen, R.J. Davey, E. Ferrari, C. Towler and G.J.T. Tiddy, *Cryst. Growth Des.*, 2002, **2**, 523.

[130] R.J. Davey, K. Allen, N. Blagden, W.I. Cross, H.F. Lieberman, M.J. Quayle, S. Righini, L. Seton and G.J.T. Tiddy, *CrystEngComm*, 2002, **4**, 257.

[131] W.C. McCrone in *Polymorphism in Physics and Chemistry of the Organic Solid State*, Vol. II eds. D.Fox, M.M. Labes, A. Weissemberg, Interscience. New York, 1965, p. 276.

[132] J. Dunitz and J. Bernstein, *Acc. Chem. Res.*, 1995, **28**, 193.

[133] J. Bernstein, R.J. Davey and J.-O. Henck, *Angew. Chem., Int. Ed. Engl.*, 1999, **38**, 3441.

[134] D. Braga and F. Grepioni, *Chem. Soc. Rev.*, 2000, **29**, 229.

[135] A. Gavezzotti and G. Filippini, *Chem. Comm.*, 1998, 287.

[136] I. Weissbuch, R. Popovitz-Biro, M. Lahav and L. Leiserowitz, *Acta. Cryst.*, 1995, **B51**, 115.

[137] J. Bernstein, *Polymorphism in Molecular Crystals*, Oxford University Press, Oxford, 2002.

[138] D.B. Amabilino and J.F. Stoddart, *Chem. Rev.*, 1995, **95**, 2725.

[139] E. Wasserman, *J. Am. Chem. Soc*, 1960, **82**, 4433.

[140] I.T. Harrison and S. Harrison, *J. Am. Chem. Soc*, 1967, **89**, 5723.

[141] F.M. Raymo and J.F. Stoddart, *Chem. Rev.*, 1999, **99**, 1643.

[142] J.-C. Chambron, C.O. Dietrich-Buchecker and J.-P. Sauvage, *Top Curr. Chem.*, 1993. **165**, 131.

[143] R. Hernandez, H.-R. Tseng, J.W. Wong, J.F. Stoddart and J.I. Zink, *J. Am. Chem. Soc.*, 2004, **126**, 3370.

[144] D.J. Cram. *Angew. Chem., Int. Ed. Engl.*, 1988, **27**, 1009.

[145] E. Fischer, *Ber. Dtsch. Chem. Ges.*, 1894, **27**, 2985.

[146] D.H. Kim in *Comprehensive Supramolecular Chemistry*, Vol. 4, ed. Y. Murakami, Pergamon, Oxford, 1996.

[147] Y. Murakami, J.-I. Kikuchi, Y. Hisaeda and O. Hayashida, *Chem. Rev.*, 1996, **96**, 721.

[148] R. Breslow and S.D. Dong, *Chem. Rev.*, 1998, **98**, 1997.

[149] Y. Murakami, J.-I. Kikuchi, T. Ohno, O. Hayashida and M. Kojima, *J. Am. Chem. Soc.*, 1990, **112**, 7672.

[150] D.E. Fenton, *Chem. Soc. Rev.*, 1999, **28**, 159.

[151] F. Toda, K. Tanaka, S. Nagamatsu and T.C.W. Mak, *Isr. J. Chem.*, 1985, **25**, 346.

[152] E. Weber, S. Nitsche, A. Wierig and I. Csöregh, *Eur. J. Org. Chem.*, 2002, 856.

[153] P. Timmerman, W. Verboom and D.N. Reinhoudt, *Tetrahedron*, 1996, **52**, 2663.

[154] Y. Aoyama, Y. Tanaka, H. Toi and H. Ogoshi, *J. Am. Chem. Soc.*, 1988. **110**, 634.

[155] Y. Aoyama, Y. Tanaka and S. Sugahara, *J. Am. Chem. Soc.*, 1989, **111**, 5397.

[156] J.L. Atwood, L.J. Barbour, M.J. Hardie, E. Lygris, C.L. Raston and H.R. Webb, *CrystEngComm*, 2001, **10**, 1.

[157] J.L. Atwood and A. Szumna, *Supramol. Chem.*, 2002, 479.

[158] M. Pietraskiewicz, O. Pietraskiewicz, W. Kolodziejski, K. Wozniak, N. Feeder, F. Benevelli and J. Klinowski, *J. Phys Chem. B*, 2000, **104**, 1921

[159] T. Friščić and L.R. MacGillivray, *J. Organometallic Chem.*, 2003, **666**, 43.

[160] B.Q. Ma and P. Coppens. *Chem. Comm.*, 2003, 412.

[161] B.Q. Ma, Y. Zhang and P. Coppens, *CrystEngComm*, 2001, **20**, 1.

[162] L.R. MacGillivray, J.L. Reid and J.A. Ripmeester, *Chem. Comm.*, 2001, 1034.

[163] H. Mansikkamäki, M. Nissinen and K. Rissanen, *Chem. Comm.*, 2002, 1902.

[164] A. Shivanyuk and J. Rebek, Jr., *Chem. Comm.*, 2001, 2424.

[165] G.W.V. Cave, M.J. Hardie, B.A. Roberts and C.L. Raston, *Eur. J. Org. Chem.*, 2001, 3227.

[166] L.R. MacGillivray, P.R. Diamente, J.L. Reid and J.A. Ripmeester, *Chem. Comm.*, 2000, 359.

[167] S. Ma, D.M. Rudkevich and J.Rebek, Jr., *J. Am. Chem. Soc.*, 1998, **120**, 4977.

[168] L.R. MacGillivray, J.L. Reid, J.L. Atwood and J.A. Ripmeester, *Crystal Engineering*, 1999, **2**, 47.

[169] S. Saito, C. Nuckolls and J. Rebek, Jr., *J. Am. Chem. Soc.*, 2000, **122**, 9628.

[170] D.J. Cram, J.M. Cram, *Container Molecules and their Guests, Monographs in Supramolecular Chemistry*, ed. J.F. Stoddart, Royal Society of Chemistry: Cambridge, 1994, Vol. 4.

Chapter 2

EXPERIMENTAL AND COMPUTATIONAL METHODS

HOST COMPOUNDS

Three host compounds were used in this study to prepare the inclusion compounds:

- The host compound, *trans*-9,10-dihydroxy-9,10-bis(p-*tert*-butylphenyl)-9,10-dihydroanthracene (abbreviated **TBDDDA**) was synthesised by the author. The synthesis was carried out using the Grignard method with anthraquinone as starting material as described below.

  All diethyl ether used in the synthesis was dried by refluxing over sodium wire followed by distillation. A solution of 100 mmol 4-*tert*-butylphenylbromide in 30 ml dry diethyl ether was prepared. 5 ml of this solution was added to a heated and stirred mixture of 2.4 g (98.7 mmol) of magnesium and 10ml diethyl ether. Once the reaction had commenced, the remainder of the solution was added dropwise to the reacting mixture, which was then allowed to reflux for two hours. The resulting Grignard reagent was added dropwise to a stirred and heated suspension of 4 g (19.2 mmol) of anthraquinone in 100 ml dry diethyl ether.

  The reaction mixture was allowed to reflux for 15-20 h and was then acidified to a pH of 2 using 2.5 M HCl, while cooling on ice. This resulted in a grey-green precipitate, which was added to 500 ml boiling acetone. The mixture was heated for a further 10 min and was then filtered hot. The filtrate was transferred to a round bottomed flask and a rotary evaporator was used to distil off approximately 400 ml of the acetone.

  The remaining solution was cooled on ice, resulting in precipitation of the product. The product was recrystallised repeatedly from acetone and then finally recrystallised from benzene to yield a white powder. The compound was heated at 120°C under vacuum to remove any included solvent. This compound was characterised by elemental analysis and NMR.

- The host compound 9,9'-(Biphenyl-4,4'-diyl)difluoren-9-ol (abbreviated **WEB24**) was supplied by Professor Edwin Weber from the Institute for Organic Chemistry, Freiberg, Germany,[1] and was used as supplied for the project.

- The host compound $1^4,1^6,5^4,5^6$-tetrahydroxy-2,4,6,8-tetrapentyl-$3^4,3^6,7^4,7^6$-tetra(p-toluenesulfonyl-oxy)-1,3,5,7(1,3)-tetrabenzenacyclooctaphane (abbreviated **TTRSC**) was synthesised by G. Arnott according to a method described in the literature,[2] and was used as supplied.

Differential scanning calorimetry (DSC) and thermal gravimetry (TG) were used to confirm the purity of all host compounds.

GUEST COMPOUNDS

N,N-Dimethylformamide (DMF), N,N-dimethylsulfoxide (DMSO) and 1,4-dioxane were supplied by BDH Laboratory Suppliers (Poole, England). N,N-Dimethylacetamide (DMA), methyl ethyl ketone (MEK), ethylamine and propylamine, as well as the pentanols and picolines were supplied by Aldrich Chemical Company, Inc. (Milwaukee, USA). Acetone and pyridine were supplied by SaarChem (Pty) Ltd (Muldersdrift, South Africa).

The guest compounds were all AR grade and were used as supplied without further purification or preparative work. DMF, DMSO, acetone, N,N-dimethylacetamide, MEK, 1,4-dioxane, pyridine and picolines were stored over dried molecular sieves.

The relevant physical properties of the various guest compounds are given in Table 2.1.

CRYSTAL GROWTH

The crystals were prepared using the method of slow evaporation. The general method followed is described below and further details for the preparation of individual inclusion compounds are given in the appropriate chapters.

Suitable crystals were obtained by stirring a solution of the host in an excess of guest while warming gently. Once dissolution had occurred, the solution was filtered through a 0.5 μm syringe filter and left to evaporate slowly at room temperature.

Table 2.1 Physical properties of guest compounds

Guest	Molecular formula	M_r ($g.mol^{-1}$)	bp (°C)*	mp (°C)*	Density** ($g.cm^{-3}$)
N,N-Dimethylformamide	C_3H_7NO	73.09	153	-61	0.9445
N,N-Dimethylsulfoxide	C_2H_6OS	78.13	189	18.45	1.100
Acetone	C_3H_6O	58.08	56.5	-94	0.788
N,N-Dimethylacetamide	C_4H_9NO	87.12	163-165	-20	0.9366
1,4-Dioxane	$C_4H_8O_2$	88.10	101.1	11.80	1.0329
Methyl Ethyl Ketone	C_4H_8O	72.10	79.6	-86	0.805
Ethylamine	C_2H_7N	45.08	16.6	-81	0.683
Propylamine	C_3H_9N	59.11	48-49	-83	0.717
1-Pentanol	$C_5H_{12}O$	88.15	137.5	-79	0.811
2-Pentanol	$C_5H_{12}O$	88.15	119.3	—	0.812
3-Pentanol	$C_5H_{12}O$	88.15	115.6	—	0.815
2-Methyl-1-butanol	$C_5H_{12}O$	88.15	128	—	0.815
3-Methyl-1-butanol	$C_5H_{12}O$	88.15	130	-117.2	0.809
2-Methyl-2-butanol	$C_5H_{12}O$	88.15	102.5	-9.0	0.806
3-Methyl-2-butanol	$C_5H_{12}O$	88.15	113-114	—	0.818
Pyridine	C_5H_5N	79.10	115.2-115.3	-41.6	0.982
2-Picoline	C_6H_7N	93.12	128-129	-70	0.944
3-Picoline	C_6H_7N	93.12	143-144	-18	0.967
4-Picoline	C_6H_7N	93.12	145	3.6	0.955

** mp and bp measured at 760mmHg, ** densities measured at 25°C*

THERMAL ANALYSIS

Thermogravimetry (TG) for all inclusion compounds with the host **TBDDDA** and differential scanning calorimetry (DSC) for all inclusion compounds in the thesis were performed on a Perkin Elmer PC7 series thermal analysis system under N_2 gas purge (flow rate of 40 ml/min). TG analyses for inclusion compounds of **WEB24** and **TTRSC** were performed on a Mettler Toledo TGA/SDTA 851e under N_2 gas purge (flow rate 30 mL/min). The Perkin Elmer TG instrument was calibrated against the Curie points of alumel (163°C) and nickel (354°C) and the balance was calibrated using a standard mass. The Mettler TG instrument was calibrated using indium (mp = 156.6°C) and aluminium (mp = 660.3°C) in an automated process in which temperature calibration, tau lag calibration and sensor calibration are performed simultaneously. The DSC instrument was calibrated using the standard materials indium (mp = 156.6°C, $\Delta H = 28.6\ J.g^{-1}$) and zinc (mp = 419.5°C).

Thermogravimetry measures the mass of a sample as a function of temperature while the sample is subjected to a controlled temperature program. In the case of inclusion compounds with volatile guests, the mass losses observed are due to guest release and therefore allow the host:guest ratios of the complexes to be determined. The percentage mass loss has a precision of approximately 1%, yielding accurate host:guest ratios.

This technique is employed extensively in the study of inclusion compounds and in this study was used for both determining the stoichiometries of the complexes as well as for measuring kinetics of desorption by isothermal TG analysis, which measures the mass loss of a sample with time at a fixed temperature. The stoichiometries obtained for the inclusion compounds were used to assign site occupancy factors when refining the crystal structures.

DSC analyses measure the difference in enthalpy between the sample and a reference, in a controlled atmosphere, as a function of temperature, while the sample and reference are subjected to a controlled temperature program. These differences in enthalpy are associated with thermal events such as guest release, phase transformation, polymorphic changes, recrystallisation and melting. DSC experiments can therefore be used to establish the onset temperatures and enthalpy changes associated with these thermal events.

For all analyses the samples were gently crushed and blotted dry in order to remove surface solvent and in each case sample sizes were in the range 2-5 mg. The samples were placed in open pans for TG analysis and for DSC experiments the samples were placed in crimped but vented aluminium pans. The experiments typically started at 30°C, with the final temperature being dependent on the melting point of the host compound.

HOT STAGE MICROSCOPY

Hot stage microscopy (HSM) is a technique used to observe the physical appearance of samples during the thermal events that occur during heating. HSM was used in this study to observe the thermal decomposition of the inclusion complexes. This technique allows the thermal events measured using TG and DSC to be correlated with the physical changes occurring in the crystal upon heating, such as guest release, recrystallisation, polymorphic transition and melting. Desorption of the guest can be detected by the evolution of gas bubbles if the crystals are immersed in an inert medium (e.g. silicone oil). The crystals also change from clear to opaque during guest loss due to a change in crystal structure.

During HSM analysis the crystals were observed under a Nikon SMZ-10 microscope fitted with a Linkam THMS 600 hot stage connected to a Linkam TP92 temperature controlling unit. The crystals were submerged in a drop of silicone oil (an inert medium) between two glass coverslips and then placed on the hot stage and subjected to heating at a constant rate of 10°C.min^{-1}. Images of the thermal events were monitored using a Sony Digital Hyper HAD colour video camera which was mounted on the microscope and these images were analysed using the Soft Imaging System program, analySIS.[3]

Differences were often observed between the onset temperatures of thermal events measured using TG and DSC and those observed using HSM. This is mainly due to physical differences of the various instruments as well as differences in particle size of the samples analysed. TG and DSC analyses were typically conducted on powdered samples, whereas single crystals were usually analysed in the case of HSM.

COMPETITION EXPERIMENTS

Competition experiments were set up to determine the selectivity of a particular host for various guests and the analyses were carried out using gas chromatography or TG analysis following the general methodology described below.

A series of mixtures of two guests was prepared such that the mole fraction of a given guest varied from 0 to 1 in steps of 0.1. A fixed amount of host compound was then added to these mixtures and dissolved by heating and stirring the solutions. In each case the guest volumes were such that the ratio of host to total guest was at least 1:20, to ensure that there was enough of the guest of lower mole fraction should the host have 100% preference for it. The solutions were then filtered through a 0.5 μm syringe filter and left to evaporate slowly at room temperature, resulting in the formation of crystals.

For the competition experiments carried out with the pentanol isomers, the resulting crystals were filtered, dried and placed in air tight glass vials with silicone seals incorporated into the screw-on lids. The vials were heated to induce desorption of the guests in the form of vapour. These vapours then condensed on the sides of the vials as the vials cooled and the resulting drops were extracted, dissolved in acetone and analysed by gas chromatography.

For the competition experiments carried out with the picoline isomers, the crystals were filtered and dried and then dissolved directly in acetone and analysed using gas chromatography. In the case of the DMF versus DMSO competition experiments, the crystals were filtered and dried and the relative percentages of each guest included in the crystals were determined using thermal gravimetry.

In each case the mother liquor was also analysed by gas chromatography.

GAS CHROMATOGRAPHY

Gas Chromatography (GC) was used to analyse the relative percentages of the various guests included in the crystals as well as the relative percentages of the guests in the starting solutions. Two gas chromatograph instruments were used in this study, which are described as follows:

For the analysis of the pentanol isomers a Varian 3400 gas chromatograph equipped with a polar, carbowax column (25 m length, 0.25 mm diameter) was used. The gas chromatograph was connected to a computer and the chromatographs were recorded and analysed using the program DELTA.[4] The operating conditions were as follows: Injector volume: 1 µL; Injector temperature: 220°C; Detector temperature: 250°C; Column temperature: 70°C; Carrier gas: Helium.

For the competition experiments with TTRSC and the picoline guests, the analyses were carried out using a Varian 3900 gas chromatograph connected to a computer and equipped with a 1177 split/splitless injector, an FID detector and a Varian fused silica column (30 m Length, 0.32 mm diameter). The chromatographs obtained were recorded and analysed using the Galaxie GC WS software.[5] The operating conditions were as follows: Injector volume: 1 µL; Injector temperature: 200°C; Detector temperature: 300°C; Column temperature: 70°C; Carrier gas: Helium.

For each set of experiments, the GC apparatus was calibrated by analysing a series of mixtures of known mole fraction of the two guests being used in that particular experiment.

^{13}C SOLID STATE CP/MAS NMR

^{13}C solid state CP/MAS NMR was used to analyse some of the inclusion compounds synthesised in this project. The spectra were obtained at room temperature on a Tecmag 200 MHz spectrometer equipped with a Doty Scientific 7 mm CP/MAS rotor using a standard CP pulse program with fixed amplitude ^{1}H decoupling during signal acquisition. Experiments were also carried out using ^{13}C solid state CP/MAS NMR to monitor the desorption of the inclusion compounds. These experiments were performed using the same spectrometer and the method is described in the appropriate chapter.

KINETICS OF ENCLATHRATION

The kinetics of enclathration of a guest in the vapour phase by a host compound was studied using an automated magnetic suspension balance constructed for this purpose, which allows the mass change of an inclusion compound with time to be monitored under controlled conditions of pressure and temperature.[6] The kinetic measurements were carried out by exposing finely powdered host compound to guest vapour at fixed temperatures, but at various pressures of guest vapour, and recording the mass increase with time.

The system, which is illustrated in Figure 2.1, consists of a jacketed reaction vessel connected to a vacuum pump, which is clamped in place below an electromagnet which is in turn suspended from an electronic balance. This electronic balance is connected to a computer. Inside the reaction vessel, the sample pan is suspended, at the end of a thin brass rod, from a permanent magnet which is press-fitted into a PTFE (teflon) screen. The reaction vessel can be rotated horizontally away from the electromagnet in order to load the sample.

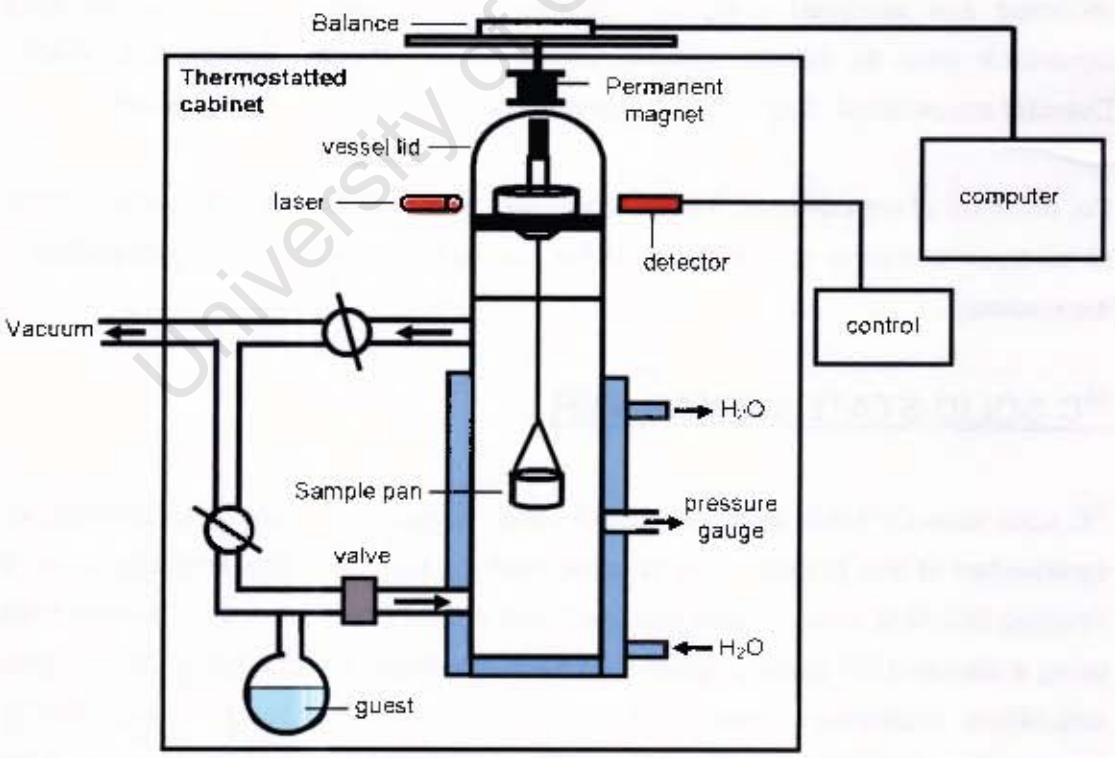

Figure 2.1 Diagram showing main features of automated magnetic suspension balance.

The pre-weighed powdered sample is placed on the sample pan which is lowered into the reaction vessel until the screen rests on a supporting plate. The vessel head is placed over the permanent magnet, thereby sealing the reaction vessel. The vessel is then swung into position and clamped so that the vessel head lies between a light source and a photodetector, which are both located on the optical platform.

The reaction vessel can be evacuated and pressure monitored by means of a manometer. The temperature is controlled by a waterbath connected to the jacketed reaction vessel and is monitored using a thermocouple. An automated system allows enough guest in the vapour phase to be introduced into the reaction vessel to achieve a desired vapour pressure. The mass increase of the sample is then recorded with time and an isothermal curve at that vapour pressure is obtained.

The resultant isotherms were converted to extent of reaction (α) versus time curves, with α defined as

$$\alpha = (m_i - m_t) / (m_i - m_f)$$

where m_i is the initial mass of the compound, m_f is the final mass of the compound and m_t is the mass of the compound at any time, t.

These curves were then fitted to various kinetic equations, of the form $f(\alpha) = kt$ using the program KINETIC[7] in order to determine the appropriate model. The kinetic equation for which the function $f(\alpha)$ was linear over the largest range of α was chosen as the best fit model.

KINETICS OF DESORPTION

The kinetics of desorption of the acetone inclusion compound with **TBDDDA** was studied using the same automated magnetic suspension balance described above. Once uptake of the guest from the vapour was complete, the system was heated to a certain temperature and then subjected to a vacuum. Mass loss with time was then recorded.

The kinetics of desorption of the inclusion compounds of **WEB24** was studied using isothermal TG analysis. These experiments were performed using the Mettler Toledo TGA/SDTA 851e instrument described previously. For each experiment

samples were crushed and blotted dry. A series of TG experiments were carried out at selected temperatures for each inclusion compound. The instrument was set to the desired temperature and once this temperature was reached, the sample was inserted and the experiment started during which the mass loss was recorded with time until guest desorption was complete. The resulting curves were analysed as described above for the kinetic curves of the enclathration process.

NUCLEATION AND CRYSTAL GROWTH

Solubility curves were determined by adding small quantities of the inclusion compound to 10 ml of the appropriate solvent in a jacketed vessel, attached to a water bath in order to control the temperature. The mass of the inclusion compound which could be dissolved at a certain temperature was noted, and this was carried out over a range of temperatures. The solubility (g/ml) was plotted against temperature to give the solubility curve.

The in-situ crystallisations were carried out using a top-hat cell, placed on the microscope stage, which is depicted in Figure 2.2. A saturated solution of the inclusion compound in the appropriate solvent was transferred to the pre-heated cell, which is surrounded by a water jacket and connected to a water bath, allowing the temperature to be controlled. The cell was then cooled to a certain temperature and the cooling crystallisation observed. Optical microscopy carried out during the investigation of nucleation and crystal growth was performed using a Zeiss Axioplan 2 polarising microscope and images were taken using a JVC TK-S300 video camera fitted to a Nikon SMZ-10 binocular.

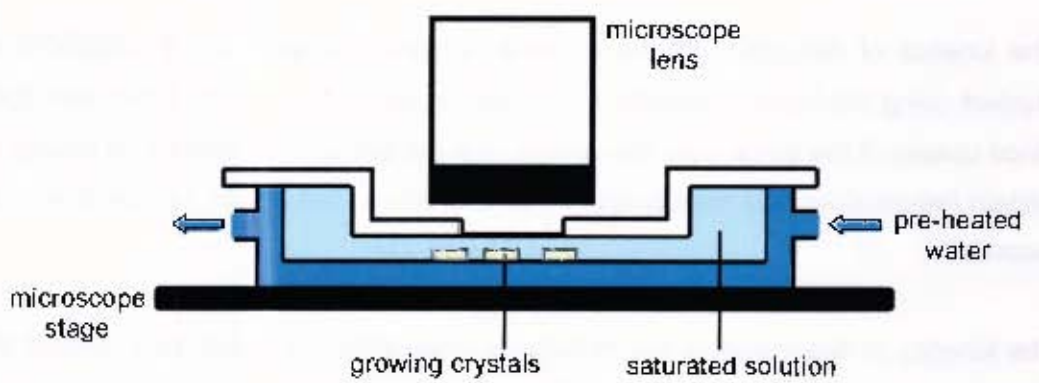

Figure 2.2 Schematic diagram of top-hat cell.

CRYSTAL STRUCTURE ANALYSIS

In all cases, a crystal of suitable size, which extinguished plane polarised light uniformly, was selected. The size of the crystals was typically between 0.1 mm and 0.5 mm in all directions and for all data collections the crystals were coated in Paratone N oil (Exxon Chemical Co., Texas, USA) before being mounted for data collection.

Preliminary cell dimensions were established from the X-ray intensity data collected on a Nonius Kappa CCD diffractometer using graphite-monochromated Mo $K\alpha$ radiation (λ = 0.71069 Å) produced at 54 kV and 23 mA using an Enraf Nonius FR590 generator. Data collections performed at low temperatures were carried out by cooling the crystals using a constant stream of nitrogen gas produced by a Cryostream cooler (Oxford Cryosystems) at a flow rate of 20 cm^3min^{-1}. Intensity data were captured at low temperature whenever possible. When problems were experienced due to severe deterioration and cracking of crystals upon cooling, the intensity data were collected at room temperature (**WEB24, WEB24•2DMA, WEB24•2ETHYL, TTRSC•2(1PENT)** and **TTRSC•6.5(4PIC)•2(H_2O)**).

The strategies for the data collections were evaluated using the COLLECT[8] software. For all structures, data were collected by the standard phi and omega scan techniques, and were scaled and reduced using DENZO-SMN[9] software. Accurate unit cell parameters were refined on all data.

All structures were solved by direct methods using SHELX-86.[10] Equivalent reflections were merged and those with $I<2\sigma(I)$ suppressed. The mean $|E^2-1|$ values were examined to confirm the space group symmetry (E is the normalised structure factor). If the $|E^2-1|$ value is close to 0.968, then the structure is centrosymmetric, whereas if the $|E^2-1|$ value is close to 0.736 then the structure is acentric.

Subsequent refinement of the structures was carried out using the program SHELX-97,[11] which employs full-matrix least-squares minimisation of the function $(\sum w(F_o^2-kF_c^2)^2)$. The agreement between the observed (F_o) and calculated (F_c) structure factors is expressed by the residual index, R, which is used to monitor the accuracy of the model and should be low if the model is satisfactory. The residual index R_1

gives the agreement between measured and calculated structure factor amplitudes for the refinement against F (equation 1), whereas the residual index R_2 expresses the agreement between intensities for the refinement against F^2 (equation 2).

$$R_1 = \frac{\Sigma \left| |F_o| - |F_c| \right|}{\Sigma |F_o|} \quad .....(1) \qquad wR_2 = \left(\frac{\Sigma w (F_o^2 - F_c^2)^2}{\Sigma w (F_o^2)^2} \right)^{1/2} \quad .....(2)$$

where w is the weighting scheme which was refined for each structure and is given by equation 3 below. Both a and b were refined for each structure and P is given by equation 4:

$$w = \frac{1}{\sigma^2 F_o^2 + (aP)^2 + bP} \quad .....(3) \qquad P = \frac{\max(0, F_o^2) + 2 F_c^2}{3} \quad .....(4)$$

The Goodness of Fit (S) is given by equation 5 and is based on F^2:

$$S = \left(\frac{\Sigma w (F_o^2 - F_c^2)^2}{n - p} \right)^{1/2} \quad .....(5)$$

where n is the number of reflections and p is the total number of parameters refined.

For all crystal structures elucidated in this study, where parts of a structure were disordered, the hydrogen atoms bonded to disordered carbon or oxygen atoms were generally not added to the final model.

COMPUTER PACKAGES

A number of computer programs were used for the analysis of the crystal structures and these are listed below:

- **Xprep**[12] was used to determine the space group and set up SHELX input files.

- The programs **SHELXS-86**[10] and **SHELXL-97**[11] were used for structure solution and refinement.

- All the structure diagrams were produced using the program **POV-RAY**[13].

- The program **LAYER**[14] was used to examine systematic absences from the X-ray intensity data and space group symmetry. This program displays the intensity data as simulated precession photographs of all levels of the reciprocal lattice.

- **SECTION**[15] was used to investigate the geometry of the voids which are formed by the packing of the host molecules in the inclusion compounds and which contain the guest molecules. This program allows a cross-section through the unit cell at any distance down a particular axis to be viewed (and was used to generate plots of these cross-sections which are presented in this thesis). If a series of these sections are viewed with the guest molecules removed and the host molecules represented with van der Waals radii, then the cavities or channels formed by the packing of the host molecules can be examined.

- **X-SEED**[16] was used as a graphical interface for SHELX-86, SHELX-97, POV-RAY and SECTION.

- **PLATON** [17] was used to calculate structural parameters and analyse host conformations.

- The **Cambridge Structural Database (CSD)** [18] was used to search for and analyse published crystal data for comparison with the crystal structures elucidated in this study.

REFERENCES

[1] E. Weber, S. Nitsche, A. Wierig and I. Csöregh, *Eur. J. Org. Chem.*, 2002, 856.

[2] O.V. Lukin, V.V. Pirozhenko and A.N. Shivanyuk, *Tetrahedron Lett.*, 1995, **36**, 7725.

[3] Soft Imaging System GmbH: Digital Solutions for Imaging and Microscopy, Version 3.1 for Windows, © 1987-2000.

[4] Delta chromatography data system for Windows, Version 5.0, © 1995-1998

[5] Galaxie Chromatography Workstation, Version 1.7.403.22, Varian, Inc. 2002.

[6] L.J. Barbour, K. Achleitner and J.R. Greene, *Thermochim. Acta*, 1992, **205**, 171.

[7] L.J. Barbour, KINETIC program, PhD Thesis, University of Cape Town, 1994.

[8] COLLECT, Data Collection Software, Nonius, Delft, The Netherlands, 1999.

[9] Z. Otwinowski and W. Minor, *Methods in Enzymology, part A: Macromolecular Crystallography*, eds. C.W. Carter Jr. and R.M. Sweet, Academic Press, 1997, Vol 276, p.307.

[10] G.M. Sheldrick, in *Crystallographic Computing*, eds. G.M. Sheldrick, C. Kruger and R. Goddard, Oxford University Press, Oxford, 1985, vol 3, p.175.

[11] G.M. Sheldrick, SHELX-97, Program for Crystal Structure Determination, University of Göttingen, Germany, 1997.

[12] XPrep, Data Preparation & Reciprocal Space Group Exploration, Version 5.1/NT, ©1997, Bruker Analytical X-ray Systems.

[13] Pov-Ray for Windows, Version 3.1e.watcom.win32, The persistence of Vision Development Team, ©1991-1999.

[14] L.J. Barbour, LAYER, A computer program for the graphic display of intensity data as simulated precession photographs, *J. Appl. Cryst.*, 1999, **32**, 351.

[15] L.J. Barbour, SECTION, A computer program for the graphic display of cross sections through a unit cell, *J. Appl. Cryst.*, 1999, **32**, 353.

[16] L.J. Barbour, *J. Supramol. Chem.*, 2001, **1**, 189; J.L. Atwood and L.J. Barbour, *Cryst. Growth Des.*, 2003, **3**, 3.

[17] A.L. Spek, PLATON, A multipurpose crystallographic tool, Version 10500, © 1980-2000.

[18] Cambridge Structural Database and Cambridge Structural Database System, Version 5.23 (April 2002), Cambridge Crystallographic Data Centre, University Chemical Laboratory, Cambridge, England.

Chapter 3

TUNABLE CLATHRATES OF THE HOST TBDDDA

*The host trans-9,10-dihydroxy-9,10-bis(p-tert-butylphenyl)-9,10-dihydroanthracene (abbreviated **TBDDDA**) forms inclusion compounds with N,N-dimethylformamide (DMF), dimethyl sulphoxide (DMSO) and acetone. In order to establish whether this host would preferentially include either DMF or DMSO, competition experiments were performed with mixtures of these guests, which yielded compounds of the type $H.nG_1.(4-n)G_2$, with n varying integrally from zero to four. Thermal analysis of these compounds has been carried out and the structures have been elucidated. The structure of the α, non-porous phase of the apohost as well as the inclusion compound with acetone and two ternary inclusion compounds (containing both acetone and either DMF or DMSO) have been elucidated and the thermal analysis of these compounds has been carried out. The kinetics of enclathration of the host with acetone vapour and the kinetics of desorption of the acetone inclusion compound have also been studied.*

For each of the structures described in this chapter the crystallographic data, experimental and refinement parameters are given in Table 3.1. Final atomic coordinates, bond lengths and angles, torsion angles, thermal parameters and tables of observed and calculated structure factors for each of the crystal structures are given in the appendices.

COMPLEX PREPARATION

Suitable crystals of the inclusion compounds were formed by slow evaporation at room temperature using the method described in Chapter 2. Suitable crystals of **TBDDDA** were obtained by crystallising the host from di-iodomethane. The ternary inclusion compounds containing DMF and DMSO as guests were set up by dissolving the host in a mixture of the two guests with various mole fractions of each guest, as described in the section of this chapter on competition experiments (page 62). The ternary inclusion compounds containing both acetone and either DMF or DMSO were prepared by dissolving the host compound in an equimolar mixture of either acetone and DMF or acetone and DMSO.

The inclusion compounds obtained as well as their abbreviations are as follows:
TBDDDA + DMF (H:G = 1:4): **TBDDDA•4DMF**
TBDDDA + DMSO (H:G = 1:4): **TBDDDA•4DMSO**
TBDDDA + acetone (H:G = 1:4): **TBDDDA•4ACE**

The abbreviations of the ternary inclusion compounds obtained are as follows:
TBDDDA•3DMF•1DMSO ($H:G_1:G_2$ = 1:3:1), **TBDDDA•2DMF•2DMSO** ($H:G_1:G_2$ = 1:2:2), **TBDDDA•1DMF•3DMSO** ($H:G_1:G_2$ = 1:1:3), **TBDDDA•2DMF•2ACE** ($H:G_1:G_2$ = 1:2:2), **TBDDDA•2DMSO•2ACE** ($H:G_1:G_2$ = 1:2:2).

The guest numbering schemes are given at the beginning of each structure analysis and the host numbering scheme is given below:

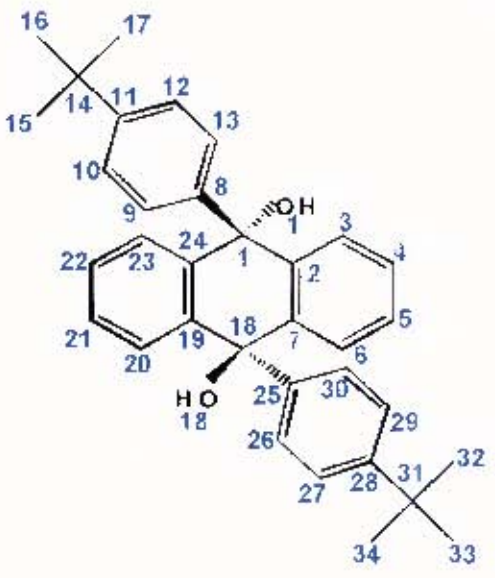

Table 3.1 Crystal data, experimental and refinement parameters

	TBDDDA	**TBDDDA•4DMF**	**TBDDDA•3DMF •1DMSO**
Molecular formula	$C_{34}H_{36}O_2$	$C_{34}H_{36}O_2$·4(C_3H_7NO)	$C_{34}H_{36}O_2$.3(C_3H_7NO).1(C_2H_6OS)
Host:guest ratio	–	1:4	1:3:1
M_r/g.mol^{-1}	476.63	769.01	774.04
Crystal symmetry	Monoclinic	Triclinic	Triclinic
Space group	P2$_1$/c	P$\bar{1}$	P$\bar{1}$
a/Å	16.6711(3)	9.0806(3)	9.0858(2)
b/Å	10.6712(2)	8.9414(4)	9.0547(2)
c/Å	24.3875(5)	14.935(1)	14.7684(4)
α/°	90	74.477(2)	107.144(1)
β/°	101.435(1)	88.693(2)	91.527(1)
γ/°	90	110.189(3)	70.236(2)
Z	6	1	1
V/Å^3	4252.4(1)	1087.67(9)	1089.00(4)
μ (Mo-Kα)/mm^{-1}	0.068	0.077	0.123
Temp of data collection (K)	173(2)	173(2)	173(2)
Range scanned, θ (°)	2.30 - 27.17	2.41 - 27.49	2.39 - 29.62
Index range	h:0-21, k:0-13, l:-31-30	h:±11, k:-10-11, l: ±19	h:±12, k:-12-11, l:+20
No. reflections collected	8950	6935	11040
No. unique reflections	8950	4771 (R_{int} = 0.0167)	5998 (R_{int} = 0.0234)
No. reflections with I>2σ(I)	6522	3093	4369
Data/restraints/parameters	8950 / 15 / 498	4771 / 1 / 262	5998 / 1 / 289
Goodness of fit, S	1.039	1.021	1.578
Final R indices (I>2σ(I))	R$_1$ = 0.0754, wR$_2$ = 0.1950	R$_1$ = 0.0585, wR$_2$ = 0.1490	R$_1$ = 0.1140, wR$_2$ = 0.3691
R indices (all data)	R$_1$ = 0.1050, wR$_2$ = 0.2203	R$_1$ = 0.0992, wR$_2$ = 0.1800	R$_1$ = 0.1402, wR$_2$ = 0.3963
Largest diff peak and hole (e.Å^{-3})	0.809; -0.559	0.268; -0.245	0.923; -0.869

Table 3.1 (cont.) Crystal data, experimental and refinement parameters

	TBDDDA•2DMF •2DMSO	**TBDDDA•1DMF •3DMSO**	**TBDDDA•4DMSO**
Molecular formula	$C_{34}H_{36}O_2.2(C_3H_7NO).2(C_2H_6OS)$	$C_{34}H_{36}O_2.1(C_3H_7NO).3(C_2H_6OS)$	$C_{34}H_{36}O_2.4(C_2H_6OS)$
Host:guest ratio	1:2:2	1:1:3	1:4
M./g.mol	779.08	784.11	789.14
Crystal symmetry	Triclinic	Triclinic	Triclinic
Space group	$P\bar{1}$	$P\bar{1}$	$P\bar{1}$
a/Å	9.1425(3)	9.0460(2)	9.0359(3)
b/Å	9.1730(3)	9.1291(2)	9.1353(3)
c/Å	14.273(1)	14.409(1)	14.4126(6)
α/°	71.356(1)	72.559(1)	72.981(1)
β/°	81.229(1)	80.132(1)	80.086(1)
γ/°	69.938(1)	71.486(2)	71.631(2)
Z	1	1	1
V/Å^3	1064.13(9)	1072.64(8)	1075.44(7)
μ (Mo-Kα)/mm^{-1}	0.173	0.218	0.264
Temp of data collection (K)	173(2)	173(2)	173(2)
Range scanned, θ (°)	2.37 - 27.48	2.38 - 25.02	2.84 - 27.48
Index range	h:-8-11, k:-11-10, l:-18-15	h: ±10, k: ±10, l:-17-14	h:±11, k: ±11, l:-15-18
No. reflections collected	5766	5797	6220
No. unique reflections	4623 (R_{int} = 0.0145)	3693 (R_{int} = 0.0164)	4370 (R_{int} = 0.0184)
No. reflections with I>2σ(I)	3419	3059	3683
Data/restraints/parameters	4623 / 3 / 254	3693 / 24 / 257	4370 / 7 / 250
Goodness of fit, S	1.019	0.967	1.054
Final R indices (I>2σ(I))	R_1 = 0.0637, wR_2 = 0.1611	R_1 = 0.0774, wR_2 = 0.1989	R_1 = 0.0889, wR_2 = 0.2377
R indices (all data)	R_1 = 0.0906, wR_2 = 0.1787	R_1 = 0.0914, wR_2 = 0.2131	R_1 = 0.1003, wR_2 = 0.2497
Largest diff peak and hole (e.Å^{-3})	0.807; -0.542	0.983; -0.982	0.748; -0.682

Table 3.1 (cont.) Crystal data, experimental and refinement parameters

	TBDDDA•4ACE	**TBDDDA•2DMF •2ACE**	**TBDDDA•2DMSO •2ACE**
Molecular formula	$C_{34}H_{38}O_2.4(C_3H_6O)$	$C_{34}H_{38}O_2.2(C_2H_7O).$ $2(C_3H_6O)$	$C_{34}H_{38}O_2.2(C_2H_6OS).$ $2(C_3H_6O)$
Host:guest ratio	1:4	1:2:2	1:2:2
M_r/g.mol	708.94	738.98	749.04
Crystal symmetry	Monoclinic	Triclinic	Triclinic
Space group	$P2_1/c$	$P\bar{1}$	P1
a/Å	8.9057(2)	8.9932(1)	8.942(2)
b/Å	26.9049(6)	9.1674(1)	9.179(2)
c/Å	9.1615(2)	14.3817(2)	14.345(3)
α/°	90	108.326(1)	72.25(3)
β/°	108.590(1)	92.808(1)	79.80(3)
γ/°	90	70.886(1)	71.09(3)
Z	2	1	1
V/Å^3	2080.62(8)	1061.57(2)	1056.9(4)
μ (Mo-Kα)/mm^{-1}	0.073	0.076	0.171
Temp of data collection (K)	173(2)	173(2)	173(2)
Range scanned, θ(°)	2.46 - 25.70	1.49 - 27.50	2.89 - 28.29
Index range	h:+10, k:-30-32, l:-11-10	h:-11-9, k: ±11, l: ±18	h: ±11, k:-12-11, l: ±19
No. reflections collected	11359	7598	7063
No. unique reflections	3911 (R_{int} = 0.0451)	4651 (R_{int} = 0.0160)	4985 (R_{int} = 0.0166)
No. reflections with I>2σ(I)	2328	3708	4006
Data/restraints/parameters	3911 / 1 / 270	4651 / 1 / 269	4985 / 1 / 240
Goodness of fit, S	1.050	1.055	1.051
Final R indices (I>2σ(I))	R_1 = 0.0600, wR_2 = 0.1673	R_1 = 0.0833, wR_2 = 0.2479	R_1 = 0.0785, wR_2 = 0.2173
R indices (all data)	R_1 = 0.1135, wR_2 = 0.1981	R_1 = 0.1003, wR_2 = 0.2650	R_1 = 0.0929, wR_2 = 0.2311
Largest diff peak and hole (e.Å^{-3})	0.378; -0.221	0.678; -0.364	0.916; -0.558

COMPETITION EXPERIMENTS

The selectivity of **TBDDDA** for DMF versus DMSO was established by carrying out competition experiments. **TBDDDA** was dissolved in mixtures of the two guests with mole fractions of DMSO ranging from 0 to 1. The resulting crystals from each solution were filtered off and analysed using thermal gravimetry. From the percentage mass losses obtained, the mole fractions of the two guests included in the crystals could be determined unambiguously.

The results of the competition experiments are illustrated in Figure 3.1. The graph shows the mole fraction of DMSO, X_{DMSO}, in the initial solution versus the mole fraction of DMSO, Z_{DMSO}, included in the crystal. The red diagonal line represents zero selectivity and the experimental data are shown in blue. From the graph it can be seen that the stoichiometry of the inclusion compounds varies in discrete steps, giving rise to five distinct compounds: **TBDDDA•4DMF**, **TBDDDA•3DMF•1DMSO**, **TBDDDA•2DMF•2DMSO**, **TBDDDA•1DMF•3DMSO** and **TBDDDA•4DMSO**. The stoichiometry can therefore be controlled by changing the composition of the liquid guest mixture. The compound **TBDDDA•1DMF•3DMSO** was difficult to isolate as when the liquid guest mixture is in the mole fraction range $X_{DMSO} = 0.5$ to $X_{DMSO} = 1.0$, the host shows a strong propensity for the formation of **TBDDDA•2DMF•2DMSO**. **TBDDDA•1DMF•3DMSO** was therefore prepared by using an initial guest mixture with $X_{DMSO} = 0.99$.

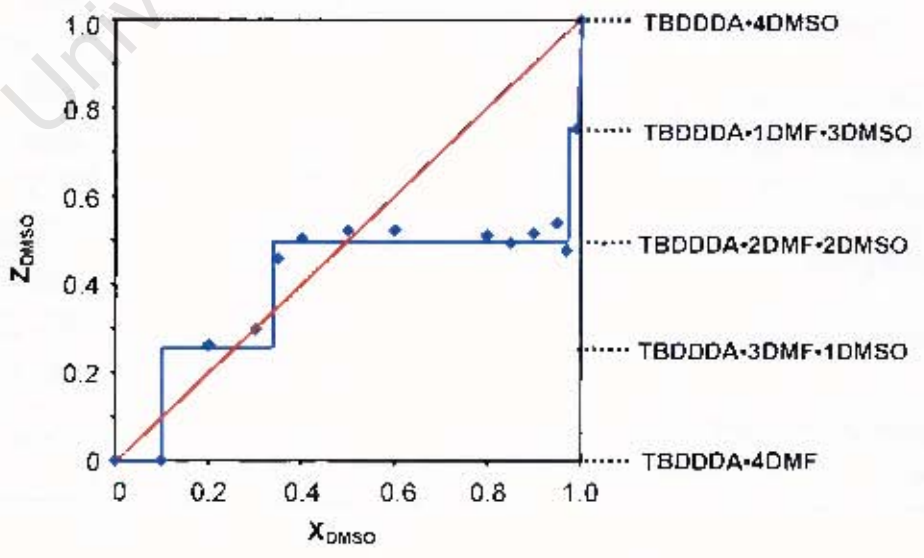

Figure 3.1 Results of the DMF versus DMSO competition experiments.

THERMAL ANALYSIS

Thermal analysis, including TG and DSC, was carried out for each of the inclusion compounds and the TG traces were used to calculate the host:guest ratios. The results of the TG and DSC analyses are summarised in Table 3.2 and Table 3.3.

The TG and DSC traces of **TBDDDA** are shown in Figure 3.2(a). The TG trace shows no mass loss and the DSC shows one endotherm at T_{on} = 266.7°C which corresponds to the melt of the host. The TG and DSC traces of **TBDDDA•4DMF** are shown in Figure 3.2(b). The TG trace shows a two step desorption, corresponding to endotherms A and B in the DSC trace. The total percentage mass loss of 37.7% shown by the TG trace corresponds to H:G = 1:4 (calc. 38.0%). Endotherm C in the DSC trace is due to the melt of the guest-free host compound. The DSC trace also shows an exotherm after guest release suggesting a phase transformation of the guest-free host compound before melting.

Figure 3.2(c) shows the TG and DSC traces for **TBDDDA•3DMF•1DMSO**. The TG trace shows that the guest is released in two steps with a total percentage mass loss of 38.6%, which corresponds to H:DMF:DMSO = 1:3:1 (calc. 38.4%). The DSC trace shows two endotherms, with endotherm A corresponding to guest release and endotherm C due to the melt of the guest-free host compound. Between these two endotherms the DSC trace displays an exotherm, once again indicating a phase transformation of the guest-free host compound before melting.

For **TBDDDA•2DMF•2DMSO**, Figure 3.2(d), guest release again occurs in two steps with a total percentage mass loss of 39.3%, which corresponds to H:DMF:DMSO = 1:2:2 (calc. 38.9%). The DSC trace shows three endotherms, A, B and C. Endotherm A and B correspond to guest release, while endotherm C represents the melt of the guest-free host compound.

The TG and DSC traces of **TBDDDA•1DMF•3DMSO** are shown in Figure 3.2(e). The TG trace shows a two step desorption with a total percentage mass loss of 40.4%, which corresponds to H:DMF:DMSO = 1:1:3 (calc. 39.2%). The DSC trace shows two endotherms with endotherm A corresponding to release of the guest and endotherm C due to melting of the guest-free host compound.

For **TBDDDA•4DMSO**, Figure 3.2(f), the TG trace shows a two step desorption with a total percentage mass loss of 40.5%, which corresponds to H:G = 1:4 (calc. 39.6%). Endotherm A in the DSC trace is due to guest release and endotherm C is caused by the melting of the guest-free host compound.

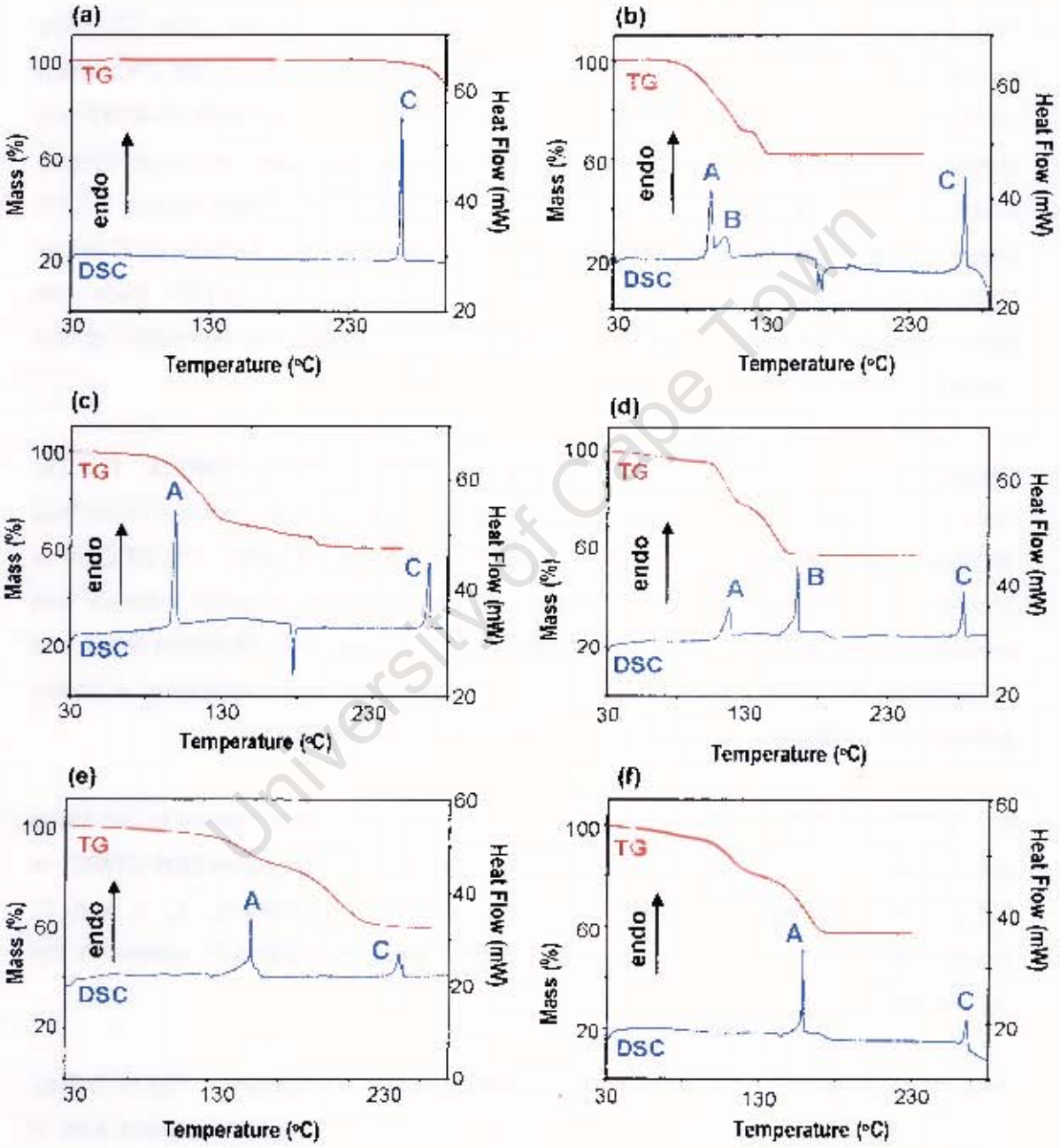

Figure 3.2 TG and DSC traces of **(a) TBDDDA**, **(b) TBDDDA•4DMF**, **(c) TBDDDA•3DMF•1DMSO**, **(d) TBDDDA•2DMF•2DMSO**, **(e) TBDDDA•1DMF•3DMSO** and **(f) TBDDDA•4DMSO**.

Figure 3.3(a) shows the TG and DSC traces of **TBDDDA•4ACE**. The TG trace shows that guest release occurs in a single step with a mass loss of 31.8% which corresponds to H:G = 1:4 (calc. 32.8%). The DSC trace shows two endotherms with endotherm A corresponding to guest release and endotherm C representing the melt of the guest-free host compound.

The TG and DSC traces of **TBDDDA•2DMF•2ACE** are shown in Figure 3.3(b). The TG trace shows a two step desorption, with corresponding endotherms, A and B, in the DSC trace. Endotherm C in the DSC trace is due to the melting of the guest-free host compound. The percentage mass loss of 37.0% shown by the TG trace corresponds to H:DMF:acetone = 1:2:2 (calc. 35.5%). There is an exotherm displayed by the DSC trace suggesting a phase change of the guest-free host compound before the melt.

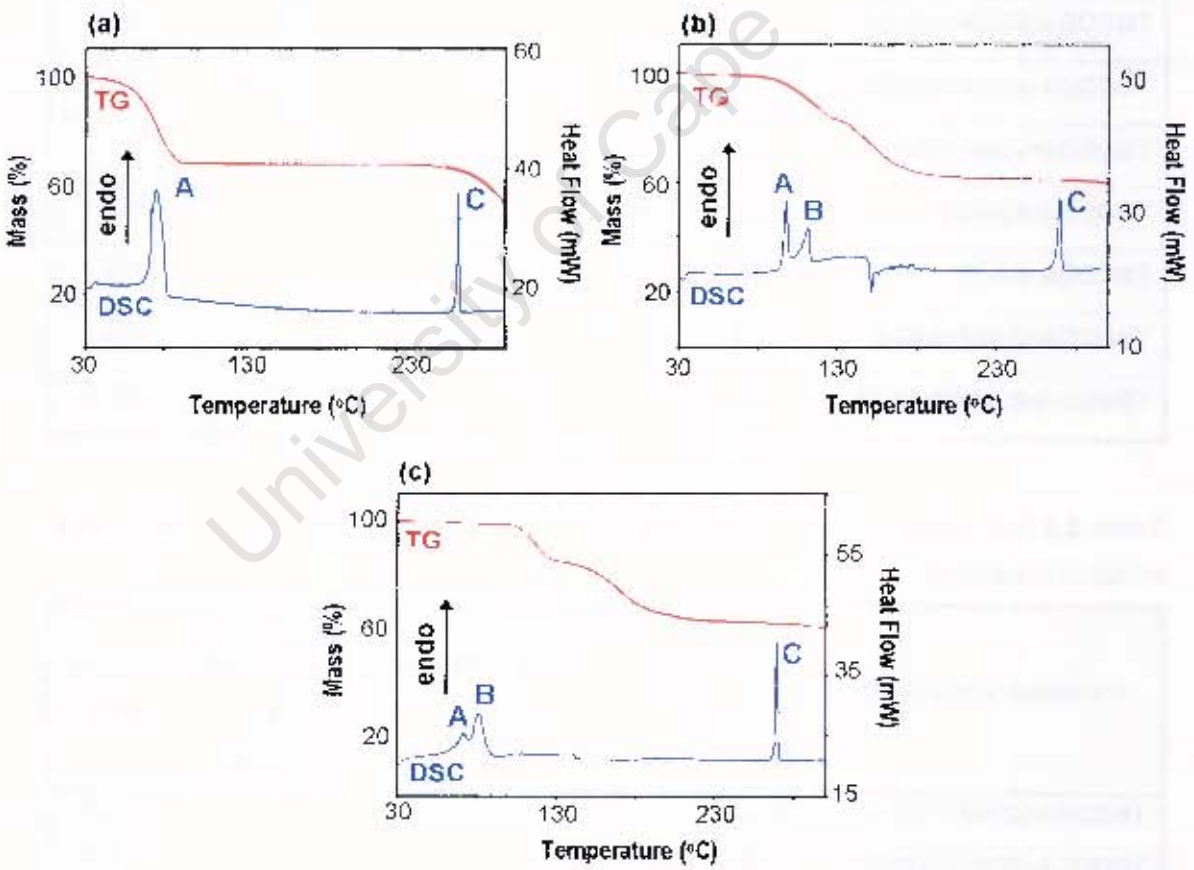

Figure 3.3 TG and DSC traces of **(a) TBDDDA•4ACE**, **(b) TBDDDA•2DMF•2ACE** and **(c) TBDDDA•2DMSO•2ACE**.

For **TBDDDA•2DMSO•2ACE**, Figure 3.3(c), the TG trace shows a two step desorption corresponding to endotherms A and B in the DSC trace. The total percentage mass loss of 36.1% shown by the TG trace corresponds to H:DMSO:acetone = 1:2:2 (calc. 36.4%). Endotherm C in the DSC trace is due to the melting of the guest-free host compound.

Table 3.2 Thermal analysis results of **TBDDDA** inclusion compounds

Inclusion Compound	TG Results		H:G ratio	DSC Results		
	Calc. % mass loss	Exp. % mass loss		T_{on} (°C) Peak A	T_{on} (°C) Peak B	T_{on} (°C) Peak C
TBDDDA	—	—	—	—	—	266.7
TBDDDA•4DMF	38.0	37.7	1:4	93.1	—	265.3
TBDDDA•3DMF•1DMSO	38.4	38.6	1:3:1	97.0	—	265.2
TBDDDA•2DMF•2DMSO	38.9	39.3	1:2:2	106.1	154.5	264.1
TBDDDA•1DMF•3DMSO	39.2	40.4	1:1:3	159.5	—	261.9
TBDDDA•4DMSO	39.6	40.5	1:4	157.4	—	263.1
TBDDDA•4ACE	32.8	31.8	1:4	70.5	—	268.3
TBDDDA•2DMF•2ACE	35.5	37.0	1:2:2	95.0	105.3	266.7
TBDDDA•2DMSO•2ACE	36.4	36.1	1:2:2	67.4	77.1	267.6

Table 3.3 TG results showing individual weight losses and stoichiometries of the ternary inclusion compounds

Inclusion compound	Mass loss (%) due to DMF loss		Mass loss (%) due to DMSO loss		Mass loss (%) due to acetone loss		$H:G_1:G_2$ ratio
	Calc.	Exp.	Calc.	Exp.	Calc.	Exp.	
TBDDDA•3DMF•1DMSO	28.3	28.6	10.1	10.0	—	—	1:3:1
TBDDDA•2DMF•2DMSO	18.8	19.0	20.1	20.3	—	—	1:2:2
TBDDDA•1DMF•3DMSO	9.3	9.5	29.9	30.9	—	—	1:1:3
TBDDDA•2DMF•2ACE	19.8	20.8	—	—	15.7	16.2	1:2:2
TBDDDA•2DMSO•2ACE	—	—	20.9	21.1	15.5	15.0	1:2:2

HOT STAGE MICROSCOPY

Hot stage microscopy (HSM) was used to observe the physical appearance of the crystals of some of the inclusion compounds during thermal decomposition. The analyses were carried out by heating the crystals at a controlled heating rate and photographs were taken during the thermal events which occurred. These photographs are shown in Figures 3.4 to 3.7.

The crystals of **TBDDDA•4DMF** (shown at room temperature in Figure 3.4(a)) became gradually opaque from room temperature (Figure 3.4(b)) and bubbles of the desorbed guest were observed from 105°C to 137°C (Figure 3.4(c)). The crystals melted at 282°C (Figure 3.4(d)).

The **TBDDDA•3DMF•1DMSO** crystals (shown at room temperature in Figure 3.5(a)) turned slowly opaque from room temperature (Figure 3.5(b)). Bubbles were observed in the silicone oil at 102°C and this guest release proceeded until 135°C (Figure 3.5(c)). Melting of the crystals took place at 279°C (Figure 3.5(d)).

Crystals of **TBDDDA•2DMF•2DMSO** (shown at room temperature in Figure 3.6(a)) became gradually opaque from room temperature, as in the above cases (Figure 3.6(b)). Bubbles of the desorbed guest were observed in the silicone oil from 109°C to 164°C (Figure 3.6(c)) and the crystals melted at 276°C (Figure 3.6(d)).

Crystals of **TBDDDA•4DMSO** (shown at room temperature in Figure 3.7(a)) also turned gradually opaque from room temperature (Figure 3.7(b)). Desorption of the guest was observed in the form of bubbles from 142°C to 174°C (Figure 3.7(c)) and melting of the crystals took place at 278°C (Figure 3.7(d)).

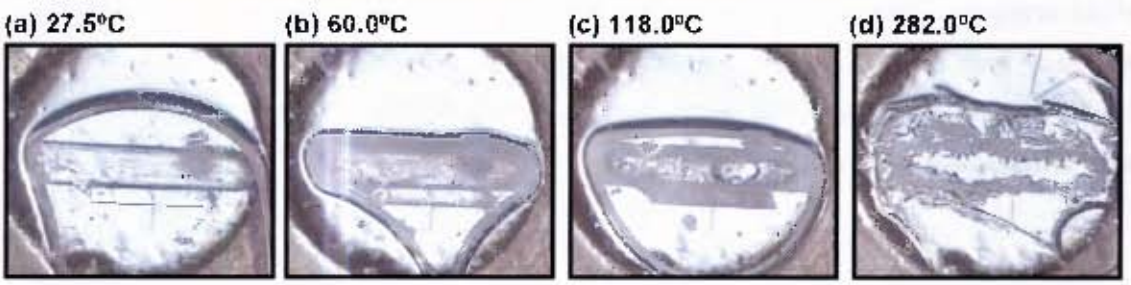

Figure 3.4 Crystals of **TBDDDA•4DMF** during thermal decomposition.

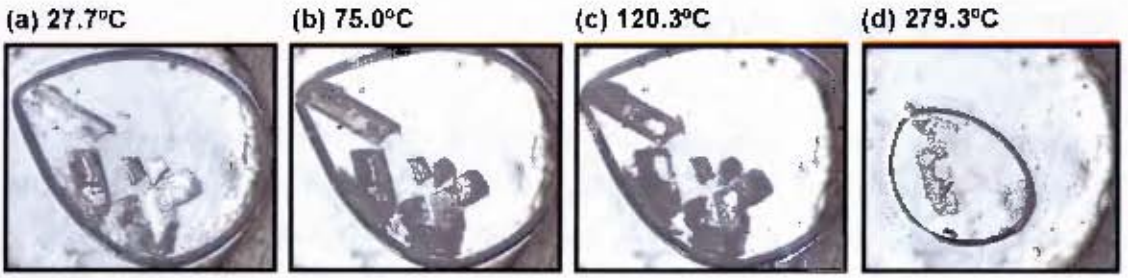

Figure 3.5 Thermal decomposition of **TBDDDA•3DMF•1DMSO** crystals.

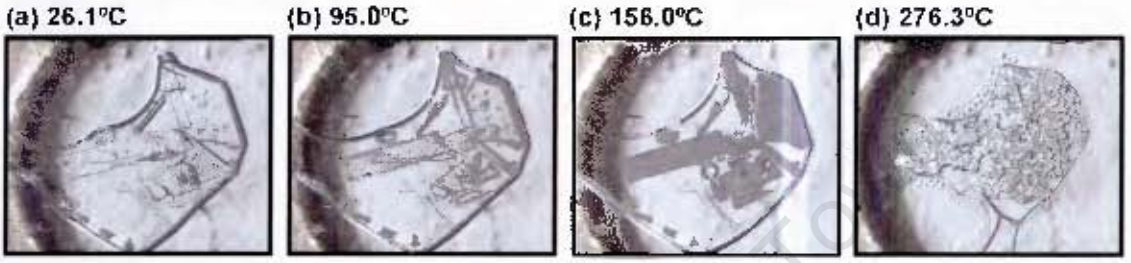

Figure 3.6 Crystals of **TBDDDA•2DMF•2DMSO** during thermal decay.

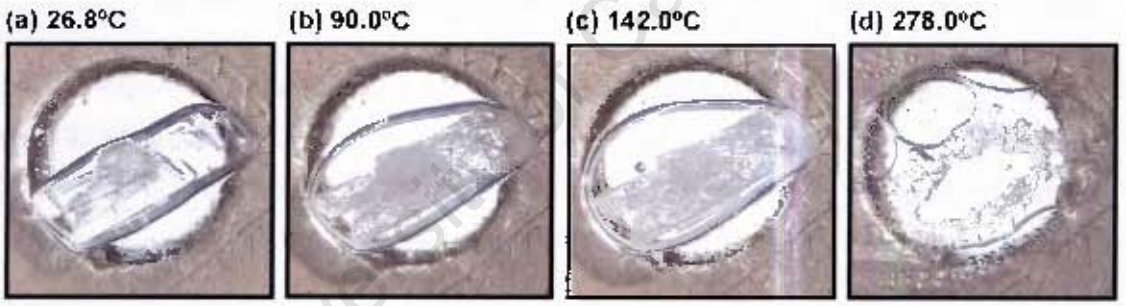

Figure 3.7 **TBDDDA•4DMSO** crystals during thermal decay.

We note that there are temperature lags between the endotherms due to guest release and host melting shown by the DSC traces versus what is observed in the HSM analysis. This is attributed to the differing geometries of the two instruments, the fact that the hot stage microscope has no purging gas, and that whereas relatively large single crystals were used in HSM, the DSC analyses were performed with crushed samples or powders.

STRUCTURE SOLUTION AND ANALYSIS

TBDDDA

$C_{34}H_{36}O_2$
Space group: $P2_1/c$
a = 16.6711(3) Å
b = 10.6712(2) Å β = 101.435(1)°
c = 24.3875(5) Å
V = 4252.4(1) Å^3
Z = 6

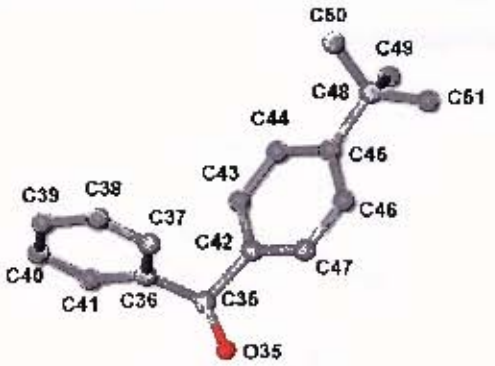

The non-porous, α-phase, the apohost, crystallises in the monoclinic crystal system, in the space group $P2_1/c$. Direct methods yielded the positions of all non-hydrogen atoms. The hydroxyl hydrogens were located in difference electron density maps and refined with simple bond length constraints. The remaining hydrogen atoms were placed with geometric constraints and refined with isotropic thermal parameters equal to $1.2xU_{eq}$ of their parent atoms. The methyl carbons of one of the *tert*-butylphenyl groups were found to be disordered over two positions, with site occupancy factors of 0.60 (atoms labelled with suffix A) and 0.40 (atoms labelled with suffix B). All non-hydrogen atoms were refined with anisotropic temperature factors, with the exception of the disordered methyl carbon atoms which were refined with isotropic temperature factors. The structure refined to $R_1 = 0.0754$.

The structure of TBDDDA has six host molecules in the unit cell and the asymmetric unit consists of one complete host molecule and one half host molecule. The numbering scheme of the half host molecule is given above, while that of the whole host molecule is given on page 58. In the unit cell, four host molecules lie in general positions and two molecules lie on centres of inversion in positions 0,1/2,0 and 0,0,1/2 (Wyckoff position *c*). The crystal packing viewed along [010] is shown in Figure 3.8.

The molecules pack to form planes perpendicular to [100]. Within these planes there is a circular pattern of hydrogen bonds which interlink eight host molecules. Host molecule A, which lies on a centre of inversion, is stabilised by a (Host A)-O35-H35····O1(Host B^1) hydrogen bond (d(O···O) = 2.813(2)Å). Host B^1 in turn hydrogen

bonds to Host B^2 via a (Host B^1)-O1-H1·····O18-(Host B^2) interaction (d(O···O) = 2.831(2)Å). These are two unique hydrogen bonds and symmetry requirements generate a further six hydrogen bonds, which interlink eight host molecules as shown in Figure 3.9. The two host molecules in the asymmetric unit have different conformations and these are discussed in more detail in Chapter 8.

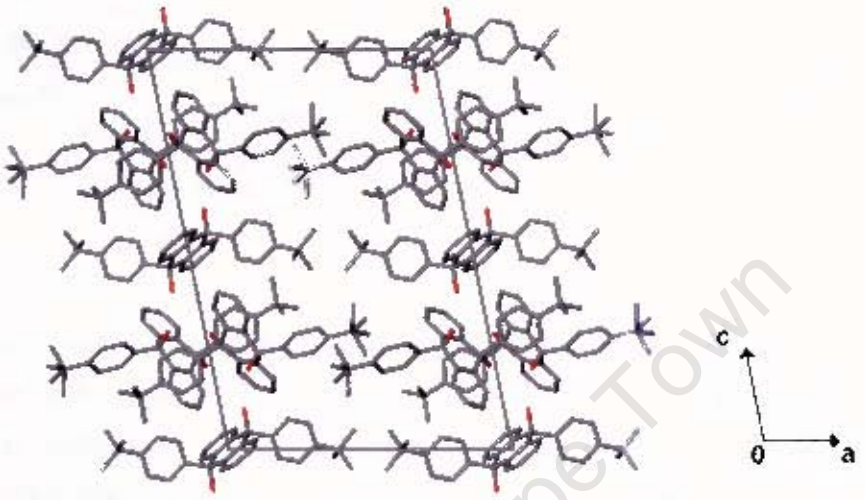

Figure 3.8 Projection of the apohost structure along [010].

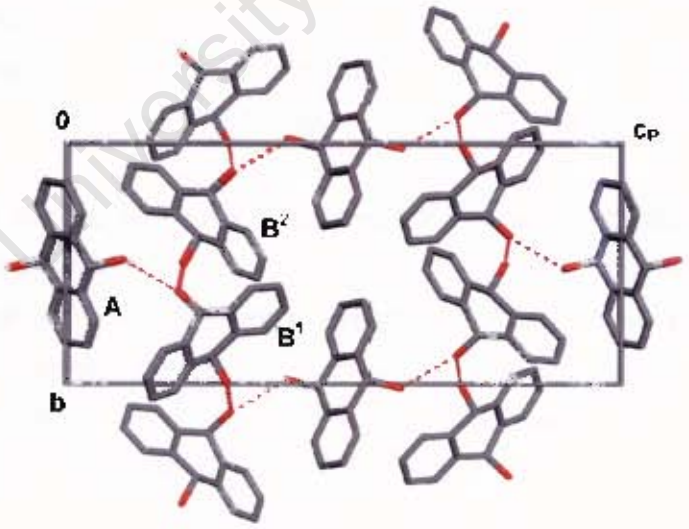

Figure 3.9 Projection of the apohost structure along [100] showing the hydrogen bonding in the structure, with the *tert*-butylphenyl groups omitted for clarity, and with B^1 at (x,y,z) and B^2 at (-x, y-1/2, ½-z).

TBDDDA•4DMF

$C_{34}H_{36}O_2.4(C_3H_7NO)$
Guest: DMF
Space group: $P\bar{1}$

a = 9.0806(3) Å	α = 74.477(2)°
b = 8.9414(4) Å	β = 88.693(2)°
c = 14.935(1) Å	γ = 110.189(3)°
V = 1087.67(9) Å^3	
Z = 1	

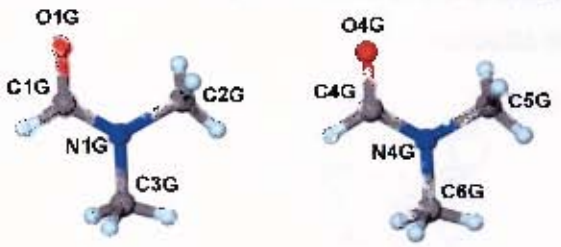

Guest 1 Guest 2

TBDDDA•4DMF crystallises in the triclinic crystal system. The mean $|E^2-1|$ values obtained by direct methods show that the structure belongs to the centrosymmetric space group $P\bar{1}$, which was confirmed by the successful refinement of the structure. The positions of all non-hydrogen host atoms were obtained by direct methods and the positions of non-hydrogen guest atoms were located in difference electron density maps. All non-hydrogen atoms were refined with anisotropic temperature factors. The hydroxyl hydrogens on the host molecule were located in difference electron density maps and refined with simple bond length constraints. All other hydrogen atoms were placed with geometric constraints and assigned isotropic temperature factors of $1.2xU_{eq}$ of their parent atoms. The structure refined successfully to $R_1 = 0.0585$.

The structure of **TBDDDA•4DMF** has Z = 1, with the asymmetric unit containing half a host molecule and two guest molecules. The space group symmetry then requires the host molecule to lie on a centre of symmetry and the host molecules were found to be located at the origin on a centre of inversion with the guests located in general positions. A projection of the structure along [010] is shown in Figure 3.10(a), along with projections of each of the other structures in this series (Figure 3.10(b) – (e)), for comparison.

From this projection it can be seen that two of the DMF guest molecules are hydrogen bonded to the host molecule via the hydroxyl groups and two are not hydrogen bonded. A diagram illustrating the hydrogen bonding in **TBDDDA•4DMF** is shown in Figure 3.11 and the hydrogen bonding details are given in Table 3.4. Table 3.12 (page 96) gives a summary and comparison of the hydrogen bonding in all of the inclusion compounds. It is interesting to note that the TG trace shows a two step

guest desorption, with concomitant endotherms in the DSC trace (Figure 3.2(b), page 64) and we can surmise that the first mass loss is due to the non-hydrogen bonded guests and the second to the hydrogen bonded guests, which are held more tightly in the structure.

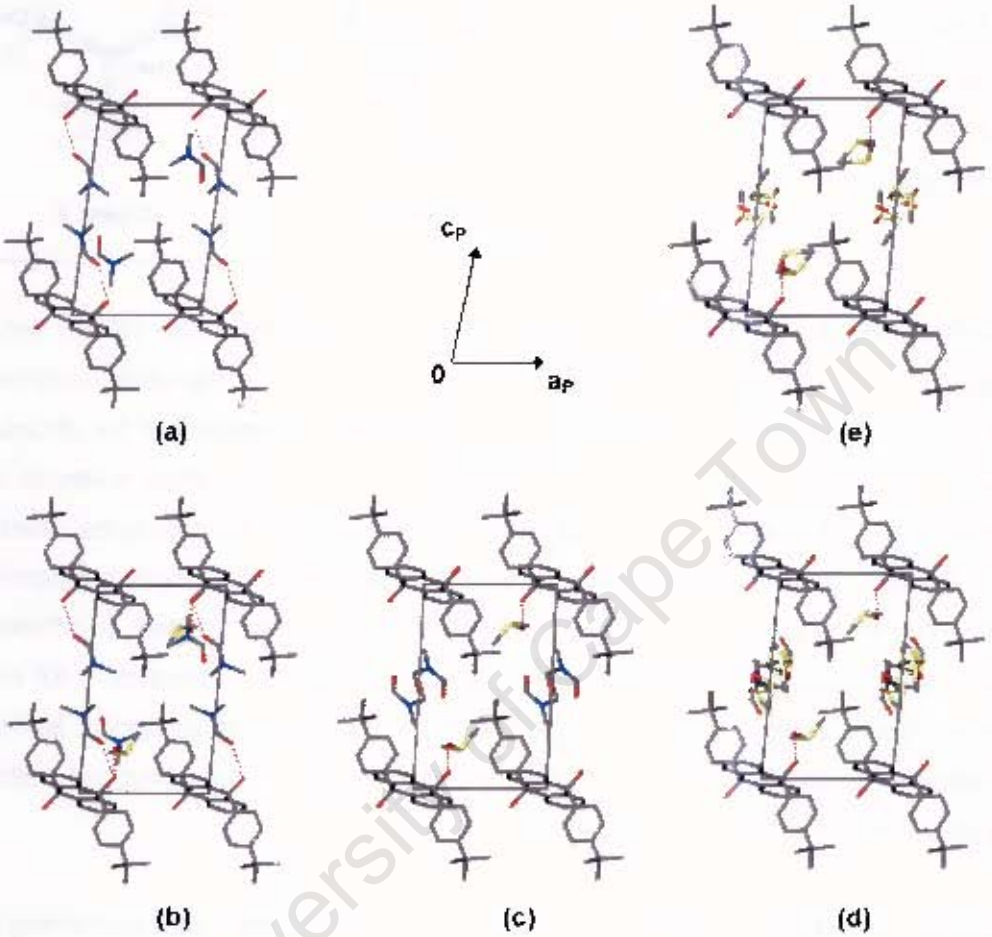

Figure 3.10 Projection of the five structures of the DMF/DMSO series along [010] with **(a) TBDDDA•4DMF**, **(b) TBDDDA•3DMF•1DMSO**, **(c) TBDDDA•2DMF•2DMSO**, **(d) TBDDDA•1DMF•3DMSO** and **(e) TBDDDA•4DMSO**.

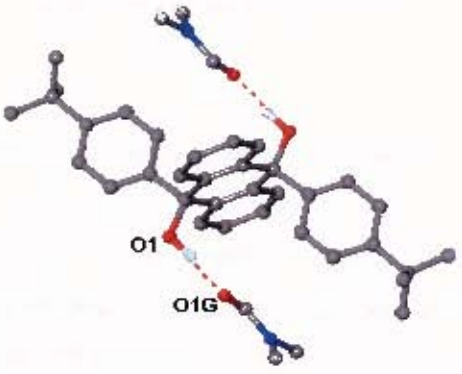

Figure 3.11 Host···guest hydrogen bonding interactions in **TBDDDA•4DMF**.

Table 3.4 Hydrogen bonding details of **TBDDDA•4DMF**

Donor (D)	Acceptor (A)	D–H/Å	D···A/Å	D–H···A/°
O1	O1G	0.980(1)	2.725(2)	172(3)

The host molecules pack to form a series of continuous ribbons in the [011] direction, which are not interlinked. The crystal packing viewed down [010] as well as down [100] is shown in Figure 3.12. The packing of the host molecules results in main channels along [010] in which the guest molecules are located. The channels were examined using the program SECTION,[1] which was used to view sections through the unit cell along [010]. These sections, with the guests omitted, are illustrated in Figure 3.13. The channels are restricted with a maximum extension of approximately 13.0 Å x 5.6 Å at 0,1/2,1/2 where the guest molecules are located. These main channels meet up with secondary undulating channels along [100] between 0.7 Å and 2.5 Å down [010] as well as between 6.5 Å and 8.3 Å down [010]. Figure 3.14 shows the packing of the host molecules, viewed down [010], with the guest molecules omitted and the host molecules represented with van der Waals radii.

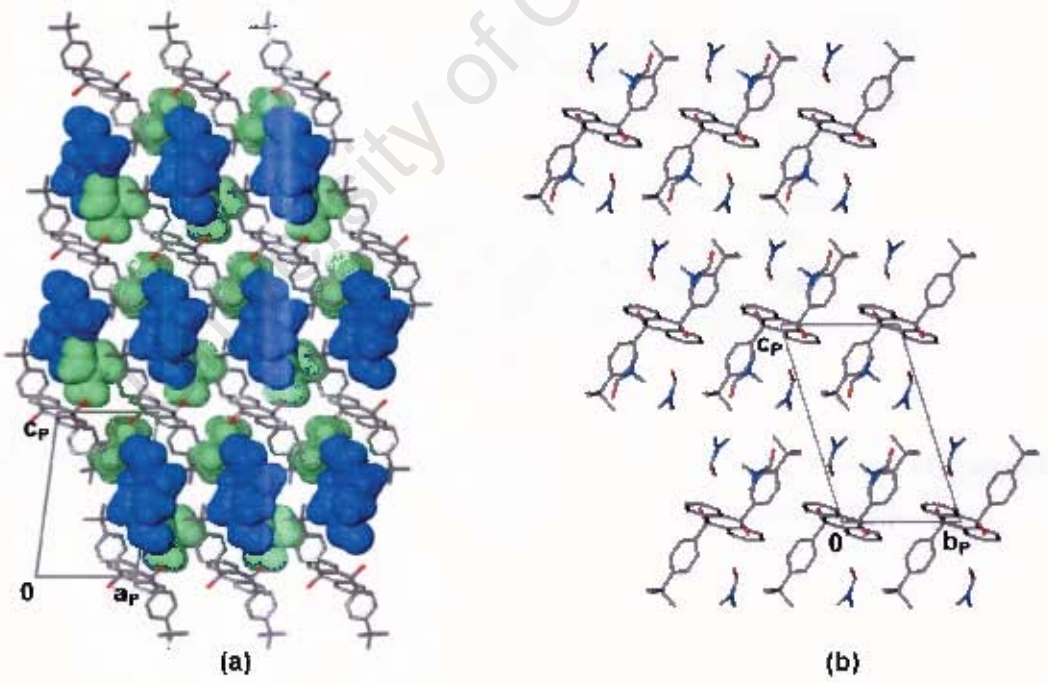

Figure 3.12 Packing diagram of **TBDDDA•4DMF** viewed **(a)** down [010] with host molecules in stick representation and guest molecules represented with van der Waals radii (hydrogen bonded guests are shown in blue and non-hydrogen bonded guests are shown in green) and **(b)** down [100].

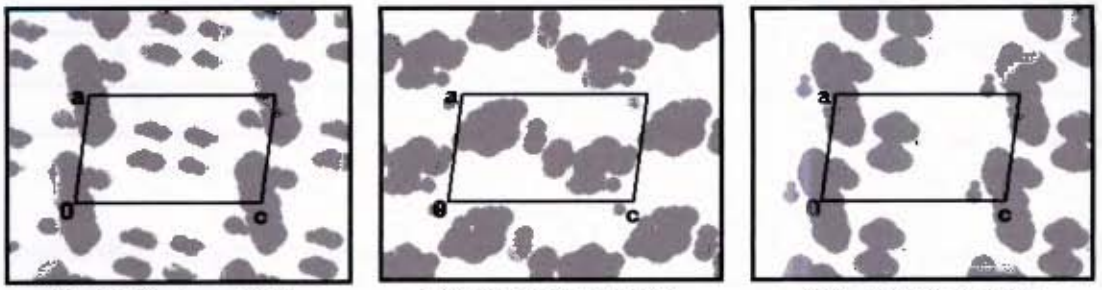

(a) 0.0 Å along [010] **(b)** 4.6 Å along [010] **(c)** 1.0 Å along [010]

Figure 3.13 SECTION plots of **TBDDDA•4DMF** (with guest molecules omitted and host molecules represented by grey areas) viewed down [010] with the unit cell sectioned at **(a)** 0.0 Å, **(b)** 4.6 Å and **(c)** 1.0 Å along [010].

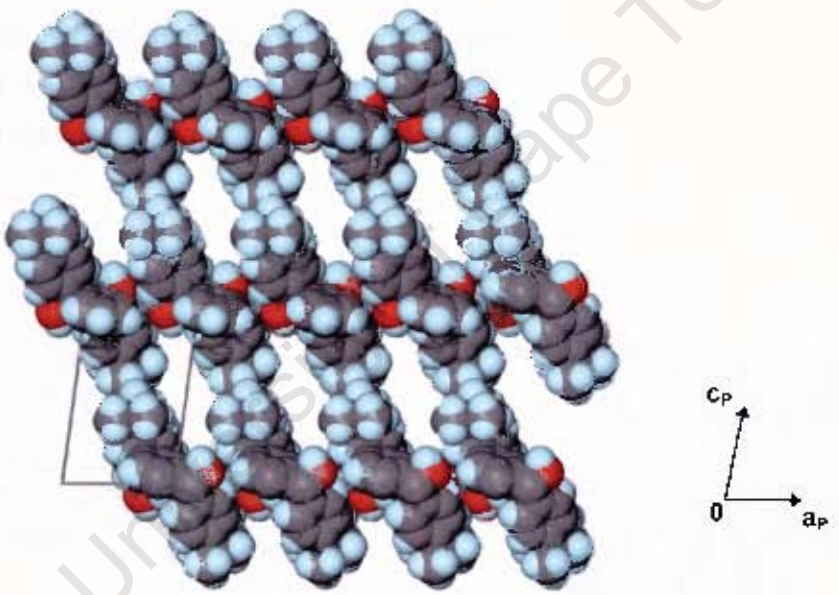

Figure 3.14 View down the channels of **TBDDDA•4DMF** along [010] with guest molecules omitted and host molecules represented with van der Waals radii.

TBDDDA•3DMF•1DMSO

$C_{34}H_{36}O_2.3(C_3H_7NO).1(C_2H_6OS)$
Guests: DMF and DMSO
Space group: $P\bar{1}$
a = 9.0858(2) Å α = 107.144(1)°
b = 9.0547(2) Å β = 91.527(1)°
c = 14.7684(4) Å γ = 70.236(2)°
V = 1089.00(4) Å^3
Z = 1

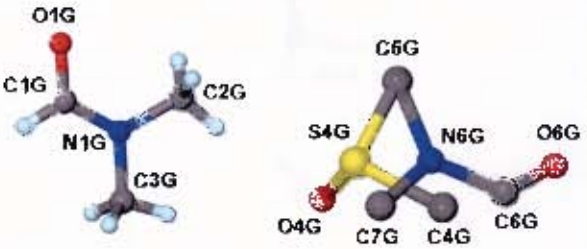

TBDDDA•3DMF•1DMSO crystallises in the triclinic system. The centrosymmetric space group $P\bar{1}$ was chosen based on the $|E^2-1|$ statistics obtained by direct methods. The positions of all non-hydrogen host atoms were obtained by direct methods and the positions of non-hydrogen guest atoms were located in difference electron density maps. In subsequent refinements all non-hydrogen atoms were refined anisotropically. The host hydroxyl hydrogen atoms were located in difference electron density maps and refined with simple bond length constraints. The remaining hydrogen atoms were placed in geometrically constrained positions and refined with isotropic temperature factors equal to $1.2xU_{eq}$ of their parent atoms. The structure refined to R_1 = 0.1140.

The asymmetric unit consists of half a host molecule and two guest molecules, as in the case of **TBDDDA•4DMF**, with Z = 1. The space group symmetry thus requires the host molecule to lie on a centre of symmetry and the host molecules were found to be located at the origin on a centre of inversion with the guests located in general positions. The unit cell contains three DMF guest molecules and one DMSO guest molecule and symmetry requires the DMSO guest to be located at two sites, each with site occupancy factors of 0.5. The DMF guest molecules were refined with site occupancy factors of 0.75 each. These values were initially derived from difference electron density maps and were subsequently refined. The difference electron density map showed that the DMF and DMSO molecules share the same general location and share a common carbon atom. Their positions were found by contouring several layers of the difference electron density map and fitting models of the guest molecules to the peaks. Figure 3.15 shows one layer of a difference electron density map used to model a partial DMF guest molecule.

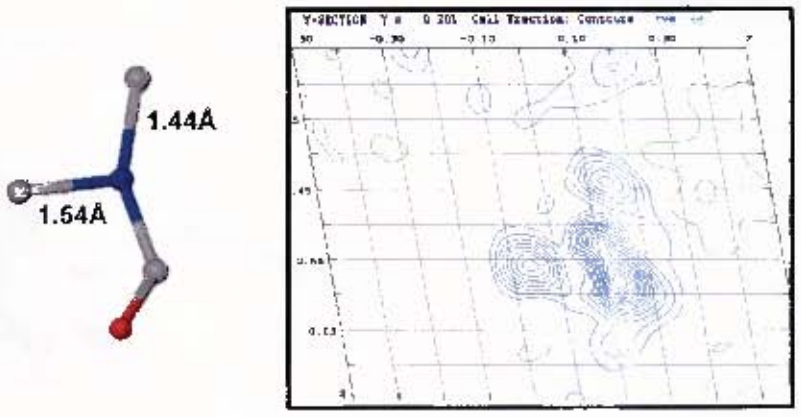

Figure 3.15 Example of a layer of a difference electron density map used to model a partial DMF guest molecule.

TBDDDA•3DMF•1DMSO is isostructural with **TBDDDA•4DMF** with respect to the packing of the host molecules and a projection of the structure along [010] is illustrated in Figure 3.10(b) (page 72). This projection shows that one of the DMF guest molecules and the DMSO guest molecule share the hydrogen bond with the hydroxyl group of the host molecule. A diagram illustrating the hydrogen bonding interactions in **TBDDDA•3DMF•1DMSO** is shown in Figure 3.16 and the hydrogen-bonding details are given in Table 3.5.

The host molecules pack to form the same restricted channels along [010] as those described for **TBDDDA•4DMF,** in which the guest molecules are situated. The crystal packing of the structure viewed along [010] and [100] is shown in Figure 3.17.

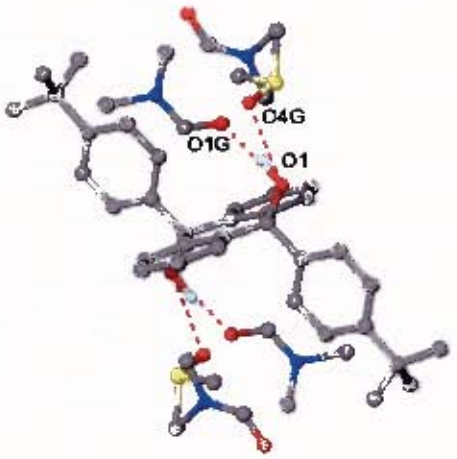

Figure 3.16 Host--guest hydrogen bonding interactions in **TBDDDA•3DMF•1DMSO**.

Table 3.5 Hydrogen bonding details of **TBDDDA•3DMF•1DMSO**

Donor (D)	Acceptor (A)	D–H/Å	D···A/Å	D–H···A/°
O1	O1G	0.980(1)	2.618(4)	168(5)
O1	O4G	0.980(1)	2.878(6)	143(4)

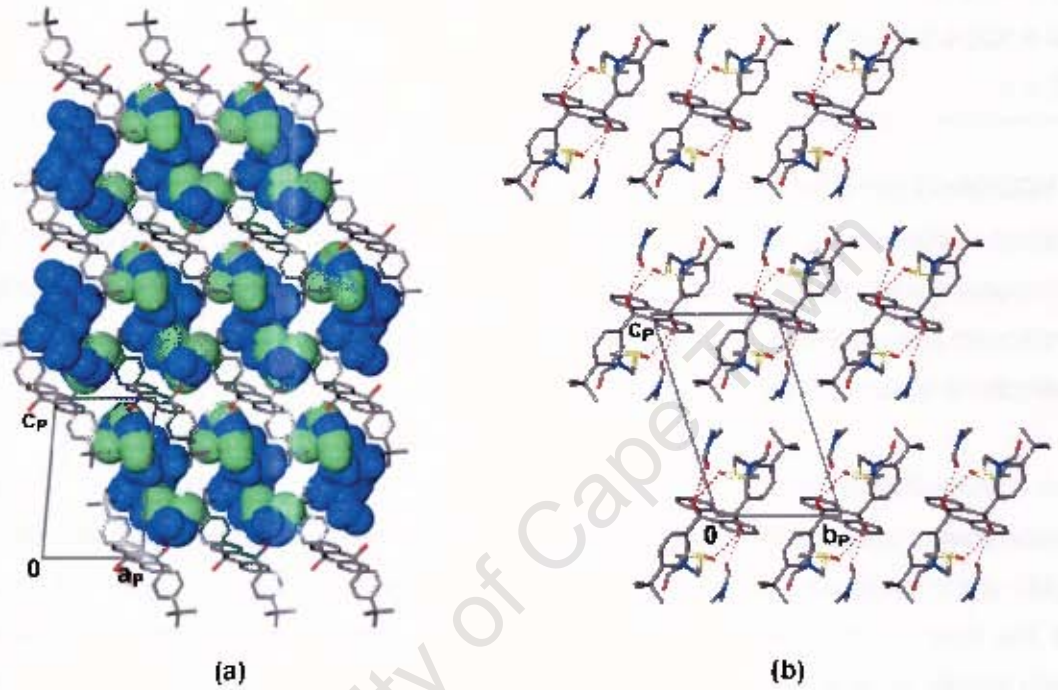

(a) (b)

Figure 3.17 Packing diagram of **TBDDDA•3DMF•1DMSO** viewed **(a)** down [010] with host molecules in stick representation and guest molecules represented with van der Waals radii (hydrogen bonded guests are shown in blue and non-hydrogen bonded guests are shown in green) and **(b)** down [100].

TBDDDA•2DMF•2DMSO

$C_{34}H_{36}O_2.2(C_3H_7NO).2(C_2H_6OS)$
Guests: DMF and DMSO
Space group: $P\bar{1}$
a = 9.1425(3) Å α = 71.356(1)°
b = 9.1730(3) Å β = 81.229(1)°
c = 14.273(1) Å γ = 69.938(1)°
V = 1064.13(9) Å^3
Z = 1

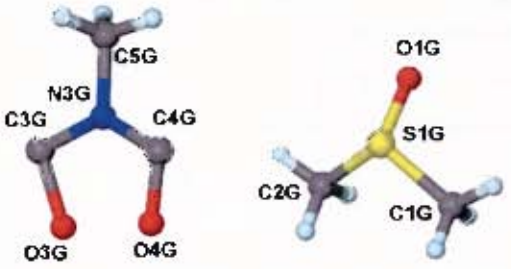

TBDDDA•2DMF•2DMSO crystallises in the triclinic crystal system. The mean $|E^2-1|$ values obtained by direct methods show that the structure belongs to the centrosymmetric space group $P\bar{1}$. Direct methods yielded the positions of all non-hydrogen host atoms and the positions of non-hydrogen guest atoms were located in difference electron density maps.

All non-hydrogen host and guest atoms were refined with anisotropic thermal parameters, with the exception of the two partial oxygen atoms in the disordered DMF guest molecule which were refined isotropically. The hydroxyl hydrogen atoms of the host molecule were located in difference electron density maps and refined with simple bond length constraints. All remaining hydrogen atoms were placed with geometric constraints and refined with isotropic thermal parameters equal to $1.2xU_{eq}$ of their parent atoms. The structure refined successfully to $R_1 = 0.0637$.

There is half a host molecule as well as two guest molecules in the asymmetric unit, with Z = 1, as in the previous structures. The host molecules were once again found to be located at the origin on a centre of inversion with the guests located in general positions. The unit cell contains two DMF guest molecules and two DMSO guest molecules. The DMF guest molecule is disordered and the oxygen atom was modelled in two positions, O3G and O4G. The site occupancy factors were allowed to refine, resulting in fractional site occupancies of 0.47 and 0.53 for O3G and O4G respectively. The disorder in the DMF guest molecule is displayed in the guest numbering scheme above.

TBDDDA•2DMF•2DMSO is isostructural with **TBDDDA•4DMF** with respect to the host molecules and the only differences are due to slight changes in the locations of the guest molecules. A projection of the structure along [010] is shown in Figure 3.10(c) (page 72) and from this projection it can be seen that the two DMSO guest molecules are hydrogen bonded to the hydroxyl group of the host molecule, while the DMF guest molecules are not involved in hydrogen bonding and are located close to a centre of symmetry at Wyckoff position *g*. A diagram illustrating the hydrogen bonding in **TBDDDA•2DMF•2DMSO** is shown in Figure 3.18 and the hydrogen bonding details are given in Table 3.6.

The packing of the host molecules results in restricted channels with the same size and shape as those described for **TBDDDA•4DMF**, with the guest molecules located in these channels. The crystal packing of the structure viewed along [010] as well as along [100] is depicted in Figure 3.19.

Figure 3.18 Host···guest hydrogen bonding interactions in **TBDDDA•2DMF•2DMSO**.

Table 3.6 Hydrogen bonding details of **TBDDDA•2DMF•2DMSO**

Donor (D)	Acceptor (A)	D–H/Å	D···A/Å	D–H···A/°
O1	O1G	0.970(1)	2.744(2)	170(3)

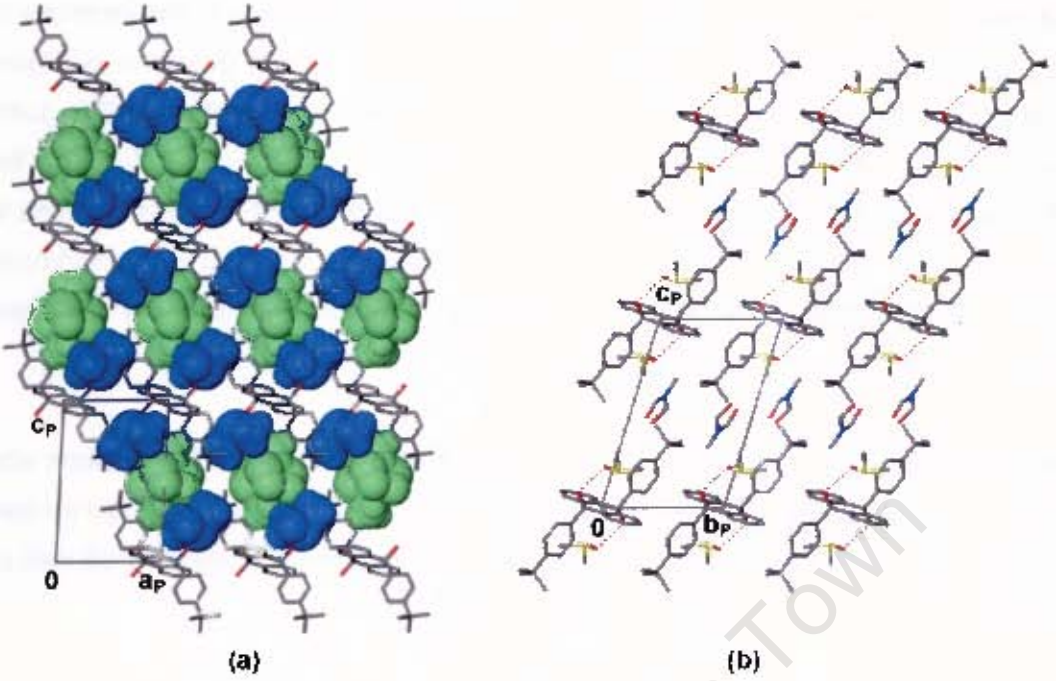

Figure 3.19 Packing diagram of **TBDDDA•2DMF•2DMSO** viewed **(a)** down [010] with host molecules in stick representation and guest molecules represented with van der Waals radii (hydrogen bonded DMSO guests are shown in blue and non-hydrogen bonded DMF guests are shown in green) and **(b)** down [100].

TBDDDA•1DMF•3DMSO

$C_{34}H_{36}O_2.(C_3H_7NO).3(C_2H_6OS)$
Guests: DMF and DMSO
Space group: $P\bar{1}$
a = 9.0460(2) Å α = 72.559(1)°
b = 9.1291(2) Å β = 80.132(1)°
c = 14.409(1) Å γ = 71.486(2)°
V = 1072.64(8) Å^3
Z = 1

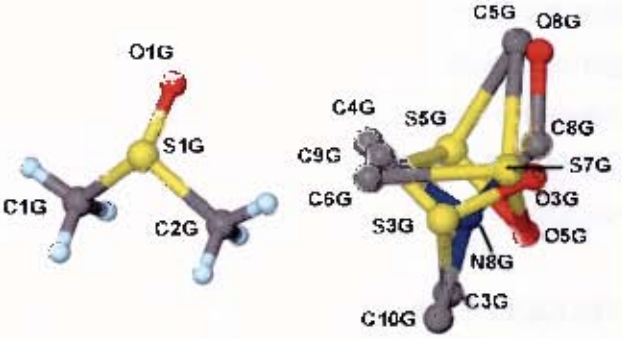

TBDDDA•1DMF•3DMSO crystallises in the triclinic system and the centrosymmetric space group $P\bar{1}$ was chosen based on the mean $|E^2-1$ values obtained by direct methods. The positions of all non-hydrogen host atoms were obtained by direct methods and the positions of non-hydrogen guest atoms were located in difference electron density maps. All non-hydrogen atoms of the host molecule, as well as those of the ordered DMSO guest molecule in the asymmetric unit, were refined with anisotropic temperature factors, while the remaining guest atoms were refined with isotropic temperature factors. The hydroxyl hydrogen atoms of the host molecule were located in difference electron density maps and refined with simple bond length constraints. All other hydrogen atoms were placed with geometric constraints and assigned isotropic temperature factors of $1.2xU_{eq}$ of their parent atoms. The structure refined to $R_1 = 0.0774$.

The asymmetric unit once again consists of half a host molecule and two guest molecules, with Z = 1. The host molecule was found to be located on the centre of inversion at the origin, while the guest molecules are located in general positions, as with the previous structures. The unit cell contains one DMF guest molecule and three DMSO guest molecules and symmetry requires the DMF guest to be located at two sites, each with site occupancy factors of 0.5. There are two whole DMSO guest molecules in the unit cell and the third DMSO guest molecule is again required to be located in two positions with site occupancy factors of 0.5. This DMSO molecule was found to be disordered and was modelled over two sites, each with a site occupancy factor of 0.25.

One of these partial molecules exhibited further disorder and the sulphur atom was modelled in two positions, S3G and S7G, with site occupancy factors of 0.15 and 0.1

respectively. These values were initially derived from difference electron density maps and were subsequently refined. The difference electron density map showed that the DMF and DMSO molecules which are located at two sites share the same general location and their positions were found by contouring several layers of the difference electron density map and fitting models of the guest molecules to the peaks, as described previously for **TBDDDA•3DMF•1DMSO**. The disorder is depicted in the guest numbering scheme above.

TBDDDA•1DMF•3DMSO is isostructural with **TBDDDA•4DMF** with respect to the packing of the host molecules and this is illustrated in Figure 3.10(d) (page 72) which gives a projection of the structure along [010]. From this projection it can be seen that the two whole DMSO guest molecules are hydrogen bonded to the host molecule via the hydroxyl groups, while the DMF guest molecule and the third DMSO guest, which are both located in two positions, are not involved in hydrogen bonding. A diagram illustrating the hydrogen bonding in **TBDDDA•1DMF•3DMSO** is shown in Figure 3.20 and the hydrogen bonding details are given in Table 3.7.

The host molecules pack to form the same restricted channels as those described for **TBDDDA•4DMF**, which contain the guest molecules. Figure 3.21 illustrates the crystal packing of the structure viewed along [010], as well as along [100].

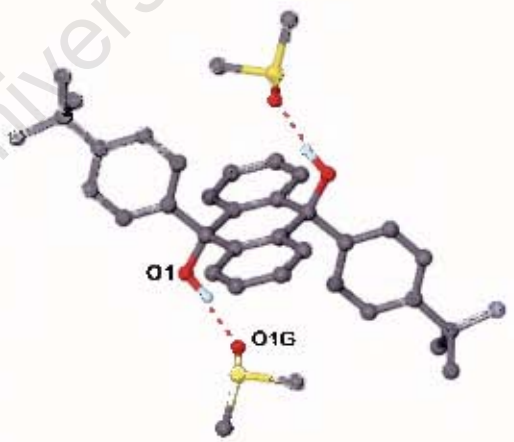

Figure 3.20 Host···guest hydrogen bonding interactions in **TBDDDA•1DMF•3DMSO**.

Table 3.7 Hydrogen bonding details of **TBDDDA•1DMF•3DMSO**

Donor (D)	Acceptor (A)	D–H/Å	D···A/Å	D–H···A/°
O1	O1G	0.970(1)	2.751(3)	159(5)

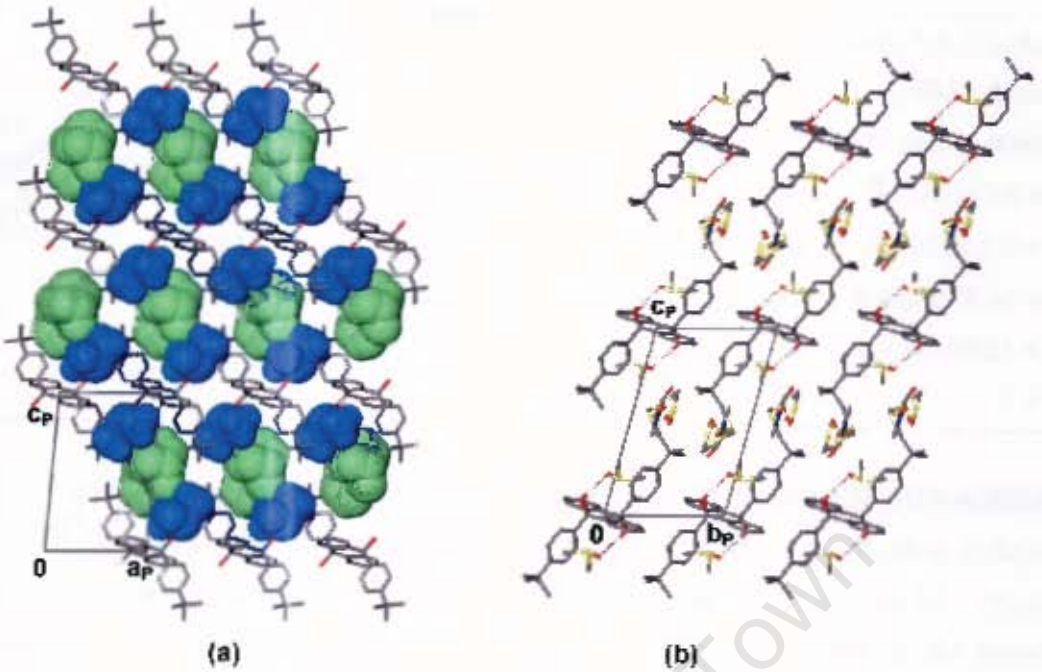

Figure 3.21 Packing diagram of **TBDDDA•1DMF•3DMSO** viewed **(a)** down [010] with host molecules in stick representation and guest molecules represented with van der Waals radii (hydrogen bonded guests are shown in blue and non-hydrogen bonded guests are shown in green) and **(b)** down [100].

TBDDDA•4DMSO

$C_{34}H_{36}O_2.4(C_2H_6OS)$
Guest: DMSO
Space group: $P\bar{1}$
a = 9.0359(3) Å α = 72.981(1)°
b = 9.1353(3) Å β = 80.086(1)°
c = 14.4126(6) Å γ = 71.631(2)°
V = 1075.44(7) Å^3
Z = 1

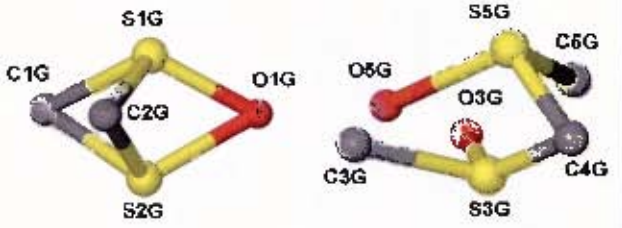

Guest 1 Guest 2

TBDDDA•4DMSO crystallises in the triclinic system and, based on the $|E^2-1|$ statistics obtained by direct methods, the centrosymmetric space group $P\bar{1}$ was chosen. All non-hydrogen atoms of the host molecule in the asymmetric unit were located using direct methods. The non-hydrogen guest atoms were located in difference electron density maps. All non-hydrogen host atoms, as well as selected non-hydrogen guest atoms, were refined anisotropically, while the remaining non-hydrogen guest atoms were refined with isotropic temperature factors. The hydroxyl hydrogen atoms of the host molecule were located in difference electron density maps and refined with simple bond length constraints. The remaining hydrogen atoms of the host molecule were placed in geometrically constrained positions and refined with isotropic thermal parameters equat to $1.2xU_{eq}$ of their parent atoms. No attempt was made to place the hydrogen atoms of the guest molecules. The structure refined to $R_1 = 0.0889$.

Once again the asymmetric unit contains half a host molecule and two guest molecules with Z = 1. This requires the host molecule to be located on a centre of symmetry and, as in the previous structures, the host molecules were found to be located at the origin on a centre of inversion, while the guests are located in general positions.

Analysis of the difference electron density maps showed that both guest molecules in the asymmetric unit were disordered and the sulphur atom of guest 1 was modelled in two positions, S1G and S2G with fractional site occupancy factors of 0.93 and 0.07 respectively. The atoms of this guest molecule were refined anisotropically, with the exception of S2G, which was refined isotropically.

The guest 2 molecule was found to be disordered over two positions, with site occupancy factors of 0.42 (molecule containing S3G, O3G and C3G) and 0.58 (molecule containing S5G, O5G and C5G) with one carbon atom, C4G, common to both partial molecules. The atoms of the guest 2 molecule were refined isotropically, except for the two sulphur atoms, which were refined with anisotropic thermal parameters. For both guest molecules, the site occupancy factors were initially assigned according to the relative peak heights in the electron density map and were then refined. The disorder in the guest molecules is depicted above in the guest numbering scheme.

TBDDDA•4DMSO is isostructural with **TBDDDA•4DMF** with respect to the packing of the host molecules, which is clearly illustrated in a projection of the structure along [010] shown in Figure 3.10(e) (page 72). From this projection it can be seen that two of the DMSO guest molecules are hydrogen bonded to the host molecule, via its hydroxyl groups, and two are not involved in hydrogen bonding. A diagram illustrating the hydrogen bonding in **TBDDDA•4DMSO** is shown in Figure 3.22 and the hydrogen-bonding details are given in Table 3.8. We can infer that the first mass loss shown by the TG trace (Figure 3.2(f), page 64) is due to the loss of the two non-hydrogen bonded guest molecules and the second due to the loss of the hydrogen bonded guests.

Figure 3.22 Host···guest hydrogen bonding interactions in **TBDDDA•4DMSO**.

Table 3.8 Hydrogen bonding details of **TBDDDA•4DMSO**

Donor (D)	Acceptor (A)	D–H/Å	D···A/Å	D–H···A/°
O1	O1G	0.970(1)	2.765(3)	167(4)

The packing of the host molecules results in the same restricted channels as those described for **TBDDDA•4DMF** and the guest molecules are located in these channels. The crystal packing of the structure viewed along [010], as well as along [100], is shown in Figure 3.23.

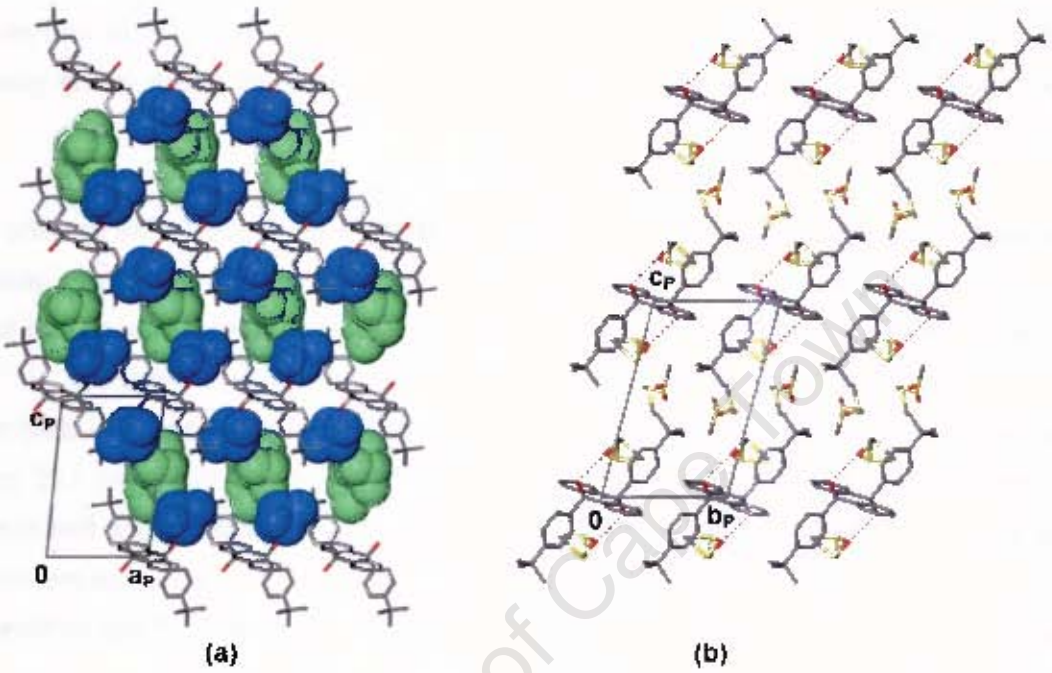

Figure 3.23 Packing diagram of **TBDDDA•4DMSO** viewed **(a)** down [010] with host molecules in stick representation and guest molecules represented with van der Waals radii (hydrogen bonded guests are shown in blue and non-hydrogen bonded guests are shown in green) and **(b)** down [100].

TBDDDA•4ACE

$C_{34}H_{36}O_2.4(C_3H_6O)$
Guest: acetone
Space group: $P2_1/c$
a = 8.9057(2) Å
b = 26.9049(6) Å β = 108.590(1)°
c = 9.1615(2) Å
V = 2080.62(8) Å^3
Z = 2

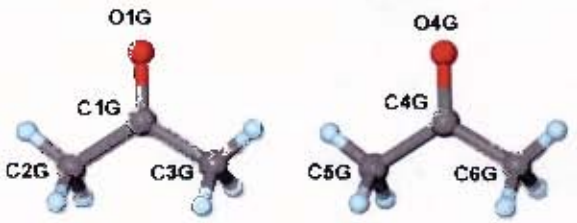

Guest 1 Guest 2

TBDDDA•4ACE crystallises in the monoclinic crystal system, in the space group $P2_1/c$. The positions of all non-hydrogen host atoms were obtained by direct methods and the positions of non-hydrogen guest atoms were located in difference electron density maps. The methyl carbons of the *tert*-butylphenyl groups of the host molecules were found to be disordered and were modelled over two positions with site occupancy factors of 0.29 (atoms labelled with suffix A) and 0.71 (atoms labelled with suffix B).

All non-hydrogen atoms were refined with anisotropic temperature factors. The hydroxyl hydrogen atoms of the host molecule were located in difference electron density maps and refined with simple bond length constraints. The remaining hydrogen atoms were placed with geometric constraints and refined with isotropic temperature factors equal to $1.2xU_{eq}$ of their parent atoms. No hydrogen atoms were placed on the disordered methyl carbons. The structure refined to $R_1 = 0.0600$.

TBDDDA•4ACE has Z = 2 and the asymmetric unit consists of half a host molecule and two guest molecules. There are two host molecules per unit cell located at 0,1/2,0 and 0,0,1/2 (Wyckoff position *c*), while the guest molecules lie in general positions in the unit cell. The crystal packing viewed along [001] and [100] is shown in Figure 3.24(a) and Figure 3.25(b) respectively. The packing of the host molecules in **TBDDDA•4ACE** results in criss-crossed channels running parallel to [100] and [001], in which the guest molecules are located. These channels meet at two locations in the unit cell: (0.2, 0.25, 0.5) and (0.8, 0.75, 0.5). The channels running parallel to [100] have a maximum cross-section of 4.1 Å x 4.1 Å, while the channels running parallel to [001] have a maximum cross-section of 5.3 Å x 8.4 Å.

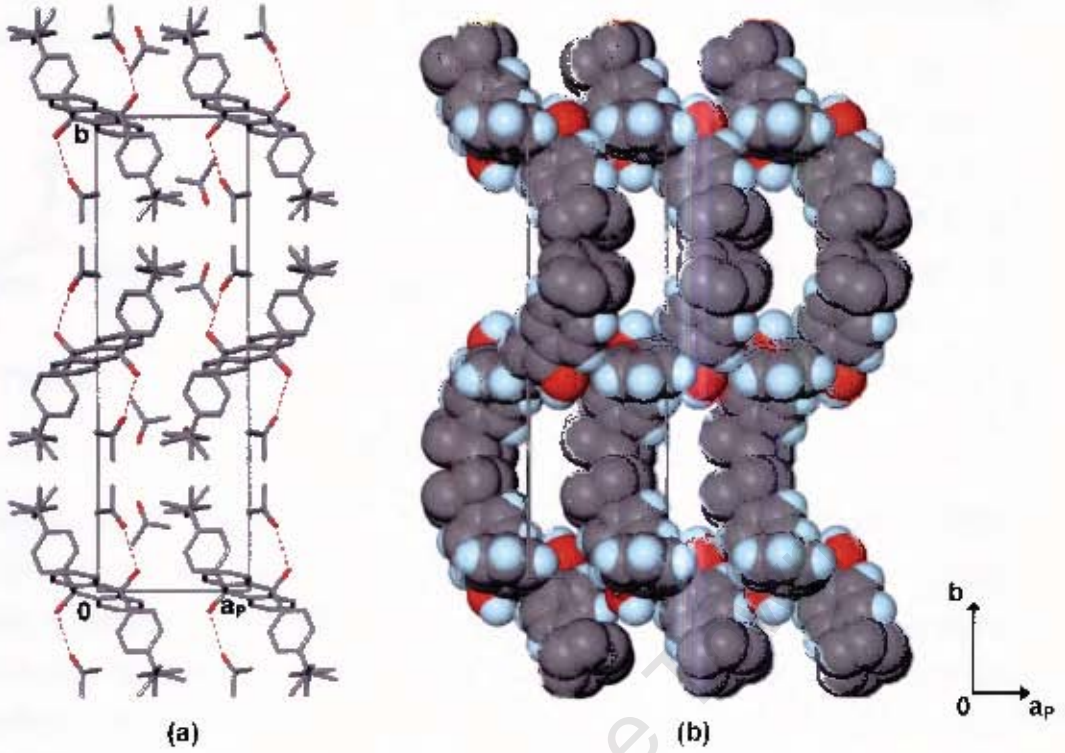

Figure 3.24 **(a)** Packing diagram of **TBDDDA•4ACE** viewed along [001] and **(b)** view down channels along [001] with guest molecules omitted and host molecules represented with van der Waals radii.

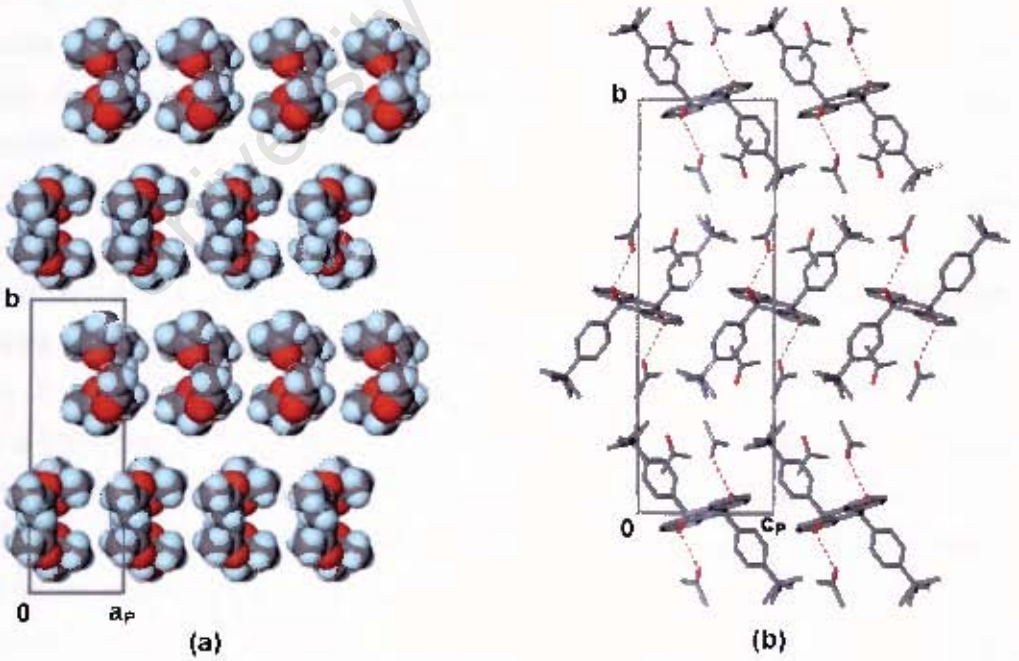

Figure 3.25 **(a)** View along [001] with host molecules omitted, showing guest molecules (represented with van der Waals radii) in channels along [100] and **(b)** Packing diagram of **TBDDDA•4ACE** viewed along [100].

These channels can be seen in Figure 3.24(b), while Figure 3.25(a) shows the rows of guest molecules located in the channels along [100]. The channels were viewed using the program SECTION,[1] which was used to view sections through the unit cell along [100]. Two of these cross sections, with the guests omitted are displayed in Figure 3.26. The channels along [001] can be clearly seen in Figure 3.26(a) and the cross-section of one the channels along [100] is highlighted in Figure 3.26(b).

Two of the guests are hydrogen bonded to the hydroxyl groups of the host molecule. The hydrogen bonding in the structure is illustrated in Figure 3.27 and hydrogen bonding details are given in Table 3.9. It is interesting to note that despite there being two hydrogen bonded guests and two guests which are not hydrogen bonded, the TG and DSC traces (Figure 3.3(a), page 65) show a single step guest desorption.

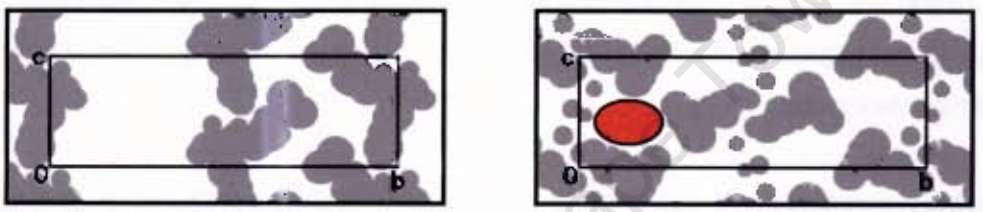

(a) 1.7 Å along [100] **(b)** 4.4 Å along [100]

Figure 3.26 SECTION plots of **TBDDDA•4ACE** (with guest molecules omitted and host molecules represented by grey areas) viewed down [100] with the unit cell sectioned at **(a)** 1.7 Å and **(b)** 4.4 Å along [100].

Figure 3.27 Host···guest hydrogen bonding interactions in **TBDDDA•4ACE**.

Table 3.9 Hydrogen bonding details of **TBDDDA•4ACE**

Donor (D)	Acceptor (A)	D–H/Å	D···A/Å	D–H···A/°
O1	O1G	0.960(1)	2.850(2)	164(3)

TBDDDA•2DMF•2ACE

$C_{34}H_{36}O_2.2(C_3H_7NO).2(C_3H_6O)$
Guests: DMF and acetone
Space group: $P\bar{1}$

a = 8.9932(1) Å	α = 108.326(1)°
b = 9.1674(1) Å	β = 92.808(1)°
c = 14.3817(2) Å	γ = 70.886(1)°
V = 1061.57(2) Å^3	
Z = 1	

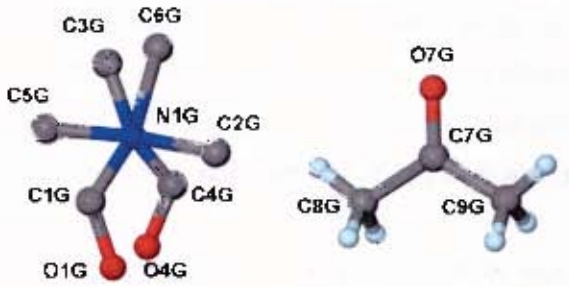

TBDDDA•2DMF•2ACE crystallises in the triclinic system. The $|E^2-1|$ values obtained by direct methods show that the structure belongs to the centrosymmetric space group $P\bar{1}$. Direct methods yielded the positions of all the non-hydrogen host atoms and the positions of non-hydrogen guest atoms were located in the difference electron density maps.

In subsequent refinements the non-hydrogen atoms of the host molecule and those of the acetone guest molecule were refined with anisotropic thermal parameters, while those of the disordered DMF molecule were refined with isotropic thermal parameters. The hydroxyl hydrogen atoms of the host molecule were located in difference electron density maps and refined with simple bond length constraints. The remaining hydrogen atoms were placed in geometrically constrained positions and assigned isotropic temperature factors equal to $1.2xU_{eq}$ of their parent atoms. No hydrogen atoms were placed on the disordered DMF guest molecule. The structure refined to R_1 = 0.0833.

The asymmetric unit consists of half a host molecule and two guest molecules, with Z = 1, as in the case of the structures in the DMF/DMSO series. The host molecule was found to be located at the origin on a centre of inversion with the guests located in general positions. The unit cell contains two DMF guest molecules and two acetone guest molecules. The DMF guest molecules are disordered over two positions and were modelled with fractional site occupancy factors of 0.72 (molecule containing atoms O1G, C1G, C2G and C3G) and 0.28 (molecule containing atoms O4G, C4G, C5G and C6G), with the two partial molecules sharing a common nitrogen site. The guest numbering scheme given above depicts the disorder in the DMF guest molecule.

TBDDDA•2DMF•2ACE is isostructural with the five compounds in the DMF/DMSO series with respect to the host molecules and the only differences are due to small changes in the location of the guest molecules. A projection of the structure along [010] is shown in Figure 3.28(a).

From this projection it can be seen that the two DMF guest molecules are hydrogen bonded to the hydroxyl groups of the host molecule, while the acetone guest molecules are not involved in hydrogen bonding. A diagram illustrating the hydrogen bonding in **TBDDDA•2DMF•2ACE** is shown in Figure 3.29 and the hydrogen-bonding details are given in Table 3.10.

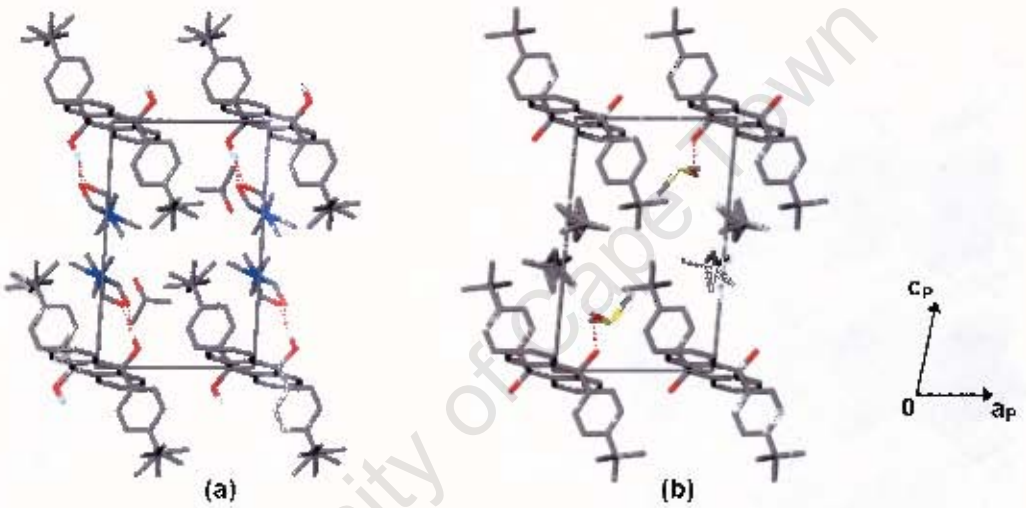

Figure 3.28 Projection of **(a) TBDDDA•2DMF•2ACE** and **(b) TBDDDA•2DMSO•2ACE** along [010].

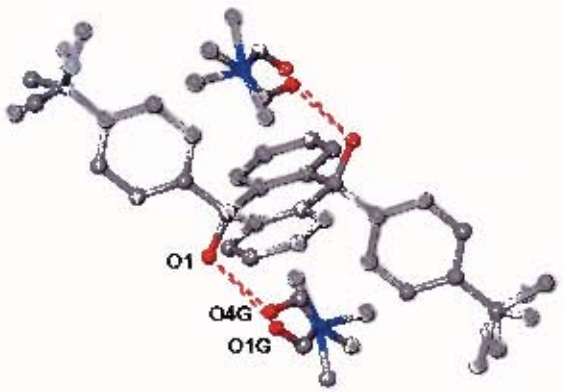

Figure 3.29 Host–guest hydrogen bonding interactions in **TBDDDA•2DMF•2ACE**.

Table 3.10 Hydrogen bonding details of **TBDDDA•2DMF•2ACE**

Donor (D)	Acceptor (A)	D–H/Å	D···A/Å	D–H···A/°
O1	O1G	0.970(1)	2.834(3)	159(3)
O1	O4G	0.970(1)	2.660(8)	161(3)

The host molecules pack to form the same restricted channels as those described for **TBDDDA•4DMF** and the guest molecules are situated in these channels. The crystal packing of the structure viewed along [010], as well as along [100] is shown in Figure 3.30.

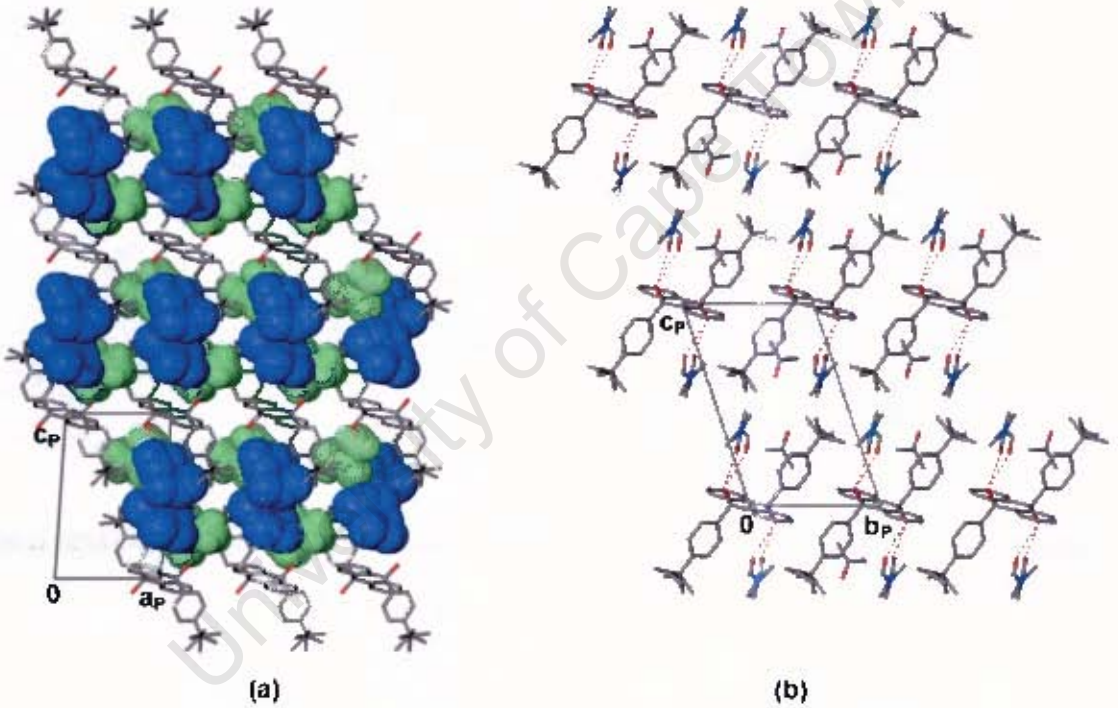

Figure 3.30 Packing diagram of **TBDDDA•2DMF•2ACE** viewed **(a)** down [010] with host molecules in stick representation and guest molecules represented with van der Waals radii (hydrogen bonded DMF guests are shown in blue and non-hydrogen bonded acetone guests are shown in green) and **(b)** down [100].

TBDDDA•2DMSO•2ACE

$C_{34}H_{36}O_2.2(C_2H_6OS).2(C_3H_6O)$
Guests: DMSO and acetone
Space group: $P\bar{1}$
a = 8.942(2) Å α = 72.25(3)°
b = 9.179(2) Å β = 79.80(3)°
c = 14.345(3) Å γ = 71.09(3)°
V = 1056.9(4) Å^3
Z = 1

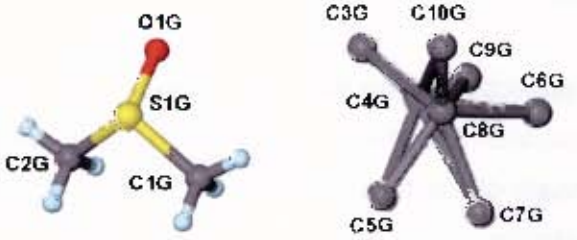

TBDDDA•2DMSO•2ACE crystallises in the triclinic system and the centrosymmetric space group $P\bar{1}$ was chosen based on the $|E^2-1$ values obtained by direct methods. The positions of all non-hydrogen host atoms were obtained by direct methods and the positions of non-hydrogen guest atoms were located in difference electron density maps.

All non-hydrogen atoms of the host molecule and of the DMSO guest molecule were refined with anisotropic temperature factors, while the non-hydrogen atoms of the acetone guest molecule, which is disordered, were refined isotropically. The hydroxyl hydrogen atoms of the host molecule were located in difference electron density maps and refined with bond length constraints. The remaining hydrogen atoms were placed with geometric constraints and refined with isotropic thermal parameters of $1.2xU_{eq}$ of their parent atoms. No hydrogen atoms were placed on the disordered acetone guest molecule. The structure refined to R_1 = 0.0785.

Once again there is half a host molecule and two guest molecules in the asymmetric unit, with Z = 1. As with the previous structures, the host molecule is required to lie on a centre of symmetry and was found to be located on the centre of inversion at the origin, while the guest molecules are located in general positions.

The unit cell contains two DMSO guest molecules and two acetone guest molecules. The acetone guest molecule is severely disordered to the extent that the oxygen atoms could not be identified and the molecule could not be modelled successfully. Instead, the eight identified atoms were assigned as carbon atoms and refined with site occupancy factors of 0.5. The disorder in the acetone guest molecule is shown in the guest numbering scheme above.

TBDDDA•2DMSO•2ACE is isostructural with **TBDDDA•2DMF•2ACE**, as well as with the five compounds in the DMF/DMSO series, with respect to the packing of the host molecules, with the only differences being due to the locations of the guests.

A projection of the structure along [010] is shown in Figure 3.28(b) (page 91), which illustrates that the two DMSO guest molecules are hydrogen bonded to the hydroxyl groups of the host molecule, while the acetone guest molecules are not involved in hydrogen bonding. A diagram illustrating the hydrogen bonding in **TBDDDA•2DMSO•2ACE** is shown in Figure 3.31 and the hydrogen-bonding details are given in Table 3.11. Table 3.12 (page 96) gives a summary of the guests and host···guest hydrogen bonding in each of the inclusion compounds for comparison.

The packing of the host molecules forms the same restricted channels as those described for **TBDDDA•4DMF**. Both guest molecules are located in these channels. The crystal packing of the structure viewed along [010] and along [100] is shown in Figure 3.32.

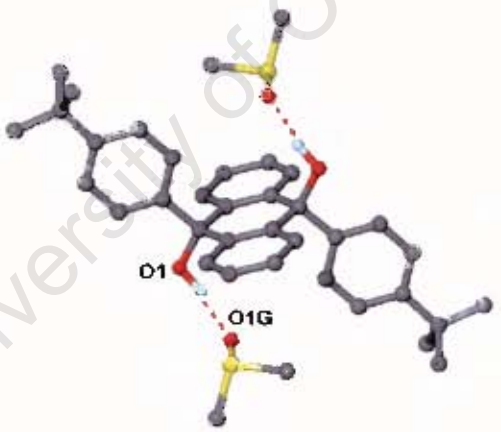

Figure 3.31 Host···guest hydrogen bonding interactions in **TBDDDA•2DMSO•2ACE**.

Table 3.11 Hydrogen bonding details of **TBDDDA•2DMSO•2ACE**

Donor (D)	Acceptor (A)	D–H/Å	D···A/Å	D–H···A/°
O1	O1G	0.970(1)	2.764(3)	169(3)

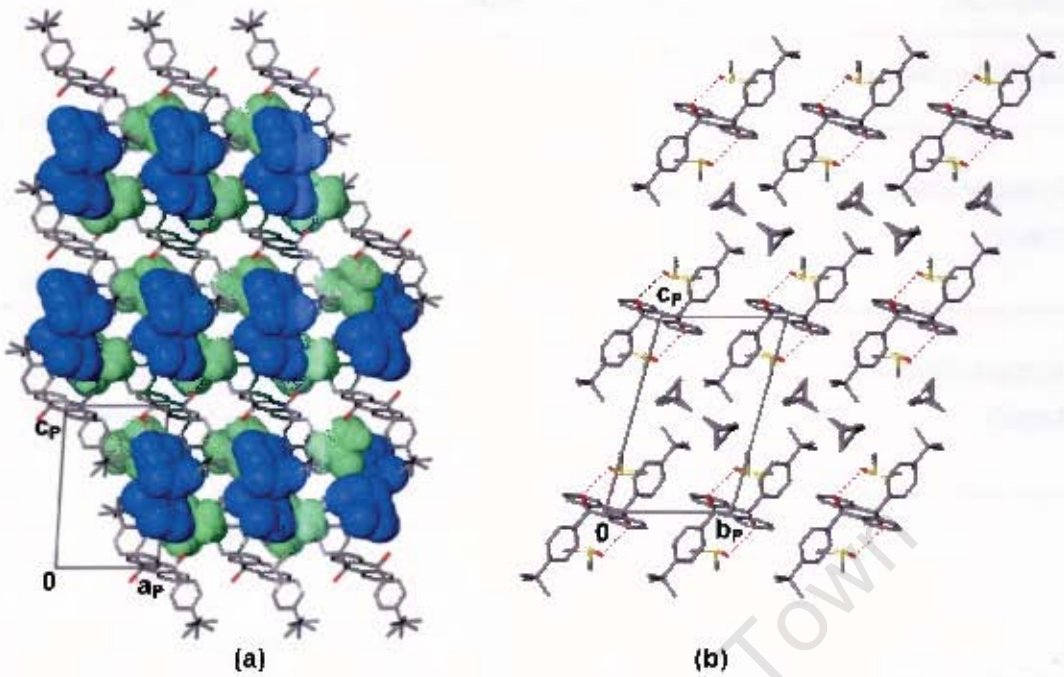

Figure 3.32 Packing diagram of **TBDDDA•2DMSO•2ACE** viewed **(a)** down [010] with host molecules in stick representation and guest molecules represented with van der Waals radii (hydrogen bonded DMSO guests are shown in blue and non-hydrogen bonded acetone guests are shown in green) and **(b)** down [100].

Table 3.12 Summary of hydrogen bonding in **TBDDDA** inclusion compounds

Compound	Guest H-bonded d(O···O)Å	Guest not H-bonded
TBDDDA•4DMF	DMF O–H·····O=C d = 2.725(2) Å	DMF Ordered
TBDDDA•3DMF•1DMSO	DMF O–H·····O=C d = 2.818(4) Å DMSO O–H·····O=S d = 2.878(6) Å	DMF Ordered, with a site occupancy factor of 0.75. DMF and DMSO share a common C atom (C5G).
TBDDDA•2DMF•2DMSO	DMSO O–H·····O=S d = 2.744(2) Å	DMF O atom disordered over two positions with site occupancy factors of 0.53 and 0.47.
TBDDDA•1DMF•3DMSO	DMSO O–H·····O=S d = 2.751(3) Å	DMF Ordered DMSO Molecule disordered over two positions, each with a site occupancy factor of 0.25. The S atom of one of the partial molecules was modelled over two positions with site occupancy factors of 0.15 and 0.1.
TBDDDA•4DMSO	DMSO O–H·····O=S d = 2.765(3) Å S atom disordered over two positions with site occupancy factors of 0.93 and 0.07.	DMSO Molecule disordered over two positions, with site occupancy factors of 0.58 and 0.42, with one C atom common to both partial molecules (C4G).
TBDDDA•4ACE	Acetone O–H·····O=C d = 2.850(2) Å	Acetone Ordered
TBDDDA•2DMF•2ACE	DMF O–H·····O=C Molecule disordered over two positions, with site occupancy factors of 0.72 and 0.28, but sharing a common N site d(O1···O1G) = 2.834(3) Å d(O1···O4G) = 2.660(8) Å	Acetone Ordered
TBDDDA•2DMSO•2ACE	DMSO O–H·····O=S d = 2.764(3) Å	Acetone Severely disordered

KINETICS OF ENCLATHRATION

The kinetics of enclathration of acetone vapour by **TBDDDA** was studied using the automated magnetic suspension balance described in Chapter 2. The kinetic measurements were carried out by exposing finely powdered host compound to acetone vapour at fixed temperatures, but at various vapour pressures of acetone, and recording the mass increase with time.

TBDDDA takes up acetone from the vapour to form the inclusion compound **TBDDDA•4ACE** with H:G = 1:4. Experiments were carried out at three temperatures: At T = 290 K experiments were performed at five different vapour pressures ranging from 86 torr to 158 torr; at T = 298 K experiments were carried out at five vapour pressures ranging from 140 torr to 223 torr and at T = 306 K experiments were carried out at four vapour pressures of acetone ranging from 161 torr to 217 torr. The data obtained were converted to extent of reaction (α) versus time curves and the curves obtained for T = 290 K are shown in Figure 3.33 as an example.

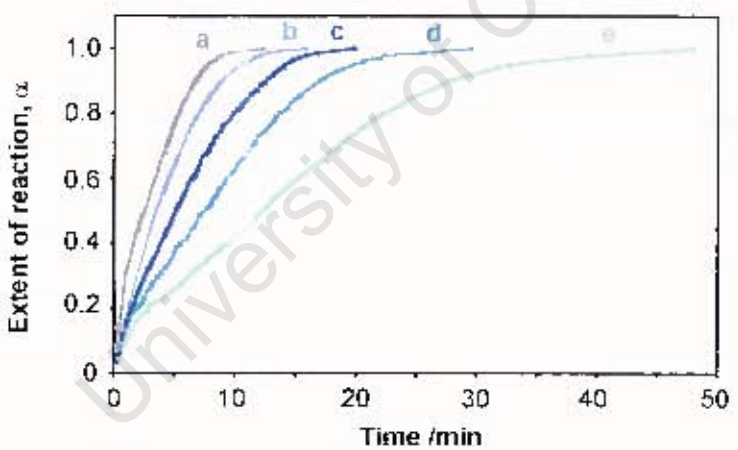

Figure 3.33 Isothermal curves at T = 290 K with vapour pressures of **(a)** 158 torr, **(b)** 140 torr, **(c)** 118 torr, **(d)** 100 torr and **(e)** 86 torr.

At each temperature the kinetic curves were found to best fit the contracting volume equation,[2] namely $f(\alpha) = 1-(1-\alpha)^{1/3}$, and the rate constants, k_{obs}, were derived. The rate of the enclathration reaction is proportional to the vapour pressure of the guest at a particular temperature and it was noted that in order for the apohost to combine with acetone, a threshold pressure, P_0, of the guest is required.

Plots of k_{obs} versus the pressure of the guest, P, are shown in Figure 3.34, and yielded the following P_0 values at the indicated temperatures: 62 torr (290 K), 115 torr (298 K), 127 torr (306 K). An interesting feature of the kinetics is that for a given pressure of acetone vapour, the rate of the reaction decreases with increasing temperature and the reaction therefore displays anti-Arrhenius behaviour. This is clearly illustrated in Figure 3.34, where for example, at a pressure of 140 torr, k_{obs} is 0.061 min ^{1} at 290 K and 0.020 min^{-1} at 298 K.

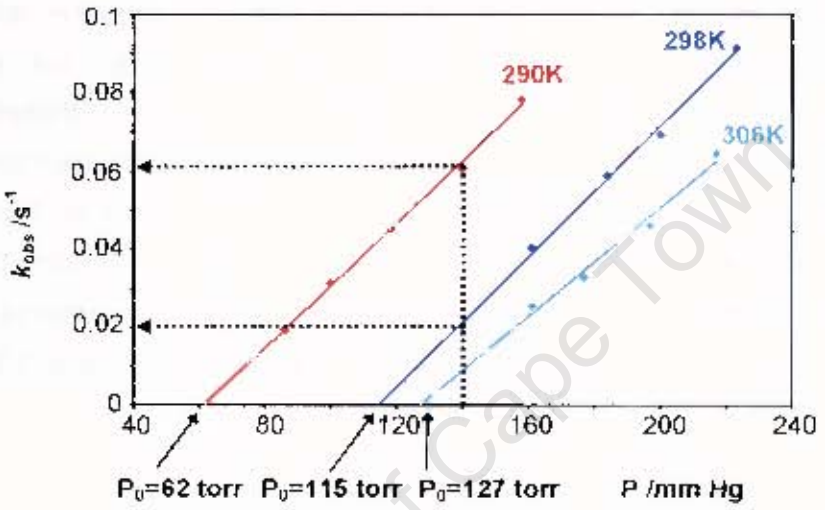

Figure 3.34 Plot of k_{obs} versus the pressure of the guest, P.

KINETICS OF DESORPTION

Using the same automated magnetic suspension balance, the kinetics of desorption of the acetone inclusion compound was studied by subjecting the system, containing the sample of the acetone inclusion compound, to vacuum at various temperatures. The resulting desorption curves were deceleratory and were converted to extent of reaction (α) versus time curves. These curves were found to fit the first order equation,[2] namely $f(\alpha) = -\ln(1-\alpha)$, over virtually the complete decomposition range (α = 0.05 to 0.95) and the rate constants, k_{obs}, were derived. The α versus time curves obtained are shown in Figure 3.35. The semilogarithmic plot of ln k_{obs} versus 1000 K/T is shown in Figure 3.36 and yielded an activation energy of 48.4 kJ.mol^{-1}.

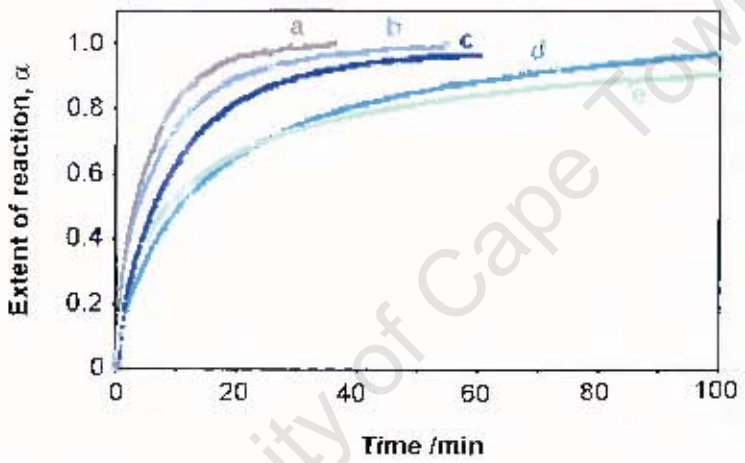

Figure 3.35 Extent of reaction (α) versus time curves for desorption of **TBDDDA•4ACE** at **(a)** 45°C, **(b)** 38°C, **(b)** 33°C, **(d)** 28°C and **(e)** 20°C.

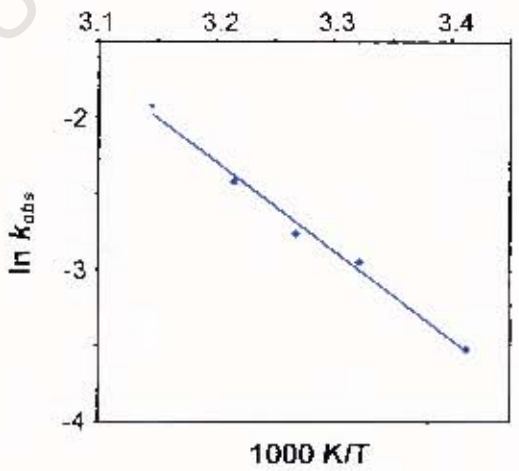

Figure 3.36 Semilogarithmic plot of ln k_{obs} versus 1000 K/T.

SUMMARY AND DISCUSSION

The inclusion chemistry of the host *trans*-9,10-dihydroxy-9,10-bis(p-*tert*-butylphenyl)-9,10-dihydroanthracene was investigated. It had previously been shown that this compound forms inclusion compounds with acetone, diethyl ether and benzene as guests.[3,4] In this study it was found that this diol host also forms inclusion compounds with the guests DMF and DMSO. Thermal analysis of these two inclusion compounds was carried out and the crystal structures were elucidated.

Competition experiments were performed in order to determine whether the host would selectively include either of these two guests. The results of these competition experiments show that, when dissolved in a mixture of the two guests, the host compound forms clathrates containing both guests in selected ratios. The graph obtained is unusual and different to the typical curves obtained for competition experiments displayed in Figure 1.6 (page 11). The result is a completely tuneable system in which five different inclusion compounds can be obtained, depending on the mole fractions of the two guests in the starting solution.

The five compounds in this series were all found to crystallise in the space group $P\bar{1}$, with a host:total guest ratio of 1:4. In each case the asymmetric unit consists of half a host molecule and two guest molecules with Z = 1. In each of the structures the host molecule is located at the origin on a centre of inversion and the compounds are isostructural with respect to the packing of the host molecules. The guest molecules are located in general positions and in each case two of the guest molecules are hydrogen bonded to the hydroxyl groups of the host molecule.

In each of the structures the host molecules are packed in a series of continuous ribbons forming restricted channels within this framework, containing the guest molecules. Within these channels, there are small variations in the positions of the guest molecules between the five structures. The changes which occur in the positions of the guest molecules are summarised in a schematic diagram given in Figure 3.37.

The structure of the non-porous α-phase was also elucidated and was found to crystallise in the space group $P2_1/c$, with one complete host molecule and one half host molecule in the asymmetric unit. There are six molecules per unit cell, four of

which are located in general positions and four of which are located on centres of inversion at Wyckoff position *c*.

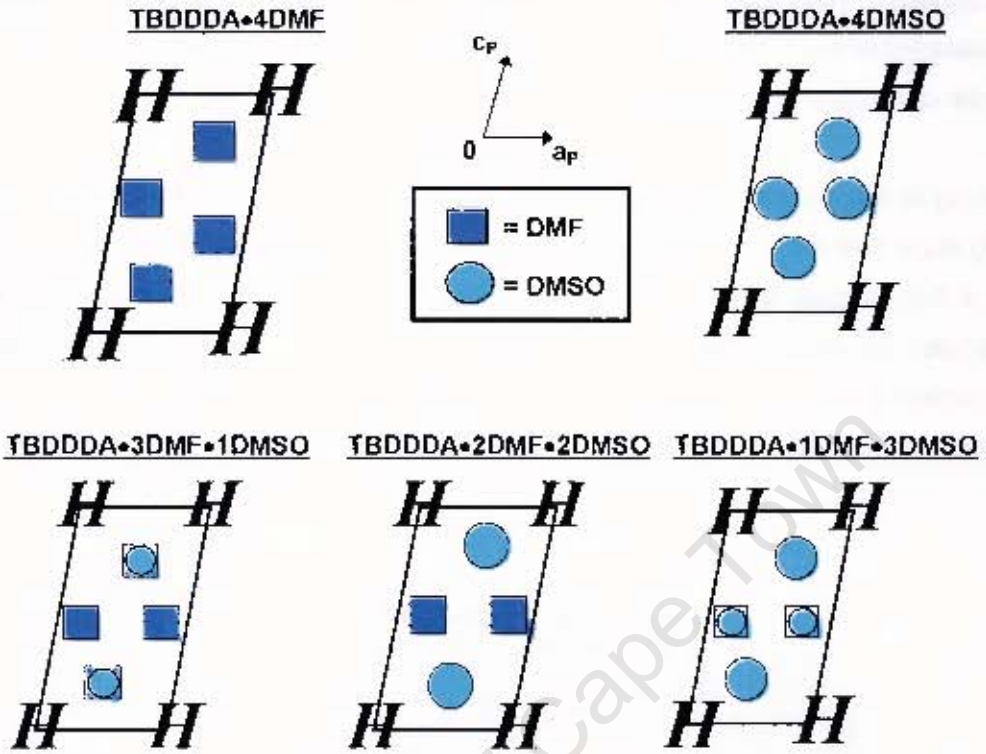

Figure 3.37 Schematic diagram summarising the differences between the five structures in the DMF/DMSO series.

The inclusion compound with acetone, **TBDDDA•4ACE**, crystallises in the space group $P2_1/c$ with H:G = 1:4 and Z = 2. The host molecules are located at Wyckoff position *c* and the guest molecules are located in general positions. The host molecules pack to form criss-crossed channels running parallel to [100] and [001] in which the guest molecules are located. **TBDDDA•2DMF•2ACE** and **TBDDDA•2DMSO•2ACE** both crystallise in the space group $P\bar{1}$ with Z = 1 and are isostructural with the compounds in the DMF/DMSO series.

The kinetics of enclathration of acetone vapour by the host was studied using an automated magnetic suspension balance and it was found that the enclathration reaction displays anti-Arrhenius behaviour. This has been observed previously for the enclathration of acetone by the related host *trans*-9,10-dihydroxy-9,10-diphenyl-9,10-dihydroanthracene.[5] This phenomenon arises from the threshold pressure, P_0,

required to start the enclathration reaction. These threshold pressures increase with increasing temperatures, which is consistent with the inclusion compound having a greater propensity to decompose at higher temperatures. This threshold pressure phenomenon has also been observed in the absorption of ethyl acetate by anthracenebisresorcinol, which was monitored by pressure measurements, X-ray powder diffraction and thermal analysis.[6]

Looking at the structure of the apohost, van der Waals plots of the surface (Figure 3.38) show that the hydroxyl groups protrude from the ab plane, which suggests that this is the reactive face, which presents free OH donors for incoming acetone gas molecules for incipient host-guest hydrogen bonding. This is similar to the situation encountered with the structure of 1,1,6,6-tetraphenyl-hexa-2,4-diyne-1,6-diol, a host compound which also enclathrates acetone vapour.[7]

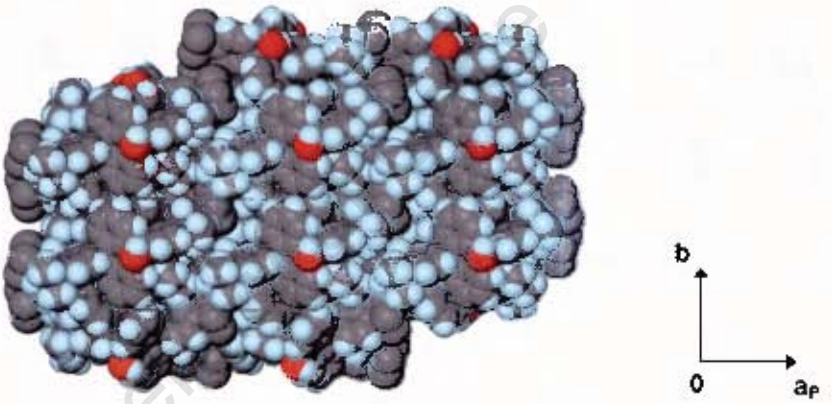

Figure 3.38 Packing of **TBDDDA** along [001] showing exposed OH groups.

The kinetics of desorption of the acetone inclusion compound was investigated and the desorption process was found to have a low activation energy of 48.4 $kJ.mol^{-1}$. Similar results were obtained for the desorption of acetone from the inclusion compound it forms with 2,2'-bis(2,7-dichloro-9-hydroxy-9-fluorenyl)-biphenyl.[8]

REFERENCES

[1] L.J. Barbour, SECTION, A computer program for the graphic display of cross sections through a unit cell, *J. Appl. Cryst.*, 1999, **32**, 353.

[2] A.K. Galwey and M.E. Brown, *Handbook of Thermal analysis and Calorimetry*, ed. M.E. Brown, Elsevier Science B.V., Amsterdam, 1998, p. 162.

[3] L.J. Barbour, *Clathration by Diol Hosts: Thermodynamics and structure*, *PhD Thesis*, University of Cape Town, 1994.

[4] L.J. Barbour, M.R. Caira and L.R. Nassimbeni, *J. Chem. Soc., Perkin Trans. 2*, 1993, 1413.

[5] L.J. Barbour, M.R. Caira and L.R. Nassimbeni, *J. Chem. Soc., Perkin Trans. 2*, 1993, 2321.

[6] T. Dewa, K. Eudo and Y Aoyama, *J. Am. Chem. Soc.*, 1998, **120**, 8933.

[7] D.R. Bond, L. Johnson, L.R. Nassimbeni and F. Toda, *J. Solid State Chem.*, 1991, **92**, 68.

[8] M.R. Caira. A. Coetzee, L.R. Nassimbeni, E. Weber and A. Wierig, *J. Chem. Soc., Perkin Trans. 2*, 1997, 237.

Chapter 4

STRUCTURE AND KINETIC REACTIVITY OF INCLUSION COMPOUNDS OF WEB24 WITH VOLATILE GUESTS

*The host 9,9'-(Biphenyl-4,4'-diyl)difluoren-9-ol (abbreviated **WEB24**) forms inclusion compounds with N,N-dimethylacetamide (DMA), 1,4-dioxane and methyl ethyl ketone (MEK). With DMA this host was found to form two different inclusion compounds with H:G ratios of 1:2 and 1:4. Thermal analysis of these compounds has been carried out and the structures have been elucidated, as well as the structure of the host α-phase, the apohost. ^{13}C solid state CP/MAS NMR was used to analyse these compounds as well as to monitor the desorption of the guest from each of these clathrates. The kinetics of desorption of the inclusion compounds with DMA and 1,4-dioxane were measured by a series of isothermal TG experiments. A brief investigation of the nucleation and crystal growth of the inclusion compound with 1,4-dioxane was carried out which involved measuring the solubility of the compound in 1,4-dioxane as well as carrying out cooling crystallisations at different temperatures.*

Crystallographic data, experimental and refinement parameters are given in Table 4.1. Final atomic coordinates, bond lengths and angles, torsion angles, thermal parameters and tables of observed and calculated structure factors for each of the crystal structures are given in the appendices.

COMPLEX PREPARATION

Suitable crystals were grown by slow evaporation at room temperature. The crystals of the apohost **WEB24** were obtained by crystallising the host from acetonitrile. Crystals of the inclusion compounds with DMA with different H:G ratios were obtained by crystallisation at different temperatures. Crystals of the inclusion compound with H:G = 1:4 were obtained by evaporating a solution of **WEB24** at 25°C, while those of the inclusion compound with DMA with H:G = 1:2 were formed by evaporating a solution of **WEB24** at 62°C.

The inclusion compounds obtained and their abbreviations are as follows:

Host α-phase: **WEB24**
WEB24 + DMA (H:G = 1:4): **WEB24•4DMA**
WEB24 + DMA (H:G = 1:2): **WEB24•2DMA**
WEB24 + 1,4-dioxane (H:G = 1:3): **WEB24•3DIOX**
WEB24 + methyl ethyl ketone (H:G = 1:2): **WEB24•2MEK**

The guest numbering schemes are given at the beginning of each structure analysis and the host numbering scheme is given below:

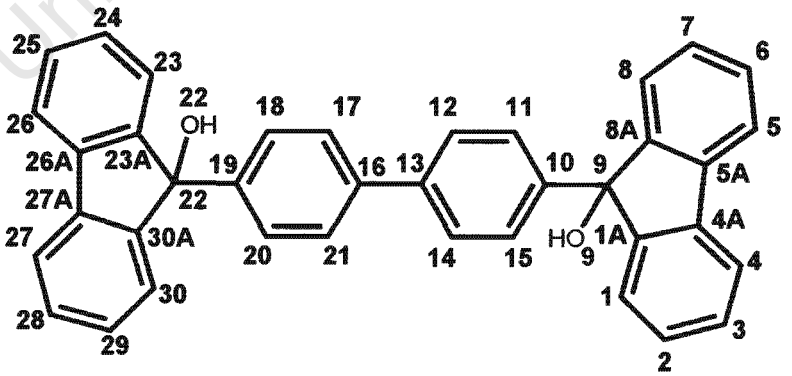

Table 4.1 Crystal data, experimental and refinement parameters

	WEB24	**WEB24•4DMA**	**WEB24•4DMA***
Molecular formula	$C_{38}H_{26}O_2$	$C_{38}H_{26}O_2.4(C_4H_9NO)$	$C_{38}H_{26}O_2.4(C_4H_9NO)$
Host:guest ratio	–	1:4	1:4
M_r/g.mol^{-1}	514.59	863.08	863.08
Crystal symmetry	Monoclinic	Triclinic	Triclinic
Space group	$P2_1/n$	$P\bar{1}$	$P\bar{1}$
a/Å	5.8002(1)	10.2961(1)	20.1219(3)
b/Å	14.4736(3)	14.9893(2)	15.1319(2)
c/Å	15.7510(3)	17.8825(3)	17.3526(3)
α/°	90	108.255(1)	108.555(1)
β/°	91.141(1)	91.524(1)	91.152(1)
γ/°	90	109.284(1)	106.749(1)
V/Å^3	1322.03(4)	2447.71(6)	4759.90(7)
Z	2	2	4
μ (Mo-Kα)/mm^{-1}	0.078	0.076	
Temperature (K)	298(2)	298(2)	113(2)
Range scanned, θ (°)	1.91 - 27.49	1.60 - 27.48	
Index range	h:0-7, k:±18, l:±20	h:-12-13, k:±19, l:±23	
No. reflections collected	5370	18802	
No. unique reflections	3027 (R_{int} = 0.0160)	11071 (R_{int} = 0.0361)	
No. reflections with I>2σ(I)	2479	5786	
Data/restraints/parameters	3027 / 1 / 185	11071 / 18 / 597	
Goodness of fit, S	1.034	1.112	
Final R indices (I>2σ(I))	R_1 = 0.0429, wR_2 = 0.1092	R_1 = 0.0849, wR_2 = 0.2356	
R indices (all data)	R_1 = 0.0540, wR_2 = 0.1162	R_1 = 0.1567, wR_2 = 0.2812	
Largest diff peak and hole (e.Å^{-3})	0.229; -0.180	0.752; -0.341	

** **WEB2•4DMA** was found to undergo a phase change at low temperature, but the data collected at 113K did not allow the structure to be refined to a satisfactory level and only unit cell parameters and the space group are reported.*

Table 4.1 (cont.) Crystal data, experimental and refinement parameters

	WEB24•2DMA	WEB24•3DIOX	WEB24•2MEK
Molecular formula	$C_{38}H_{26}O_2$. $2(C_4H_9NO)$	$C_{38}H_{26}O_2$. $3(C_4H_8O_2)$	$C_{38}H_{26}O_2$. $2(C_4H_8O)$
Host:guest ratio	1:2	1:3	1:2
M_r/g.mol^{-1}	688.83	778.90	658.80
Crystal symmetry	Triclinic	Monoclinic	Monoclinic
Space group	$P\bar{1}$	$P2_1/c$	$P2_1/n$
a/Å	7.9629(3)	13.1096(3)	7.7993(1)
b/Å	9.0266(4)	12.8883(2)	21.9845(4)
c/Å	13.5092(7)	12.0038(2)	21.0296(4)
α/°	77.015(2)	90	90
β/°	83.033(2)	92.247(1)	94.552(1)
γ/°	84.212(2)	90	90
V/Å^3	936.47(7)	2026.61(7)	3594.4 (1)
Z	1	2	4
μ(Mo-Kα)/mm^{-1}	0.077	0.085	0.076
Temperature (K)	298(2)	173(2)	173(2)
Range scanned, θ (°)	1.55 - 25.35	1.55 - 27.50	1.94 - 26.39
Index range	h:±9, k:±10, l:-11-16	h: ±17, k:15 -16, l: ±15	h: ±9, k:-27-25, l:-26-20
No. reflections collected	4708	7890	17155
No. unique reflections	3328 (R_{int} = 0.0169)	4628 (R_{int} = 0.0221)	7320 (R_{int} = 0.0382)
No. reflections with I>2σ(I)	2008	3355	5889
Data/restraints/parameters	3328 / 1 / 242	4628 / 1 / 266	7320 / 2 / 463
Goodness of fit, S	1.007	1.027	1.018
Final R indices (I>2σ(I))	R_1 = 0.0697, wR_2 = 0.1740	R_1 = 0.0469, wR_2 = 0.1045	R_1 = 0.0441, wR_2 = 0.1039
R indices (all data)	R_1 = 0.1197, wR_2 = 0.2065	R_1 = 0.0731, wR_2 = 0.1161	R_1 = 0.0583, wR_2 = 0.1120
Largest diff peak and hole (e.Å^{-3})	0.563; -0.271	0.288; -0.206	0.218; -0.182

THERMAL ANALYSIS

The thermal analysis results for each of the inclusion compounds are given in Table 4.2 and the TG and DSC traces are illustrated in Figure 4.1.

The TG and DSC traces of the apohost, **WEB24**, are given in Figure 4.1(a). The TG trace shows no mass loss, while the DSC trace shows one endotherm, endotherm C, at 308.0°C which corresponds to the melt.

The TG and DSC traces of **WEB24•4DMA** are shown in Figure 4.1(b). The TG trace shows a two step desorption with a total mass loss of 39.7%, which agrees with the calculated value for H:G = 1:4 (calc. 40.4%). The first mass loss represents the loss of two guest molecules and a transformation from the inclusion compound with H:G = 1:4 to another stable inclusion compound with H:G = 1:2. The second mass loss represents the loss of the remaining two guest molecules from the inclusion compound to form the guest-free host compound. The two step mass loss in the TG trace corresponds to endotherms A and B in the DSC trace. The third endotherm labelled C corresponds to the melting of the guest-free host compound.

For **WEB24•3DIOX**, Figure 4.1(c), the TG trace shows that the 1,4-dioxane guest is released in a single step corresponding to endotherm A in the DSC trace. The percentage mass loss of 34.0% shown by the TG trace corresponds to H:G = 1:3 (calc. 33.9%). Endotherm C in the DSC trace is due to the melt of the guest-free host compound.

In the case of **WEB24•2MEK**, Figure 4.1(d), guest release occurs in one step with a percentage mass loss of 21.1%, which corresponds to H:G = 1:2 (calc. 21.9%). The DSC trace shows two endotherms, A and C. Endotherm A corresponds to guest release, while endotherm C represents the melt of the guest-free host compound.

We note the difference in melting point of the apohost **WEB24** versus the host resulting from desorption of the three host-guest compounds (Table 4.2). This suggests the possibility of two different polymorphs. However, the solid state NMR spectra of the apohost and the three desorbed compounds are practically identical and the possibility of a new polymorph was not investigated further.

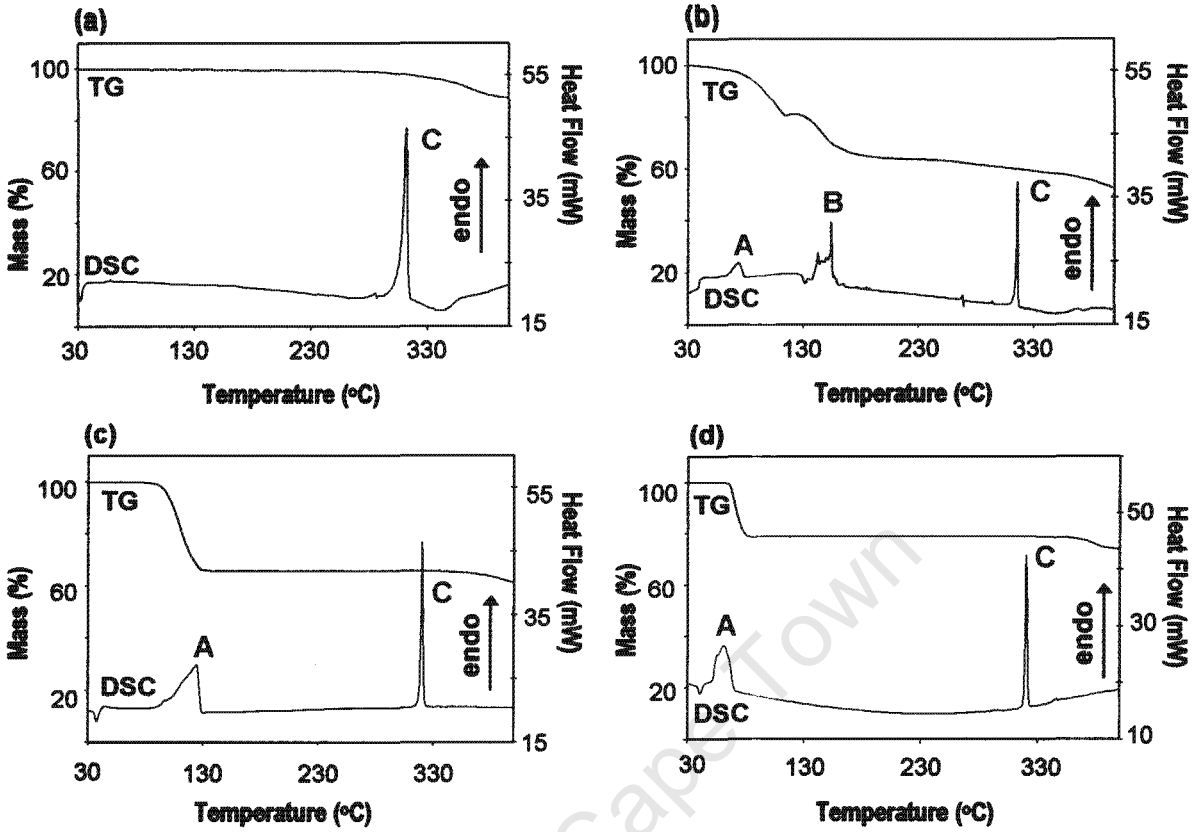

Figure 4.1 TG and DSC traces of **(a) WEB24, (b) WEB24•4DMA, (c) WEB24•3DIOX** and **(d) WEB24•2MEK.**

Table 4.2 Thermal analysis results of **WEB24** inclusion compounds

Inclusion Compound	TG Results		H:G ratio	DSC Results		
	Calc. % mass loss	Exp. % mass loss		T_{on}(°C) Peak A	T_{on}(°C) Peak B	T_{on}(°C) Peak C
WEB24	—	—	—	—	—	308.0
WEB24•4DMA	40.4	39.7	1:4	65.0	152.8	313.8
WEB24•3DIOX	33.9	34.0	1:3	104.4	—	317.8
WEB24•2MEK	21.9	21.1	1:2	50.7	—	318.0

HOT STAGE MICROSCOPY

Crystals of the inclusion compounds were observed during thermal decomposition using hot stage microscopy (HSM) and the images obtained are shown in Figures 4.2 to 4.4.

The **WEB24•4DMA** crystals (shown at room temperature in Figure 4.2(a)) became gradually opaque from 85°C to 145°C (Figure 4.2(b)). Between 145°C and 178°C the guest was released in the form of bubbles and recrystallisation took place simultaneously (Figure 4.2(c)). Melting occurred between 335°C and 336°C (Figure 4.2(d)).

The crystals of **WEB24•3DIOX** (shown at room temperature in Figure 4.3(a)) became opaque between 76°C and 85°C (Figure 4.3(b)) and, following this, bubbles of the desorbed guest were observed (Figure 4.3(c)). The crystals melted between 330°C and 331°C (Figure 4.3(d)).

The **WEB24•2MEK** crystals (shown at room temperature in Figure 4.4(a)) became gradually opaque from 30°C (Figure 4.4(b)) and bubbles of desorbed guest were observed between 63°C and 90°C (Figure 4.4(c)). The crystals melted from 332°C to 333°C (Figure 4.4(d)).

Figure 4.2 Thermal decomposition of **WEB24•4DMA** crystals.

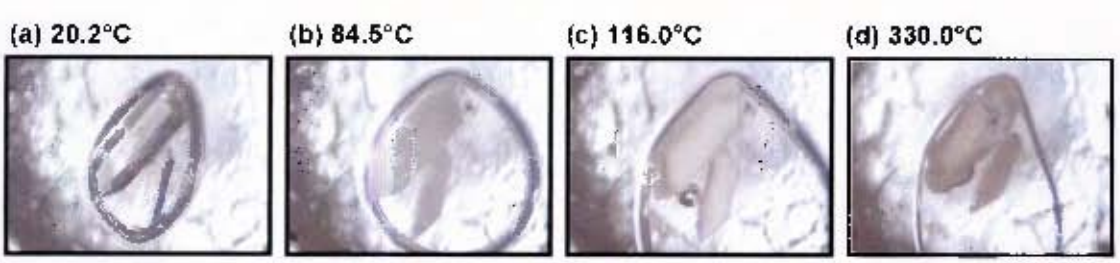

Figure 4.3 Crystals of **WEB24•3DIOX** during thermal decay.

STRUCTURE SOLUTION AND ANALYSIS

WEB24

$C_{38}H_{26}O_2$
Space group: $P2_1/n$
a = 5.8002(1) Å
b = 14.4736(3) Å β = 91.141(1)°
c = 15.7510(3) Å
V = 1322.03(4) Å^3
Z = 2

WEB24 crystallises in the monoclinic crystal system, in the space group $P2_1/n$. The positions of all non-hydrogen host atoms were obtained by direct methods. In subsequent refinements these atoms were refined with anisotropic temperature factors. The hydroxyl hydrogen atoms on the host molecule were located in the difference electron density maps and refined with simple bond length constraints and independent temperature factors. All other hydrogen atoms were placed with geometric constraints and refined with isotropic thermal parameters equal to $1.2xU_{eq}$ of their parent atoms. The structure refined to $R_1 = 0.0429$.

The structure of **WEB24** has Z = 2 with the asymmetric unit containing half a host molecule. The host molecule is located on a centre of inversion at Wyckoff position *d*. There is no hydrogen bonding between the molecules, which are packed in layers perpendicular to the a-axis.

In a particular layer, the packing pattern approximates the plane group c2mm. Within this pattern, the molecules orientated in one direction are displaced half a unit cell length along [100] upward or downward from those orientated in the other direction. The structure shows a sawtooth pattern along [101]. The crystal packing viewed down the a-axis and viewed along [101] is shown in Figure 4.5.

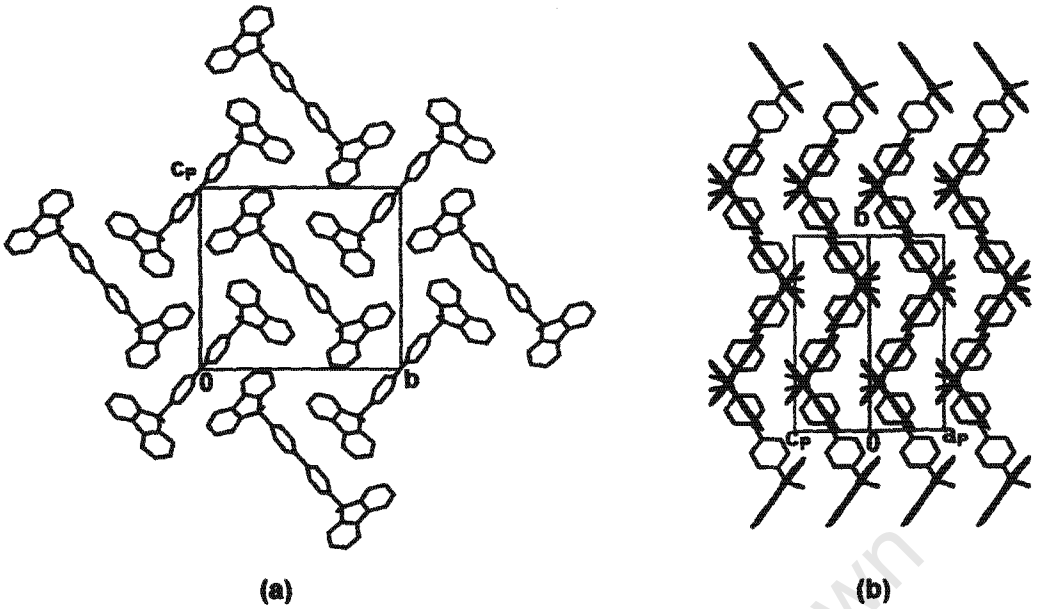

Figure 4.5 Packing diagrams of **WEB24** viewed **(a)** along [100] and **(b)** along [101].

WEB24•4DMA

$C_{38}H_{26}O_2.4(C_4H_9NO)$
Guest: N,N-dimethylacetamide
Space group: $P\bar{1}$

a = 10.2961(1) Å	α = 108.255(1)°
b = 14.9893(2) Å	β = 91.524(1)°
c = 17.8825(3) Å	γ = 109.284(1)°
V = 2447.71(6) Å^3	
Z = 2	

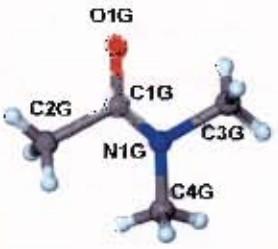

Guest 1

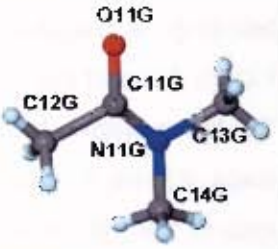

Guest 2

WEB24•4DMA was found to undergo a phase change when cooled to 113 K. Single crystal X-ray data were collected at both 298 K and 113 K. The structure at 113 K however could not be refined to a satisfactory level and so only the unit cell parameters and space group for this structure are reported. The structure of **WEB24•4DMA** at 298 K belongs to the triclinic crystal system and the centrosymmetric space group $P\bar{1}$ was chosen based on the $|E^2-1|$ values obtained by direct methods.

Direct methods yielded the positions of all non-hydrogen host atoms. The non-hydrogen guest atoms were located in difference electron density maps. All non-hydrogen atoms were refined with anisotropic temperature factors. The host hydroxyl hydrogen atoms were located in the difference electron density maps and refined with simple bond length constraints and independent temperature factors. All other hydrogen atoms were placed with geometric constraints and assigned isotropic temperature factors of $1.2xU_{eq}$ of their parent atoms. Due to the data being collected at 298K, the values of the U_{eq} of the guest atoms are high (maximum = 0.22 Å^2). The guest numbering scheme is given above and guest 3 and guest 4 were numbered in the same way with, for example, the oxygen atoms labelled O21G and O31G. The structure refined to R_1 = 0.0849.

WEB24•4DMA has Z = 2 and H:G = 1:4. The asymmetric unit consists of one host molecule and four guest molecules. Both the host molecules and guest molecules are located in general positions. Packing diagrams of the structure viewed down [100] and [001] are shown in Figure 4.6. The host molecules are packed in layers which lie parallel to the ac plane and are located at y = 0.25 and y = 0.75, giving rise

to a very open structure. The guest molecules are located between these layers. Each host molecule is hydrogen bonded to two of the guest molecules via the hydroxyl groups. The other two guest molecules are not involved in hydrogen bonding. A diagram illustrating the hydrogen bonding in **WEB24•4DMA** is shown in Figure 4.7 and the hydrogen bonding details are given in Table 4.3. We note that the TG trace shows a two step desorption, with corresponding endotherms in the DSC trace (Figure 4.1(b), page 110), and we can infer that the first mass loss is due to the loss of the non-hydrogen bonded guest molecules and the second due to the loss of the hydrogen bonded guests, which are held more tightly in the structure.

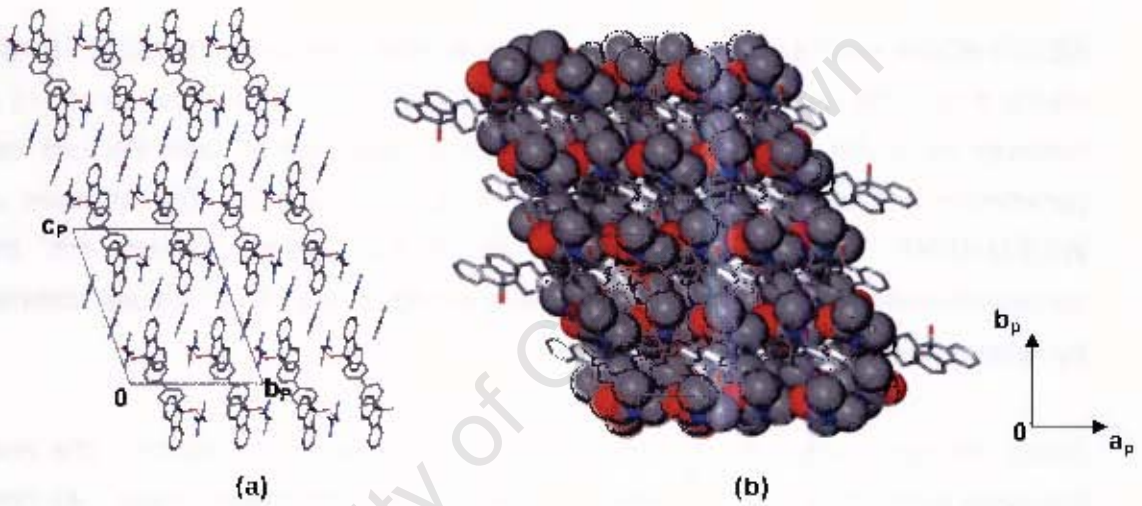

Figure 4.6 Packing diagrams of **WEB24•4DMA** viewed **(a)** down [100] and **(b)** down [001], with the guest molecules represented with van der Waals radii.

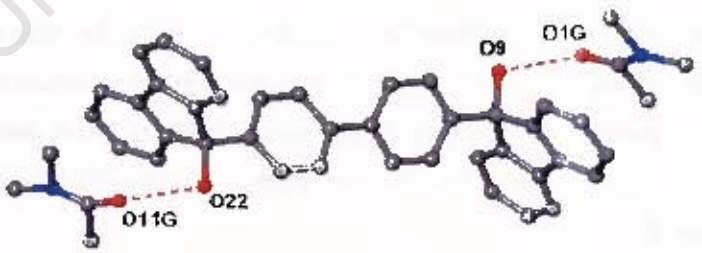

Figure 4.7 Host···guest hydrogen bonding in **WEB24•4DMA**.

Table 4.3 Hydrogen bonding details in **WEB24•4DMA**

Donor (D)	Acceptor (A)	D–H/Å	D···A/Å	D–H···A/°
O9	O1G	0.970(1)	2.721(3)	172(3)
O22	O11G	0.970(1)	2.747(3)	178(4)

WEB24•2DMA

$C_{38}H_{26}O_2.2(C_4H_9NO)$	
Guest: N,N-dimethylacetamide	
Space group: $P\bar{1}$	
a = 7.9629(3) Å	α = 77.015(2)°
b = 9.0266(4) Å	β = 83.033(2)°
c = 13.5092(7) Å	γ = 84.212(2)°
V = 936.47(7) Å^3	
Z = 1	

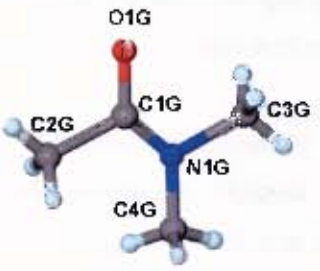

WEB24-2DMA belongs to the triclinic crystal system. The E^2-1 | values obtained by direct methods show that the structure belongs to the centrosymmetric space group, $P\bar{1}$, which was confirmed by the successful refinement of the structure. The positions of all non-hydrogen host atoms were obtained by direct methods. The non-hydrogen guest atoms were located in difference electron density maps and all non-hydrogen atoms were refined with anisotropic temperature factors.

The hydroxyl hydrogen atoms on the host molecule were located in the difference electron density maps and refined with simple bond length constraints and independent temperature factors. All remaining hydrogen atoms were placed in geometrically constrained positions and refined with isotropic temperature factors of 1.2xU_{eq} of their parent atoms. The structure refined to R_1 = 0.0697.

The structure of **WEB24•2DMA** has Z = 1 and H:G = 1:2. There is half a host molecule and one guest molecule in the asymmetric unit. The host molecules are located on a centre of inversion at Wyckoff position *d* and the N,N-dimethylacetamide guest molecules are located in general positions.

The crystal packing is shown in Figure 4.8, viewed (a) down the b-axis and (b) down the a-axis. The host molecules pack to form channels along [-1 0 1] in which the guest molecules are situated. These channels can be clearly seen in Figure 4.9. The channels were also examined using the program SECTION,[1] which was used to view sections through the unit cell down the a-axis. These sections are illustrated in Figure 4.10.

The cross-section of the channels can be seen shifting through the cell along the c-axis, which corresponds to channels along [-1 0 1]. The cross-sectional area of the channels is approximately 5.9 Å x 7.1 Å where the guests are located and varies only slightly from this size.

Each host molecule is hydrogen bonded to two guest molecules via the hydroxyl groups. A diagram illustrating the hydrogen bonding in **WEB24•2DMA** is shown in Figure 4.11 and the hydrogen bonding details are given in Table 4.4.

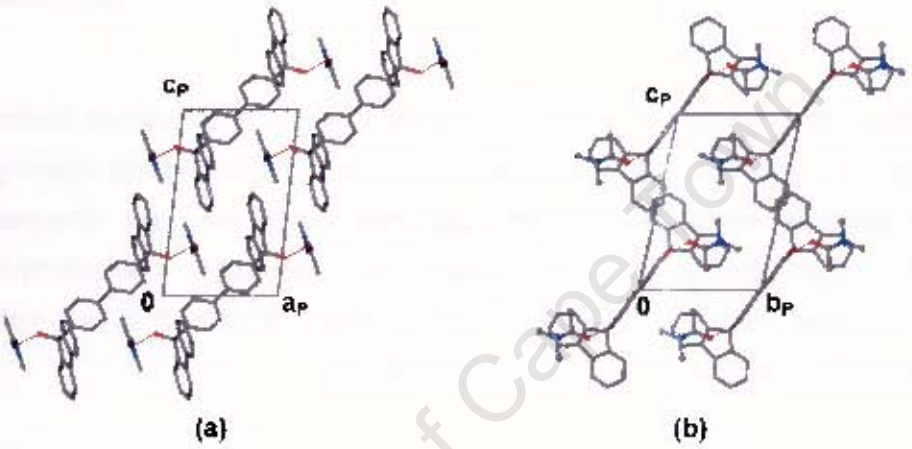

Figure 4.8 Packing diagram of **WEB24•2DMA** viewed down **(a)** the b-axis and **(b)** the a-axis (guest molecules are shown in ball and stick representation for clarity).

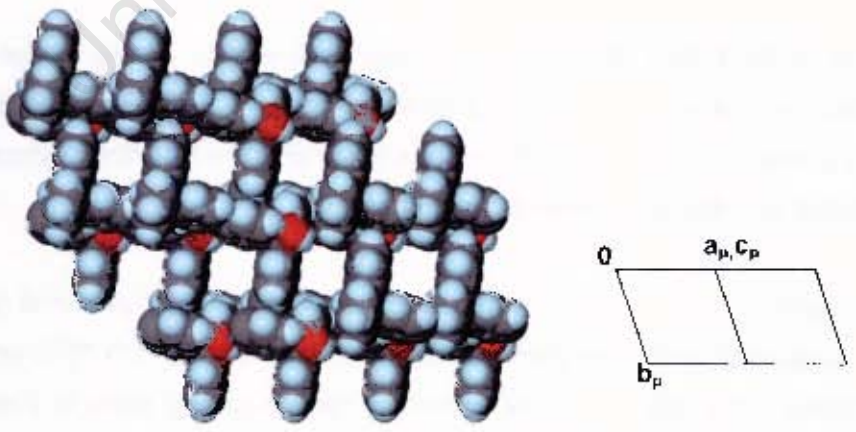

Figure 4.9 View down the channels of **WEB24•2DMA** along [-1 0 1] with the guests omitted and the host molecules represented with van der Waals radii.

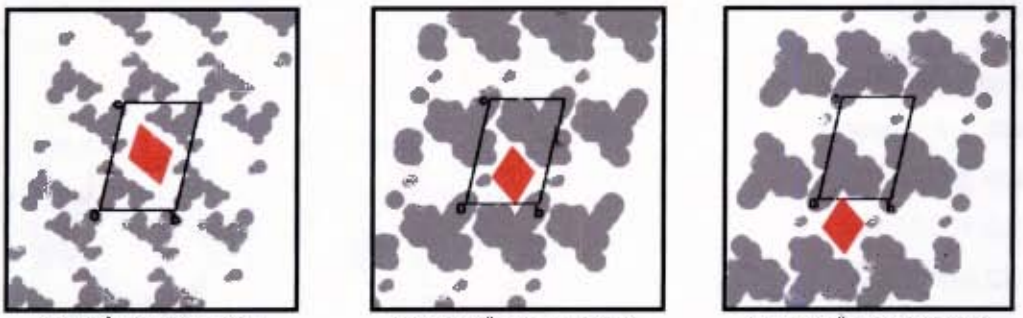

(a) 0 Å along [100] (b) 1.6 Å along [100] (c) 6.3 Å along [100]

Figure 4.10 SECTION plots of **WEB24•2DMA** (with guest molecules omitted and host molecules represented by grey areas) viewed down [100] with the unit cell sectioned at **(a)** 0 Å, **(b)** 1.6 Å and **(c)** 6.3 Å along [100]. The shifting cross-section of one of the channels along [-1 0 1] is highlighted in red.

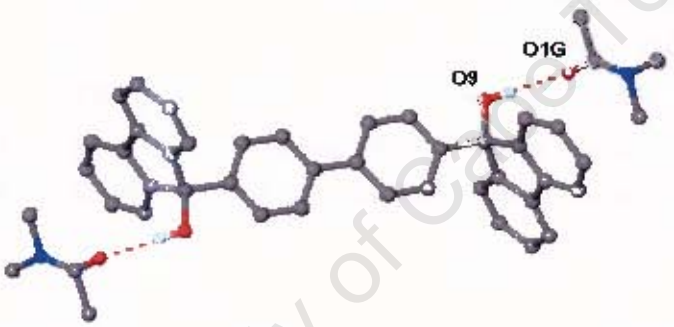

Figure 4.11 Host···guest hydrogen bonding in **WEB24•2DMA.**

Table 4.4 Hydrogen bonding details of **WEB24•2DMA**

Donor (D)	Acceptor (A)	D–H/Å	D···A/Å	D–H···A/°
O9	O1G	0.96(2)	2.744(3)	173(3)

WEB24•3DIOX

$C_{38}H_{26}O_2.3(C_4H_8O_2)$
Guest: 1,4-dioxane
Space group: $P2_1/c$
a = 13.1096(3) Å
b = 12.8883(2) Å β = 92.247(1)°
c = 12.0038(2) Å
V = 2026.61(7) Å^3
Z = 2

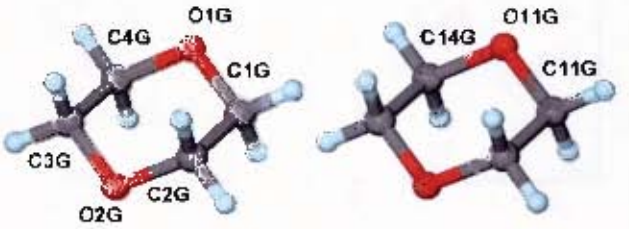

Guest 1 Guest 2

WEB24•3DIOX belongs to the monoclinic crystal system and crystallises in the space group $P2_1/c$. Direct methods yielded the positions of all non-hydrogen host atoms. The non-hydrogen guest atoms were located in difference electron density maps and in subsequent refinements all non-hydrogen atoms were refined with anisotropic temperature factors. The host hydroxyl hydrogens were located in the difference electron density maps and refined with simple bond length constraints and independent temperature factors. All remaining hydrogen atoms were placed with geometric constraints and refined with isotropic temperature factors equal to $1.2xU_{eq}$ of their parent atoms. The structure refined to $R_1 = 0.0469$.

WEB24•3DIOX has Z = 2 with H:G = 1:3. The asymmetric unit consists of half a host molecule and one and a half guest molecules. The host molecules are located on a centre of inversion at Wyckoff position *d*. The half guest molecules in the asymmetric unit (labelled guest 2) are located on centres of inversion at Wyckoff position *c* and the guest 1 molecules are located in general positions. The crystal packing viewed down [001] is shown in Figure 4.12.

The structure is very open and the host molecules pack to form zigzagged layers perpendicular to the a-axis giving rise to channels along [001] in which the 1,4-dioxane guest molecules are located. These channels can be seen in Figure 4.13, viewed down [001]. The channels can be viewed using the program SECTION,[1] which shows that the channels shift in position and also change in size along the c-axis. Sections through the unit cell down [001] are shown in Figure 4.14. Looking down the c-axis, the channels initially have a cross-section of approximately 9.4 Å x 7.4 Å with the centres of the channels at half a unit cell length along the b-axis.

There is a guest 2 molecule located in the channel at 0 Å along the c-axis. Between 1.5 Å and 4.6 Å along the c-axis, the channels are split into two parts by the host molecules. There are two guest 1 molecules located at 1.9 Å and 4.0 Å along the c-axis and at these locations the narrowed part of the channel in which the guest is situated has a cross-section of 7.4 Å x 4.6 Å. The channels then reform to their original size of approximately 9.4 Å x 7.4 Å at half a unit cell length along the c-axis with the centres of the channels now at 0 Å along the b-axis. There is a guest 2 molecule located in the channel at this location.

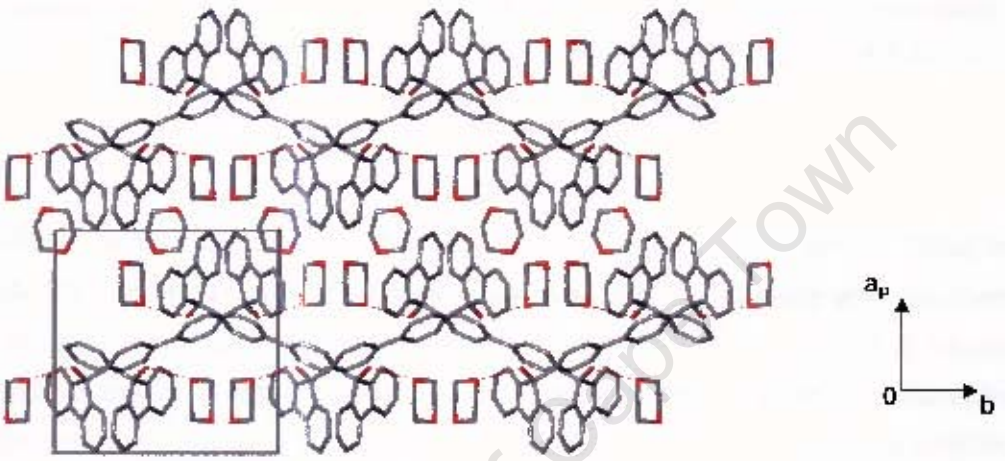

Figure 4.12 Packing diagram of **WEB24•3DIOX** viewed down [001].

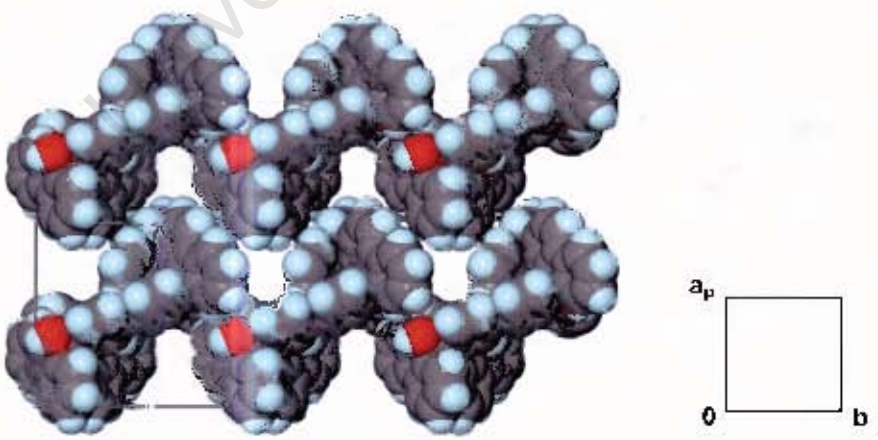

Figure 4.13 View down [001] showing the channels of **WEB24•3DIOX** with the guests omitted and the host molecules represented with van der Waals radii.

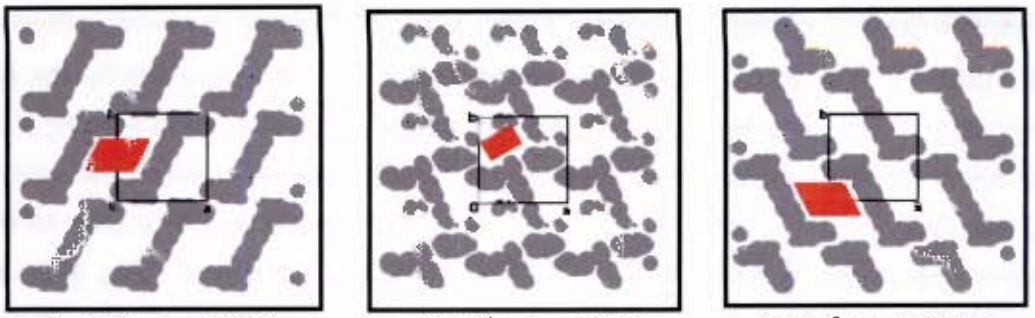

(a) 0 Å along [001] (b) 4 Å along [001] (c) 6 Å along [001]

Figure 4.14 SECTION plots of **WEB24•3DIOX** (with guest molecules omitted and host molecules represented by grey areas) viewed down [001] with the unit cell sectioned at (a) 0 Å, (b) 4 Å and (c) 6 Å along [001]. The channel in which a guest is located at that height in the unit cell is highlighted in red.

The guest 1 molecules located in general positions are hydrogen bonded to the host molecules, whereas the guest 2 molecules located on centres of inversion are not involved in hydrogen bonding. Both 1,4-dioxane guest molecules are in the chair conformation. The hydrogen bonding in the structure is shown in Figure 4.15 and the hydrogen bonding details are given in Table 4.5. Despite guest 1 being hydrogen bonded to the host and guest 2 not being hydrogen bonded, we note that the TG and DSC traces shown in Figure 4.1(c) (page 110) show a one step desorption.

Figure 4.15 Host···guest hydrogen bonding in **WEB24•3DIOX.**

Table 4.5 Hydrogen bonding details in **WEB24•3DIOX**

	Acceptor (A)	D–H/Å	D···A/Å	D–H···A/°
O9	O1G	0.970(1)	2.743(1)	164(2)

WEB24•2MEK

$C_{38}H_{26}O_2.2(C_4H_8O)$
Guest: Methyl ethyl ketone
Space group: $P2_1/n$
a = 7.7993(1) Å
b = 21.9845(4) Å β = 94.552(1)°
c = 21.0296(4) Å
V = 3594.4(1) Å^3
Z = 4

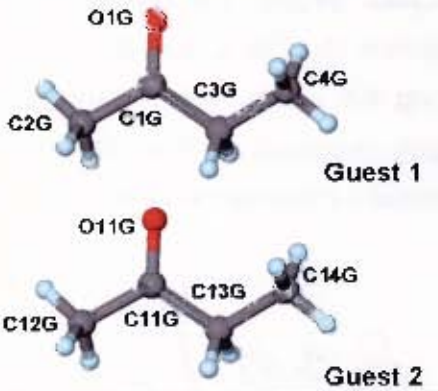

WEB24•2MEK crystallises in the monoclinic crystal system in the space group $P2_1/n$. All non-hydrogen atoms of the host molecule in the asymmetric unit were located by direct methods and non-hydrogen guest atoms were located in the difference electron density maps. All non-hydrogen host and guest atoms were refined anisotropically. The host hydroxyl hydrogens were located in the difference electron density maps and refined with simple bond length constraints and independent temperature factors. All remaining hydrogen atoms were placed with geometric constraints and assigned isotropic temperature factors of $1.2xU_{eq}$ of their parent atoms. The structure refined to $R_1 = 0.0441$.

WEB24•2MEK has Z = 4 and H:G = 1:2. There are two half host molecules and two methyl ethyl ketone guest molecules in the asymmetric unit. The two different guest molecules have been labelled as guest 1 and guest 2 in the numbering scheme above and the guests have been represented in two different colours in the packing diagrams in order to distinguish between the two. The four host molecules are located in pairs at different centres of inversion, Wyckoff positions *b* and *d*, while the guest molecules are both located in general positions.

The host molecules pack to form a distorted version of the pattern seen in the **WEB24** structure. This packing of the host molecules can be seen when the unit cell is viewed down the a-axis. Packing diagrams of the structure viewed down [100] and [010] are given in Figure 4.16 and the packing along [101] is illustrated in Figure 4.17(a). In the unit cell there are undulating channels running along [101] which contain both independent MEK guest molecules and these channels can be seen in Figure 4.17(b). Guest 1 is centred at 0.27, 0.93, 0.71 and guest 2 at 0.15, 0.71, 0.46.

The channels along [101] were studied using the program SECTION[1] by viewing sections through the unit cell down the c-axis. These sections are illustrated in Figure 4.18. The cross-section of the channels can be seen shifting through the cell along the a-axis, which corresponds to channels along [101]. The channels are highly restricted, with a maximum cross-sectional area of 8.0 Å x 8.2 Å and a minimum cross-sectional area of 2.0 Å x 2.4 Å.

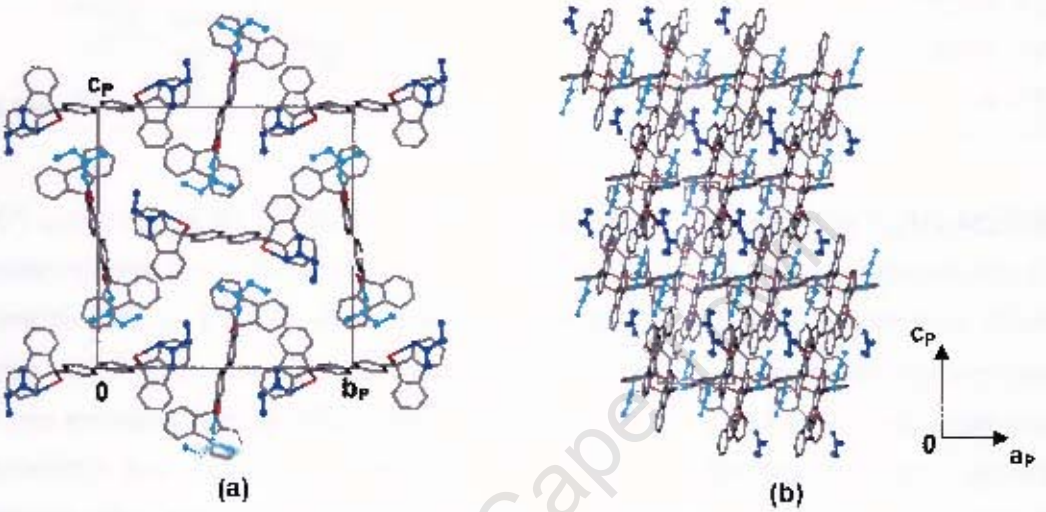

Figure 4.16 Packing diagram of **WEB24•2MEK** viewed **(a)** down [100] and **(b)** down [010] with guest molecules shown in ball and stick representation for clarity and guest 1 shown in dark blue and guest 2 shown in light blue.

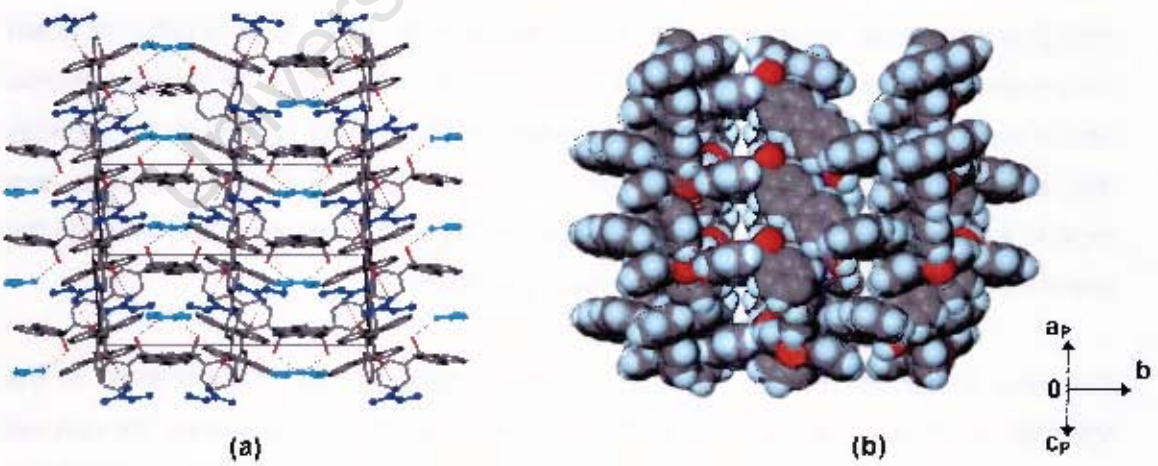

Figure 4.17 Packing diagrams of **WEB24•2MEK** viewed down [101], **(a)** with guest molecules shown in ball and stick representation for clarity and guest 1 shown in dark blue and guest 2 shown in light blue and **(b)** showing the channels down [101] with the guest molecules omitted and the host molecules represented with van der Waals radii.

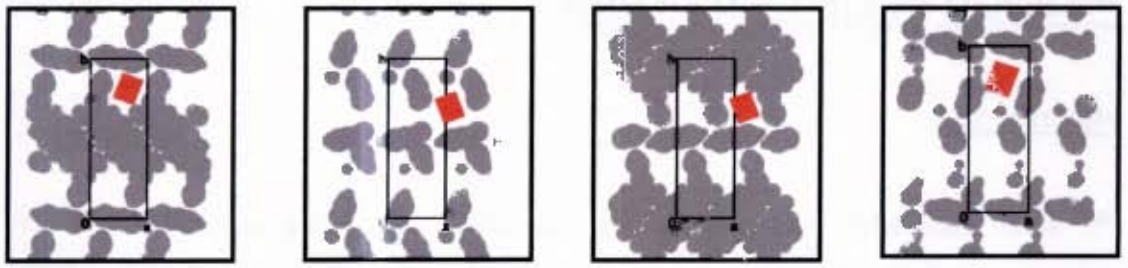

(a) 0 Å along [001] **(b)** 7.5 Å along [001] **(c)** 10.5 Å along [001] **(d)** 18.4 Å along [001]

Figure 4.18 SECTION plots of **WEB24•2MEK** (with guest molecules omitted and host molecules represented by grey areas) viewed down [001] with the unit cell sectioned at **(a)** 0 Å, **(b)** 7.5 Å, **(c)** 10.5 Å and **(d)** 18.4 Å along [001]. The shifting cross-section of one of the channels down [101] is highlighted in red.

Both methyl ethyl ketone guest molecules are hydrogen bonded to the host molecules via the hydroxyl groups. The hydrogen bonding in **WEB24•2MEK** is shown in Figure 4.19 and hydrogen bonding details are given in Table 4.6.

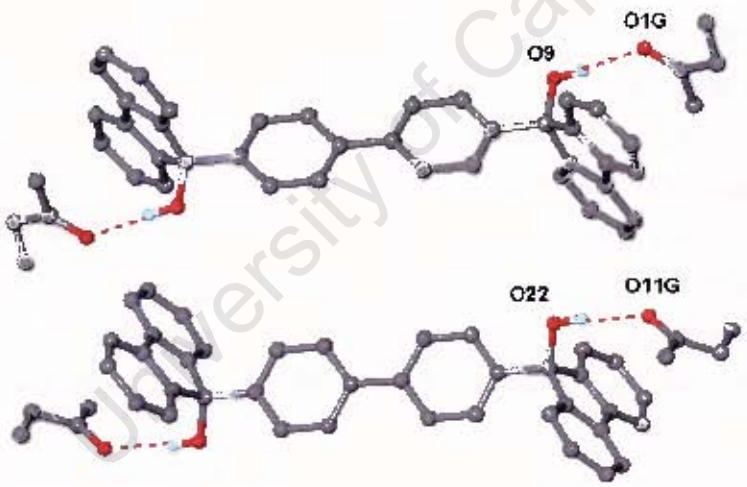

Figure 4.19 Host···guest hydrogen bonding in **WEB24•2MEK**.

Table 4.6 Hydrogen bonding details in **WEB24•2MEK**

Donor (D)	Acceptor (A)	D–H/Å	D···A/Å	D–H···A/°
O9	O1G	0.970(1)	2.772(2)	169(2)
O22	O11G	0.89(2)	2.787(2)	174(2)

^{13}C SOLID STATE CP/MAS NMR

Introduction

^{13}C solid state NMR has become an important tool for studying solid inclusion compounds. Early applications of solid state NMR in chemistry have been discussed by Fyfe.[2] An introduction to the basics of solid state NMR, emphasising applications in supramolecular chemistry has also been given by J. Ripmeester and C. Ratcliffe.[3]

Generally there is relatively little difference in isotropic chemical shifts in solution and in the solid state. The differences which do occur are often due to packing effects or hydrogen bonding, or due to the fact that conformations are locked in the solid state whereas these are averaged in solution. In the solid state, chemical shift differences can arise from chemically equivalent, but crystallographically inequivalent nuclei, which means that the ^{13}C NMR spectrum can give information about the content of the unit cell of the crystal.[3]

In solid state NMR the magnetic shielding experienced by a nuclear spin in a molecule varies with the orientation of the molecule with respect to the external applied magnetic field. In solution on the other hand, random tumbling of the molecules averages the shielding to an isotropic value. This results in the NMR linewidths of solid state spectra generally being much broader than those in solution, as the solid state NMR lineshapes result from the statistical distribution of all possible crystalline orientations. In addition there are direct nuclear dipole-dipole interactions in solids, which are averaged to zero in solution, which lead to further broadening.[4]

Three techniques are usually combined to obtain high-resolution solid state spectra of dilute spin-1/2 nuclei (eg. ^{13}C) in the solid state:[5]

(1) cross-polarisation (CP) from abundant spins

(2) magic angle spinning (MAS)

(3) high-power heteronuclear decoupling

CP allows dilute spins (eg. ^{13}C) to borrow magnetisation from abundant spins (eg. ^{1}H). It also reduces the recycle time between radiofrequency pulses. Magic angle spinning involves spinning solid samples very rapidly about an axis inclined at an angle of 54.74° with respect to the external applied magnetic field direction.[6] This

angle is called the magic angle and is the angle at which the spatial dependencies of many NMR interactions are averaged to their isotropic values. High-power heteronuclear decoupling is used during acquisition to remove dipolar interactions.

^{13}C Solid state CP/MAS NMR spectra

^{13}C solid state CP/MAS NMR was used to analyse **WEB24**, **WEB24•4DMA**, **WEB24•2DMA**, **WEB24•3DIOX** and **WEB24•2MEK**. The spectra obtained are given in Figure 4.20 (a)-(e). The spinning sidebands in each spectrum were identified by running the spectrum at two different spinning speeds and are indicated by blue stars. The guest resonances in the spectra of the inclusion compounds are shown by red arrows.

In each case a spectrum was also run under dipolar dephasing conditions to assist in the assignment of the host resonances. Under dipolar dephasing conditions, resonances of carbon atoms which have hydrogen atoms attached do not usually appear in the spectrum, so only quaternary carbon resonances remain. In Figure 4.20 the resonances in each spectrum which disappear under dipolar dephasing conditions are shown in a light blue box.

A solution spectrum of the guest-free host compound was also run to assist with assignments of the host resonances. This spectrum is shown in Figure 4.21. In solution the host molecule has a centre of symmetry as well as a plane of symmetry through the molecule. We therefore expect to see resonances of eleven different carbon atoms. The spectral assignments made are given in Table 4.7 and the numbering of the host molecule in solution is given with the spectrum in Figure 4.21.

Looking at the host structure in the solid state, the asymmetric unit consists of half a host molecule. We therefore expect to see 19 different carbon atoms in the spectrum. This increase in the number of different carbon atoms can be seen by the increased number of splittings in the solid state spectrum of **WEB24** (Figure 4.20(a)). This results in the spectrum being complicated and difficult to assign, but partial assignments are given, as is the case for the host resonances of all the spectra.

The assignments for the solid state spectrum of **WEB24** are given in Table 4.8, and those of the inclusion compounds are given in Table 4.9. The numbering of the host and the guest molecules for the solid state spectra are given with the spectra in Figure 4.20.

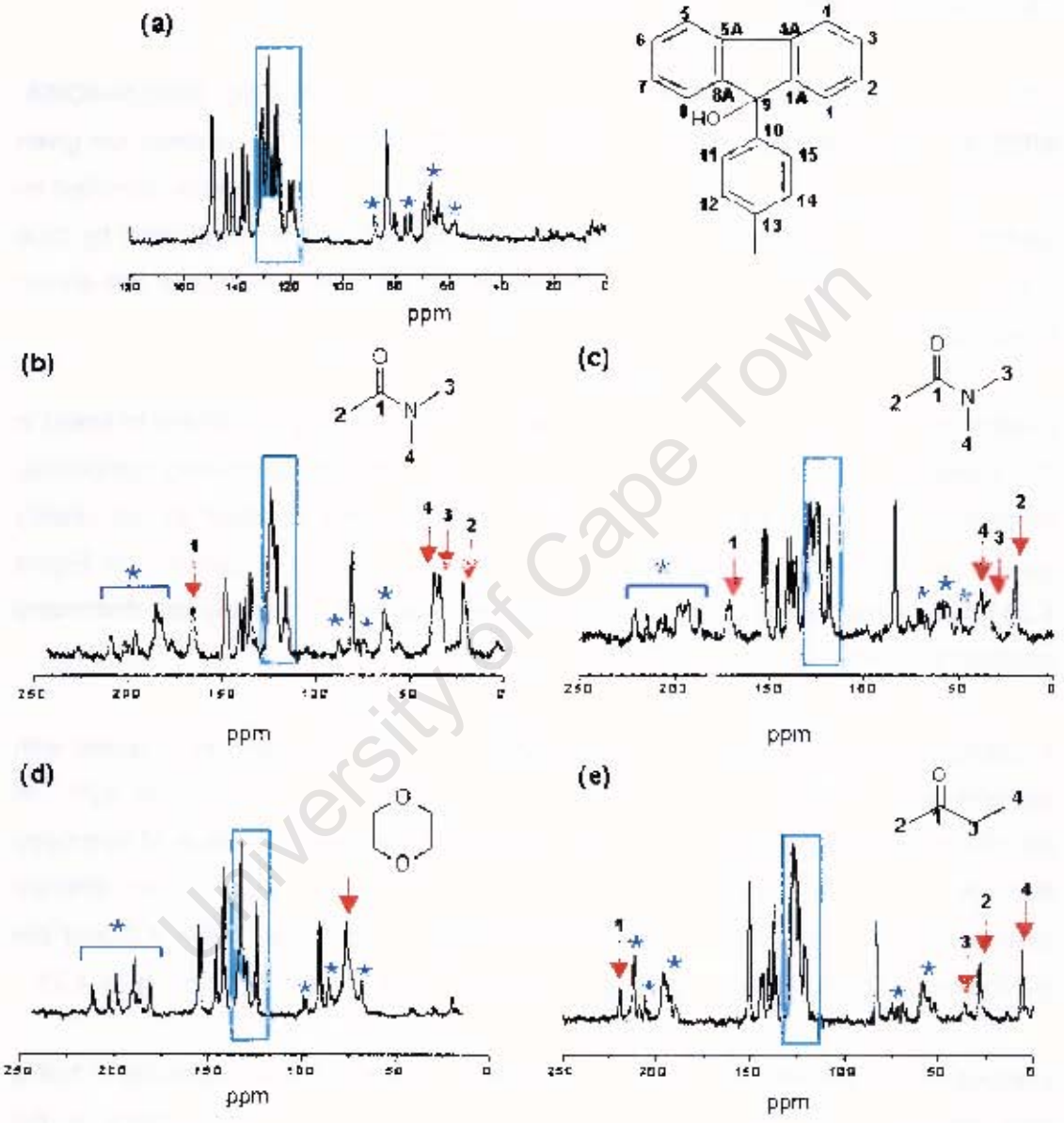

Figure 4.20 ^{13}C CP/MAS spectra of **(a) WEB24**, **(b) WEB24•4DMA**, **(c) WEB24•2DMA**, **(d) WEB24•3DIOX**, **(e) WEB24•2MEK** at 297K (600 scans at 5 s intervals, 5 μs 90° ^{1}H pulse, contact time = 2 ms). [⋆ = spinning sidebands, ↓ = guest resonances, [ ] = resonances that disappear under dipolar dephasing conditions]

In the spectrum of **WEB24•4DMA** (Figure 4.20(b)), the host resonances are not the same as those of **WEB24**. The resonances of C1A and C8A have split as well as the resonances of the other quaternary carbon atoms. There is a large amount of overlap of the non-quaternary carbon resonances. The guest resonances are shown by red arrows. Of these, the C1 resonance is most downfield, the C2 resonance is most upfield and is split, indicating that there is more than one guest molecule in the asymmetric unit, and the C3 and C4 resonances are found at 36.1 ppm and 38.5 ppm respectively.

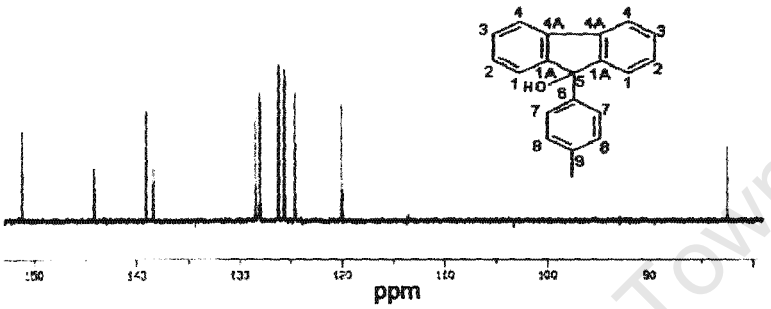

Figure 4.21 ^{13}C NMR solution spectrum of **WEB24** host powder.

From the spectrum of **WEB24•2DMA** (Figure 4.20(c)), it can be clearly seen from the host resonances that there has been a change of phase. There are also differences in the guest resonances. For example, the C2 resonance is not split, which is expected for this structure as the asymmetric unit contains only one N,N-dimethylacetamide guest molecule. The C3 and C4 resonances appear as asymmetric doublets, which is expected as they are attached to a nitrogen atom.

In the spectrum of **WEB24•3DIOX** (Figure 4.20(d)), the host resonances again have a different appearance from any of the previous spectra. The guest resonance is overlapping the spinning sidebands, but it looks as if it is split, which is possible as the asymmetric unit of the **WEB24•3DIOX** structure has one and a half 1,4-dioxane molecules. There could therefore be up to six resonances. The **WEB24•2MEK** spectrum (Figure 4.20(e)) also shows different host resonances from the previous spectra. The carbonyl carbon (C1) resonance of the guest molecule is found furthest downfield and the C4 resonance is furthest upfield. In the asymmetric unit of the **WEB24•2MEK** structure there are two methyl ethyl ketone guest molecules and therefore we could expect to see splitting in the guest resonances.

Table 4.7 ^{13}C Solution NMR isotropic shift and assignments of host **WEB24**

Shift	Assignment C atom	
WEB24		
151.3	1A	Q
144.2	9	Q
139.0	4A	Q
138.3	6	Q
128.6	1	CH
128.0	7	CH
126.2	3	CH
125.7	8	CH
124.7	2	CH
120.1	4	CH
82.4	5	Q

Table 4.8 ^{13}C Solid State NMR isotropic shifts and assignments of host **WEB24**

Shift	Assignment C atom	
WEB24		
149.4	1A, 8A	Q
144.7,142.4,138.2, 136.4	4A, 5A, 10, 13	Q
130.6,128.2,126.4, 125.3,123.8,120.3, 118.8	1-8, 11, 12, 14, 15	CH
83.2	9	Q

Notes for tables 4.7, 4.8 and 4.9

- Q = quaternary carbon
- Partial assignments are given where the complete assignment is not known.

Table 4.9 ^{13}C Solid State NMR isotropic shifts and assignments of **WEB24** clathrates

Shift	Assignment C atom	
WEB24•4DMA		
WEB24		
152.5	1A,8A	Q
145.1 - 135.2	4A,5A,10,13	Q
128.7 - 118.4	1-8,11,12,14,15	CH
84.0	9	Q
DMA		
169.7	1	Q
38.5	4	CH_3
36.1	3	CH_3
23.8-20.5	2	CH_3
WEB24•2DMA		
WEB24		
154.1, 152.4	1A,8A	Q
145.9 - 136.1	4A,5A,10,13	Q
130.3 - 118.8	1-8,11,12,14,15	CH
84.4	9	Q
DMA		
171.3	1	Q
40.4	4	CH_3
35.8	3	CH_3
20.1	2	CH_3
WEB24•3DIOX		
WEB24		
154.1, 152.4	1A,8A	Q
144.3 - 138.1	4A,5A,10,13	Q
129.5 - 120.1	1-8,11,12,14,15	CH
83.6	9	Q
1,4-DIOXANE		
68.0	1	CH_2
WEB24•2MEK		
WEB24		
151.2	1A,8A	Q
144.3-135.6	4A,5A,10,13	Q
127.9-120.5	1-8,11,12,14,15	CH
82.8	7	Q
MEK		
219.7	1	Q
36.1	3	CH_2
27.8	2	CH_3
6.6	4	CH_3

Desorption of WEB24 clathrates

Desorption of the inclusion compounds was monitored using ^{13}C solid state CP/MAS NMR. This was carried out by running a spectrum, then removing the sample from the rotor and heating it for a period of time in the oven, then repacking and running another spectrum. This was repeated a number of times for each sample at intervals along the curve obtained by TG analysis.

Figure 4.22(a) shows the series of spectra obtained during the partial guest loss of **WEB24•4DMA**, resulting in the **WEB24•2DMA** complex. Through the series a change in the guest resonances can be seen. The C2 resonance loses its splitting and becomes a single peak and the structure on the C3 and C4 resonances changes. Through the series the host resonances also change significantly, indicating a phase change. The spectra show that this phase change occurs simultaneously to the partial guest loss.

Figure 4.22(b) displays the series of spectra obtained during the guest loss from **WEB24•2DMA** to form the guest-free host compound. As the sample is heated, the guest resonances decrease in size until they disappear completely. As the guest loss occurs, the host resonances also show a change of phase occurring simultaneously to the guest release.

Figure 4.22(c) shows the spectra obtained during the desorption of **WEB24•3DIOX**. As the sample is heated, the 1,4-dioxane resonance decreases and eventually disappears. The host resonances show a phase change which occurs simultaneously to the loss of the guest.

Figure 4.22(d) gives the series of spectra taken during the release of guest from **WEB24•2MEK**. Through the series the guest peaks decrease and then disappear to form the guest-free host compound. Once again a simultaneous phase change is shown by the host resonances.

The final spectra in each of the above series are identical, indicating that in each case the guest-free host compound formed by desorption has the same structure. These structures are also the same as that of the original host compound.

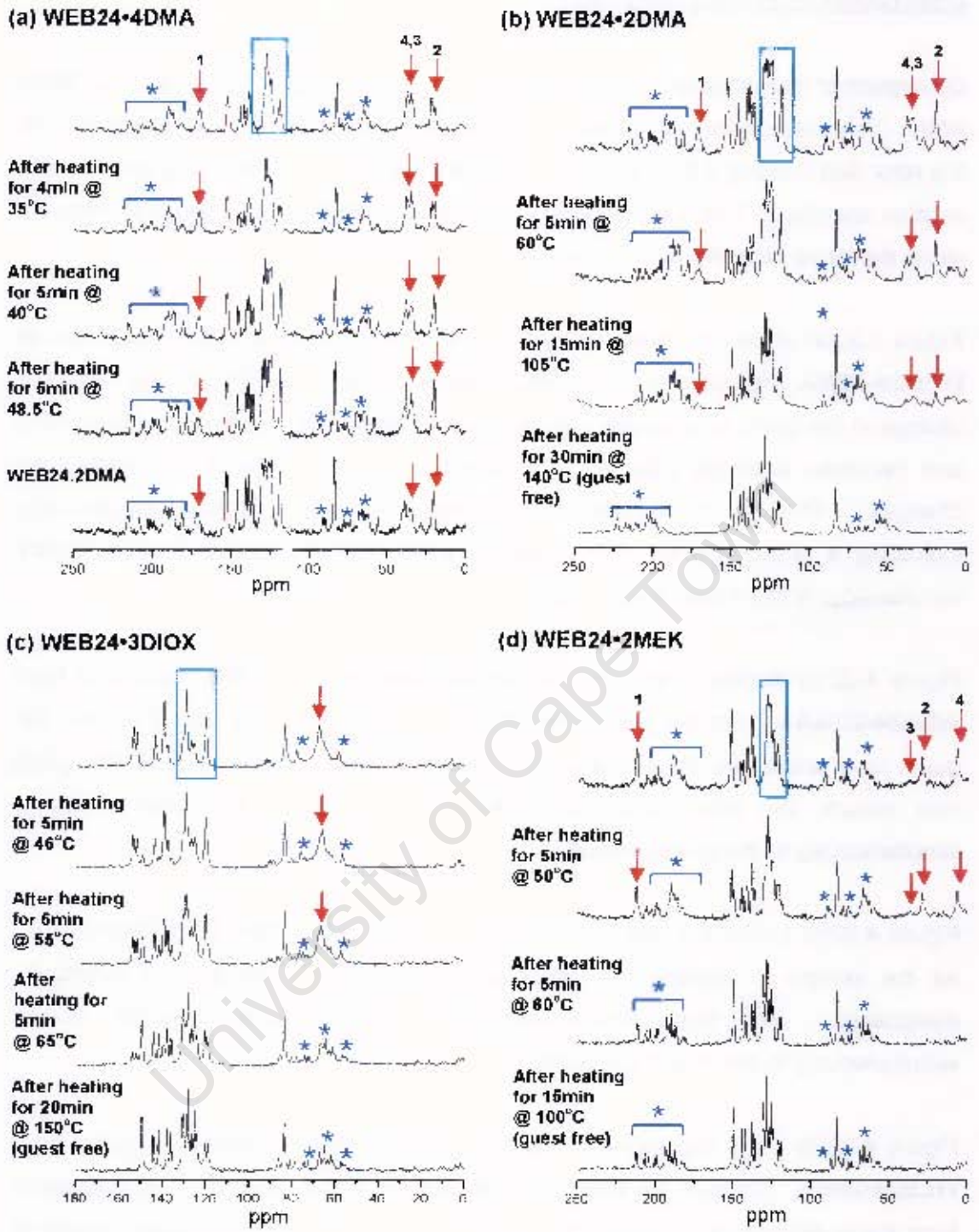

Figure 4.22 ^{13}C CP/MAS spectra of **(a) WEB24•4DMA** (800 scans at 15 s intervals, 5 μs 90° ^{1}H pulse, contact time = 2 ms) , **(b) WEB24•2DMA** (300 scans at 10 s intervals, 5 μs 90° ^{1}H pulse, contact time = 2 ms) , **(c) WEB24•3DIOX** (600 scans at 5 s intervals, 5 μs 90° ^{1}H pulse, contact time = 2 ms) and **(d)** ^{13}C CP/MAS spectra of **WEB24•2MEK** (600 scans at 5 s intervals, 5 μs 90° ^{1}H pulse, contact time = 2 ms)

KINETICS OF DESORPTION

The kinetics of desorption of both **WEB24•4DMA** and **WEB24•3DIOX** were analysed by carrying out a series of isothermal TG experiments. In the case of **WEB24•4DMA**, the first desorption step, resulting in the stable compound **WEB24•2DMA**, was separated from the second desorption step by selecting appropriate temperatures for these experiments. Once the first desorption step was complete, the sample was removed and the temperature was then raised for the second desorption step and the sample replaced. Figure 4.23 shows a typical example in which the mass loss versus time curve along with the temperature program used is shown.

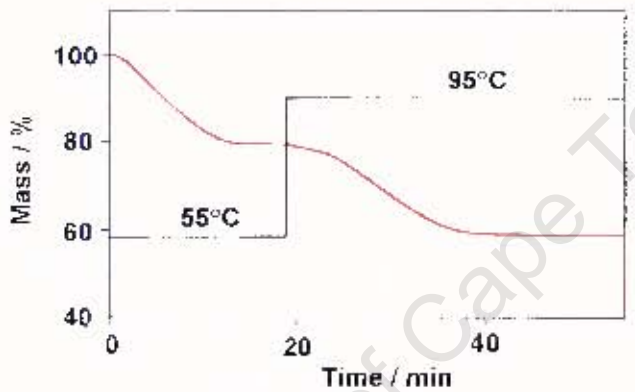

Figure 4.23 Example of a set of isothermal TG experiments carried out with **WEB24•4DMA**, as well as the temperature program used.

Isothermal TG experiments were carried out over the temperature range 40-65°C at intervals of 5°C for the first step and over the temperature range 90-110°C, also at intervals of 5°C, for the second step. The mass loss versus time curves obtained were converted to extent of reaction (α) versus time curves. The α versus time curves obtained for both the first and second desorption steps were best described by the Prout-Tompkins equation,[7] namely $f(\alpha) = \ln[\alpha/(1-\alpha)]$, over an α-range of 0.05-0.95 and the rate constants, k_{obs}, were derived. The semilogarithmic plots of $\ln k_{obs}$ versus $1000\ K/T$ are shown in Figure 4.24 and yield activation energies of 79.1 kJ.mol^{-1} and 115.4 kJ.mol^{-1} for the first and second steps respectively.

The desorption of **WEB24•3DIOX** takes place in a single step and isothermal TG experiments were carried out over the temperature range 70-90°C at intervals of 5°C.

The α versus time curves obtained were best fitted to the first order equation[7], $f(\alpha) = -\ln(1-\alpha)$ over an α-range of 0.05-0.95. The semilogarithmic plot of $\ln k_{obs}$ versus 1000 K/T is shown in Figure 4.25 and yields an activation energy of 95.5 kJ.mol^{-1}.

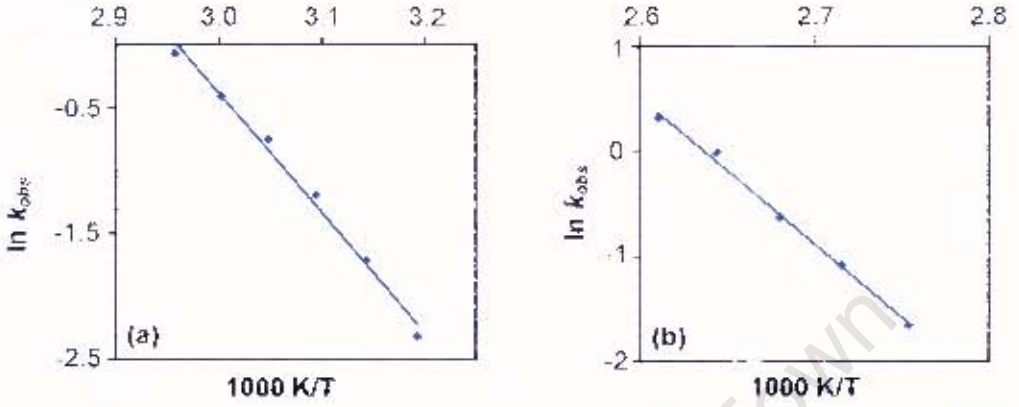

Figure 4.24 Semilogarithmic plots of $\ln k_{obs}$ versus 1000 K/T for **(a)** the first step and **(b)** the second step of the desorption of **WEB24•4DMA**.

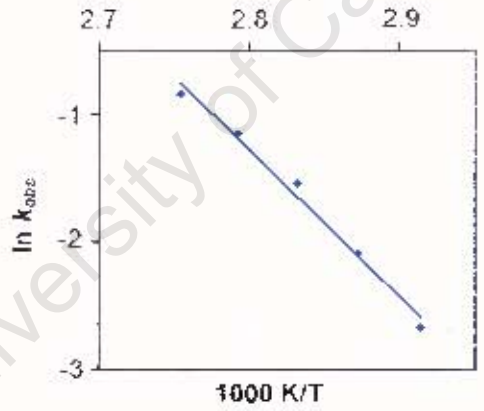

Figure 4.25 Semilogarithmic plot of $\ln k_{obs}$ versus 1000 K/T for the desorption of **WEB24•3DIOX**.

Table 4.10 Kinetic parameters for desorption of **WEB24•4DMA** and **WEB24•3DIOX**

Inclusion compound	Temperature range (°C)	Alpha range	Kinetic equation	E_a (kJ.mol^{-1})
WEB24•4DMA - 1st step	40-65	0.05-0.95	$f(\alpha) = \ln[\alpha/(1-\alpha)]$	79.1
- 2nd step	90-110	0.05-0.95	$f(\alpha) = \ln[\alpha/(1-\alpha)]$	115.4
WEB24•3DIOX	70-90	0.05-0.95	$f(\alpha) = -\ln(1-\alpha)$	95.5

NUCLEATION AND CRYSTAL GROWTH

A brief study of the nucleation and crystal growth of **WEB24•3DIOX** was carried out, which involved measuring the solubility curve of this compound in 1,4-dioxane and then crystallising the compound by cooling from saturated solutions at various temperatures and examining the resulting crystals using optical microscopy.

The solubility curve of **WEB24•3DIOX** was determined by measuring the solubility over the temperature range 20°C to 85°C and the solubility versus temperature curve plotted. This plot is given in Figure 4.26 and gave a smooth curve with no indication that above a certain temperature the host alone is formed preferentially to the inclusion compound. A solution whose composition lies above the curve has a greater amount of dissolved solute than the equilibrium value and is thus supersaturated.

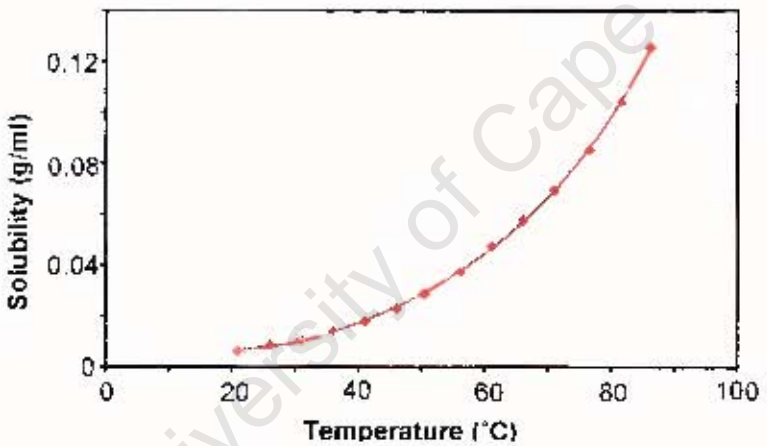

Figure 4.26 Solubility versus temperature plot for **WEB24•3DIOX** in 1,4-dioxane.

WEB24•3DIOX was crystallised at 50°C, 60°C and 70°C from saturated solutions set up at 66°C, 76°C and 86°C respectively. The supersaturation of each solution at the crystallisation temperature was calculated using the equation:

$$\text{Supersaturation} = \ln\left[\frac{\text{mass of inclusion compound in supersaturated state}}{\text{mass of inclusion compound in saturated phase}}\right]$$

and was found to be 0.684 for the crystallisation at 50°C, 0.638 for the crystallisation at 60°C and 0.610 for the crystallisation at 70°C.

Optical microscopy was used to examine the morphology of the crystals, but there did not appear to be any change in morphology for the different crystallisations. Photographs of the crystals are shown in Figure 4.27.

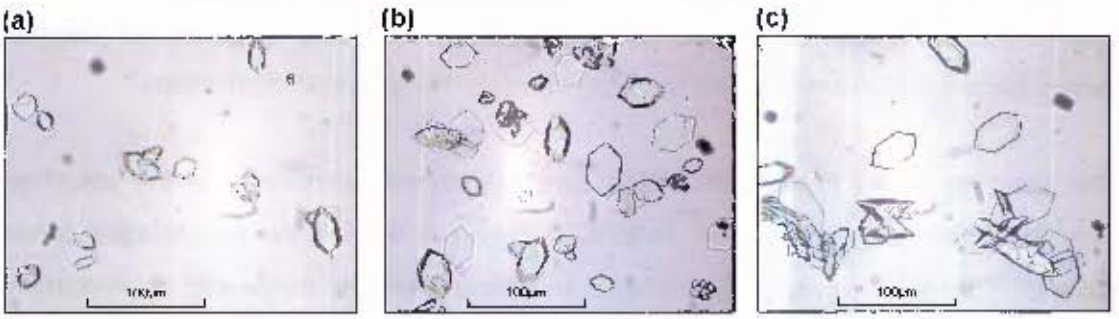

Figure 4.27 Crystals of **WEB24•3DIOX** formed at **(a)** 50°C from a saturated solution at 66°C, **(b)** 60°C from a saturated solution at 76°C and **(c)** 70°C from a saturated solution at 86°C.

An in-situ cooling crystallisation of **WEB24•3DIOX** at 50°C was observed using optical microscopy. This crystallisation was set up by making a saturated solution of **WEB24•3DIOX** in 1,4-dioxane at 66°C. The hot solution was transferred to a pre-heated top-hat cell (placed on the microscope stage), surrounded by a water jacket and connected to a water bath, allowing the temperature to be controlled. The temperature of the cell was lowered to 50°C, allowing the crystallisation of **WEB24•3DIOX** to be observed. Selected images are shown in Figure 4.28.

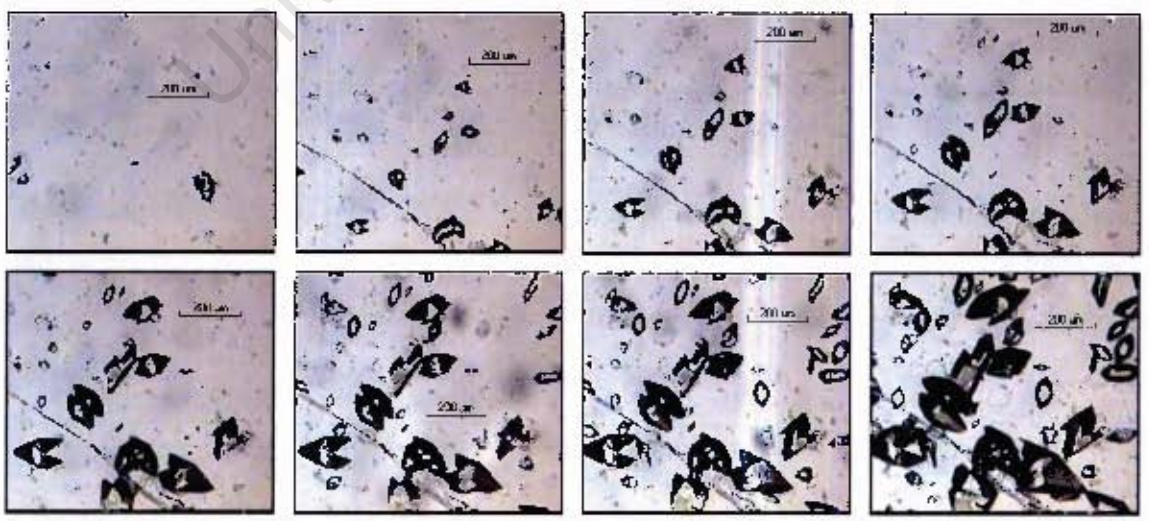

Figure 4.28 Images taken during crystallisation of **WEB24•3DIOX.**

SUMMARY AND DISCUSSION

Various inclusion compounds of the host **WEB24** were analysed using a number of methods such as thermal analysis, crystal structure analysis and ^{13}C solid state CP/MAS NMR.

WEB24 was found to crystallise in the space group $P2_1/n$ with $Z = 2$ and half a host molecule in the asymmetric unit. The host molecules are located on centres of inversion and there is no hydrogen bonding between them. The molecules pack to form a sawtooth pattern viewed down [101]. **WEB24** was found to form inclusion compounds with **N**,N-dimethylacetamide, 1,4-dioxane and methyl ethyl ketone. The H:G ratios were determined by thermal gravimetry and were found to be 1:2 for the complex with methyl ethyl ketone and 1:3 for the complex with 1,4-dioxane. **WEB24** forms two inclusion complexes with N,**N**-dimethylacetamide with **H**:G ratios of 1:2 as well as 1:4

It has been noted that the difference between the onset temperature, T_{on}, and the normal boiling point of the guest, T_b, is a measure of the relative stability of an inclusion compound.[8] The endotherm due to guest release for **WEB24•3DIOX** occurs at $T_{on} = 104°C$ ($T_{on} - T_b = +3°C$). This is more stable than the dioxane inclusion compound formed with triphenylsilanol[9] ($T_{on} - T_b = -16°C$), but less stable than the clathrate with 10,11-dihydro-5-phenyl-5**H**-dibenzo[a,d]cyclo-hepten-5-ol[10] ($T_{on} - T_b = +21°C$).[8] For **WEB24•2MEK**, $T_{on} = 51°C$ ($T_{on} - T_b = -29°C$), and compares with the MEK inclusion compounds formed with 1,1,6,6-tetraphenyl-hexa-2,4-diyne-1,6-diol[10] ($T_{on} - T_b = -30°C$) and cholic acid[11] ($T_{on} - T_b = -10°C$). In the case of **WEB24•4DMA** the two endotherms occur at $T_{on} = 65°C$ and 153°C, corresponding to $T_{on} - T_b$ values of -100°C and -12°C, showing that the intermediate **WEB24•2DMA** is more stable.

The structures of the inclusion compounds formed by this host are all significantly different. **WEB24•4DMA** crystallises in the space group $P\bar{1}$ with $Z = 2$ and H:G = 1:4. The asymmetric unit consists of one host molecule and four guest molecules. **WEB24•2DMA** crystallises in the space group $P\bar{1}$ and has $Z = 1$ and H:G = 1:2, with half a host molecule and one guest molecule in the asymmetric unit. **WEB24•3DIOX** crystallises in the space group $P2_1/c$ and has $Z = 2$ with H:G = 1:3. The asymmetric unit consists of half a host molecule and one and a half guest molecules.

WEB24•2MEK crystallises in the space group $P2_1/n$ and has Z = 4 and H:G = 1:2, with two half host molecules and two guest molecules in the asymmetric unit. In the structures of each of the inclusion compounds, with the exception of **WEB24•4DMA**, the host molecules are located on centres of inversion and in all of the structures there are two guests hydrogen bonded to each host molecule via the hydroxyl groups. In the structures of **WEB24•4DMA** and **WEB24•3DIOX** there are additional guests which are not hydrogen bonded to the host molecules.

WEB24•4DMA has an open structure, with the host molecules packing to form layers parallel to the ac plane, between which the guests are located. In each of the other inclusion compounds the guests are located in channels, although the channels vary significantly among the three structures. In **WEB24•2DMA** the guests are located in general positions in channels along [-1 0 1], which have a fairly constant cross-sectional diameter. The stabilities of **WEB24•4DMA** and **WEB24•2DMA**, given by T_{on} -T_b, can thus be correlated to the structures as the structure of **WEB24•4DMA** is more open than that of **WEB24•2DMA**, resulting in a less stable structure from which the guest can be released more easily.

WEB24•3DIOX has a very open structure, with the guests located in channels along [001] which have wider and narrower sections. The guest molecules which are hydrogen bonded to the host are located in general positions in the narrower parts of the channels and the non hydrogen bonded guests are located on centres of symmetry in the wider parts of the channels. **WEB24•2MEK** has restricted channels which run along [101]. Both guests in the asymmetric unit are located in these channels in general positions.

^{13}C solid state CP/MAS NMR was also used to analyse the inclusion compounds and to monitor the desorption of the guest from each of the **WEB24** clathrates. The results show that in each case the guest loss and the phase change to the structure of the host alone are intimately connected and occur simultaneously.

Solid state NMR has been shown to be a very effective method of analysis and has a number of important applications in supramolecular chemistry. This technique complements diffraction studies and often gives unique information about the asymmetric unit in the crystal, which can be particularly helpful when there is lattice disorder in the structure.[12] This combination of solid state NMR and single crystal

X-ray diffraction has been used in a number of studies to obtain complementary information and an improved structural model.[13,14,15,16,17] Defining a structure in terms of dynamics is important for understanding the molecular recognition processes that occur in host-guest systems,[12] and NMR measurements can be used to acquire information about the types of motion present in a crystal structure,[18,19,20,21,22] as well as motional rates and activation energies.[23,24] The technique usually used to study guest dynamics is temperature dependent ^{2}H NMR lineshape studies.[12] Such studies could be carried out on the **WEB24** host-guest compounds described in this chapter in order to gain additional insight into the motion of the guest molecules within the host lattices.

Isothermal TG experiments were used to study the kinetics of desorption of both **WEB24•4DMA** and **WEB24•3DIOX**. The desorption of **WEB24•3DIOX** takes place in a single step and was found to be a first order process with an activation energy of 95.5 kJ.mol^{-1}. The desorption of **WEB24•4DMA** takes place in two steps and the isothermal curves obtained for both steps were found to fit the Prout-Tompkins equation. The first and second steps were found to have activation energies of 79.1 kJ.mol^{-1} and 115.4 kJ.mol^{-1} respectively. It is interesting to note that in inclusion compounds H.nG which desorb in two steps:

$$H{\bullet}nG \xrightarrow{E_1} H{\bullet}(n\text{-}m)G + mG\uparrow \xrightarrow{E_2} H + (n\text{-}m)G\uparrow \quad (n>m)$$

the activation energy E_1 for the first step is smaller than that of the second step E_2. This occurred with the inclusion compound formed between the host **H1** = 2,2'-bis(2,7-dichloro-9-hydroxy-fluorenyl)biphenyl with dioxane[25] in which the desorption reaction:

$$H1{\bullet}3.5\ DIOX \rightarrow H1{\bullet}1.5DIOX \rightarrow H1$$

yielded values of E_1 = 34 kJ.mol^{-1} and E_2 = 111 kJ.mol^{-1}. Similar results were obtained with the host binaphthol, BINAP, with dioxane, which formed the inclusion compound BINAP•3.5DIOX that decomposed to the intermediate BINAP•1.5DIOX and subsequently to the apohost **BINAP**. Here the activation energies measured were E_1 = 61 kJ.mol^{-1} and E_2 = 86 kJ.mol^{-1}. In this latter case both the starting and intermediate inclusion compounds were isolated by crystallisation at different temperatures.[26] We note that inclusion compounds with different guest:host ratios may be prepared from the same host-guest system by changing the crystallisation temperature.

The general rules linking guest/host ratios, the topologies of the ensuing compounds and crystallisation temperature have been formulated by Ibragimov [27] and state

(i) the guest/host ratio decreases as the crystallisation temperature increases.

(ii) the topology changes from low to high temperature as intercalate → tubulate › cryptate → apohost

These trends are illustrated in Figure 4.29 which shows that the compounds with high guest/host ratios generally have the more open structures. These in turn would decay easily to intermediates with lower guest/host ratios by a desorption process of low activation energy. The intermediate, with a lower guest/host ratio is then likely to be more stable and decay with a higher activation energy. This is indeed what occurred in the desorption of **WEB24•4DMA** › **WEB24•2DMA** → **WEB24**.

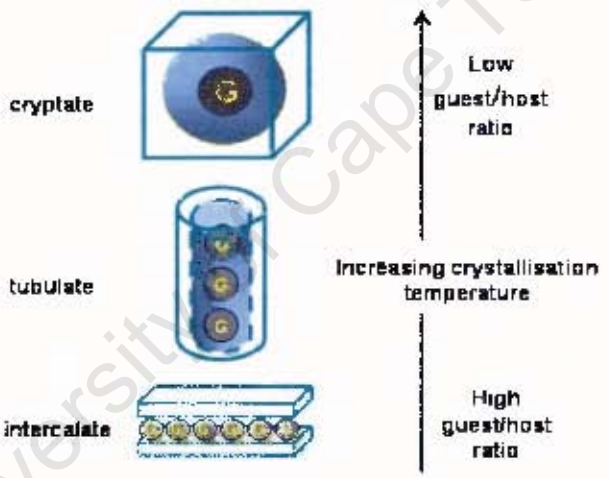

Figure 4.29 Schematic diagram showing relationship between crystallisation temperature, H:G ratio and topology of inclusion compounds.[28]

As part of a brief study of nucleation and crystal growth, the solubility curve of **WEB24.3DIOX** was measured and it was found that the solubility of **WEB24.3DIOX** in 1,4-dioxane increases uniformly with temperature, with no evidence of another phase. Crystallisations carried out at various temperatures along the curve from supersaturated solutions did not show any differences in morphology. At each temperature the crystals appear as elongated hexagonal plates and observation of the crystallisation in situ showed that the crystals first develop as these flat plates and then grow in thickness.

REFERENCES

[1] L.J. Barbour, SECTION, A computer program for the graphic display of cross sections through a unit cell, *J. Appl. Cryst.*, 1999, **32**, 353.

[2] Colin Fyfe, *Solid State NMR for chemists*, CFC Press, Guelph, 1983.

[3] J.A. Ripmeester and C.I. Ratcliffe in *Inclusion Compounds*, Vol. 5, eds. J.L. Atwood, J.E.D. Davies and D.D. MacNicol, 1991, Chapter 2.

[4] R.E. Wasylishen in *Encyclopedia of Nuclear Magnetic Resonance*, eds. D.M. Grant and R.K. Harris, John Wiley & Sons, Ltd., New York, 1996, p 1685.

[5] E.O. Stejskal and J.D. Memory, *High-Resolution NMR in the Solid State: Fundamentals of CP/MAS*, Oxford University Press, New York, 1994.

[6] D.L. Bryce, G.M. Bernard, M. Gee, M.D. Lumsden, K. Eichele and R.E. Wasylishen, *Canadian Journal of Analytical Sciences and Spectroscopy*, 2001, **46**, 46.

[7] A.K. Galwey and M.E. Brown, *Handbook of Thermal analysis and Calorimetry*, ed. M.E. Brown, Elsevier Science B.V., Amsterdam, 1998, p. 162.

[8] M.R. Caira, L.R. Nassimbeni, M.L. Niven, W.-D. Schubert, E. Weber and N. Dörpinghaus, *J. Chem. Soc., Perkin Trans. 2*, 1990, 2129.

[9] S.A. Bourne, L. Johnson, C. Marais, L.R. Nassimbeni, E. Weber, K. Skobridis and F. Toda, *J. Chem. Soc., Perkin Trans. 2*, 1991, 1707.

[10] L. Johnson, L.R. Nassimbeni and F. Toda, *Acta Crystallogr.*, 1992, B**48**, 827.

[11] M.R. Caira, L.R. Nassimbeni and J.L. Scott, *J. Chem. Crystallogr.*, 1994, **24**, 783.

[12] J. A. Ripmeester and C.I. Ratcliffe in *Spectroscopic and Computational Studies of Supramolecular Systems*, ed. J.E.D. Davies, 1992, Chapter 1.

[13] G.D Enright, C.I. Ratcliffe and J.A. Ripmeester, *Molecular Physics*, 1999, **97**, 1193.

[14] R. Haase, D.S. Meinhold, B. Thomas, E. Weber, G. Rheinwald, *Structural Chemistry*, 2002, **13**, 471.

[15] M. Pietraszkiewicz, O. Pietraszkiewicz, W. Kolodziejski, K. Wozniak, N. Feeder, F. Benevelli and J. Klinowski, *J. Phys. Chem. B*, 2000, **104**, 1921.

[16] E.B. Brouwer, K.A. Udachin, G.D. Enright, C.I. Ratcliffe and J.A. Ripmeester, *Chem. Comm.*, 1998, 587.

[17] P. Zaderenko, M.S. Gil, P. López, P. Ballesteros, I. Fonsec and A. Albert, *Acta Cryst.*, 1997, B**53**, 961.

[18] G.A. Facey, C.I. Ratcliffe and J.A. Ripmeester, *J. Phys. Chem.*, 1995, **99**, 12249.

[19] M. Bach-Verges, S.J. Kitchin, K.D.M. Harris, M. Zugic and C.A. Koh, , *J. Phys. Chem. B*, 2001, **105**, 2699.

[20] E.B. Brouwer, G D. Enright, C.I. Ratcliffe, G.A. Facey and J.A. Ripmeester, *J. Phys. Chem. B*, 1999, **103**, 10604.

[21] H.C. Canuto, S.J. Heyes, S. Aime, R. Gobetto and F. Napolitano, *J. Chem. Soc., Dalton Trans.*, 2000, **22**, 4075.

[22] E. Zaborowski, H. Zimmermann and S. Vega, *J. Am. Chem. Soc.*, 1998, **120**, 8113.

[23] P.S. Sidhu, G.D. Enright, J.A. Ripmeester and G.H. Penner, *J. Phys. Chem. B*, 2002, **106**, 8569.

[24] P.S. Sidhu, G.H. Penner, K.R. Jeffrey, B. Zhao, Z.L. Wang and I. Goh, *J. Phys. Chem. B*, 1997, **101**, 9087.

[25] M.R. Caira, A. Coetzee, L.R. Nassimbeni, E. Weber and A. Wierig, *J. Chem. Soc., Perkin Trans. 2*, 1995, 281.

[26] L.R. Nassimbeni and H. Su, *J. Phys. Org. Chem.*, 2000, **13**, 368.

[27] B.T. Ibragimov, *J. Incl. Phenom. Macrocyclic Chem.*, 1999, **34**, 345.

[28] L.R. Nassimbeni, *Acc. Chem. Res.*, 2003, **36**, 631.

Chapter 5

INCLUSION OF ETHYLAMINE AND PROPYLAMINE BY THE HOST WEB24

COMPLEX PREPARATION

Suitable crystals of the inclusion compounds with ethylamine and propylamine were grown by slow evaporation at room temperature. For the ethylamine inclusion compound, because ethylamine is such a volatile guest, the solution was left to evaporate in a screw-top glass vial with a 1 mm hole in the lid, which was in turn placed inside a sealed larger glass vial. This was done in order to slow down the evaporation of ethylamine by causing back pressure.

The inclusion compounds obtained as well as their abbreviations are as follows:

WEB24 + ethylamine (H:G = 1:1): **WEB24•ETHYL**
WEB24 + ethylamine (H:G = 1:2): **WEB24•2ETHYL**
WEB24 + propylamine (H:G = 1:2): **WEB24•2PROPYL**

The guest numbering schemes are given at the beginning of each structure analysis and the host numbering scheme is the same as that given in Chapter 4 and is shown again below:

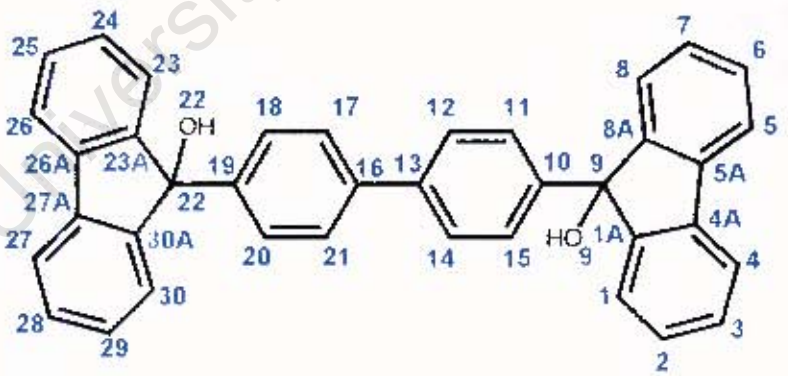

*The host 9,9'-(Biphenyl-4,4'-diyl)difluoren-9-ol (abbreviated **WEB24**) also forms inclusion compounds with ethylamine and propylamine, each with H:G = 1:2. Thermal analysis of these compounds has been carried out and the structures have been elucidated. The kinetics of enclathration of both ethylamine vapour and propylamine vapour by **WEB24** were studied using an automated magnetic suspension balance. These experiments were carried out at two temperatures and various vapour pressures for each guest and it was found that enclathration of ethylamine vapour by **WEB24** yields an inclusion compound with H:G = 1:1. The kinetics of desorption of each of the inclusion compounds were also measured by carrying out a series of isothermal TG experiments.*

The crystallographic data, experimental and refinement parameters for the structures discussed in this chapter are given in Table 5.1. Final atomic coordinates, bond lengths and angles, torsion angles, temperature factors and tables of observed and calculated structure factors for each of the crystal structures are given in the appendices.

Table 5.1 Crystal data, experimental and refinement parameters

	WEB24•2ETHYL	**WEB24•2PROPYL**
Molecular formula	$C_{38}H_{26}O_2.2(C_2H_7N)$	$C_{38}H_{26}O_2.2(C_3H_9N)$
Guest	ethylamine	propylamine
Host:guest ratio	1:2	1:2
M_r/g.mol^{-1}	604.76	632.81
Crystal symmetry	Triclinic	Orthorhombic
Space group	$P\bar{1}$	$Pca2_1$
a/Å	7.6344(2)	14.9762(3)
b/Å	13.2521(5)	14.2481(2)
c/Å	17.3520(4)	16.7632(2)
α/°	76.326(1)	90
β/°	89.954(1)	90
γ/°	73.703(1)	90
Z	2	4
V/Å^3	1633.19(7)	3576.1(1)
μ(Mo-Kα)mm^{-1}	0.075	0.071
Temp of data collection (K)	293(2)	203(2)
Range scanned, θ(°)	1.21 - 27.13	2.86 - 27.87
Index range	h:±9, k:±16, l:±22	h:±19, k:±18, l:±21
No. reflections collected	12909	8112
No. unique reflections	7042 (R_{int} = 0.0269)	8112
No. reflections with I>2σ(I)	5234	5561
Data/restraints/parameters	7042 / 2 / 425	8112 / 3 / 443
Goodness of fit, S	1.019	1.027
Final R indices (I>2σ(I))	R_1 = 0.0491, wR_2 = 0.1226	R_1 = 0.0544, wR_2 = 0.1276
R indices (all data)	R_1 = 0.0737, wR_2 = 0.1367	R_1 = 0.0930, wR_2 = 0.1446
Largest diff peak and hole (e.Å^{-3})	0.538; -0.599	0.566; -0.301

THERMAL ANALYSIS

Thermal analysis, including TG and DSC, was carried out for each of the inclusion compounds and the host:guest ratio was determined from the mass loss shown by the TG trace. The TG and DSC traces obtained are given in Figure 5.1 and the results of the analyses are summarised in Table 5.2.

Figure 5.1(a) shows the TG and DSC traces for **WEB24•ETHYL**. The TG trace shows that guest desorption takes place in a single step, corresponding to endotherm A in the DSC trace. The percentage mass loss of 7.3% shown by the TG trace corresponds to H:G = 1:1 (calc. 8.0%). Endotherm C in the DSC trace is due to the melt of the guest-free host compound.

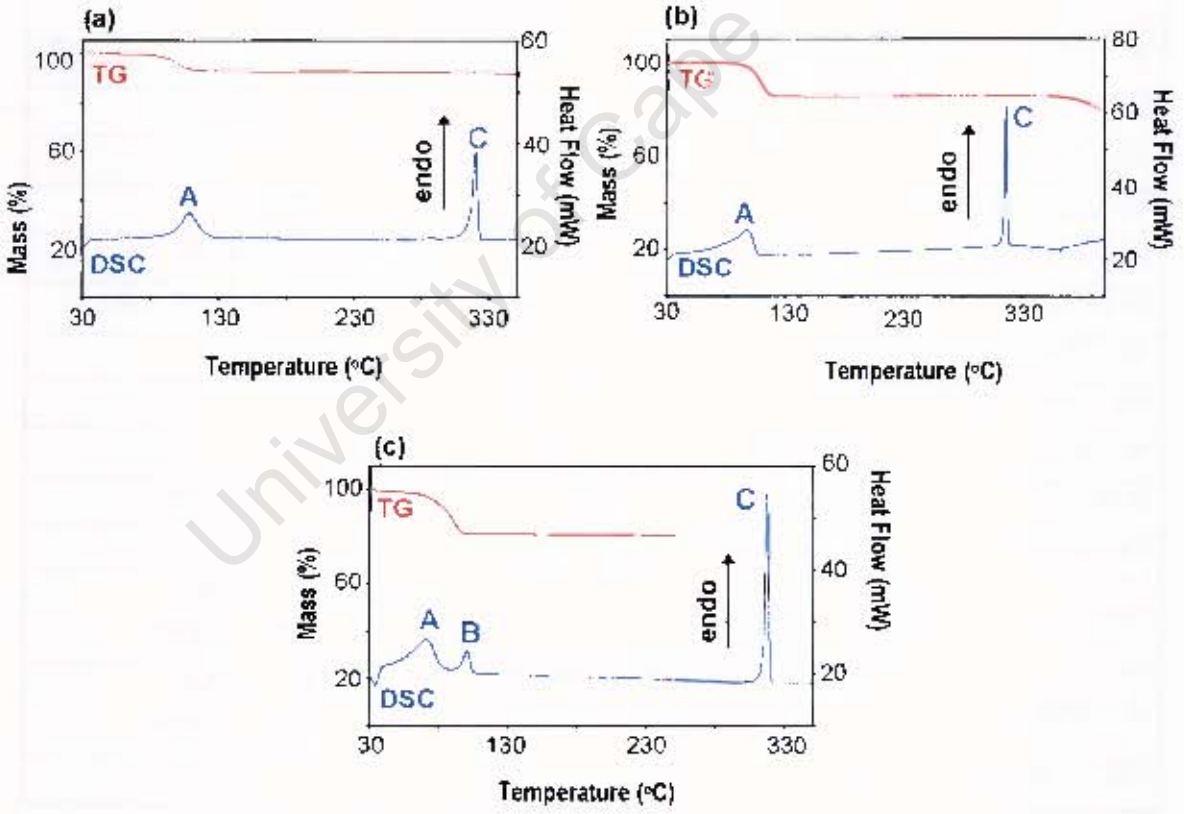

Figure 5.1 TG and DSC traces of **(a) WEB24•ETHYL**, **(b) WEB24•2ETHYL** and **(c) WEB24•2PROPYL**.

The TG and DSC traces of **WEB24•2ETHYL** are shown in Figure 5.1(b). The TG trace shows that the ethylamine guest is released in a single step corresponding to endotherm A in the DSC trace. The percentage mass loss of 14.5% shown by the TG trace corresponds to H:G = 1:2 (calc. 14.9%). Endotherm C in the DSC trace is due to the melt of the guest-free host compound.

For **WEB24•2PROPYL**, Figure 5.1(c), guest release occurs in one step with a percentage mass loss of 17.8%, which corresponds to H:G = 1:2 (calc. 18.7%). The DSC trace shows three endotherms, A, B and C. Endotherms A and B correspond to guest release, while endotherm C represents the melt of the guest-free host compound.

Table 5.2 Thermal analysis results of **WEB24** inclusion compounds

Inclusion Compound	TG Results		H:G ratio	DSC Results		
	Calc. % mass loss	Exp. % mass loss		T_{on} (°C) Peak A	T_{on} (°C) Peak B	T_{on} (°C) Peak C
WEB24•ETHYL	8.0	7.3	1:1	96.2	—	315.1
WEB24•2ETHYL	14.9	14.5	1:2	77.6	—	321.7
WEB24•2PROPYL	18.7	17.8	1:2	52.68	95.03	314.11

HOT STAGE MICROSCOPY

The decomposition of crystals of **WEB24•2ETHYL** and **WEB24•2PROPYL** with heating was observed using hot stage microscopy (HSM). Photographs of the thermal decay of **WEB24•2ETHYL** and **WEB24•2PROPYL** are shown in Figures 5.2 and 5.3 respectively.

The **WEB24•2ETHYL** crystal (shown at room temperature in Figure 5.2(a)) began to turn opaque at 60°C and bubbles of the desorbed guest were observed from 86°C to 120°C (Figure 5.2(b) and (c)). Recrystallisation and then melting of the crystals occurred between 334°C and 341°C (Figure 5.2(d) and (e)).

Crystals of **WEB24•2PROPYL** (shown at room temperature in Figure 5.3(a)) became gradually opaque between 50°C and 76°C (Figure 5.3(b) and (c)). Discolouration of the crystals occurred at 316°C (Figure 5.3(d)) and melting of the crystals was observed between 327°C and 330°C (Figure 5.3(e)).

Once again, the temperature differences between the endotherms displayed in the DSC traces and what is observed during HSM analysis are attributed to physical differences in the instruments and particle size of the samples.

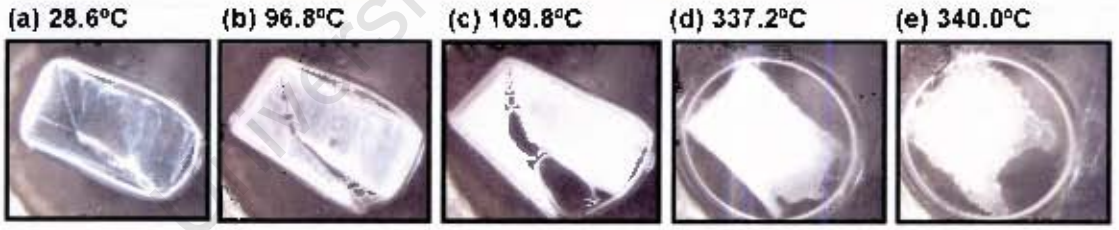

Figure 5.2 Crystals of **WEB24•2ETHYL** during thermal decomposition.

Figure 5.3 Thermal decomposition of **WEB24•2PROPYL** crystals.

STRUCTURE SOLUTION AND ANALYSIS

WEB24•2ETHYL

$C_{38}H_{26}O_2.2(C_2H_7N)$
Guest: ethylamine
Space group: $P\bar{1}$

a = 7.6344(2) Å	α = 76.362(1)°
b = 13.2521(5) Å	β = 89.954(1)°
c = 17.3520(4) Å	γ = 73.703(1)°
V = 1633.19(7) $Å^3$	
Z = 2	

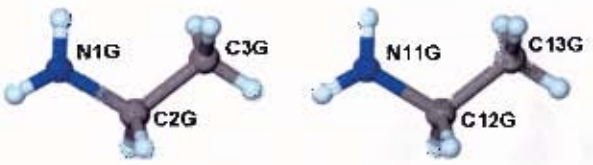

Guest 1 Guest 2

WEB24•2ETHYL belongs to the triclinic crystal system. The E^2-1 values obtained by direct methods show that the structure belongs to the centrosymmetric space group $P\bar{1}$, which was confirmed by the successful refinement of the structure.

The positions of all non-hydrogen host atoms were obtained by direct methods and the non-hydrogen guest atoms were located in difference electron density maps. In subsequent refinements all non-hydrogen atoms were refined with anisotropic temperature factors. The hydroxyl hydrogens on the host molecule were located in difference electron density maps and refined with bond length constraints. All other hydrogen atoms were placed with geometric constraints and refined with isotropic temperature factors equal to $1.2xU_{eq}$ of their parent atoms. The structure refined to $R_1 = 0.0491$.

The structure of **WEB24•2ETHYL** has Z = 2 and H:G = 1:2. The asymmetric unit consists of one host molecule and two guest molecules with both the host molecules and the ethylamine guest molecules located in general positions.

The crystal packing is shown in Figure 5.4, viewed down [001] and [100]. The host molecules pack to form channels down [010] in which the guest molecules are situated. These channels can be clearly seen in Figure 5.5, which shows the crystal packing viewed down [010]. The channels were examined using the program SECTION,[1] which was used to view sections through the unit cell down the b-axis. These sections are illustrated in Figure 5.6.

There are two channels through each unit cell centred at x = 0.5 and z = 0 and 0.5. The channel at z = 0 contains the guest 1 molecules and that at z = 0.5 contains the guest 2 molecules. The channels have a minimum cross-sectional area of approximately 4.1 Å x 2.8 Å at 1.30 Å, 6.60 Å and 11.90 Å down [010] (Figure 5.6(a)). They have a maximum cross-sectional area of approximately 5.4 Å x 4.2 Å where the guests are located at 4.35 Å and 8.90 Å down [010] (Figure 5.6(b)).

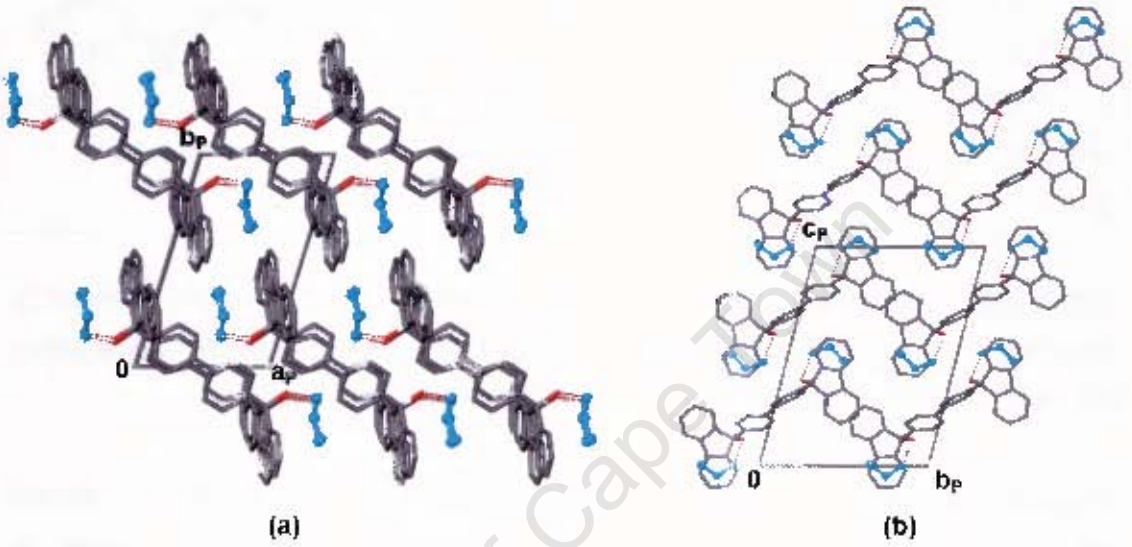

Figure 5.4 Packing diagram of **WEB24•2ETHYL** viewed **(a)** down [001] and **(b)** down [100], with the guest molecules shown in blue for clarity.

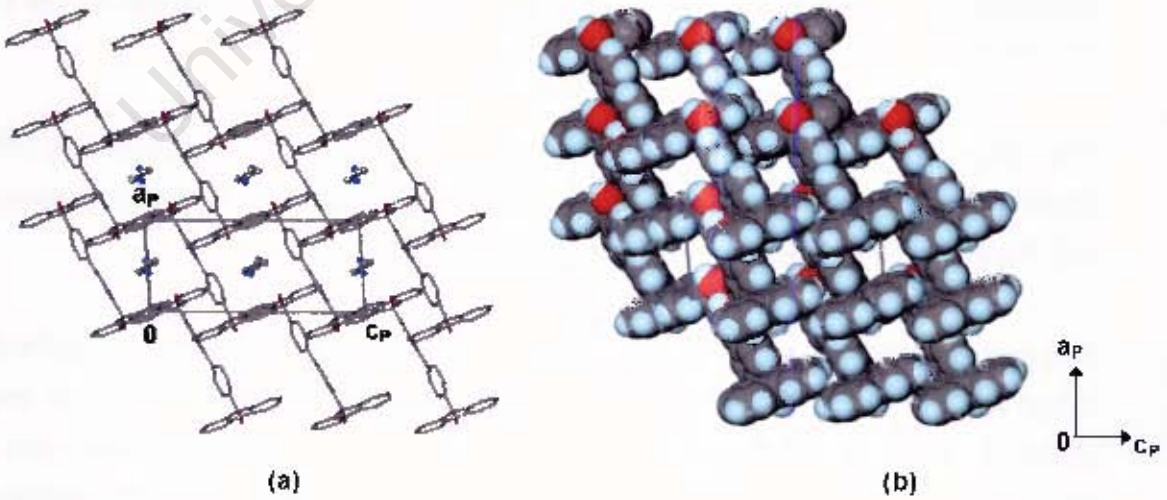

Figure 5.5 **(a)** Packing of **WEB24•2ETHYL** down [010] and **(b)** Space-filling projection down [010] showing the channels of **WEB24•2ETHYL**, with the guest molecules omitted.

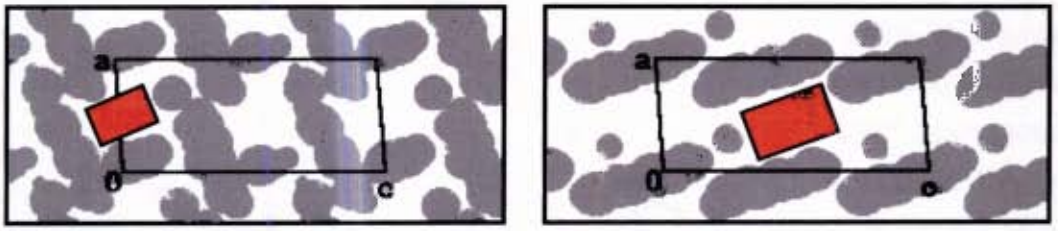

(a) 1.30 Å along [010] **(b)** 4.35 Å along [010]

Figure 5.6 SECTION plots of **WEB24•2ETHYL** (with guest molecules omitted and host molecules represented by grey areas) viewed down [010] with the unit cell sectioned at **(a)** 1.30 Å and **(b)** 4.35 Å along [010].

Each host molecule is hydrogen bonded to two guest molecules via the hydroxyl groups. A diagram illustrating the hydrogen bonding in **WEB24•2ETHYL** is shown in Figure 5.7 and the hydrogen bonding details are given in Table 5.3.

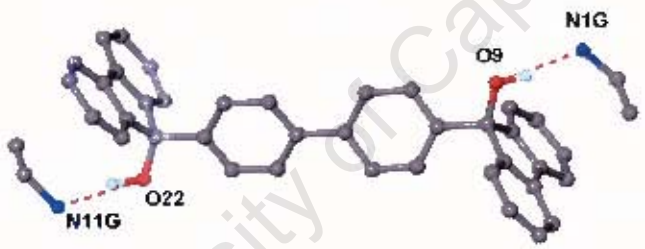

Figure 5.7 Host–guest hydrogen bonding in **WEB24•2ETHYL**.

Table 5.3 Hydrogen bonding details of **WEB24•2ETHYL**

Donor (D)	Acceptor (A)	D–H/Å	D···A/Å	D–H···A/°
O9	N1G	0.960(1)	2.847(2)	170(2)
O22	N11G	0.960(1)	2.792(2)	166(2)

WEB24•2PROPYL

$C_{38}H_{26}O_2.2(C_3H_9N)$
Guest: propylamine
Space group: $Pca2_1$
a = 14.9762(3) Å
b = 14.2481(2) Å
c = 16.7632(2) Å
V = 3576.1(1) Å^3
Z = 4

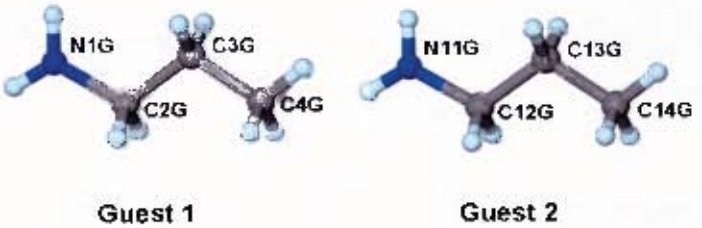

Guest 1 Guest 2

WEB24•2PROPYL belongs to the orthorhombic crystal system and crystallises in the space group $Pca2_1$. The positions of all the non-hydrogen host atoms were obtained by direct methods. The non-hydrogen guest atoms were located in difference electron density maps and in subsequent refinements all non-hydrogen atoms were refined with anisotropic temperature factors. The hydroxyl hydrogens on the host molecule were located in difference electron density maps and refined with bond length constraints. The remaining hydrogen atoms were placed in geometrically constrained positions and refined with isotropic temperature factors equal to $1.2xU_{eq}$ of their parent atoms. The structure refined to $R_1 = 0.0544$.

The structure of **WEB24•2PROPYL** has Z = 4 and H:G = 1:2. The asymmetric unit consists of one host molecule and two guest molecules with both the host and guest molecules located in general positions.

The crystal packing is shown in Figure 5.8 viewed down [100] and [010], as well as in Figure 5.9(a) which shows the packing of the structure viewed down [001]. The host molecules pack to form channels along [001] in which the guest molecules are situated and these channels can be clearly seen in Figure 5.9(b). The channels were also examined using the program SECTION,[1] which was used to view sections through the unit cell down the c-axis and these sections are illustrated in Figure 5.10.

There are two channels through each unit cell which undulate in size and position along [010] and are located at 0 and 0.5 of a unit cell length along [100]. The eight guest molecules in the unit cell are divided between the two channels, with two guest 1 molecules and two guest 2 molecules located in each channel.

The channels have a maximum cross-sectional area of approximately 4.2 Å x 10.8 Å, at 1.0 Å and 9.4 Å down [001] (Figure 5.10(a)) and a minimum cross-sectional area of approximately 5.8 Å x 4.8 Å at 3.9 Å and 12.2 Å along [001]. Sections through the unit cell down [010] and [100] depicting the channels are given in Figures 5.10(b) and (c) respectively.

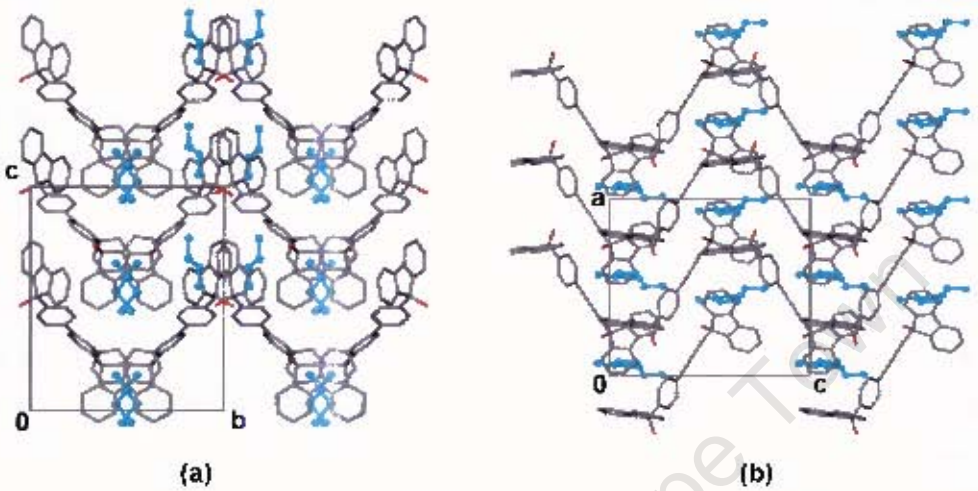

Figure 5.8 Packing diagram of **WEB24•2PROPYL** viewed **(a)** down [100] and **(b)** down [010] with the host molecules shown in stick representation and the guest molecules in ball and stick representation and coloured blue for clarity.

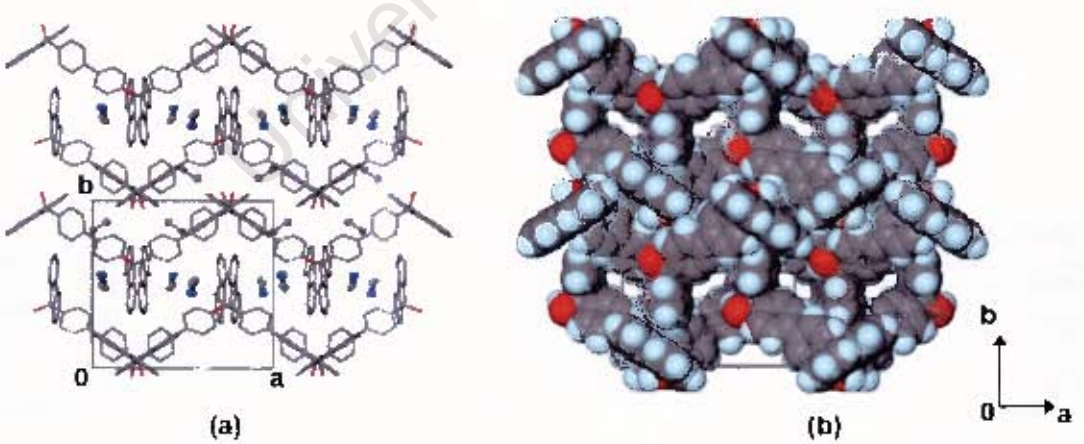

Figure 5.9 **(a)** Packing diagram of **WEB24•2PROPYL** viewed down [001] and **(b)** Space-filling projection down [001] showing the channels of **WEB24•2PROPYL**, with the guest molecules omitted.

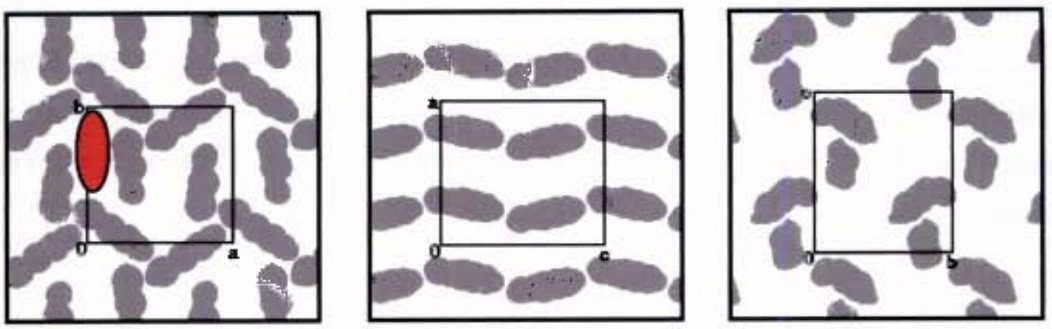

(a) 1.0 Å along [001] **(b)** 7.1 Å along [010] **(c)** 7.5 Å along [100]

Figure 5.10 SECTION plots of **WEB24•2PROPYL** (with guest molecules omitted and host molecules represented by grey areas) viewed with the unit cell sectioned at **(a)** 1.0 Å down [001], **(b)** 7.1 Å down [010] and **(c)** 7.5 Å along [100].

Each host molecule is hydrogen bonded to two guest molecules via the hydroxyl groups. A diagram illustrating the hydrogen bonding in **WEB24•2PROPYL** is shown in Figure 5.11 and the hydrogen bonding details are given in Table 5.4.

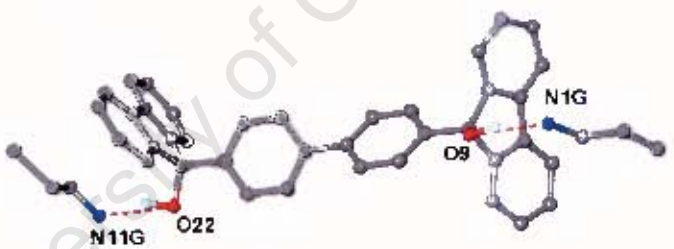

Figure 5.11 Host···guest hydrogen bonding in **WEB24•2PROPYL**.

Table 5.4 Hydrogen bonding details of **WEB24•2PROPYL**

Donor (D)	Acceptor (A)	D–H/Å	D···A/Å	D–H···A/°
O9	N1G	0.960(1)	2.805(3)	167(3)
O22	N11G	0.970(1)	2.760(4)	158(3)

KINETICS OF ENCLATHRATION

The kinetics of enclathration of ethylamine vapour as well as propylamine vapour by **WEB24** were studied using the automated magnetic suspension balance described in detail in Chapter 2. In both cases the kinetic measurements were taken by exposing finely powdered host compound to guest vapour at fixed temperatures, but at various pressures of the guest, and recording the mass increase with time.

WEB24 readily absorbs ethylamine from the vapour to form a clathrate with H:G = 1:1, in contrast to the H:G ratio of 1:2 obtained in the crystals grown from solution. Ethylamine has a high vapour pressure at room temperature, allowing the kinetics of the enclathration reaction to be studied over a wide range of vapour pressures. At T = 283 K experiments were performed with vapour pressures varying from 150 torr to 350 torr and at T = 293 K with vapour pressures varying from 200 torr to 400 torr. Figure 5.12 shows an isothermal curve for the enclathration of ethylamine at both T = 283 K and T = 293 K and at a vapour pressure of 350 torr as an example.

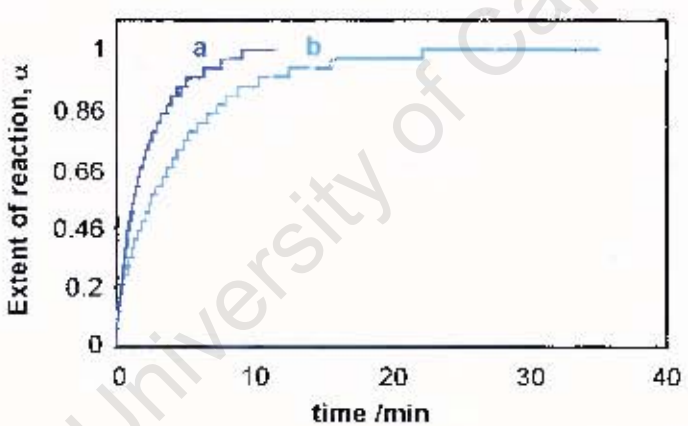

Figure 5.12 Isothermal curves for the enclathration of ethylamine by **WEB24** at a vapour pressure of 350 torr and at temperatures of **(a)** 283 K and **(b)** 293 K.

The kinetic results at both temperatures were fitted to the first order equation,[2] namely, $f(\alpha) = -\ln(1-\alpha)$, over an α-range of 0.1 to 0.7 and the rate constants, k_{obs}, were derived. Under isothermal conditions the velocity of guest uptake is proportional to the vapour pressure of the guest and it was found that there is a threshold pressure, P_0, below which the reaction does not take place. The plot of k_{obs} versus the pressure of the guest is shown in Figure 5.13, which yielded the P_0 values of 92

torr at 283 K and 154 torr at 293 K. For a given pressure of ethylamine, the rate of the reaction decreases with increasing temperature, ie. the enclathration reaction shows anti-Arrhenius behaviour.

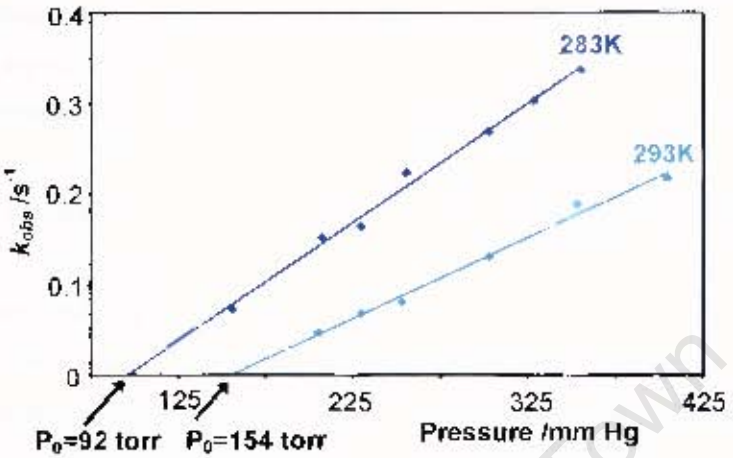

Figure 5.13 Plot of k_{obs} versus the pressure of the guest.

The enclathration of **WEB24** with propylamine vapour yielded a clathrate with H:G = 1:2. This is the same as the H:G ratio obtained in the crystals grown from solution. The kinetics of this reaction were studied at two temperatures and various vapour pressures of propylamine. At T = 298 K experiments were performed with vapour pressures varying from 237 torr to 292 torr and at T = 308 K with vapour pressures varying from 295 torr to 342 torr. The isothermal curve at T = 298 K and a vapour pressure of 250 torr as well as at T = 308 K and a vapour pressure of 340 torr are shown as examples in Figure 5.14.

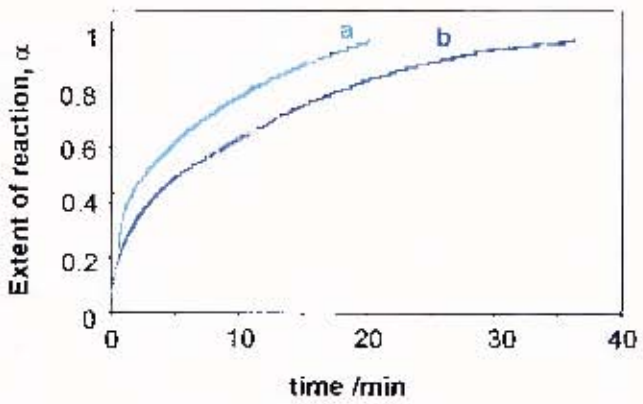

Figure 5.14 Isothermal curves for the enclathration of propylamine by **WEB24** at **(a)** T = 308 K and a vapour pressure of 340 torr and **(b)** T = 298 K and a vapour pressure of 250 torr.

The kinetic results at both temperatures were fitted to the contracting volume equation,[2] namely $f(\alpha)=1-(1-\alpha)^{1/3}$, over an α–range of 0.1 to 0.95 and the rate constants, k_{obs}, were derived. We note once again that there is a threshold pressure, P_0, below which the reaction does not take place. The plot of k_{obs} versus the pressure of the guest is shown in Figure 5.15, which yielded the following P_0 values at the indicated temperatures: 205 torr (298 K), 259 torr (308 K). Once again the enclathration reaction displays anti-Arrhenius behaviour, in that for a given pressure of ethylamine, the rate of the reaction decreases with increasing temperature. The kinetic parameters for the enclathration reactions of **WEB24** with ethylamine and propylamine vapour are given in Table 5.5.

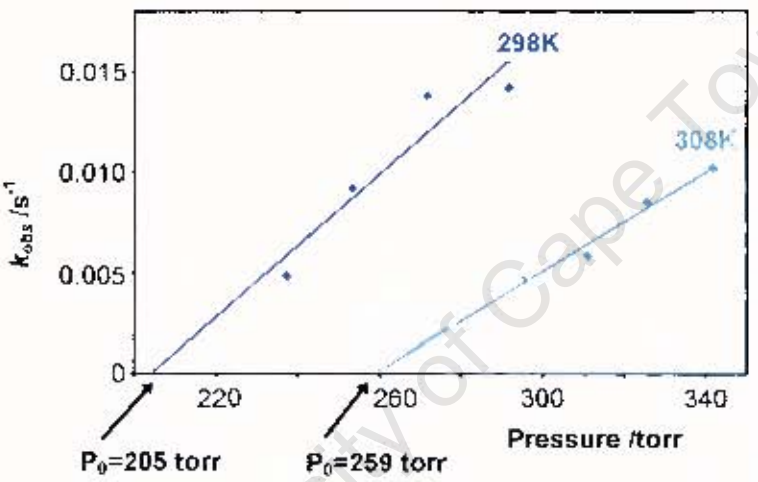

Figure 5.15 Plot of k_{obs} versus the pressure of the guest.

Table 5.5 Kinetic parameters for the enclathration of ethylamine and propylamine by **WEB24**

Guest	Temp (K)	Pressure range (torr)	Alpha range	Kinetic equation	P_0 (torr)
Ethylamine	283	150-350	0.1 – 0.7	$f(\alpha) = -\ln(1-\alpha)$	92
	293	200-400	0.1 – 0.7	$f(\alpha) = -\ln(1-\alpha)$	154
Propylamine	298	237-292	0.1 – 0.95	$f(\alpha) = 1-(1-\alpha)^{1/3}$	205
	308	295-342	0.1 – 0.95	$f(\alpha) = 1-(1-\alpha)^{1/3}$	259

KINETICS OF DESORPTION

The kinetics of desorption of **WEB24•ETHYL**, **WEB24•2ETHYL** and **WEB24•2PROPYL** were analysed by carrying out a series of isothermal TG experiments.

The desorption of **WEB24•ETHYL** takes place in a single step and isothermal TG experiments were carried out over the temperature range 70-90°C at intervals of 5°C. The data were converted to extent of reaction (α) versus time curves which are shown in Figure 5.16. These curves were found to fit the second order equation,[2] namely $f(\alpha) = 1/(1-\alpha)$, over an α-range of 0.05 to 0.90 and the rate constants, k_{obs}, were derived. The semilogarithmic plot of ln k_{obs} versus 1000 K/T is shown in Figure 5.18(a) and yields an activation energy of 103.1 kJ.mol^{-1}.

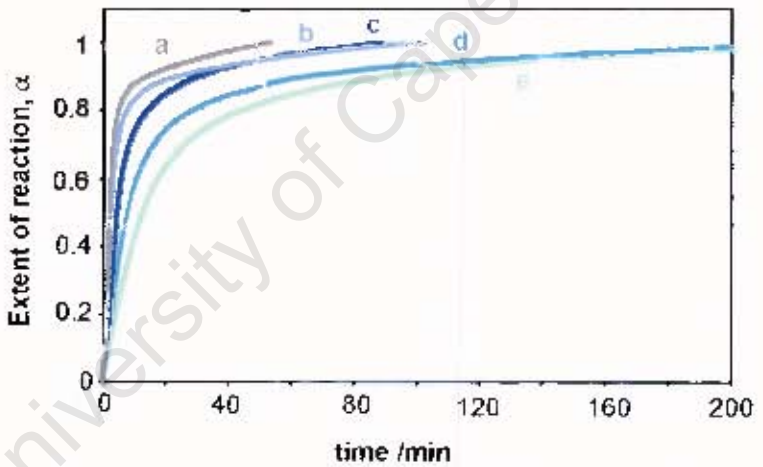

Figure 5.16 Isothermal curves showing α versus time for **WEB24•ETHYL** at **(a)** 90°C, **(b)** 85°C, **(c)** 80°C, **(d)** 75°C and **(e)** 70°C.

The desorption of **WEB24•2ETHYL** also takes place in a single step and isothermal TG experiments were carried out over the temperature range 70-90°C at intervals of 5°C. The data were converted to extent of reaction (α) versus time curves which are displayed in Figure 5.17. These curves were found to fit the first order equation,[2] namely $f(\alpha) = -\ln(1-\alpha)$, over an α-range of 0.05 to 0.90 and the rate constants, k_{obs}, were derived. The semilogarithmic plot of ln k_{obs} versus 1000 K/T is shown in Figure 5.18(b) and yields an activation energy of 122.1 kJ.mol^{-1}.

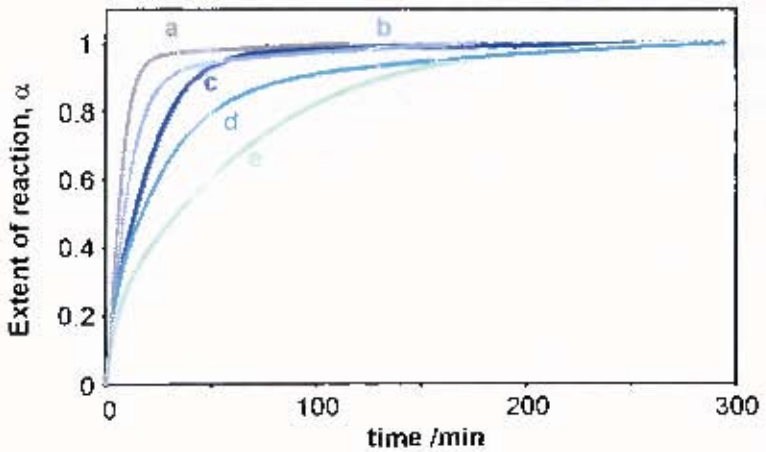

Figure 5.17 Isothermal curves showing α versus time for **WEB24•2ETHYL** at **(a)** 90°C, **(b)** 85°C, **(c)** 80°C, **(d)** 75°C and **(e)** 70°C.

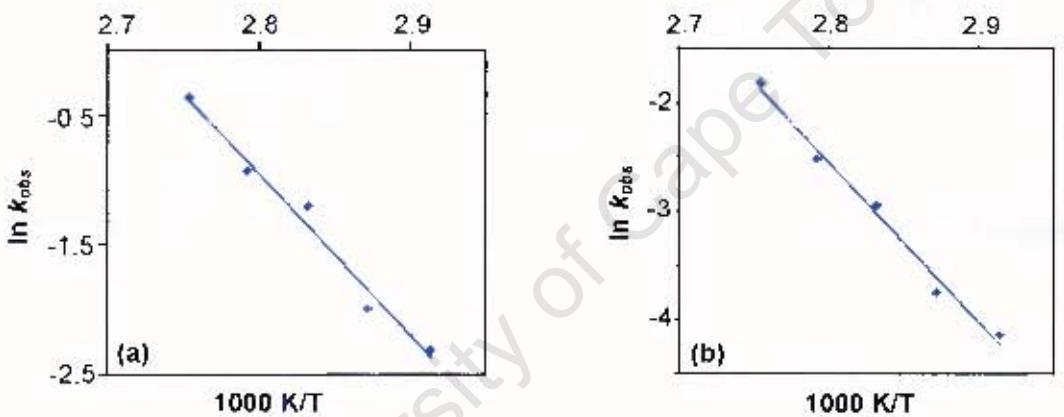

Figure 5.18 Semilogarithmic plots of ln k_{obs} *versus* 1000 *K/T* for the desorption of **(a) WEB24•ETHYL** and **(b) WEB24•2ETHYL**.

The desorption of **WEB24•2PROPYL** was also found to take place in a single step and the kinetics of desorption were analysed by carrying out a series of isothermal TG experiments over the temperature range 55-75°C at intervals of 5°C. The data were converted to extent of reaction (α) versus time curves, which are given in Figure 5.19. These curves were found to fit the second order equation[2], $f(\alpha) = 1/(1-\alpha)$, over an α-range of 0.20 to 0.80 and the rate constants, k_{obs}, were derived. The semilogarithmic plot of ln k_{obs} versus 1000 *K/T* is shown in Figure 5.20 and gives an activation energy of 159.6 kJ.mol^{-1}. The kinetic parameters for the desorption of **WEB24•ETHYL**, **WEB24•2ETHYL** and **WEB24•2PROPYL** are given in Table 5.6.

The semilogarithmic plot shown in Figure 5.20 is not linear and the activation energy obtained represents an 'average' value. We note however that the application of the Arrhenius equation to solids is theoretically questionable and open to wide interpretation. The author has noted significant papers on this subject by M.E. Brown[3,4] in which he cautions against placing too great an emphasis on the values obtained for the pre-exponential factor and the activation energy.

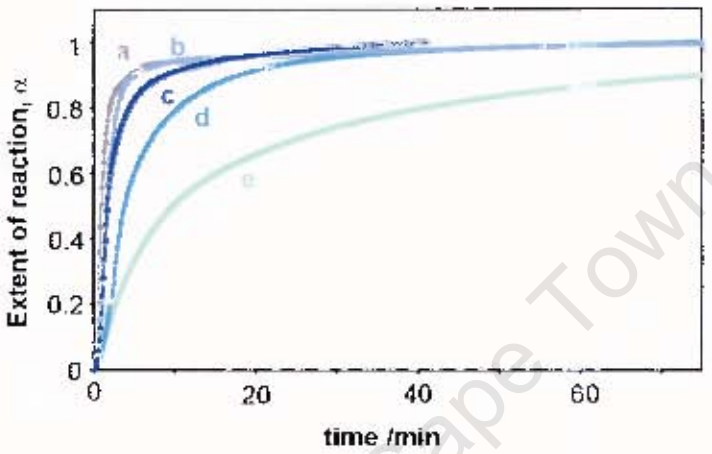

Figure 5.19 Isothermal curves showing α versus time for **WEB24•2PROPYL** at **(a)** 75°C, **(b)** 70°C, **(c)** 65°C, **(d)** 60°C and **(e)** 55°C.

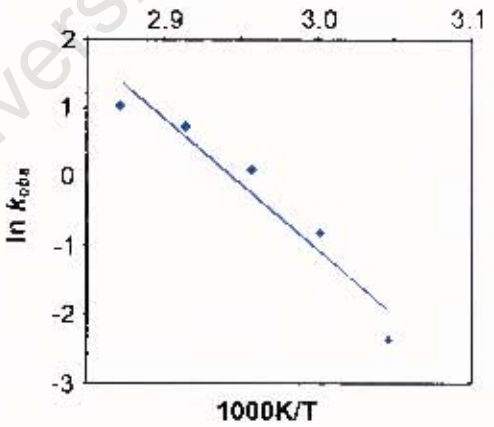

Figure 5.20 Semilogarithmic plot of ln k_{obs} *versus* 1000 K/*T* for the desorption of **WEB24•2PROPYL**.

Table 5.6 Kinetic parameters for the desorption of **WEB24•ETHYL, WEB24•2ETHYL** and **WEB24•2PROPYL**

Inclusion compound	Temperature range (°C)	Alpha range	Kinetic equation	E_a (kJ.mol^{-1})
WEB24•ETHYL	70-90	0.05 – 0.9	$f(\alpha) = 1/(1-\alpha)$	103.1
WEB24•2ETHYL	70-90	0.05 – 0.9	$f(\alpha) = -\ln(1-\alpha)$	122.1
WEB24•2PROPYL	55-75	0.2 – 0.8	$f(\alpha) = 1/(1-\alpha)$	159.6

SUMMARY AND DISCUSSION

Inclusion compounds formed with the host **WEB24** and guests ethylamine and propylamine have been studied. Thermal analysis was carried out and the structures have been elucidated. The kinetics of enclathration of the host with these two guests has been examined as well as the kinetics of desorption of **WEB24•ETHYL**, **WEB24•2ETHYL** and **WEB24•2PROPYL**.

The H:G ratios were determined by thermal gravimetry and both of the inclusion compounds were found to have H:G = 1:2. **WEB24•2ETHYL** crystallises in the space group $P\bar{1}$ with Z = 2 and **WEB24•2PROPYL** crystallises in the space group $Pca2_1$ with Z = 4. In both structures the asymmetric unit consists of one host molecule and two guest molecules, with both the host molecules and guest molecules located in general positions. The hydrogen bonding pattern is similar in both structures and in each case there are two guest molecules hydrogen bonded to the hydroxyl groups of the host molecule.

The crystal packing in the two structures is similar and in both cases the host molecules pack to form channels in which the guest molecules are situated. In **WEB24•2ETHYL** the guest molecules are located in channels down [010], with the guest 1 molecules situated in one channel and the guest 2 molecules situated in a different channel. The channels in the **WEB24•2PROPYL** structure, which are found along [001], contain both guest 1 and guest 2 molecules.

The kinetics of enclathration of ethylamine vapour, as well as propylamine vapour, by the host was studied using an automated magnetic suspension balance. We note once again, as in the case of enclathration of acetone vapour by **TBDDDA**, described in Chapter 3, that for a given pressure of guest vapour, the rate of the reaction decreases with increasing temperature. This anti–Arrhenius behaviour is observed for the enclathration of both ethylamine and propylamine vapour by **WEB24** and arises once again due to the greater propensity of the inclusion compounds to decompose at higher temperatures.

Figure 5.21 shows a space-filling projection of **WEB24** down [100]. From this projection it can be seen that there are exposed hydroxyl groups which protrude from the [011] face. This suggests that this may be the reactive face from which the host

compound can form host-guest hydrogen bonds via the hydroxyl groups with incoming ethylamine or propylamine gas molecules resulting in the formation of **WEB24•ETHYL** and **WEB24•2PROPYL**.

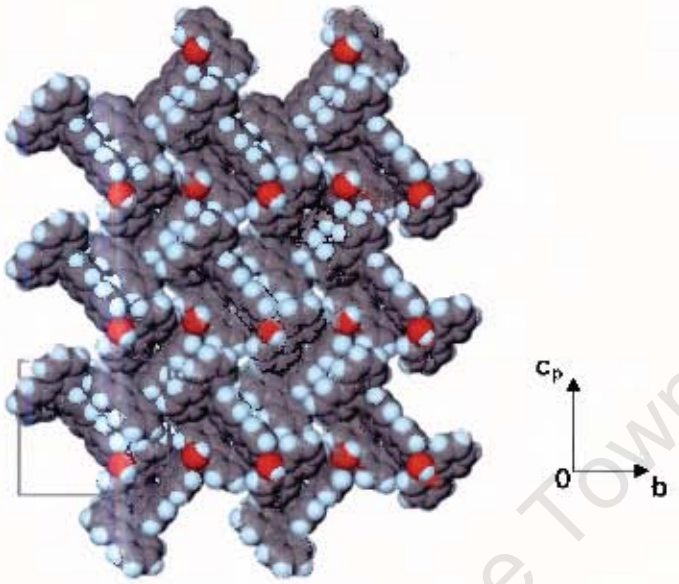

Figure 5.21 Packing of **WEB24** along [100] showing exposed OH groups.

The kinetics of desorption of **WEB24•ETHYL**, **WEB24•2ETHYL** and **WEB24•2PROPYL** were also studied and the results showed the desorption processes to have activation energies of 103.1 $kJ.mol^{-1}$ and 122.1 $kJ.mol^{-1}$ for **WEB24•ETHYL** and **WEB24•2ETHYL** respectively. As might be expected, the desorption of the inclusion compound with H:G = 1:2 requires a higher activation energy than that of the inclusion compound with H:G = 1:1. The desorption process of **WEB24•2PROPYL** was found to have an activation energy of 159.6 $kJ.mol^{-1}$, which is greater than that for either of the inclusion compounds with ethylamine.

REFERENCES

[1] L.J. Barbour, SECTION, A computer program for the graphic display of cross sections through a unit cell, *J. Appl. Cryst.*, 1999, **32**, 353.

[2] A.K. Galwey and M.E. Brown, *Handbook of Thermal analysis and Calorimetry*, ed. M.E. Brown, Elsevier Science B.V., Amsterdam, 1998, p. 162.

[3] M.E. Brown, *Journal of Thermal Analysis*, 1997, **49**, 17.

[4] A.K. Galwey and M.E. Brown, *Proc. R. Soc. Lond. A*, 1995, **450**, 501.

Chapter 6

SELECTIVITY OF THE HOST TTRSC FOR PENTANOL ISOMERS

*The host $1^4,1^6,5^4,5^6$-tetrahydroxy-2,4,6,8-tetrapentyl-$3^4,3^6,7^4,7^6$-tetra(p-toluenesulfonyl-oxy)-1,3,5,7(1,3)-tetrabenzenacyclooctaphane (abbreviated **TTRSC**) forms inclusion compounds with seven pentanol isomers, namely 1-pentanol, 2-pentanol, 3-pentanol, 2-methyl-1-butanol, 3-methyl-1-butanol, 2-methyl-2-butanol and 3-methyl-2-butanol. Thermal analysis of these compounds has been carried out which shows that they all have H:G = 1:2 and their structures have been elucidated and compared. Competition experiments were also carried out with a number of pairs of guests in order to establish the selectivity of **TTRSC** for some of the pentanols and thereby investigate the capability of this host for the separation of pentanol isomers. The solubility curve of the inclusion compound with 1-pentanol was measured and cooling crystallisations at different temperatures were carried out as part of the brief study of nucleation and crystal growth.*

Crystallographic data, experimental and refinement parameters are given in Table 6.1. Final atomic coordinates, bond lengths and angles, torsion angles, thermal parameters and tables of observed and calculated structure factors for each of the crystal structures are given in the appendices.

COMPLEX PREPARATION

Suitable crystals of the inclusion compounds were formed by the method of slow evaporation as described in Chapter 2.

The inclusion compounds obtained and their abbreviations are as follows:

TTRSC + 1-pentanol (H:G = 1:2): **TTRSC•2(1PENT)**
TTRSC + 2-pentanol (H:G = 1:2): **TTRSC•2(2PENT)**
TTRSC + 3-pentanol (H:G = 1:2): **TTRSC•2(3PENT)**
TTRSC + 2-methyl-1-butanol (H:G = 1:2): **TTRSC•2(2M1B)**
TTRSC + 3-methyl-1-butanol (H:G = 1:2): **TTRSC•2(3M1B)**
TTRSC + 2-methyl-2-butanol (H:G = 1:2): **TTRSC•2(2M2B)**
TTRSC + 3-methyl-2-butanol (H:G = 1:2): **TTRSC•2(3M2B)**

The guest numbering schemes are given at the beginning of each structure analysis and the host numbering scheme is shown below:

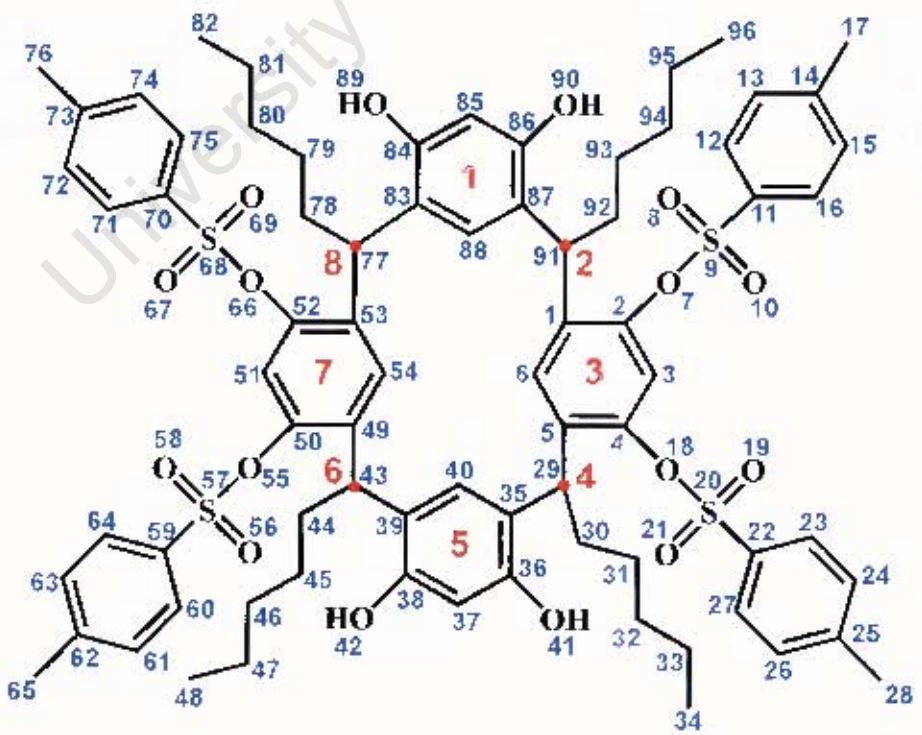

Table 6.1 Crystal data, experimental and refinement parameters

	TTRSC•2(1PENT)	**TTRSC•2(2PENT)**	**TTRSC•2(2M1B)**	**TTRSC•2(3M1B)**
Molecular formula	$C_{76}H_{68}O_{16}S_4 \cdot 2(C_5H_{12}O)$	$C_{76}H_{68}O_{16}S_4 \cdot 2(C_5H_{12}O)$	$C_{76}H_{68}O_{16}S_4 \cdot 2(C_5H_{12}O)$	$C_{76}H_{68}O_{16}S_4 \cdot 2(C_5H_{12}O)$
Guest	1-pentanol	2-pentanol	2-methyl-1-butanol	3-methyl-1-butanol
Host:guest ratio	1:2	1:2	1:2	1:2
M_r/g.mol^{-1}	1562.08	1562.08	1562.08	1562.08
Crystal symmetry	Orthorhombic	Orthorhombic	Orthorhombic	Orthorhombic
Space group	Pcca	Pcca	Pcca	Pcca
a/Å	60.711(1)	61.1635(6)	60.926(1)	61.0866(7)
b/Å	11.4430(2)	11.4335(1)	11.1517(2)	11.4465(1)
c/Å	24.3637(5)	24.3952(2)	24.4772(7)	24.4263(2)
α/°	90	90	90	90
β/°	90	90	90	90
γ/°	90	90	90	90
Z	8	8	8	8
V/Å^3	16925.7(6)	17059.9(3)	16630.4(7)	17079.5(3)
μ (Mo-Kα)/mm^{-1}	0.178	0.177	0.181	0.177
Temp of data collection (K)	293(2)	203(2)	213(2)	203(2)
Range scanned, θ(°)	2.21 - 25.47	2.22 - 21.94	1.79 - 25.02	3.15 - 23.22
Index range	h:0-73, k:0-13, l:0-29	h:-63-64, k:±12, l:±25	h:+71, k:0-13, l:±28	h:-65-66, k:±12, l:±27
No. reflections collected	14590	15464	29303	19023
No. unique reflections	14590	9145 (R_{int} = 0.0162)	11039 (R_{int} = 0.0928)	10817 (R_{int} = 0.0353)
No. reflections with I>2σ(I)	5783	7823	5615	7138
Data/restraints/ parameters	14590 / 4 / 954	9145 / 4 / 962	11039 / 30 / 959	10817 / 4 / 977
Goodness of Fit, S	1.017	1.061	1.052	1.029
Final R indices (I>2σ(I))	R_1 = 0.0934, wR_2 = 0.2569	R_1 = 0.0780, wR_2 = 0.2130	R_1 = 0.0923, wR_2 = 0.2444	R_1 = 0.0801, wR_2 = 0.2093
R indices (all data)	R_1 = 0.2118, wR_2 = 0.3321	R_1 = 0.0890, wR_2 = 0.2239	R_1 = 0.1900, wR_2 = 0.2959	R_1 = 0.1255, wR_2 = 0.2375
Largest diff peak and hole (e.Å^{-3})	0.522; -0.379	0.511; -0.478	0.821; -0.535	0.518; -0.410

Table 6.1 (cont.) Crystal data, experimental and refinement parameters

	TTRSC•2(3PENT)	TTRSC•2(2M2B)	TTRSC•2(3M2B)
Molecular formula	$C_{76}H_{88}O_{16}S_4$. $2(C_5H_{12}O)$	$C_{76}H_{88}O_{16}S_4$. $2(C_5H_{12}O)$	$C_{76}H_{88}O_{16}S_4$. $2(C_5H_{12}O)$
Guest	3-pentanol	2-methyl-2-butanol	3-methyl-2-butanol
Host:guest ratio	1:2	1:2	1:2
M_r/g.mol^{-1}	1562.08	1562.08	1562.08
Crystal symmetry	Monoclinic	Monoclinic	Monoclinic
Space group	$P2_1/n$	$P2_1/n$	$P2_1/n$
a/Å	19.3857(2)	19.2199(1)	19.2340(2)
b/Å	22.3884(2)	22.3700(2)	11.2713(2)
c/Å	19.7808(3)	19.9958(2)	19.9335(3)
α/°	90	90	90
β/°	101.634(1)	101.870(1)	102.640(1)
γ/°	90	90	90
Z	4	4	2
V/Å^3	8408.8(2)	8413.3(1)	4216.7(1)
μ (Mo-Kα)/mm^{-1}	0.179	0.184	0.179
Temp of data collection (K)	173(2)	173(2)	203(2)
Range scanned, θ(°)	2.68 - 27.88	1.34 - 28.29	2.77 – 27.87
Index range	h:±25, k:±29, l:±26	h:±25, k:±29, l:±26	h:±25, k: ±14, l:±26
No. reflections collected	38696	40462	18920
No. unique reflections	19912 (R_{int} = 0.0770)	20714 (R_{int} = 0.0481)	9932 (R_{int} = 0.0449)
No. reflections with I>2σ(I)	9805	12127	5306
Data/restraints/ parameters	19912 / 4 / 1002	20714 / 4 / 1001	9932 / 2 / 486
Goodness of Fit, S	1.017	1.036	1.050
Final R indices (I>2σ(I))	R_1 = 0.0706, wR_2 = 0.1760	R_1 = 0.0668, wR_2 = 0.1770	R_1 = 0.0776, wR_2 = 0.2153
R indices (all data)	R_1 = 0.1613, wR_2 = 0.2121	R_1 = 0.1253, wR_2 = 0.2070	R_1 = 0.1465, wR_2 = 0.2566
Largest diff peak and hole (e.Å^{-3})	0.536; -0.440	0.668; -0.569	0.570; -0.451

THERMAL ANALYSIS

Thermal analysis, including TG and DSC, was carried out for each of the inclusion compounds and in each case the TG trace showed a host:guest ratio of 1:2. The results of the TG and DSC analyses are summarised in Table 6.2.

The TG and DSC traces of **TTRSC** are shown in Figure 6.1(a). The TG trace shows no mass loss and the DSC trace shows a single endotherm with T_{on} = 211.3°C which corresponds to the melt of the host.

The TG and DSC traces of **TTRSC•2(1PENT)** are shown in Figure 6.1(b). The TG trace shows a single step desorption, corresponding to endotherm A in the DSC trace. The percentage mass loss of 11.0% shown by the TG trace corresponds to H:G = 1:2 (calc. 11.3%). Endotherm B in the DSC trace is due to the melt of the guest-free host compound.

For **TTRSC•2(2PENT)**, Figure 6.1(c), guest release occurs in a multiple step process with a total percentage mass loss of 11.6%, which corresponds to H:G = 1:2 (calc. 11.3%). In the DSC trace, guest release is shown by complex endotherm A, while endotherm B represents the melt of the guest-free host compound.

Figure 6.1(d) shows the TG and DSC traces for **TTRSC•2(2M1B)**. The TG trace shows that the guest is released in two steps with a total percentage mass loss of 11.6%, which corresponds to H:G = 1:2 (calc. 11.3%). Endotherm A in the DSC trace represents desorption of the guest and endotherm B is due to the melt of the guest-free host compound.

The TG and DSC traces of **TTRSC•2(3M1B)** are shown in Figure 6.1(e). The TG trace shows a single step desorption, with a corresponding endotherm, endotherm A, in the DSC trace followed by a second endotherm, endotherm B, due to the melting of the guest-free host compound. The percentage mass loss of 11.5% shown by the TG trace corresponds to H:G = 1:2 (calc. 11.3%).

Figure 6.1(f) shows the TG and DSC traces of **TTRSC•2(3PENT)**. The TG trace shows that guest release occurs in multiple steps with a total mass loss of 10.2% which corresponds to H:G = 1:2 (calc. 11.3%). The DSC trace shows two endotherms with complex endotherm A corresponding to loss of the guest and endotherm B representing the melt of the guest-free host compound.

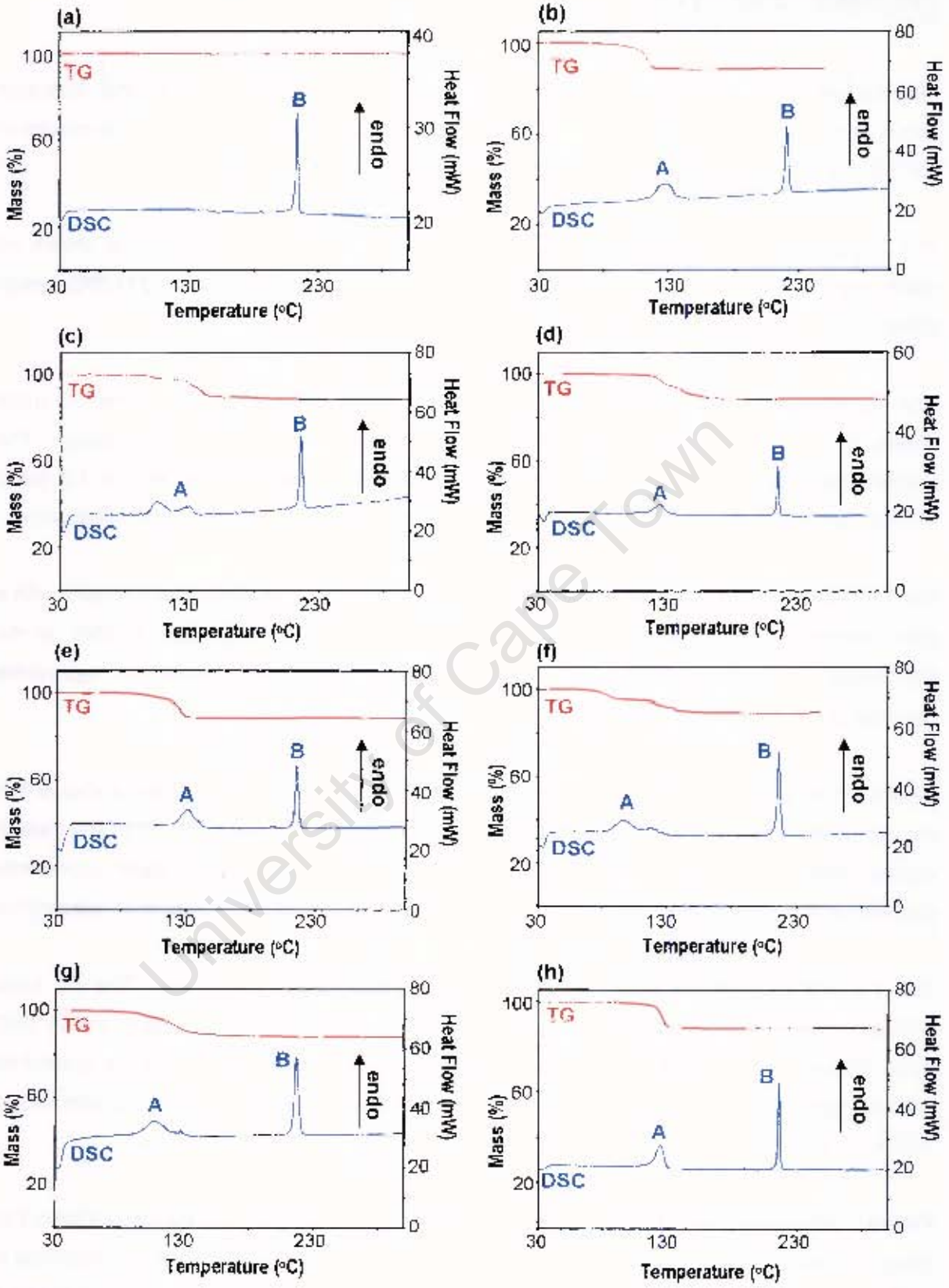

Figure 6.1 TG and DSC traces of **(a) TTRSC**, **(b) TTRSC•2(1PENT)**, **(c) TTRSC•2(2PENT)**, **(d) TTRSC•2(2M1B)**, **(e) TTRSC•2(3M1B)**, **(f) TTRSC•2(3PENT)**, **(g) TTRSC•2(2M2B)** and **(h) TTRSC•2(3M2B)**.

For **TTRSC•2(2M2B)**, Figure 6.1(g), the TG trace shows a two step desorption corresponding to endotherm A in the DSC trace. The percentage mass loss of 11.6% shown by the TG trace corresponds to H:G = 1:2 (calc. 11.3%). Endotherm B in the DSC trace is due to melting of the guest-free host compound.

Figure 6.1(h) shows the TG and DSC traces of **TTRSC•2(3M2B)**. It can be seen from the TG trace that guest release occurs in a single step with a percentage mass loss of 11.8% corresponding to H:G = 1:2 (calc. 11.3%). The DSC trace shows two endotherms with endotherm A due to guest release and endotherm B corresponding to the melt of the guest-free host compound.

Table 6.2 Thermal analysis results of **TTRSC** inclusion compounds

Inclusion Compound	TG Results		H:G ratio	DSC Results	
	Calc. % mass loss	Exp. % mass loss		T_{on} (°C) Peak A	T_{on} (°C) Peak B
TTRSC•2(1PENT)	11.3	11.0	1:2	116.7	218.3
TTRSC•2(2PENT)	11.3	11.6	1:2	98.1	214.8
TTRSC•2(2M1B)	11.3	11.6	1:2	116.1	213.5
TTRSC•2(3M1B)	11.3	11.5	1:2	121.4	214.9
TTRSC•2(3PENT)	11.3	10.2	1:2	85.2	215.0
TTRSC•2(2M2B)	11.3	11.6	1:2	94.8	215.0
TTRSC•2(3M2B)	11.3	11.8	1:2	117.6	214.1

HOT STAGE MICROSCOPY

Crystals of each of the inclusion compounds formed with TTRSC were observed during thermal decomposition by hot stage microscopy (HSM). Photographs were taken during the thermal events which occurred and these images are shown in Figures 6.2 to 6.8.

The **TTRSC•2(1PENT)** crystals (shown at room temperature in Figure 6.2(a)) began to turn opaque at 120°C (Figure 6.2(b)) and bubbles of the desorbed guest were observed in the silicone oil between 127°C and 151°C, during which time the crystals became completely opaque (Figure 6.2(c)). The crystals melted between 220°C and 221°C (Figure 6.2(d)). The crystals of **TTRSC•2(2PENT)** (shown at room temperature in Figure 6.3(a)) started to become opaque at 98°C and from 106°C to 140°C bubbles of desorbed guest were released (Figure 6.3(b) and (c)). At 200°C further bubbles were observed until the crystals melted between 224°C and 225°C (Figure 6.3(d)).

The **TTRSC•2(2M1B)** crystals (shown at room temperature in Figure 6.4(a)) became slowly opaque from 107°C and bubbles of desorbed guest were observed in the silicone oil from 125°C to 175°C (Figure 6.4(b) and (c)). Melting of the crystals took place between 224°C and 225°C (Figure 6.4(d)). The **TTRSC•2(3M1B)** crystals (shown at room temperature in Figure 6.5(a)) began to change from clear to opaque at 90°C (Figure 6.5(b)). Bubbles were observed in the silicone oil at 133°C and this guest release proceeded until 156°C (Figure 6.5(c)). The crystals melted between 221°C and 222°C (Figure 6.5(d)).

The crystals of **TTRSC•2(3PENT)** (shown at room temperature in Figure 6.6(a)) began to turn opaque at 94°C and at the same temperature bubbles of desorbed guest were observed (Figure 6.6(b) and (c)). This guest release was complete at 125°C and the crystals melted between 224°C and 225°C (Figure 6.6(d)).

The **TTRSC•2(2M2B)** crystals (shown at room temperature in Figure 6.7(a)) released bubbles of desorbed guest between 97°C and 106°C and simultaneously became opaque (Figure 6.7(b) and (c)). Melting took place between 222°C and 223°C (Figure 6.7(d)). The crystals of **TTRSC•2(3M2B)** (shown at room temperature in Figure 6.8(a)) started to become opaque at 120°C. Bubbles were observed from 126°C until 158°C (Figure 6.8(b)) and the crystals melted between 221°C and 222°C (Figure 6.8(c)).

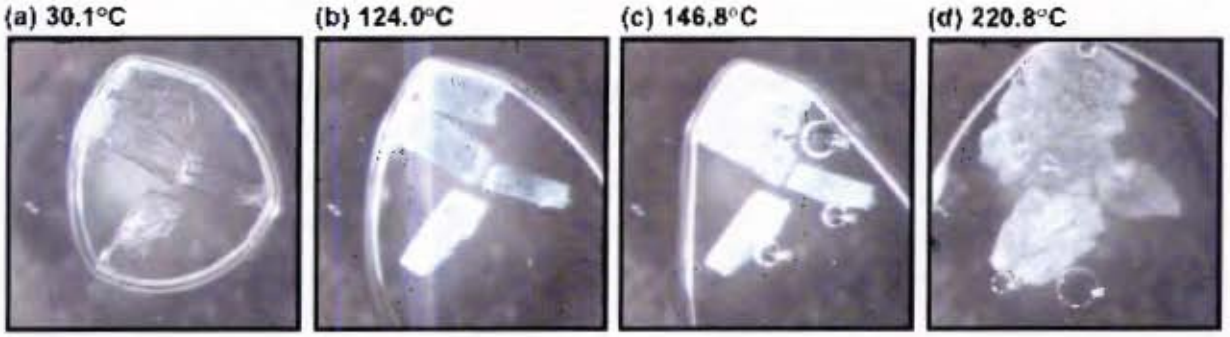

Figure 6.2 Crystals of **TTRSC•2(1PENT)** during thermal decomposition.

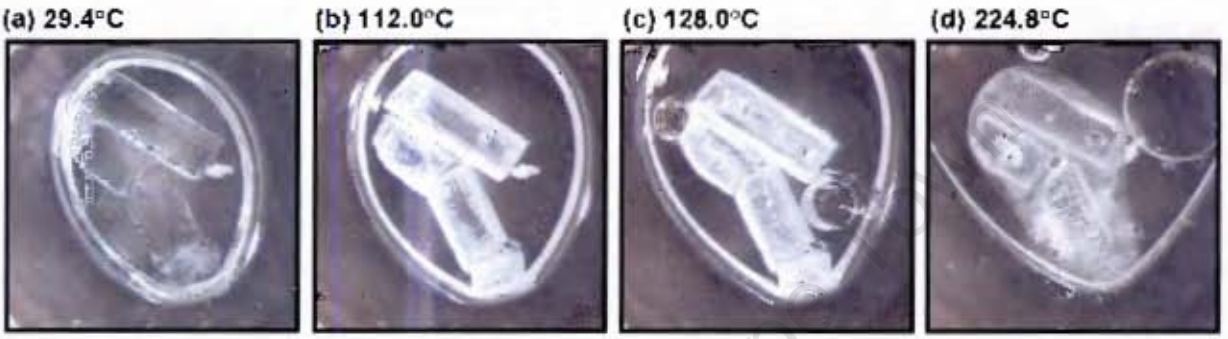

Figure 6.3 Thermal decay of **TTRSC•2(2PENT)** crystals.

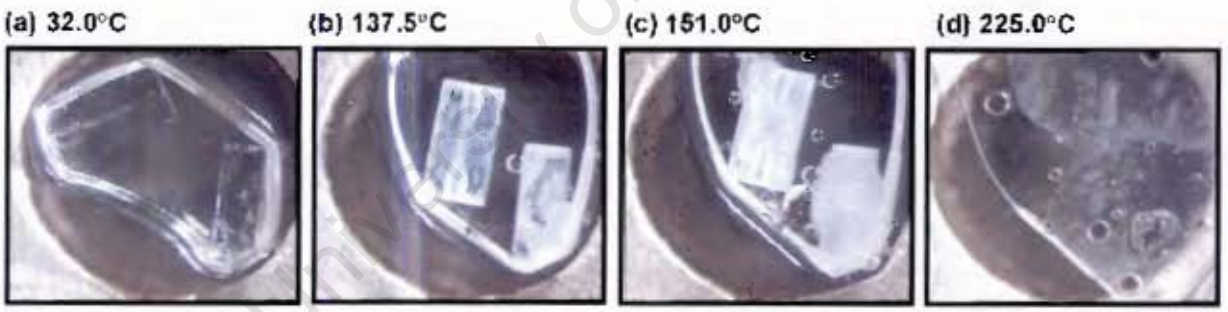

Figure 6.4 **TTRSC•2(2M1B)** crystals during thermal decay.

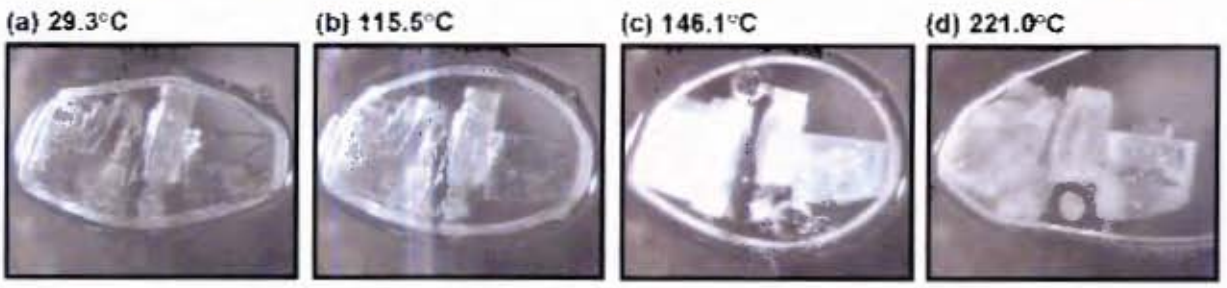

Figure 6.5 Thermal decomposition of **TTRSC•2(3M1B)** crystals.

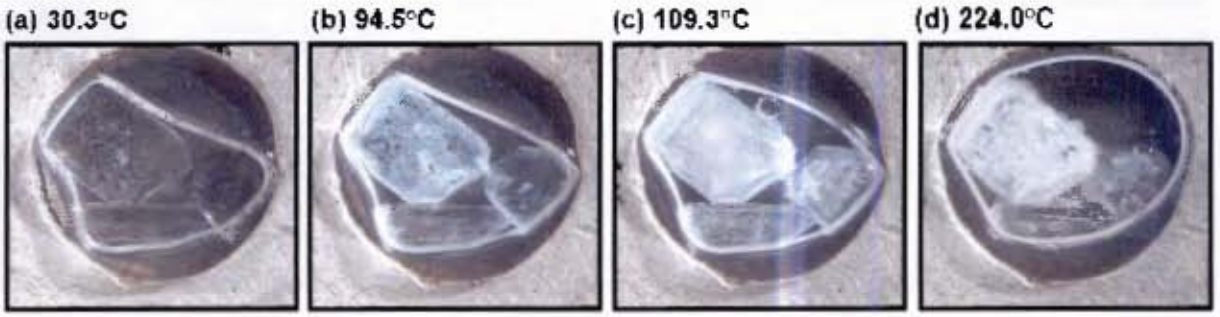

Figure 6.6 Crystals of **TTRSC•2(3PENT)** during thermal decay.

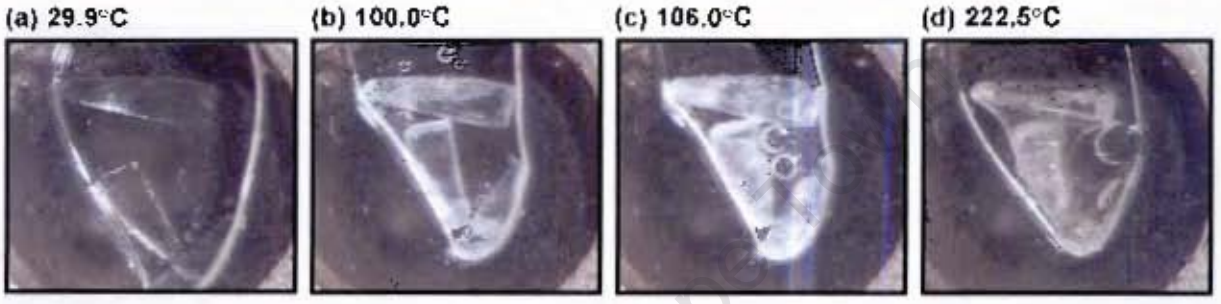

Figure 6.7 Thermal decomposition of crystals of **TTRSC•2(2M2B).**

Figure 6.8 **TTRSC•2(3M2B)** crystals during thermal decay.

STRUCTURE SOLUTION AND ANALYSIS

TTRSC•2(1PENT)

$C_{76}H_{88}O_{16}S_4.2(C_5H_{12}O)$
Guest: 1-pentanol
Space group: Pcca
a = 60.711(1) Å
b = 11.4430(2) Å
c = 24.3637(5) Å
V = 16925.7(6) Å^3
Z = 8

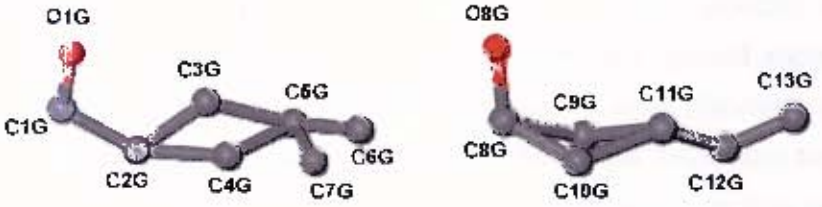

Guest 1 Guest 2

1-pentanol: HO-CH_2-CH_2-CH_2-CH_2-CH_3

TTRSC•2(1PENT) was found to crystallise in the orthorhombic crystal system, in the space group Pcca. The positions of all non-hydrogen host atoms were obtained by direct methods and the positions of non-hydrogen guest atoms were located in difference electron density maps. The hydroxyl hydrogens on the host molecule were located in difference electron density maps and refined with bond length constraints. All other hydrogen atoms were placed with geometric constraints and refined with isotropic temperature factors equal to $1.2xU_{eq}$ of their parent atoms. All non-hydrogen atoms of the host molecule, except for the disordered alkyl chain carbon atoms, as well as the oxygen atoms of the guest molecules were refined with anisotropic temperature factors. The remaining guest atoms and the disordered alkyl chain carbon atoms were refined isotropically. The structure refined to R_1 = 0.0934.

Three of the alkyl chains of the host molecule exhibit disorder with atoms C45, C82, C95 and C96 disordered over two positions. The two partial atoms are labelled with suffixes A and B in each case and the disorder is depicted in Figure 6.9. In the guest 1 molecule, the carbon atoms at positions 3 and 5 were found to be disordered over two positions and in the guest 2 molecule, the carbon atom at position 2 was modelled over two positions. The site occupancy factors of the partial atoms for both the host and guest molecules are given in Table 6.3 (page 179). The disorder in the guest molecules is depicted in the guest numbering scheme above. In each case the temperature factors of the two partial atoms were forced to refine to the same value. This value was then fixed and the site occupancy factors were allowed to refine to give a total site occupancy of one. The refined site occupancy factors were then fixed and the isotropic temperature factors of the two partial atoms were allowed to refine independently.

The structure of **TTRSC•2(1PENT)** has Z = 8, with the asymmetric unit containing one host molecule and two guest molecules. Both the host and guest molecules are located in general positions. The crystal packing viewed along [010] is shown in Figure 6.10. The host molecules pack to form undulating channels along [001] which are shown in Figure 6.11. The channels were examined using the program SECTION,[3] which was used to view sections through the unit cell down the c-axis. These sections are illustrated in Figure 6.12. The channels have a maximum cross-section of approximately 7.6 Å x 8.0 Å, where the guest molecules are located and a minimum cross-section of approximately 5.7 Å x 3.8 Å. They shift along the b-axis, with both the minimum and maximum cross-sections located at y = 0 and x = 0.12, 0.36, 0.63 and 0.88. In Figure 6.12, the minimum and maximum cross-sections of the channels located at x = 0.63 (Figure 6.12(a) and (b)) and x = 0.12 (Figure 6.12(c) and (d)) are highlighted in red.

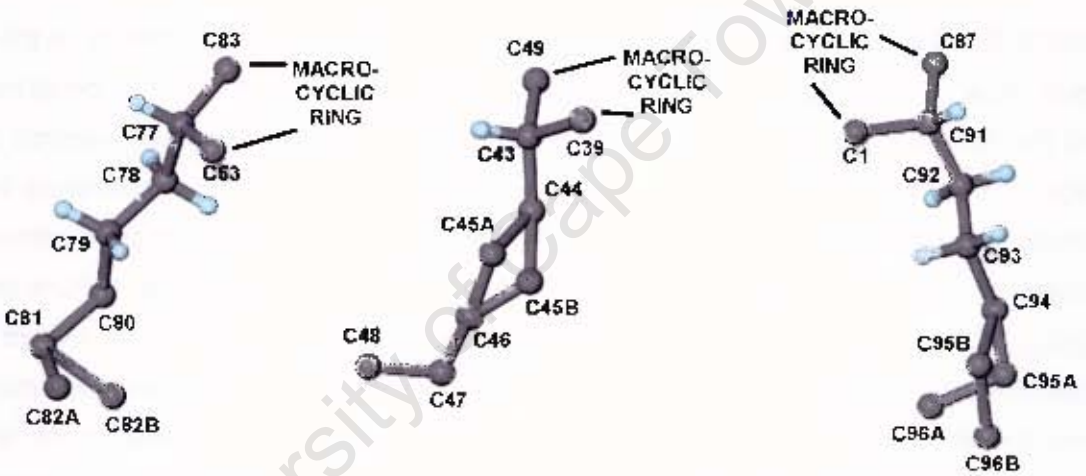

Figure 6.9 Disorder in alkyl chains of host molecule in **TTRSC•2(1PENT)**.

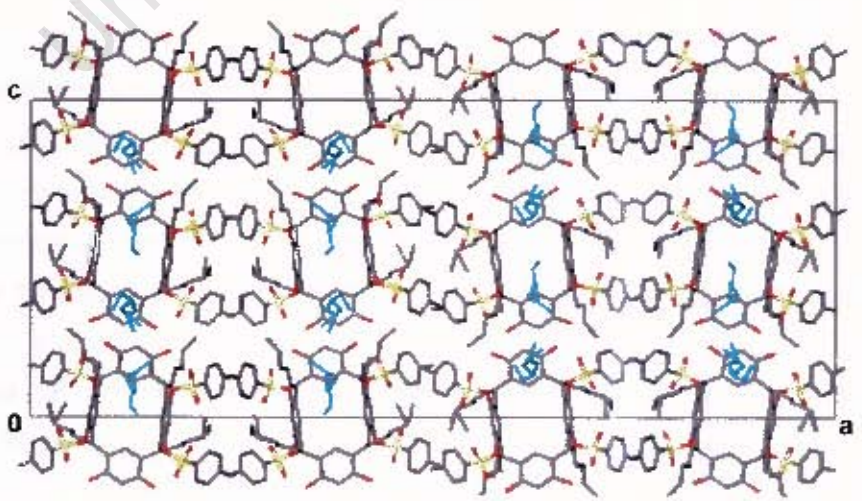

Figure 6.10 Packing diagram of **TTRSC•2(1PENT)** viewed along [010] with guest molecules shown in blue for clarity.

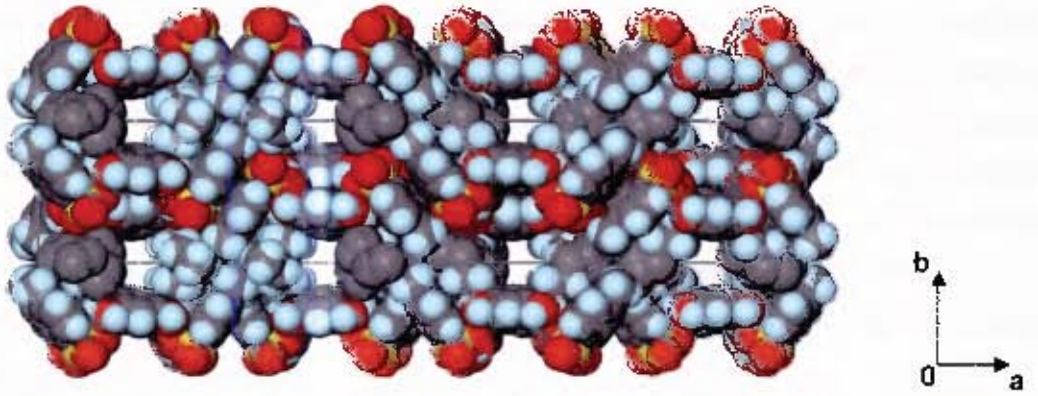

Figure 6.11 View down the channels of **TTRSC•2(1PENT)** along [001] with guest molecules omitted and host molecules represented with van der Waals radii.

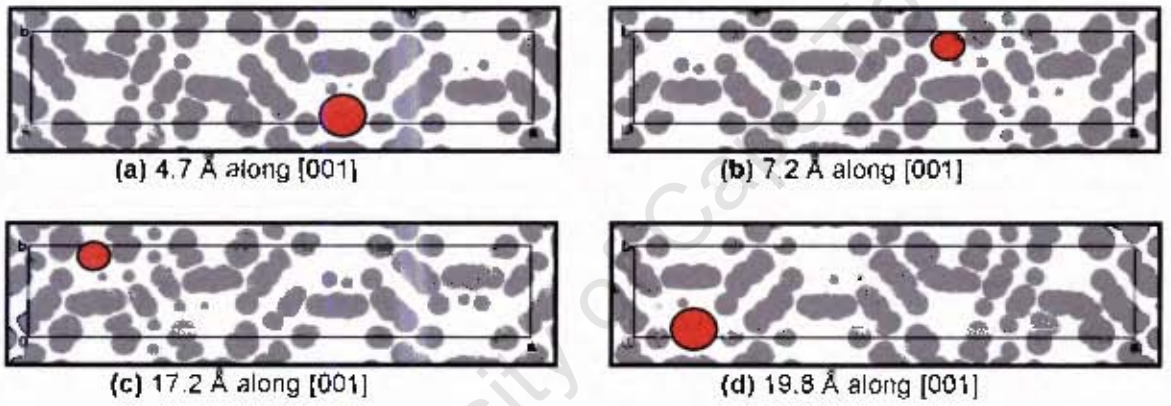

Figure 6.12 SECTION plots of **TTRSC•2(1PENT)** (with guest molecules omitted and host molecules represented by grey areas) viewed down [001] with the unit cell sectioned at **(a)** 4.7 Å, **(b)** 7.2 Å, **(c)** 17.2 Å and **(d)** 19.8 Å along [001].

The same hydrogen bonding pattern is exhibited by all seven of the inclusion compounds and so this pattern will be described here only once. In each case both guest molecules are hydrogen bonded to the host molecule via (Host)-O-H•••OH(Guest). The structures are all additionally stabilised by hydrogen bonding which occurs between the host molecules from the hydroxyl groups which are not hydrogen bonded to the guests, to one of the oxygen atoms on the tosylate groups of the next host. The hydrogen bonding in **TTRSC•2(1PENT)** is illustrated in Figure 6.13 and details for all of the structures are given in Table 6.4 (page 194).

In addition to these hydrogen bonds there are close contacts between the guest 1 oxygen atom and O66 as well as O67, which are found in a tosylate group of the host molecule. These close contacts vary in length among the structures from 3.0 Å to 3.4 Å (close contact to O66) and from 3.2 Å to 3.6 Å (close contact to O67). Similarly there are close contacts between the guest 2 oxygen atom and O18 and O21, which vary in length among the structures from 3.1 Å to 3.5 Å (close contact to O18) and from 3.1 Å to 3.6 Å (close contact to O21). Although hydrogen atoms have not been placed on the guest molecules in all of the structures, it is likely that these interactions represent weak hydrogen bonds.

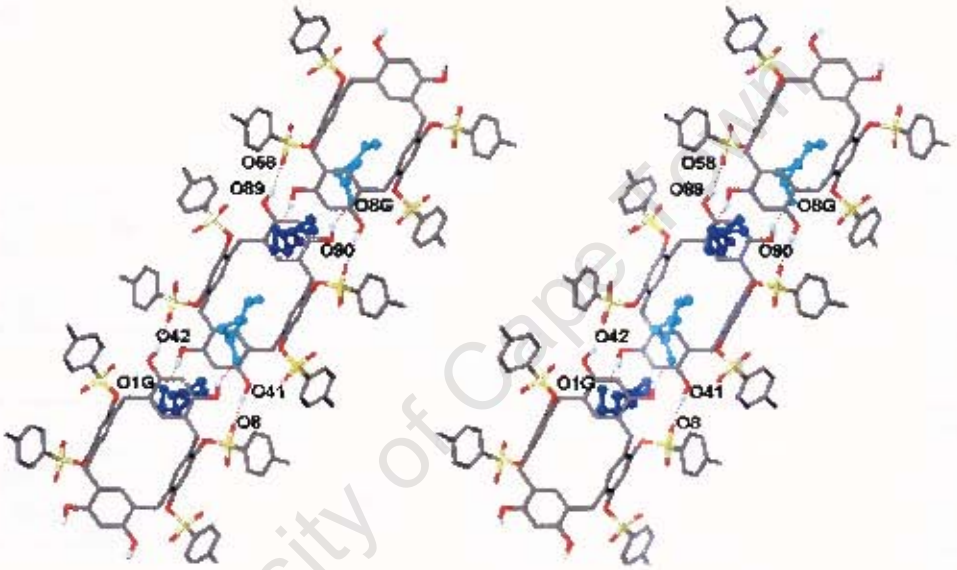

Figure 6.13 Stereoview of hydrogen bonding interactions in **TTRSC•2(1PENT)** showing guest 1 molecules in dark blue and guest 2 molecules in light blue and with the alkyl chains of the host molecule omitted for clarity.

Table 6.3 Site occupancy factors of partial disordered atoms

Inclusion compound	Host alkyl chain atoms				Guest atoms			
	Partial atom pair		Site occupancy factors		Partial atom pair		Site occupancy factors	
	Atom 1	Atom 2	Atom 1	Atom 2	Atom 1	Atom 2	Atom 1	Atom 2
TTRSC•2(1PENT)	C45A	C45B	0.64	0.36	C3G	C4G	0.59	0.41
	C82A	C82B	0.47	0.53	C5G	C6G	0.49	0.51
	C95A	C95B	0.63	0.37	C9G	C10G	0.68	0.32
	C96A	C96B	0.63	0.37	—	—	—	—
TTRSC•2(2PENT)	C34A	C34B	0.64	0.36	O1G	O2G	0.59	0.41
	C45A	C45B	0.38	0.62	C3G	C4G	0.45	0.55
	C46A	C46B	0.61	0.39	C5G	C6G	0.56	0.44
	C81A	C81B	0.55	0.45	C9G	C10G	0.54	0.46
	C96A	C96B	0.66	0.34	O11G	O12G	0.65	0.35
	—	—	—	—	C14G	C15G	0.69	0.31
	—	—	—	—	C16G	C17G	0.63	0.37
	—	—	—	—	C19G	C20G	0.56	0.44
TTRSC•2(2M1B)	C45A	C45B	0.64	0.36	C2G	C3G	0.56	0.44
	C81A	C81B	0.55	0.45	C5G	C6G	0.46	0.54
	C82A	C82B	0.55	0.45	C7G	C8G	0.46	0.54
	—	—	—	—	C9G	C10G	0.60	0.40
	—	—	—	—	C14G	C17G	0.60	0.40
	—	—	—	—	C15G C16G	C18G	0.30 0.30	0.60
TTRSC•2(3M1B)	—	—	—	—	C9G	C10G	0.63	0.37
TTRSC•2(3PENT)	C79A	C79B	0.80	0.20	—	—	—	—
	C80A	C80B	0.82	0.18	—	—	—	—
	C93A	C93B	0.62	0.38	—	—	—	—
	C94A	C94B	0.69	0.31	—	—	—	—
TTRSC•2(2M2B)	C46A	C46B	0.53	0.47	C3G	C4G	0.77	0.23
	C94A	C94B	0.67	0.33	C11G	C12G	0.73	0.27
TTRSC•2(3M2B)	C33A	C33B	0.55	0.45	C1G	C7G	0.58	0.42
	C34A	C34B	0.57	0.43	C3G	C4G	0.58	0.42
	C93A	C93B	0.70	0.30	C2G	C8G	0.58	0.42
	C94A	C94B	0.69	0.31	—	—	—	—

TTRSC•2(2PENT)

$C_{76}H_{88}O_{16}S_4.2(C_5H_{12}O)$
Guest: 2-pentanol
Space group: Pcca
a = 61.1635(6) Å
b = 11.4335(1) Å
c = 24.3952(2) Å
V = 17059.9(3) Å^3
Z = 8

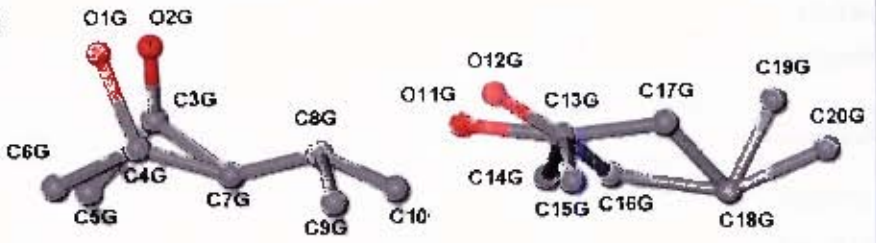

2-pentanol: CH_3-CH(OH)-CH_2-CH_2-CH_3

TTRSC•2(2PENT) was also found to crystallise in the orthorhombic crystal system, in the space group Pcca. The positions of all non-hydrogen host atoms were obtained by direct methods and the positions of non-hydrogen guest atoms were located in difference electron density maps.

All non-hydrogen atoms of the host molecule were refined anisotropically, with the exception of disordered carbon atoms in the alkyl chains. These disordered atoms as well as the non-hydrogen guest atoms were refined with isotropic temperature factors. The hydroxyl hydrogens on the host molecule were located in difference electron density maps and refined with bond length constraints. The rest of the hydrogen atoms were placed in geometrically constrained positions and assigned isotropic temperature factors of $1.2xU_{eq}$ of their parent atoms. The structure refined to $R_1 = 0.0780$.

All four of the alkyl chains of the host molecule as well as both the guest molecules show some degree of disorder. Atoms C34, C45, C46, C81 and C96 in the alkyl chains of the host molecule are disordered over two positions with the two partial atoms labelled with suffixes A and B in each case. This disorder is illustrated in Figure 6.14. In the guest 1 molecule, the oxygen atom was found to be disordered over two positions, as were the carbon atoms in positions 1, 2 and 5. The oxygen atom in the guest 2 molecule, as well as the carbon atoms in positions 1, 3 and 5 were also modelled over two positions. The site occupancy factors of the partial atoms for both the host and guest molecules are given in Table 6.3 (page 179). The disorder in the guest molecules is depicted in the guest numbering scheme above. The disorder in both the host and guest molecules was treated in the same way as described for **TTRSC•2(1PENT)**.

TTRSC•2(2PENT) has Z = 8 and is isostructural with **TTRSC•2(1PENT)** with respect to the packing of the host molecules, with both the host and guest molecules located in general positions. The host molecules pack to form channels with the same dimensions and positions as those described for **TTRSC•2(1PENT)**. The hydrogen bonding in **TTRSC•2(2PENT)** is illustrated in Figure 6.15 and hydrogen bonding details are given in Table 6.4 (page 194).

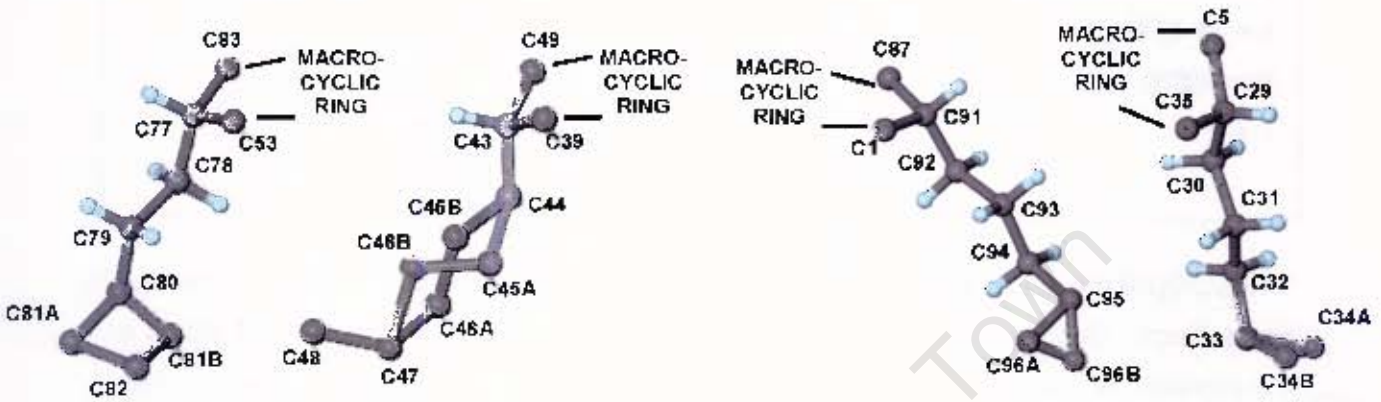

Figure 6.14 Disorder in alkyl chains of host molecule in **TTRSC•2(2PENT)**.

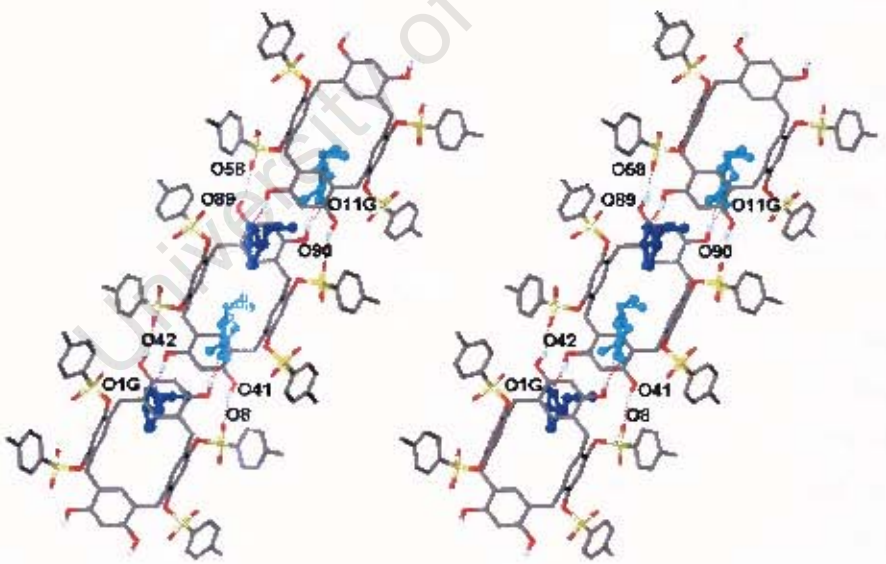

Figure 6.15 Stereoview of hydrogen bonding interactions in **TTRSC•2(2PENT)** showing guest 1 molecules in dark blue and guest 2 molecules in light blue and with the alkyl chains of the host molecule omitted for clarity.

TTRSC•2(2M1B)

$C_{76}H_{88}O_{16}S_4.2(C_5H_{12}O)$
Guest: 2-methyl-1-butanol
Space group: Pcca
a = 60.926(1) Å
b = 11.1517(2) Å
c = 24.4772(7) Å
V = 16630.4(7) Å^3
Z = 8

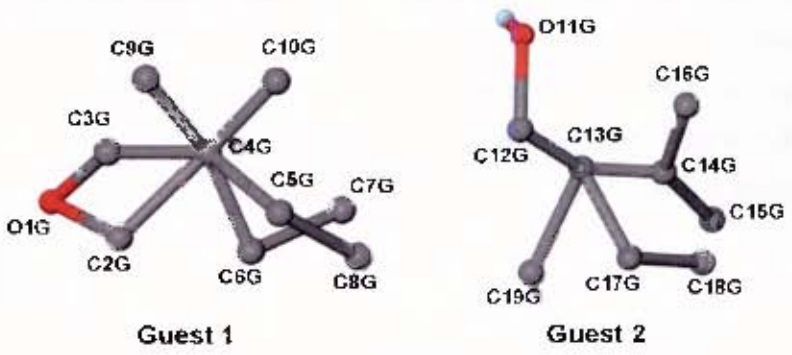

2-methyl-1-butanol: HO-CH_2-CH(CH_3)-CH_2-CH_3

TTRSC•2(2M1B) was found to belong to the orthorhombic crystal system, in the space group Pcca. Direct methods yielded the positions of all the non-hydrogen host atoms and the positions of non-hydrogen guest atoms were located in difference electron density maps. All non-hydrogen atoms of the host molecule were refined with anisotropic thermal parameters, with the exception of disordered alkyl chain carbon atoms which were refined isotropically. The non-hydrogen atoms of the guest molecules were also refined with isotropic temperature factors.

The hydroxyl hydrogens on the host molecule were located in difference electron density maps and refined with bond length constraints. The remainder of the hydrogen atoms were placed in geometrically constrained positions and refined with isotropic temperature factors equal to $1.2xU_{eq}$ of their parent atoms. The structure refined to $R_1 = 0.0923$.

Both of the guest molecules and two of the alkyl chains in the host molecule exhibit disorder. Atoms C45, C81 and C82 in the alkyl chains of the host molecule were found to be disordered and were modelled over two positions with the partial atoms labelled with suffixes A and B in each case. Figure 6.16 illustrates this disorder. In the guest 1 molecule, the carbon atoms at positions 1, 3 and 4 as well as the methyl carbon atom were modelled over two positions, while in the guest 2 molecule, the carbon atom at position 3 was found to be disordered over two positions and the carbon atom at position 4 was modelled over three positions. The site occupancy factors of the partial atoms for both the host and guest molecules are given in Table 6.3 (page 179). The disorder in the guest molecules is depicted in the guest numbering scheme above. The disorder in both the host and guest molecules was modelled using the method described for **TTRSC•2(1PENT)**.

TTRSC•2(2M1B) has Z = 8 and is isostructural with **TTRSC•2(1PENT)** with respect to the packing of the host molecules, with both the host and guest molecules located in general positions. The host molecules pack to form channels with the same dimensions and positions as those described for **TTRSC•2(1PENT)**. The hydrogen bonding in **TTRSC•2(2M1B)** is illustrated in Figure 6.17 and hydrogen bonding details are given in Table 6.4 (page 194).

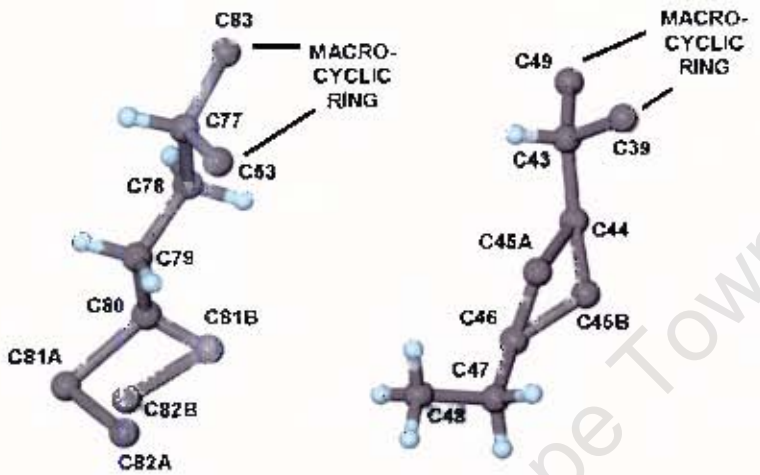

Figure 6.16 Disorder in alkyl chains of host molecule in **TTRSC•2(2M1B)**.

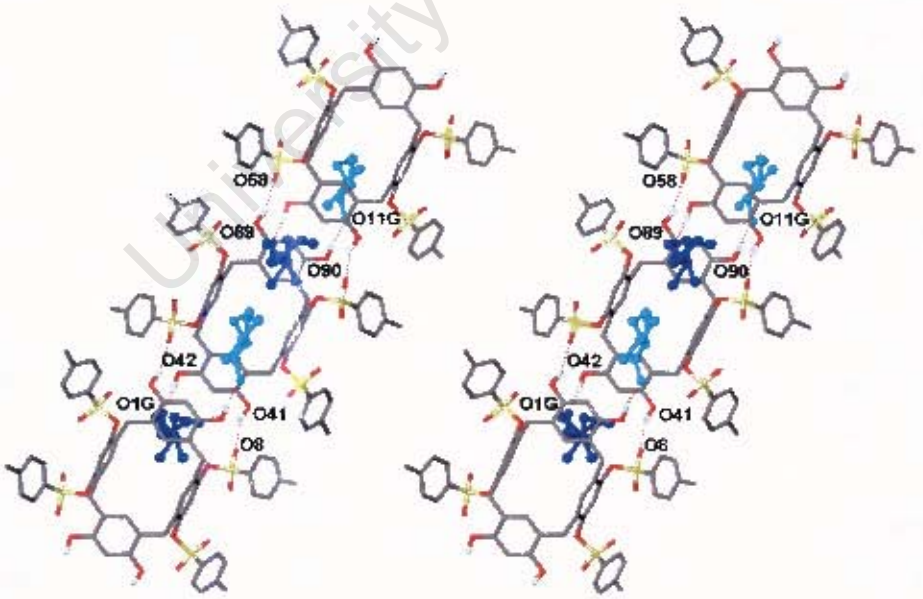

Figure 6.17 Stereoview of hydrogen bonding interactions in **TTRSC•2(2M1B)** showing guest 1 molecules in dark blue and guest 2 molecules in light blue and with the alkyl chains of the host molecule omitted for clarity.

TTRSC•2(3M1B)

$C_{76}H_{88}O_{16}S_4.2(C_5H_{12}O)$
Guest: 3-methyl-1-butanol
Space group: Pcca
a = 61.0866(7) Å
b = 11.4465(1) Å
c = 24.4263(2) Å
V = 17079.5(3) Å^3
Z = 8

Guest 1

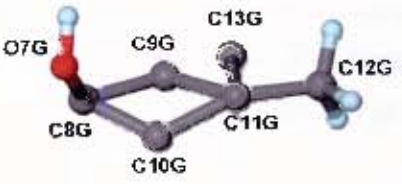

Guest 2

3-methyl-1-butanol: $HO\text{-}CH_2\text{-}CH_2\text{-}CH(CH_3)\text{-}CH_3$

TTRSC•2(3M1B) was found to crystallise in the orthorhombic crystal system, in the space group Pcca. The positions of all non-hydrogen host atoms were obtained by direct methods and the positions of non-hydrogen guest atoms were located in difference electron density maps. The non-hydrogen atoms of the host molecule as well as those of the ordered guest molecule were refined with anisotropic thermal parameters. The non-hydrogen atoms of the disordered guest molecule were refined with isotropic thermal parameters with the exception of the oxygen atom which was refined anisotropically.

The hydroxyl hydrogens on the host molecule were located in difference electron density maps and refined with bond length constraints. The remaining hydrogen atoms were placed in geometrically constrained positions and refined with isotropic temperature factors equal to $1.2xU_{eq}$ of their parent atoms. The structure refined to $R_1 = 0.0801$.

There are no disordered atoms in the host molecule or guest 1 molecule. The carbon atom at position 2 in the guest 2 molecule was found to be disordered and was modelled over two positions. The site occupancy factors of the partial atoms are given in Table 6.3 (page 179) and the disorder is depicted in the guest numbering scheme above. The disorder was treated in the same way as described for **TTRSC•2(1PENT)**.

TTRSC•2(3M1B) has Z = 8 and is isostructural with **TTRSC•2(1PENT)** with respect to the packing of the host molecules, with both the host and guest molecules located in general positions. The host molecules pack to form channels with the same dimensions and positions as those described for **TTRSC•2(1PENT)**. The hydrogen bonding in **TTRSC•2(3M1B)** is illustrated in Figure 6.18 and hydrogen bonding details are given in Table 6.4 (page 194).

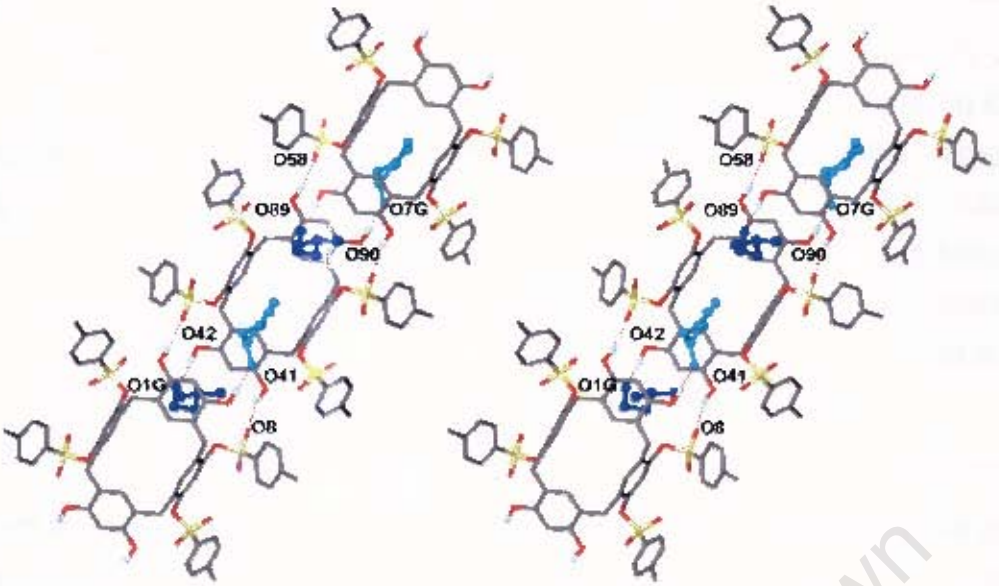

Figure 6.18 Stereoview of hydrogen bonding interactions in **TTRSC-2(3M1B)** showing guest 1 molecules in dark blue and guest 2 molecules in light blue and with the alkyl chains of the host molecule omitted for clarity.

TTRSC•2(3PENT)

$C_{76}H_{88}O_{16}S_4.2(C_5H_{12}O)$
Guest: 3-pentanol
Space group: $P2_1/n$
a = 19.3857(2) Å
b = 22.3884(2) Å β = 101.634(1)°
c = 19.7808(3) Å
V = 8408.8(2) Å^3
Z = 4

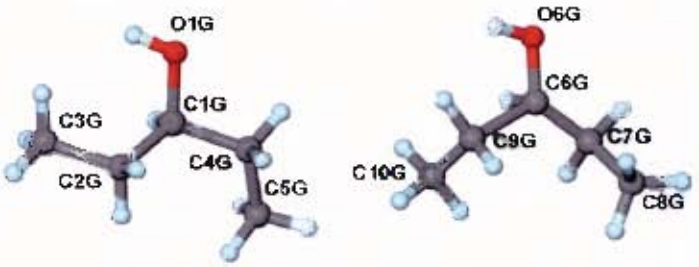

Guest 1 Guest 2

3-pentanol: CH_3-CH_2-CH(OH)-CH_2-CH_3

TTRSC•2(3PENT) was found to crystallise in the monoclinic crystal system, in the space group $P2_1/n$. Direct methods yielded the positions of all non-hydrogen host atoms and positions of the non-hydrogen guest atoms were located in difference electron density maps. All host and guest non-hydrogen atoms were refined anisotropically, with the exception of disordered alkyl chain carbon atoms of the host molecule which were refined isotropically. The hydroxyl hydrogens on the host molecule were located in difference electron density maps and refined with bond length constraints. The rest of the hydrogen atoms were placed in geometrically constrained positions and assigned isotropic temperature factors of $1.2xU_{eq}$ of their parent atoms. The structure refined to $R_1 = 0.0706$.

Atoms C79, C80, C93 and C94 in the alkyl chains of the host molecule were found to be disordered over two positions and the partial atoms were labelled with suffixes A and B in each case. This disorder is illustrated in Figure 6.19 and the site occupancy factors of the partial atoms are given in Table 6.3 (page 179). The disorder was modelled using the method described for **TTRSC•2(1PENT)**.

The structure of **TTRSC•2(3PENT)** has Z = 4 with the asymmetric unit containing one host molecule and two guest molecules. Both the host and guest molecules are located in general positions. The crystal packing of **TTRSC•2(3PENT)** viewed along [010] is shown in Figure 6.20. The host molecules pack together resulting in the formation of cavities in which the guest molecules are located. These cavities were examined using the program SECTION,[1] which was used to view sections through the unit cell down the b-axis. These sections are illustrated in Figure 6.21, with the maximum cross-section of each of the cavities highlighted in red. The cavities have dimensions 4.0 Å x 11.2 Å x 13.7 Å and four of these cavities are located in each unit cell centred at [0.75, 0.1, 0], [0.25, 0.4, 0.5], [0.75, 0.6,

0.5] and [0.25, 0.9, 0]. Each cavity contains two guest molecules, including one guest 1 molecule and one guest 2 molecule. The cavities can be clearly seen in Figure 6.22 which shows the crystal packing viewed along [100]. The hydrogen bonding in **TTRSC•2(3PENT)** is illustrated in Figure 6.23 and hydrogen bonding details are given in Table 6.4 (page 194).

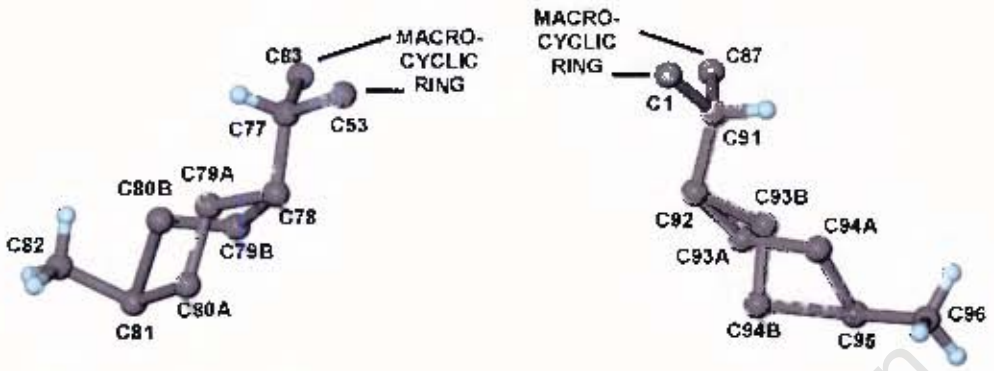

Figure 6.19 Disorder in alkyl chains of host molecule in **TTRSC•2(3PENT)**.

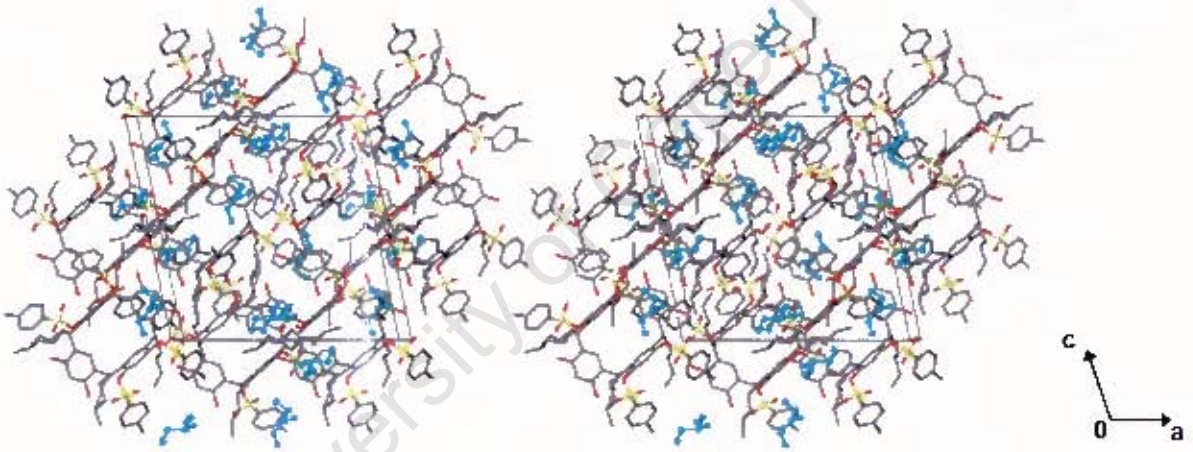

Figure 6.20 Stereoview of packing of **TTRSC•2(3PENT)** viewed along [010] with guest molecules shown in blue and in ball and stick representation for clarity.

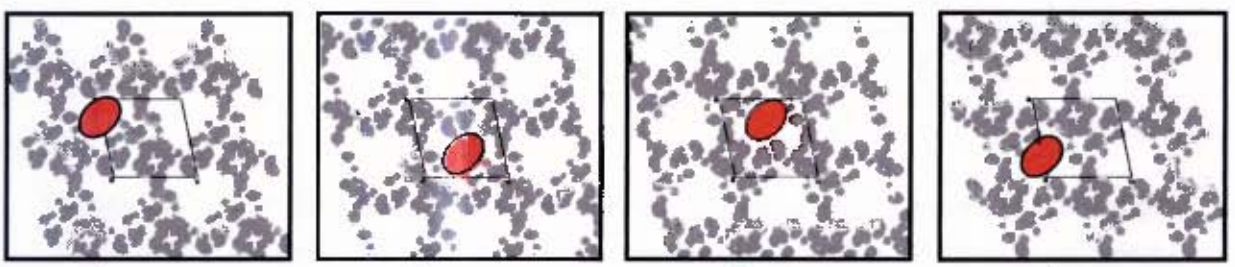

(a) 2.4 Å along [010] **(b)** 8.8 Å along [010] **(c)** 13.6 Å along [010] **(d)** 20.0 Å along [010]

Figure 6.21 SECTION plots of **TTRSC•2(3PENT)** (with guest molecules omitted and host molecules represented by grey areas) viewed down [010] with the unit cell sectioned at **(a)** 2.4 Å, **(b)** 8.8 Å, **(c)** 13.6 Å and **(d)** 20.0 Å along [010].

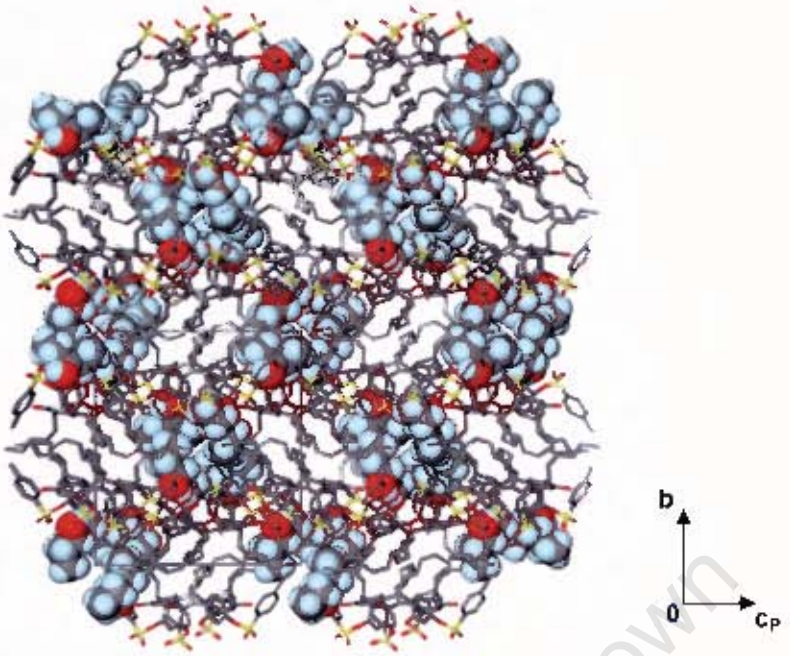

Figure 6.22 Packing diagram of **TTRSC•2(3PENT)** viewed along [100], showing the cavities containing the guest molecules, with the host molecules in stick representation and the guest molecules represented with van der Waals radii.

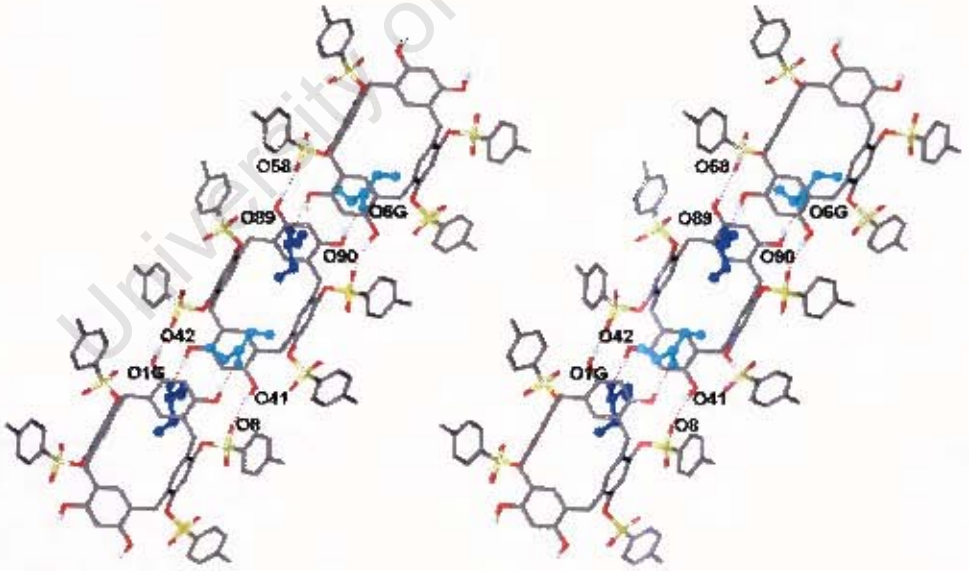

Figure 6.23 Stereoview of hydrogen bonding interactions in **TTRSC•2(3PENT)** showing guest 1 molecules in dark blue and guest 2 molecules in light blue and with the alkyl chains of the host molecule omitted for clarity.

TTRSC•2(2M2B)

$C_{76}H_{88}O_{16}S_4.2(C_5H_{12}O)$
Guest: 2-methyl-2-butanol
Space group: $P2_1/n$
a = 19.2199(1) Å
b = 22.3700(2) Å β=101.870(1)°
c = 19.9958(3) Å
V = 8413.3(1) Å^3
Z = 4

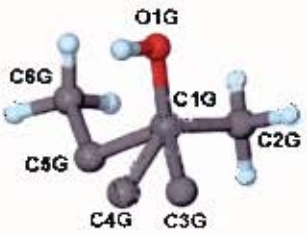

Guest 1

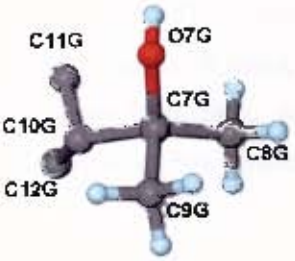

Guest 2

2-methyl-2-butanol: CH_3-CH_2-CH(OH)-CH_3 (CH_3 branch)

TTRSC•2(2M2B) was found to belong to the monoclinic crystal system, in the space group $P2_1/n$. The positions of all non-hydrogen host atoms were obtained by direct methods and the positions of non-hydrogen guest atoms were located in difference electron density maps. All non-hydrogen host atoms were refined with anisotropic temperature factors, except in the case of disordered carbon atoms in the alkyl chains which were refined isotropically. The non-hydrogen atoms of the guest molecules were also refined with anisotropic temperature factors, with the exception of disordered atoms which were refined isotropically.

The hydroxyl hydrogens on the host molecule were located in difference electron density maps and refined with bond length constraints. The rest of the hydrogen atoms were placed in geometrically constrained positions and refined with isotropic temperature factors equal to $1.2xU_{eq}$ of their parent atoms. The structure refined to $R_1 = 0.0668$.

Atoms C46 and C94 in the alkyl chains of the host molecule are disordered over two positions and the partial atoms were labelled with suffixes A and B. The disorder is shown in Figure 6.24. In the guest 1 molecule the methyl carbon atom was found to be disordered over two positions and in the guest 2 molecule the carbon atom at position 4 was modelled over two positions. The site occupancy factors of the partial atoms of both the host and guest molecules are given in Table 6.3 (page 179). The disorder in the guest molecules is depicted in the guest numbering scheme above. The disorder in both the host and guest molecules was treated in the same way as described for **TTRSC•2(1PENT)**.

The structure of **TTRSC•2(2M2B)** has Z = 4 and is isostructural with **TTRSC•2(3PENT)** with respect to the host molecules, with both the host and guest molecules located in general positions. The host molecules pack together resulting in the formation of cavities in which the guest molecules are located. These cavities have the same dimensions and positions as those described for **TTRSC•2(3PENT)**. The hydrogen bonding in **TTRSC•2(2M2B)** is illustrated in Figure 6.25 and hydrogen bonding details are given in Table 6.4 (page 194).

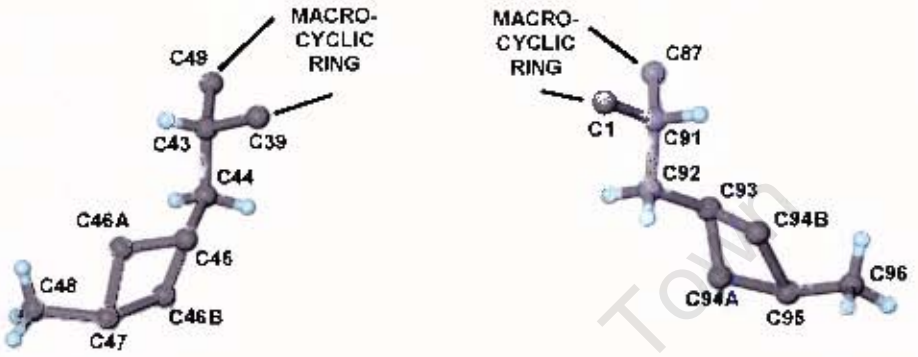

Figure 6.24 Disorder in alkyl chains of host molecule in **TTRSC•2(2M2B)**.

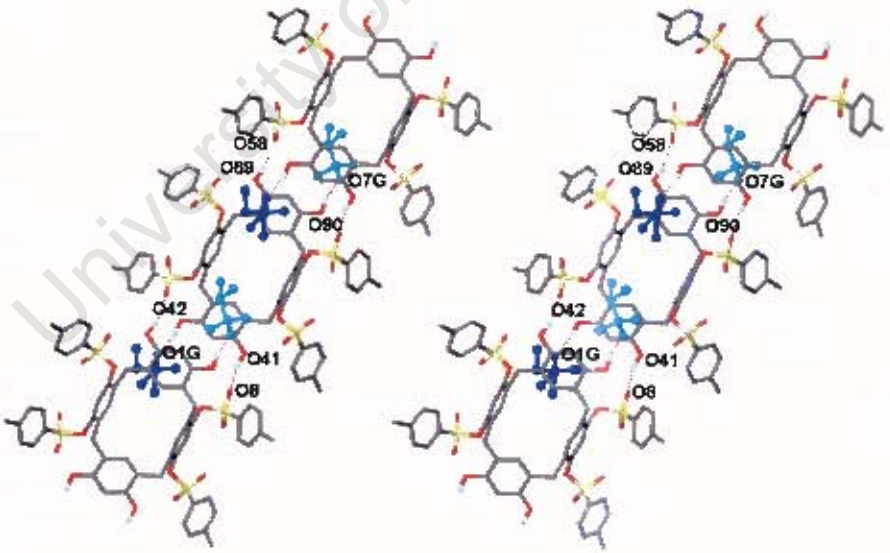

Figure 6.25 Stereoview of hydrogen bonding interactions in **TTRSC•2(2M2B)** showing guest 1 molecules in dark blue and guest 2 molecules in light blue and with the alkyl chains of the host molecule omitted for clarity.

TTRSC•2(3M2B)

$C_{76}H_{88}O_{16}S_4.2(C_5H_{12}O)$

Guest: 3-methyl-2-butanol

Space group: P2/n

a = 19.2340(2) Å

b = 11.2713(2) Å β = 102.640(1)°

c = 19.9335(3) Å

V = 4216.7(1) Å^3

Z = 2

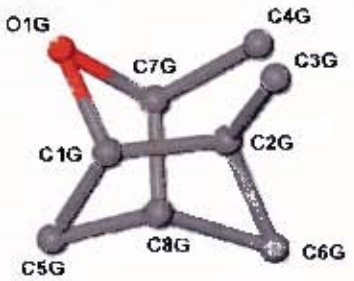

3-methyl-2-butanol:

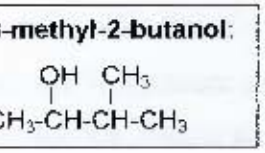

TTRSC•2(3M2B) crystallises in the monoclinic crystal system, in the space group P2/n. Direct methods yielded the positions of all non-hydrogen host atoms and positions of the non-hydrogen guest atoms were located in difference electron density maps. In subsequent refinements all non-hydrogen atoms of the host molecule were refined with anisotropic thermal parameters, with the exception of disordered carbon atoms in the alkyl chains which were refined isotropically. The guest oxygen atoms were refined with anisotropic thermal parameters, while the remaining non-hydrogen guest atoms were refined isotropically. The hydroxyl hydrogens on the host molecule were located in difference electron density maps and refined with bond length constraints and the remaining hydrogen atoms were placed in geometrically constrained positions and assigned isotropic temperature factors of $1.2xU_{eq}$ of their parent atoms. The structure refined to $R_1 = 0.0776$.

Atoms C33, C34, C93 and C94 in the alkyl chains of the host molecule were found to be disordered over two positions. The partial atoms were labelled with suffixes A and B and the disorder is depicted in Figure 6.26. The guest molecule was also found to be disordered and the molecule was modelled over two positions, with the oxygen atom and two of the three terminal carbon atoms common to both partial molecules. The site occupancy factors of the partial atoms of both the host and guest molecules are given in Table 6.3 (page 179). The disorder in the guest molecules is depicted in the guest numbering scheme above and the disorder in both the host and guest molecules was modelled using the method described for **TTRSC•2(1PENT)**. In the case of the guest molecule, the partial guest atoms in each molecule were forced to refine to the same site occupancy factors.

The structure of **TTRSC•2(3M2B)** has Z = 2, with the asymmetric unit containing one half of a host molecule and one guest molecule. The host molecules are located on two-fold axes at Wyckoff position *f* and the guest molecules are located in general positions. The crystal

packing viewed along [010] is shown in Figure 6.27. The structure of **TTRSC•2(3M2B)** has strong similarities to that of **TTRSC•2(1PENT)** in that the unit cell of the former has a similar value of 'b', and the 'a' vector of **TTRSC•2(1PENT)**, of length 60.711(1) Å, is approximately the same as double the value of $\vec{c} - \vec{a}$ = 2 x 30.565 = 61.130 Å.

The topology of the space in which the guests reside is similar in that the host molecules pack to form sharply narrowed, hour-glass shaped channels, which are seen in cross-section in Figure 6.28, and which undulate and shift along the b-axis as discussed previously in the **TTRSC•2(1PENT)** structure. However, in this case the channels are along [101], and have a maximum cross-section of 7.7 Å x 7.5 Å where the guests are located at [0.75, 0.27, 0.25] and [0.25, 0.78, 0.75] respectively. The hydrogen bonding in **TTRSC•2(3M2B)** is illustrated in Figure 6.29 and hydrogen bonding details are given in Table 6.4 (page 194).

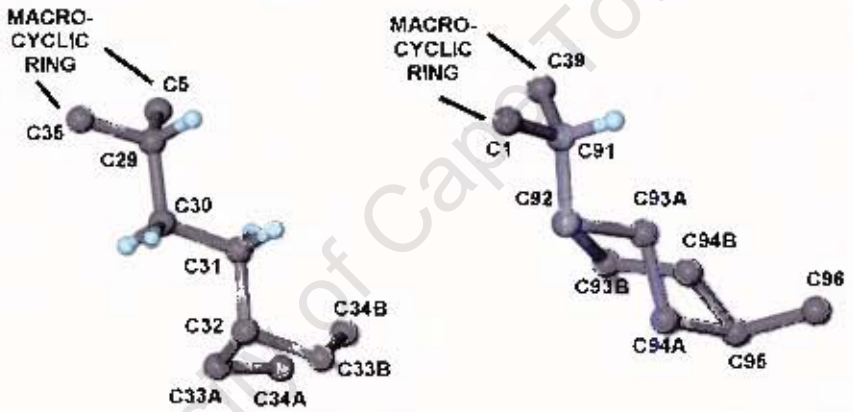

Figure 6.26 Disorder in alkyl chains of host molecule in **TTRSC•2(3M2B)**.

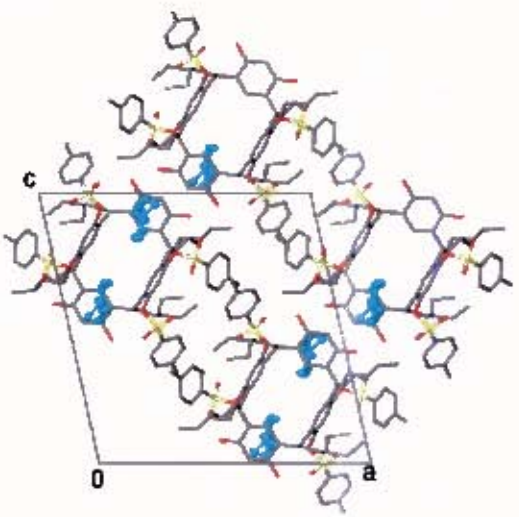

Figure 6.27 Packing diagram of **TTRSC•2(3M2B)** viewed down [010] with guest molecules shown in blue for clarity.

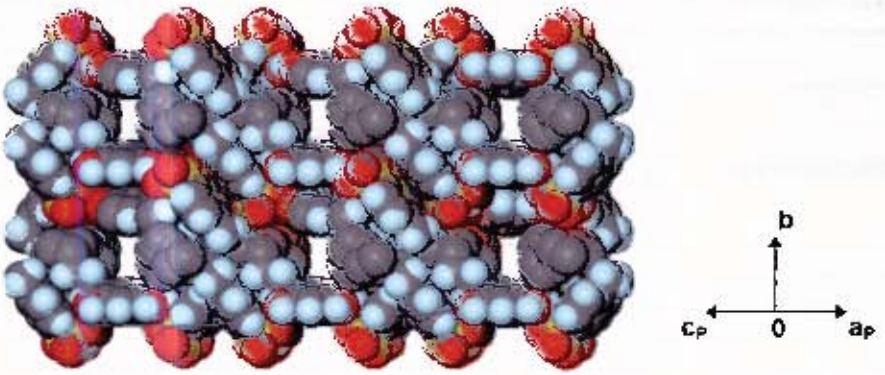

Figure 6.28 View down the channels of **TTRSC•2(3M2B)** along [101] with guest molecules omitted and host molecules represented with van der Waals radii.

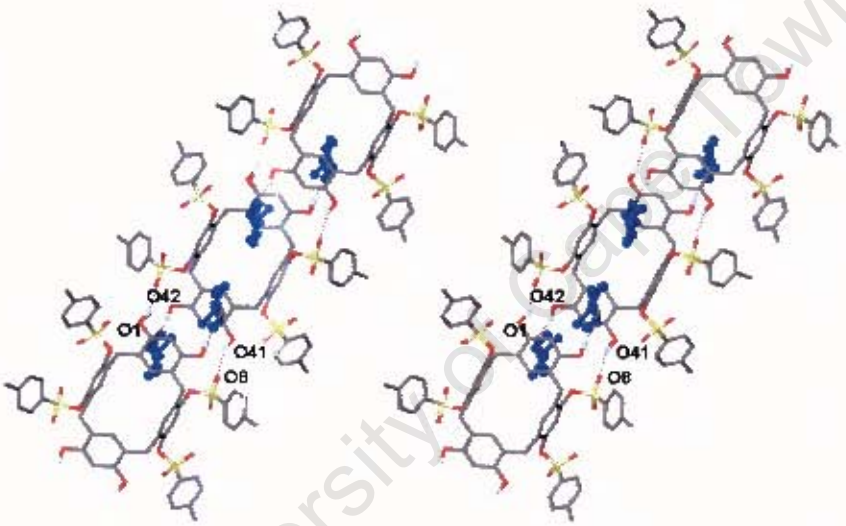

Figure 6.29 Stereoview of hydrogen bonding in **TTRSC•2(3M2B)** with the guest molecules shown in blue and the alkyl chains of the host molecule omitted for clarity.

Table 6.4 Hydrogen bonding details of **TTRSC** inclusion compounds with pentanol isomers

	D-H...A	D-H (Å)	D...A (Å)	D-H-A(°)
TTRSC•2(1PENT)	O41-H41...O8[a]	0.970(1)	2.753(6)	171(9)
	O42-H42...O1G	0.980(1)	2.715(6)	160(5)
	O89-H89...O58[b]	0.971(4)	2.788(6)	158(8)
	O90-H90...O8G	0.984(8)	2.681(6)	134(7)
TTRSC•2(2PENT)	O41-H41...O8[a]	0.960(1)	2.773(5)	157(5)
	O42-H42...O1G	0.980(1)	2.716(7)	173(6)
	O42-H42...O2G	0.980(1)	2.689(9)	150(5)
	O89-H89...O58[b]	0.970(1)	2.763(4)	156(6)
	O90-H90...O11G	0.970(1)	2.744(6)	166(6)
	O90-H90...O12G	0.970(1)	2.73(1)	149(6)
TTRSC•2(2M1B)	O41-H41...O8[b]	0.970(3)	2.762(6)	150(4)
	O42-H42...O1G	0.980(1)	2.673(7)	170(6)
	O89-H89...O58[a]	0.960(1)	2.868(6)	160(4)
	O90-H90...O11G	0.980(1)	2.675(6)	147(7)
TTRSC•2(3M1B)	O41-H41...O8[a]	0.970(1)	2.758(5)	157(5)
	O42-H42...O1G	0.980(1)	2.702(6)	172(6)
	O89-H89...O58[b]	0.960(1)	2.810(5)	166(8)
	O90-H90...O7G	0.980(1)	2.681(5)	175(6)
TTRSC•2(3PENT)	O41-H41...O8[c]	0.960(1)	2.869(3)	165(3)
	O42-H42...O1G	0.980(1)	2.679(3)	166(4)
	O89-H89...O58[d]	0.970(1)	2.740(3)	176(5)
	O90-H90...O6G	0.980(1)	2.709(4)	147(3)
TTRSC•2(2M2B)	O41-H41...O8[c]	0.960(1)	2.800(3)	143(4)
	O42-H42...O1G	0.980(1)	2.688(3)	161(3)
	O89-H89...O58[d]	0.960(1)	2.850(2)	162(3)
	O90-H90...O7G	0.980(1)	2.700(3)	162(3)
TTRSC•2(3M2B)	O41-H41...O8[e]	0.960(1)	2.792(3)	143(4)
	O42-H42...O1G	0.980(1)	2.672(3)	159(4)

[a] Symmetry codes: x,-y+1,z+1/2, [b] Symmetry codes: x,-y+1,z-1/2

[c] Symmetry codes: x-1/2,-y+3/2,z-1/2, [d] Symmetry codes: x+1/2,-y+3/2,z+1/2

[e] Symmetry codes: x-1/2,-y+2,z

COMPETITION EXPERIMENTS

The selectivity of the host for some of the pentanol isomers was established by carrying out competition experiments between pairs of guests. The results of the competition experiments are illustrated in Figure 6.30. Each graph shows the mole fraction X of one of the guests in the initial solution versus the mole fraction Z of the same guest included by the host. In each graph the red diagonal line (x = y) represents zero selectivity and the blue curve represents the experimental results.

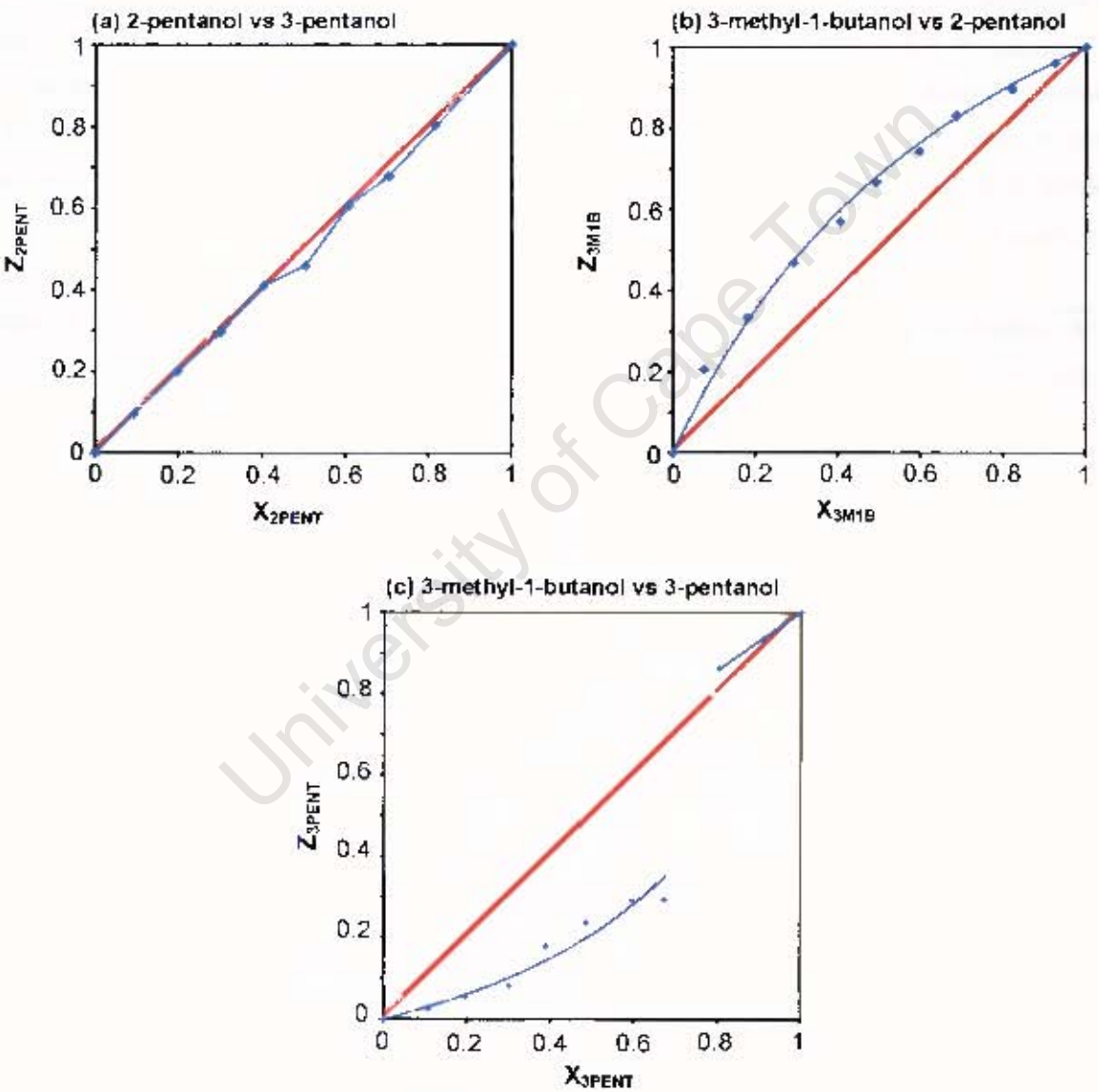

Figure 6.30 Results of the competition experiments of **TTRSC** with **(a)** 2-pentanol versus 3-pentanol, **(b)** 3-methyl-1-butanol versus 2-pentanol and **(c)** 3-methyl-1-butanol versus 3-pentanol.

It can be seen from Figure 6.30(a) that the host does not show any preference for either 2-pentanol or 3-pentanol as the experimental data follows the line representing zero selectivity very closely. Following Ward,[2] we have calculated the selectivity constant for each of the competition experiments, which is defined as $K_{A,B} = Z_A/Z_B \times X_B/X_A$ ($X_A + X_B = 1$). For the 2-pentanol versus 3-pentanol competition experiment in which the host shows no selectivity, $K_{2PENT:3PENT} \approx 1$.

The results obtained for the 3-methyl-1-butanol versus 2-pentanol competition experiment are illustrated in Figure 6.30(b) and we note that 3-methyl-1-butanol is enclathrated preferentially to 2-pentanol over the whole concentration range with a selectivity constant of $K_{3M1B:2PENT} = 2.2$. Figure 6.30(c) shows the results obtained for the 3-methyl-1-butanol versus 3-pentanol competition experiment. These results show that 3-methyl-1-butanol is also enclathrated preferentially to 3-pentanol, although only when the mole fraction of 3-pentanol is less than or equal to 0.7 and within this range $K_{3M1B:3PENT} = 4.0$. For mole fractions of 3-pentanol above 0.7, the host shows a slight preference for 3-pentanol.

The selectivity shown by the host for complexation with the pentanol isomers therefore follows the trend: 3-methyl-1-butanol > 2-pentanol ≈ 3-pentanol.

NUCLEATION AND CRYSTAL GROWTH

As part of the brief study of nucleation and crystal growth, the solubility curve of **TTRSC•2(1PENT)** in 1-pentanol was determined. The solubility was measured over the range 20°C to 95°C and the solubility versus temperature curve plotted. This plot is given in Figure 6.31.

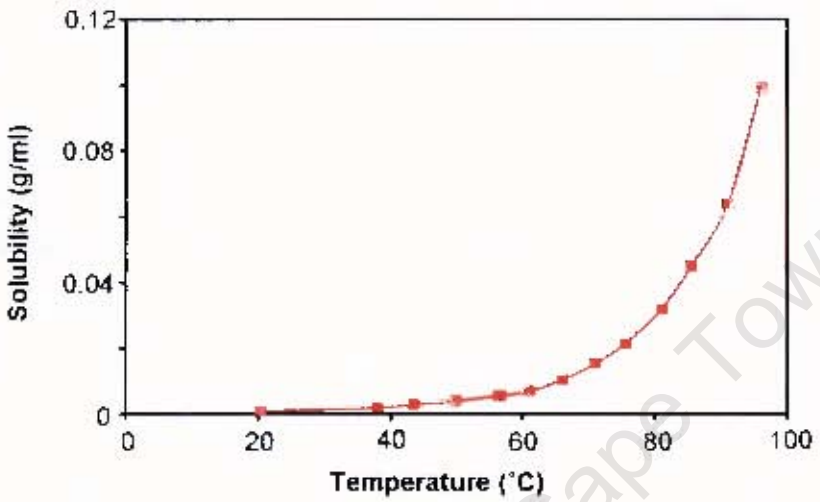

Figure 6.31 Solubility versus temperature plot for **TTRSC•2(1PENT)** in 1-pentanol.

TTRSC•2(1PENT) was crystallised at 20°C, 40°C, 60°C and 80°C from saturated solutions set up at 50°C, 61°C, 75°C and 96°C respectively. The supersaturation of each solution at the crystallisation temperature was calculated, using the equation

$$\text{Supersaturation} = \ln\left[\frac{\text{mass of inclusion compound in supersaturated state}}{\text{mass of inclusion compound in saturated phase}}\right]$$

and found to be 1.386 for the crystallisation at 20°C, 1.253 for the crystallisation at 40°C, 1.196 for the crystallisation at 60°C and 1.194 for the crystallisation at 80°C. Optical microscopy was used to study the morphology of the crystals obtained, but no changes in morphology for the various crystallisations were evident. Photographs of the crystals are shown in Figure 6.32.

An in-situ cooling crystallisation of **TTRSC•2(1PENT)** at 60°C was observed using optical microscopy. This crystallisation was set up by making a saturated solution of **TTRSC•2(1PENT)** in 1-pentanol at 75°C. The hot solution was then transferred to a top-hat cell, which was pre-heated and placed on the microscope stage. The temperature of the top-hat cell was lowered to 60°C and the crystallisation of **TTRSC•2(1PENT)** observed. Selected images are shown in Figure 6.33.

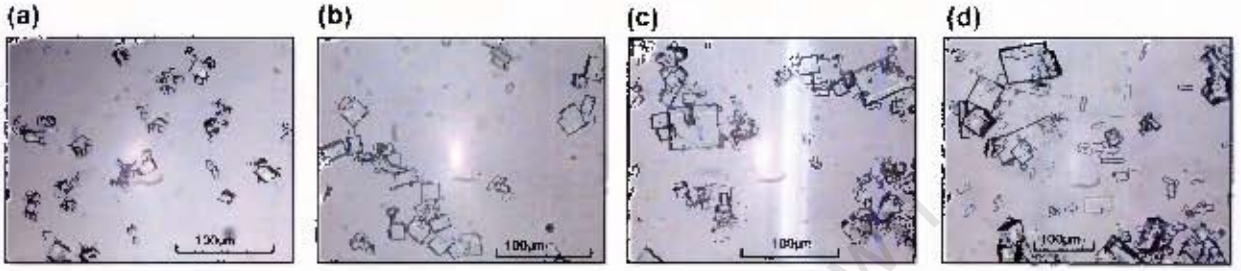

Figure 6.32 Crystals of **TTRSC•2(1PENT)** formed at **(a)** 20°C from a saturated solution at 50°C, **(b)** 40°C from a saturated solution at 61°C, **(c)** 60°C from a saturated solution at 75°C and **(d)** 80°C from a saturated solution at 96°C.

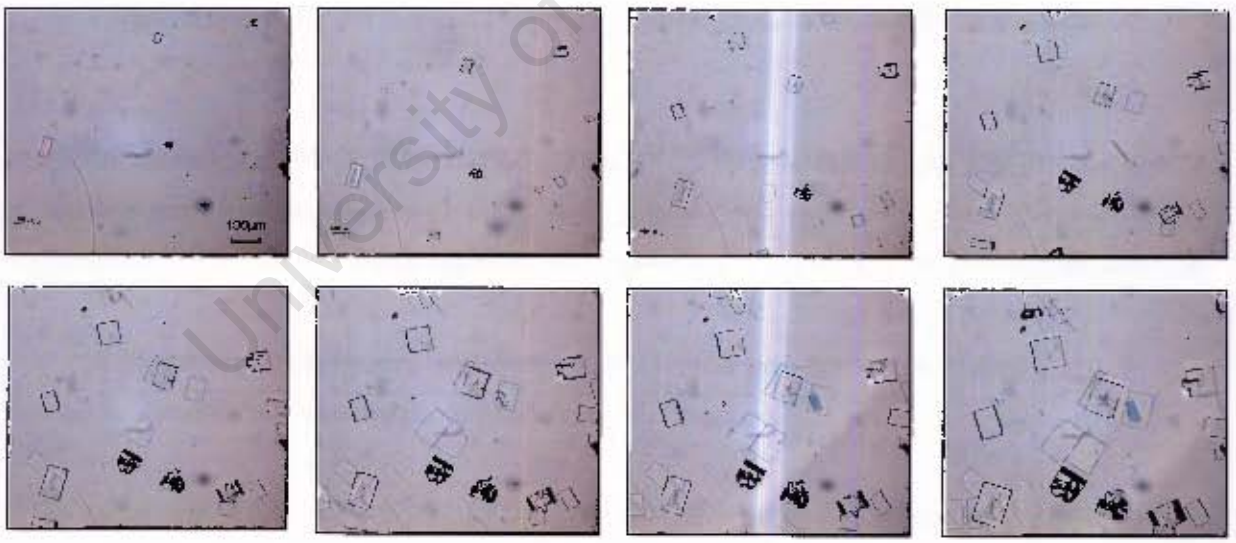

Figure 6.33 Images taken during crystallisation of **TTRSC•2(1PENT)**.

SUMMARY AND DISCUSSION

TTRSC is a resorcinarene host with four substituted tosylate groups on the upper rim and pentyl groups on the lower rim. Inclusion compounds formed with this host and the seven pentanol isomers as guests have been examined. Thermal analysis has been carried out, including TG, DSC and HSM. The TG traces obtained show that each of the inclusion compounds has H:G = 1:2 and the structures of the host-guest compounds have been elucidated and compared. Competition experiments were carried out with pairs of guests in order to study the selectivity of this host for some of the pentanol isomers.

It was found that these compounds form three types of structures and in each of these types the guests are captured between the molecules of resorcinarene rather than within the cavity of the resorcinarene. **TTRSC•2(1PENT)**, **TTRSC•2(2PENT)**, **TTRSC•2(2M1B)** and **TTRSC•2(3M1B)** all crystallise in the space group Pcca with Z = 8. The asymmetric unit consists of one host molecule and two guest molecules. They are isostructural with respect to the host molecules which pack to form undulating channels along [001] in which the guest molecules are located, with both the host and guest molecules in general positions.

TTRSC•2(3PENT) and **TTRSC•2(2M2B)** both crystallise in the space group $P2_1/n$ with Z = 4. The asymmetric unit consists of one host molecule and two guest molecules and both the host and guest molecules are located in general positions. They are isostructural with respect to the host molecules which pack together resulting in the formation of cavities in which the guest molecules are situated. There are four of these cavities in each unit cell, with each cavity containing two guest molecules. **TTRSC•2(3M2B)** crystallises in the space group P2/n with Z = 2. There is half a host molecule and one guest molecule in the asymmetric unit. The host molecules are located on two-fold axes at Wyckoff position *f*, while the guest molecules are located in general positions. The host molecules pack to form restricted channels along [101] which are very similar to those of **TTRSC•2(1PENT)** and the guest molecules are located in these channels.

The same hydrogen bonding pattern is shown by all seven of the inclusion compounds. In each case both guest molecules are hydrogen bonded to the host molecule and the structures are additionally stabilised by hydrogen bonding between the host molecules. In addition to these hydrogen bonds there are weaker interactions between the guest oxygen atoms and oxygen atoms in the tosylate groups of the host molecules.

As part of the brief nucleation and crystal growth study, the solubility curve of **TTRSC•2(1PENT)** was measured and it was found that the solubility in 1-pentanol increases uniformly with temperature, with no indication that above a certain temperature the host alone is formed preferentially to the inclusion compound. Crystallisations were carried out from supersaturated solutions at various temperatures along the curve, but no differences in morphology were evident. At each temperature the crystals were in the form of rectangular plates.

Competition experiments were performed in order to determine the selectivity of this host for some of the pentanol guests. Studies of the selectivity of other resorcinarene hosts for various guests have been carried out. Examples include the selectivity of a hydrogen-bonded molecular capsule for benzene, p-xylene and toluene[3] and selectivity of a resorcinarene host with long alkyl chains for several cyclohexanediols.[4]

From the results of this study, it can be seen that the host does not show any preference for either 2-pentanol or 3-pentanol, but the 3-methyl-1-butanol versus 2-pentanol competition experiment shows that 3-methyl-1-butanol is enclathrated preferentially to 2-pentanol over the whole concentration range, with a selectivity constant of $K_{3M1B:2PENT} = 2.2$. 3-methyl-1-butanol is also enclathrated preferentially to 3-pentanol with a selectivity constant of $K_{3M1B:3PENT} = 4.0$, although only when the mole fraction of 3-pentanol is less than or equal to 0.7. For mole fractions of 3-pentanol above 0.7, the host shows a slight preference for 3-pentanol.

The results of these competition experiments were correlated with the thermal stabilities of the host-guest systems by examining the DSC data. As mentioned previously, the difference between the onset temperature, T_{on} and the normal boiling point of the guest, T_b, has been found to be a measure of the stability of an inclusion compound.[5] These values have been determined for each of the inclusion compounds and the results are given in Table 6.5. These compounds given in order of decreasing stability are therefore as follows: **TTRSC•2(3M2B)** > **TTRSC•2(2M2B)** > **TTRSC•2(3M1B)** > **TTRSC•2(2M1B)** > **TTRSC•2(1PENT)** > **TTRSC•2(2PENT)** > **TTRSC•2(3PENT)**. These stabilities correspond to the results of the competition experiments as they show that the preferentially included guest forms the more stable inclusion compound in each case.

Table 6.5 Differences between onset temperature of guest release(T_{on}) and boiling point of guest(T_b)

Inclusion Compound	Onset Temperature, T_{on} (°C)	Boiling point, T_b (°C)	T_{on}-T_b(°C)
TTRSC•2(3M2B)	117.6	113.0	4.6
TTRSC•2(2M2B)	94.8	102.5	-7.7
TTRSC•2(3M1B)	121.4	130.0	-8.6
TTRSC•2(2M1B)	116.1	128.0	-11.9
TTRSC•2(1PENT)	116.7	137.5	-20.8
TTRSC•2(2PENT)	98.1	119.3	-21.3
TTRSC•2(3PENT)	85.2	115.6	-30.4

REFERENCES

[1] L.J. Barbour, SECTION. A computer program for the graphic display of cross sections through a unit cell, *J. Appl. Cryst.*, 1999, **32**, 353.

[2] A. M. Pivovar, K.T. Holman and M.D. Ward, *Chem. Mater.*, 2001, **13**, 3018.

[3] T. Heinz, D.M. Rudkevich, and J. Rebek, Jr., *Nature*, 1998, **394**, 764.

[4] Y. Kikuchi, Y. Kato, Y. Tanaka, H. Toi and Y. Aoyama, *J. Am. Chem. Soc.*, 1991, **113**, 1349.

[5] M.R. Caira, L.R. Nassimbeni, M.L. Niven, W.-D. Schubert, E. Weber and N.Dörpinghaus, *J. Chem. Soc., Perkin Trans. 2*, 1991, 1707.

Chapter 7

INCLUSION OF PYRIDINE AND PICOLINE ISOMERS BY THE HOST TTRSC

*The host $1^4,1^6,5^4,5^6$-tetrahydroxy-2,4,6,8-tetrapentyl-$3^4,3^6,7^4,7^6$-tetra(p-toluene-sulfonyl-oxy)-1,3,5,7(1,3)-tetrabenzenacyclooctaphane (abbreviated **TTRSC**) also forms inclusion compounds with pyridine, 2-picoline, 3-picoline and 4-picoline. Thermal analysis of these compounds has been carried out and from the TG analysis the host:guest ratios were determined. The structures have been elucidated from single crystal X-ray diffraction data and have been compared. Competition experiments were carried out to determine whether this host shows any selectivity between 3-picoline and 4-picoline.*

For each of the structures described in this chapter the crystallographic data, experimental and refinement parameters are given in Table 7.1. Final atomic coordinates, bond lengths and angles, torsion angles, thermal parameters and tables of observed and calculated structure factors for each of the crystal structures are given in the appendices.

COMPLEX PREPARATION

In each case suitable crystals were prepared using the general method of slow evaporation at room temperature, as described in Chapter 2, with the only difference being that a small amount of water was added to each solution. This was done as it proved extremely difficult to keep the solution dry, even using dry picolines, as water could be taken up from the atmosphere and the host was found to include water molecules as well as the picoline guest molecules in some cases. Thus for consistency, equally wet solvents were used.

The inclusion compounds obtained as well as their abbreviations are as follows:

TTRSC + pyridine (H:G = 1:6): **TTRSC•6PYR**
TTRSC + 2-picoline (H:G = 1:5): **TTRSC•5(2PIC)**
TTRSC + 3-picoline (H:G:H_2O =1:4.5:0.5): **TTRSC•4.5(3PIC)•0.5(H_2O)**
TTRSC + 4-picoline (H:G:H_2O =1:6.5:2): **TTRSC•6.5(4PIC)•2(H_2O)**

The guest numbering schemes are given at the beginning of each structure analysis and the host numbering scheme is the same as that given in Chapter 6 and is shown below:

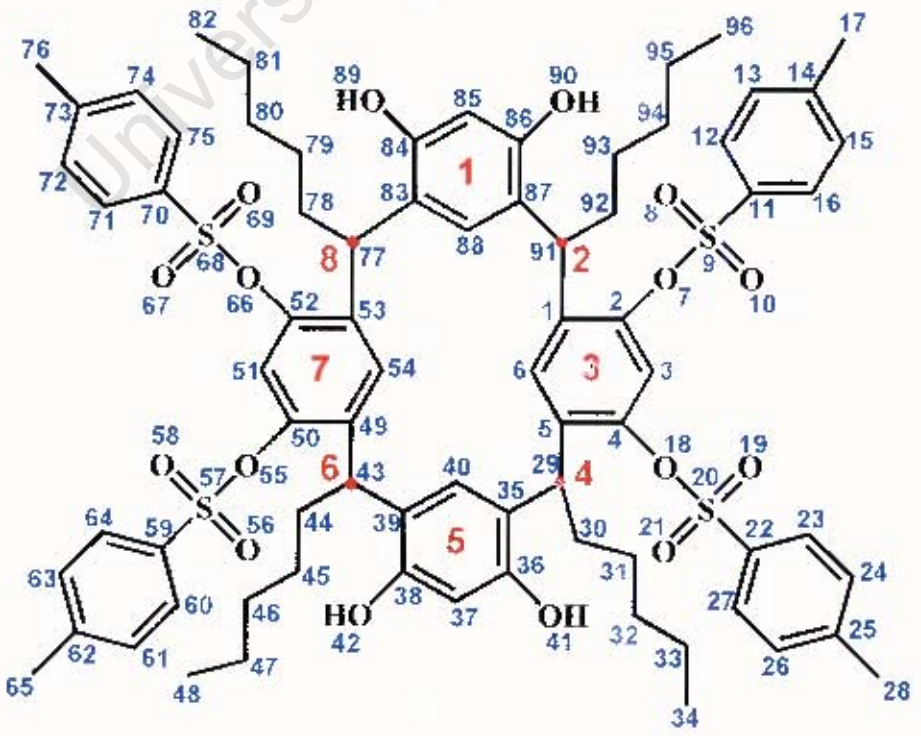

Table 7.1 Crystal data, experimental and refinement parameters

	TTRSC•6PYR	**TTRSC•5(2PIC)**
Molecular formula	$C_{70}H_{88}O_{10}S_4.6(C_5H_5N)$	$C_{76}H_{88}O_{10}S_4.5(C_6H_7N)$
Guest	pyridine	2-picoline
Host:guest ratio	1:6	1:5
M_r/g.mol^{-1}	1860.30	1851.33
Crystal symmetry	Triclinic	Triclinic
Space group	P1	$P\bar{1}$
a/Å	15.4030(5)	13.6878(2)
b/Å	21.2691(7)	16.3438(3)
c/Å	21.2829(9)	22.3279(5)
α/°	113.073(2)	77.892(1)
β/°	98.256(2)	86.092(1)
γ/°	108.881(2)	83.396(1)
Z	2	2
V/Å^3	5769.2(4)	4581.1(2)
μ(Mo-Kα)/mm^{-1}	0.141	0.167
Temp of data collection (K)	193(2)	113(2)
Range scanned, θ (°)	2.88 - 27.41	1.80 - 27.91
Index range	h:±19, k:±27, l:±27	h:-18-17, k:±21, l:-28-29
No. reflections collected	40659	72434
No. unique reflections	24369 (R_{int} = 0.0643)	21799 (R_{int} = 0.0561)
No. reflections with I>2σ(I)	10612	14737
Data/restraints/parameters	24369 / 4 / 903	21799 / 4 / 1172
Goodness of fit, S	1.349	0.980
Final R indices (I>2σ(I))	R_1 = 0.1466, wR_2 = 0.3967	R_1 = 0.0546, wR_2 = 0.1303
R indices (all data)	R_1 = 0.2429, wR_2 = 0.4588	R_1 = 0.0956, wR_2 = 0.1515
Largest diff peak and hole (e.Å^{-3})	2.356;-2.003	0.823; -0.559

Table 7.1 (cont.) Crystal data, experimental and refinement parameters

	TTRSC•4.5(3PIC)•0.5(H_2O)	**TTRSC•6.5(4PIC)•2(H_2O)**
Molecular formula	$C_{76}H_{68}O_{16}S_4.4.5(C_6H_7N).$ $0.5(H_2O)$	$C_{76}H_{68}O_{16}S_4.6.5(C_6H_7N).$ $2(H_2O)$
Guest	3-picoline, H_2O	4-picoline, H_2O
Host:guest ratio	1:4.5:0.5	1:6.5:2
M_r/g.mol^{-1}	1813.78	1944.46
Crystal symmetry	Monoclinic	Triclinic
Space group	C2/c	P1
a/Å	44.8472(3)	16.9366(1)
b/Å	20.7901(2)	17.9477(2)
c/Å	23.3348(2)	19.4997(2)
α/°	90	104.495(1)
β/°	117.239(1)	96.671(1)
γ/°	90	105.445(1)
Z	8	2
V/Å^3	19344.1(3)	5424.27(9)
μ(Mo-Kα)/mm^{-1}	0.166	0.152
Temp of data collection (K)	113(2)	293(2)
Range scanned, θ (°)	1.63 - 27.88	2.55 – 27.87
Index range	h:-45-58, k:-27-25, l:-30-27	h:±22, k:±23, l:±25
No. reflections collected	69690	46049
No. unique reflections	22846 (R_{int} = 0.0498)	25436 (R_{int} = 0.0319)
No. reflections with I>2σ(I)	14370	16716
Data/restraints/parameters	22846 / 4 / 1072	25436 / 4 / 1238
Goodness of fit, S	1.042	0.995
Final R indices (I>2σ(I))	R_1 = 0.0811, wR_2 = 0.2117	R_1 = 0.0687, wR_2 = 0.1768
R indices (all data)	R_1 = 0.1296, wR_2 = 0.2447	R_1 = 0.1114, wR_2 = 0.2041
Largest diff peak and hole (e.Å^{-3})	1.487; -0.725	1.108; -0.655

THERMAL ANALYSIS

Thermal analysis, including TG and DSC, was carried out for each of the inclusion compounds and the TG traces were used to calculate the H:G ratios in each case. The results of the TG and DSC analyses are summarised in Table 7.2.

The TG and DSC traces of **TTRSC•6PYR** are shown in Figure 7.1(*a*). The TG trace shows that guest release occurs in two steps with concomitant endotherms A and B in the DSC trace, where endotherm A is a double peak. The total mass loss of 24.9% shown by the TG trace corresponds to H:G = 1:6 (calc. 25.5%). Endotherm C in the DSC trace is due to the melt of the guest-free host compound.

The TG and DSC traces of **TTRSC•5(2PIC)** are shown in Figure 7.1(*b*). The TG trace shows a two step desorption which corresponds to endotherms A and B in the DSC trace, where endotherm B is a double peak. The TG trace shows a total mass loss of 24.5% which corresponds to H:G = 1:5 (calc. 25.2%). Endotherm C in the DSC trace represents the melt of the guest-free host compound. There are some smaller endotherms evident in the DSC trace which suggest phase transformations of the host compound, occurring after guest desorption but prior to the melt of the host compound.

The TG and DSC traces of **TTRSC•4.5(3PIC)•0.5(H_2O)** are shown in Figure 7.1(*c*). The TG trace shows that guest release occurs in a multiple step process with a total mass loss of 23.5% which corresponds to H:G:H_2O = 1:4.5:0.5 (calc. 23.6%). The DSC trace shows two main endotherms, A and B, representing guest release as well as an endotherm suggesting a phase transformation of the guest-free host compound before the melt, which is represented by endotherm C.

The TG and DSC traces of **TTRSC•6.5(4PIC)•2(H_2O)** are shown in Figure 7.1(*d*). The TG trace shows a multiple step guest desorption, with a total mass loss of 29.7% which corresponds to H:G:H_2O = 1:6.5:2 (calc. 31.6%). The DSC trace shows multiple endotherms corresponding to guest release and also shows evidence of phase transformations of the host compound, occurring after guest desorption but prior to the melt. Endotherm C represents the melt of the guest-free host compound.

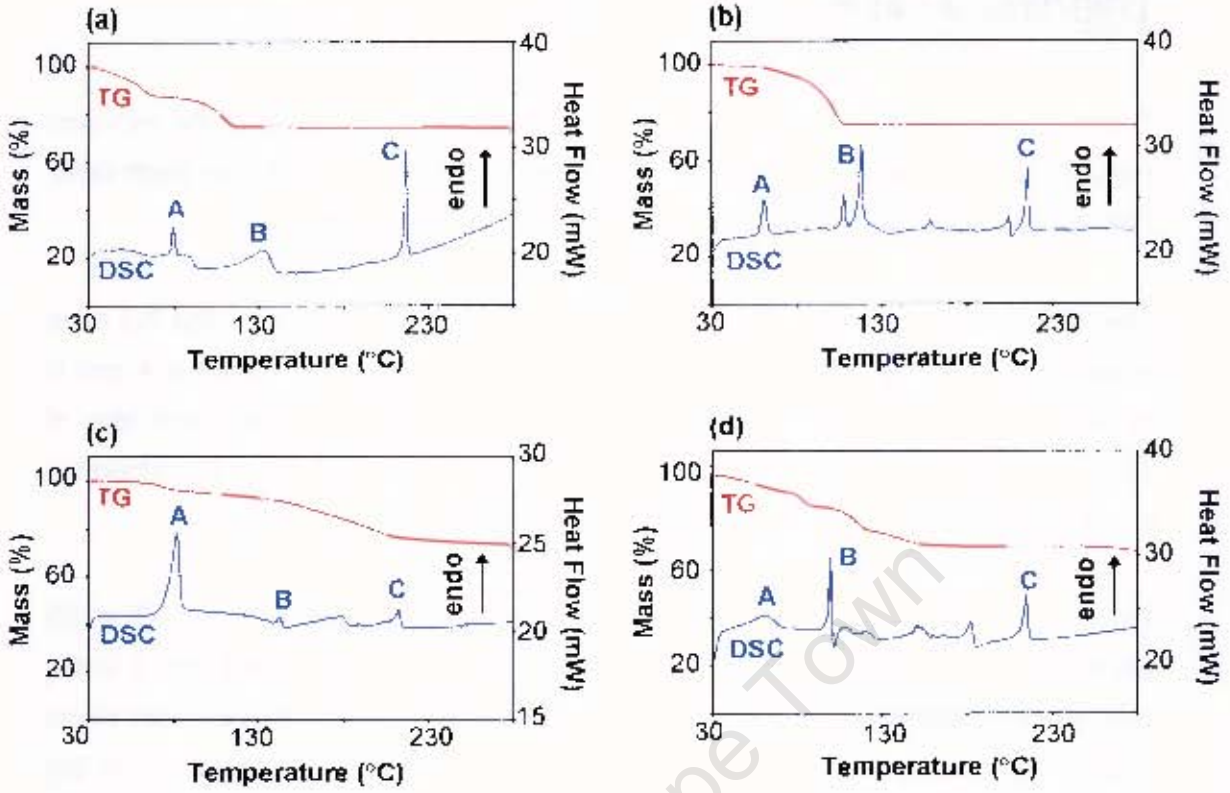

Figure 7.1 TG and DSC traces of **(a) TTRSC•6PYR. (b) TTRSC•5(2PIC), (c) TTRSC•4.5(3PIC)•0.5(H_2O)** and **(d) TTRSC•6.5(4PIC)•2(H_2O).**

Table 7.2 Thermal analysis results of **TTRSC** inclusion compounds

Inclusion Compound	TG Results		H:G ratio	DSC Results		
	Calc. % mass loss	Exp. % mass loss		T_{on} (°C) Peak A	T_{on} (°C) Peak B	T_{on} (°C) Peak C
TTRSC•6PYR	25.5	24.9	1:6	77.3	117.7	214.9
TTRSC•5(2PIC)	25.2	24.5	1:5	57.8	115.5	213.1
TTRSC•4.5(3PIC) •0.5(H_2O)	23.6	23.5	1:4.5:0.5	74.9	139.2	209.9
TTRSC•6.5(4PIC) •2(H_2O)	31.6	29.7	1:6.5:2	46.4	97.8	211.4

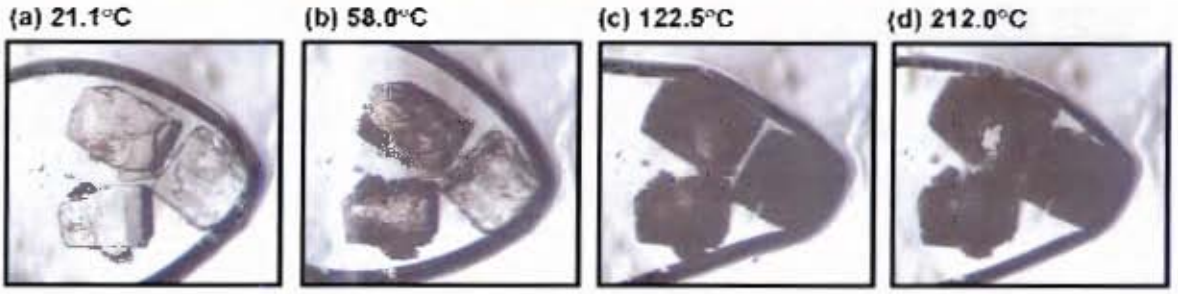

Figure 7.3 Crystals of **TTRSC•5(2PIC)** during thermal decay.

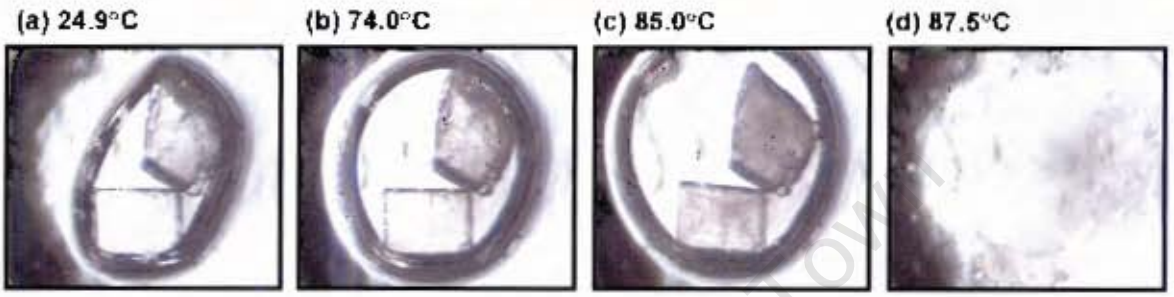

Figure 7.4 Thermal decay of **TTRSC•4.5(3PIC)•0.5(H_2O)** crystals.

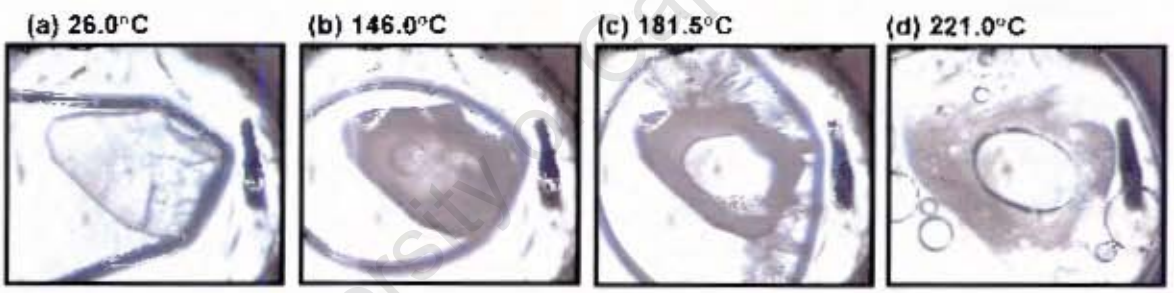

Figure 7.5 **TTRSC•6.5(4PIC)•2(H_2O)** crystals during thermal decomposition.

HOT STAGE MICROSCOPY

Hot stage microscopy (HSM) was used to observe crystals of the inclusion compounds during thermal decay and the photographs taken are displayed in Figure 7.2 to Figure 7.5.

The crystals of **TTRSC•6PYR** (shown at room temperature in Figure 7.2(a)) went slowly opaque from room temperature with the most rapid change occurring between 66.0°C and 75.0°C, during which time bubbles could also be seen forming in the crystals. From 143°C bubbles of desorbed guest were released (Figure 7.2(b)) with some recrystallisation occurring at the same time (Figure 7.2(c)). The crystals melted at 220.0°C (Figure 7.2(d)).

The **TTRSC•5(2PIC)** crystals (shown at room temperature in Figure 7.3(a)) changed from clear to opaque between 53.0°C and 64.0°C (Figure 7.3(b)) and bubbles of guest were formed in the crystals between 120°C and 140°C (Figure 7.3(c)). The crystals melted at 212.0°C (Figure 7.3(d)). Crystals of **TTRSC•4.5(3PIC)•0.5(H_2O)** (shown at room temperature in Figure 7.4(a)) became gradually opaque from room temperature (Figure 7.4(b) and (c)). At 86°C, vigorous guest release occurred in the form of bubbling, which resulted in the crystals being broken apart completely and dispersed (Figure 7.4(d)). The crystals melted at 210.0°C.

The **TTRSC•6.5(4PIC)•2(H_2O)** crystals (shown at room temperature in Figure 7.5(a)) turned slowly opaque from room temperature and from 71.0°C bubbles of desorbed guest were released (Figure 7.5(b)). From 180.0°C, recrystallisation along with further release of bubbles took place (Figure 7.5(c)) until the crystals melted at 221.0°C (Figure 7.5(d)).

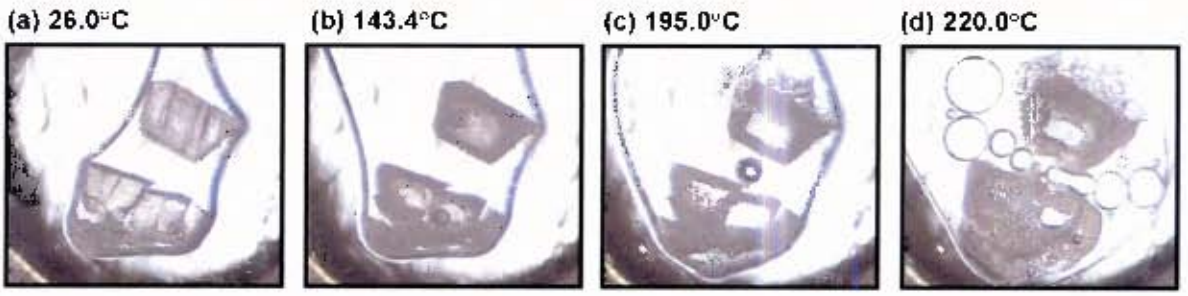

Figure 7.2 Thermal decomposition of **TTRSC•6PYR** crystals.

Two of the alkyl chains of the host molecule were found to be disordered and atoms C33, C34, C95 and C96 were modelled over two positions, with the two partial atoms labelled with suffixes A and B in each case. This disorder is illustrated in Figure 7.6 and the site occupancy factors of the partial atoms are given in Table 7.7 (page 227).

The site occupancy factors were initially assigned based on peak heights and the temperature factors of the two partial atoms were forced to refine to the same value. This value was then fixed and the site occupancy factors were allowed to refine to give a total site occupancy of one. The refined site occupancy factors were then fixed and the isotropic temperature factors of the two partial atoms were allowed to refine independently.

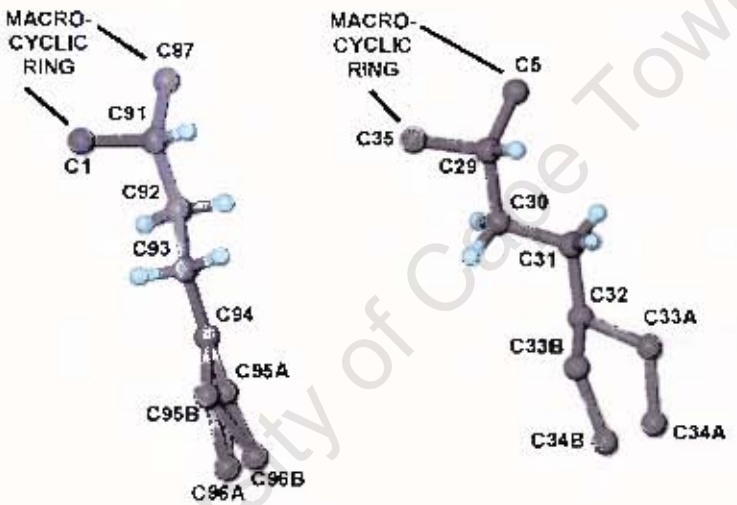

Figure 7.6 Disorder in alkyl chains of host molecule.

The structure of **TTRSC•6PYR** has Z = 2 and the asymmetric unit consists of one host molecule and six guest molecules, which are placed over seven positions with site occupancy factors of 0.87. Both the host and guest molecules are located in general positions. The crystal packing viewed along [100] and [010] is shown in Figure 7.7. The host molecules pack to form channels along [100] which are shown in Figure 7.8. The channels were examined using the program SECTION,[1] which showed the channels to be located at y = 1/2, z = 1/2 and have a fairly constant cross-sectional area of approximately 18.4 Å x 11.6 Å.

STRUCTURE SOLUTION AND ANALYSIS

TTRSC•6PYR

$C_{76}H_{88}O_{16}S_4.6(C_5H_5N)$
Guest: pyridine
Space group: $P\bar{1}$

a = 15.4030(5) Å	α = 113.073(2)°
b = 21.2691(7) Å	β = 98.256(2)°
c = 21.2829(9) Å	γ = 108.881(2)°
V = 5769.2(4) Å^3	
Z = 2	

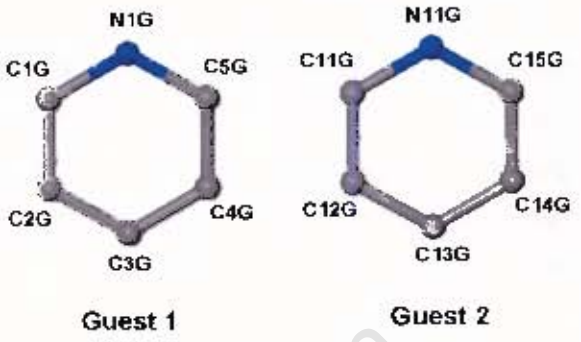

Guest 1 Guest 2

TTRSC•6PYR crystallises in the triclinic crystal system. The $|E^2-1|$ values obtained by direct methods show that the structure belongs to the centrosymmetric space group $P\bar{1}$. The positions of all non-hydrogen atoms of the host molecule were obtained by direct methods and the positions of non-hydrogen guest atoms were located in difference electron density maps. All non-hydrogen atoms of the host molecule were refined with anistropic thermal parameters, with the exception of disordered carbon atoms in the alkyl chains. Non-hydrogen atoms of the guest molecules were refined isotropically, with the exception of the nitrogen atoms of the guest molecules which are hydrogen bonded to the host.

Pyridine guest molecules were located in seven positions in the asymmetric unit and so the atoms of all the guest molecules were refined with site occupancy factors of 0.87 so as to satisfy the H:G ratio of 1:6. The hydroxyl hydrogens on the host molecule were located in difference electron density maps and refined with bond length constraints. The remaining hydrogen atoms were placed in geometrically constrained positions and assigned isotropic temperature factors of $1.2xU_{eq}$ of their parent atom. No attempt was made to place hydrogen atoms on the guest molecules which had high thermal parameters. The structure could not be refined to a satisfactory level and numerous attempts to obtain better quality crystals and data were unsuccessful. The structure refined to R_1 = 0.1466, but has been included here for completeness of this section of work and for comparison with the other structures in this chapter. The guest numbering scheme is given above and guests 3, 4, 5, 6 and 7 were numbered in the same way with, for example, the nitrogen atoms labelled N21G, N31G, N41G. N51G and N61G.

Four of the partial pyridine guest molecules are hydrogen bonded to the host molecule via the hydroxyl groups. The remaining guest molecules are not involved in hydrogen bonding. The hydrogen bonding in **TTRSC•6PYR** is depicted in Figure 7.9 and the hydrogen bonding details are given in Table 7.3. The TG and DSC traces show that guest release occurs in two steps and we can surmise that the loss of the non-hydrogen bonded pyridine guests occurs first, followed by the loss of the hydrogen bonded guests.

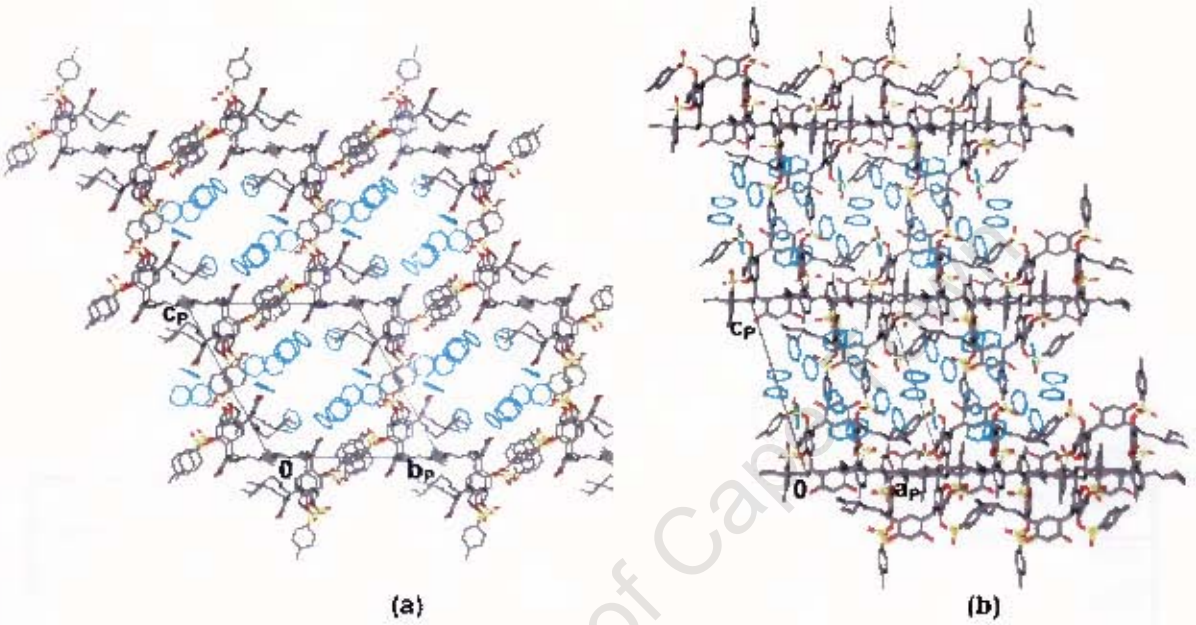

Figure 7.7 Packing diagrams of **TTRSC•6PYR** viewed along **(a)** [100] and **(b)** [010].

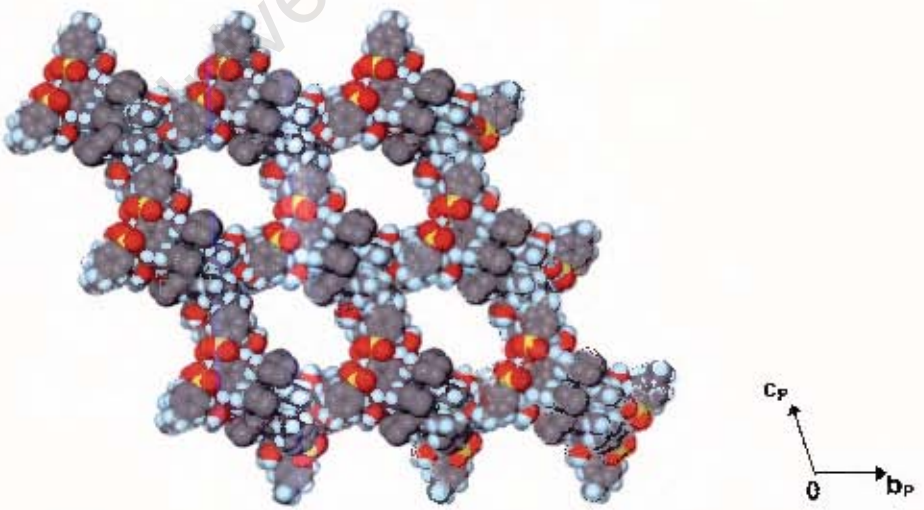

Figure 7.8 Space-filling projection of **TTRSC•6PYR**, viewed along [100], with the guest molecules omitted.

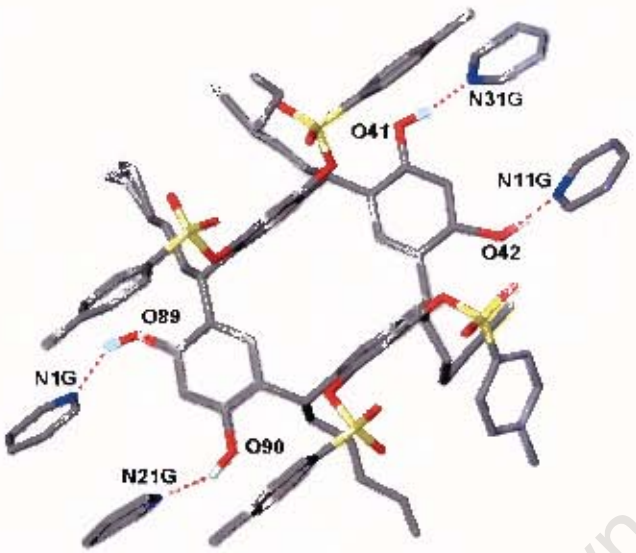

Figure 7.9 Hydrogen bonding interactions in **TTRSC•6PYR**.

Table 7.3 Hydrogen bonding details of **TTRSC•6PYR**

Donor (D)	Acceptor (A)	D–H/Å	D···A/Å	D–H···A/°
O41	N31G	0.970(1)	2.713(5)	171(5)
O42	N11G	0.98(1)	2.366(2)	160(5)
O89	N21G	0.960(2)	2.833(5)	136(7)
O90	N1G	0.960(1)	2.846(5)	148(11)

TTRSC•5(2PIC)

$C_{76}H_{88}O_{16}S_4.5(C_6H_7N)$	
Guest: 2-picoline	
Space group: $P\bar{1}$	
a = 13.6878(2) Å	α = 77.892(1)°
b = 16.3438(3) Å	β = 86.092(1)°
c = 22.3279(5) Å	γ = 83.396(1)°
V = 4851.1(2) Å^3	
Z = 2	

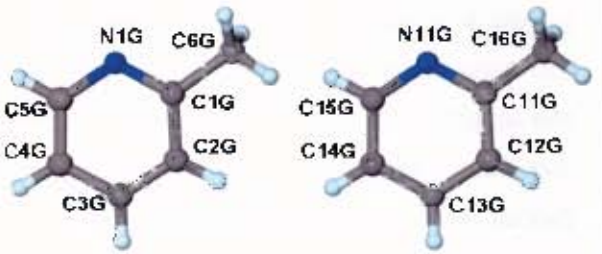

Guest 1 Guest 2

TTRSC•5(2PIC) crystallises in the triclinic crystal system. The centrosymmetric space group $P\bar{1}$ was chosen based on the $|E^2-1|$ values obtained by direct methods. The positions of all non-hydrogen atoms of the host molecule were obtained by direct methods and the positions of non-hydrogen guest atoms were located in difference electron density maps. All non-hydrogen host atoms were refined with anisotropic thermal parameters, with the exception of disordered alkyl chain carbon atoms, which were refined isotropically. One of the guest molecules was found to be disordered over two positions and the atoms of this molecule were refined isotropically, while the remainder of the non-hydrogen guest atoms were refined anisotropically. The hydroxyl hydrogens on the host molecule were located in difference electron density maps and refined with bond length constraints. The rest of the hydrogen atoms were placed with geometric constraints and refined with isotropic temperature factors equal to $1.2xU_{eq}$ of their parent atoms. The structure refined to $R_1 = 0.0546$.

One of the alkyl chains of the host molecules exhibits disorder and this disorder is illustrated in Figure 7.10(a). Atoms C79, C80, C81 and C82 were found to be disordered. Atoms C79 and C82 were modelled over two positions and the two partial atoms were labelled with suffixes A and B in each case. Atoms C80 and C81 were modelled over three positions and the partial atoms were labelled with suffixes A, B and C. For the atoms disordered over two positions, the disorder was treated as described for **TTRSC•6PYR**. The atoms disordered over three positions were assigned site occupancy factors based on their peak heights.

One of the guest molecules was found to be disordered over two positions with site occupancy factors of 0.71 (molecule containing N41G) and 0.29 (molecule containing N51G). This disorder, along with the atom labelling, is depicted in Figure 7.10(b).

The site occupancy factors of the partial atoms of both the host and guest molecules are given in Table 7.7 (page 227). The atom labelling for the ordered guest molecules is given in the guest numbering scheme above for two of the 2-picoline guests and guest 3 and guest 4 were numbered in the same way with, for example, the nitrogen atoms labelled N21G and N31G. When modelling the guest disorder, the temperature factors of the atoms of each partial molecule were forced to refine to the same value. This value was then fixed and the site occupancy factors of the two partial molecules were allowed to refine to give a total site occupancy of one. The refined site occupancy factors were then fixed and the isotropic temperature factors of the atoms were allowed to refine independently.

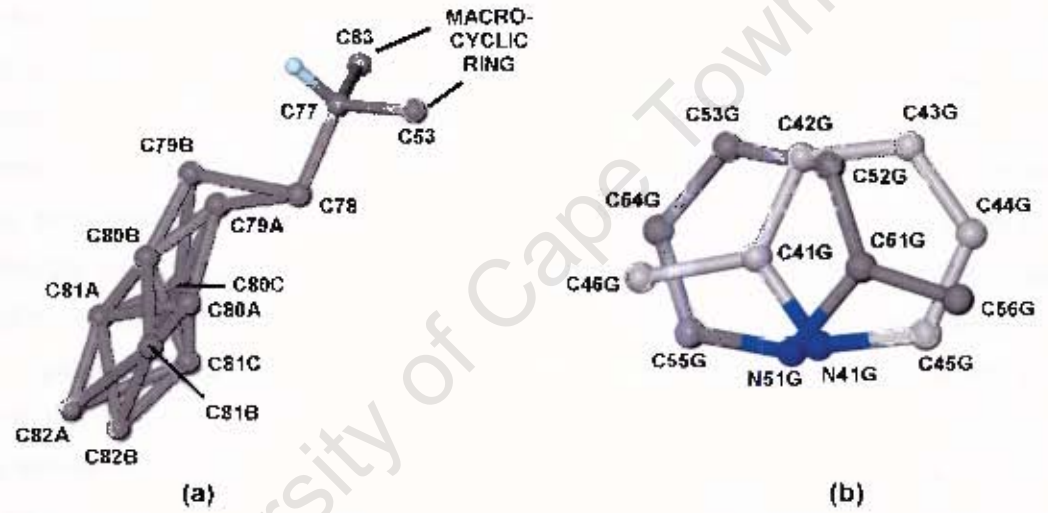

Figure 7.10 Disorder **(a)** in alkyl chain of host molecule and **(b)** of 2-picoline guest molecule in **TTRSC•5(2PIC)**.

The structure of **TTRSC•5(2PIC)** has Z = 2 and the asymmetric unit consists of one host molecule and five guest molecules. Both the host and guest molecules are located in general positions The crystal packing viewed along [010] and [100] is shown in Figure 7.11. The host molecules pack to form main channels along [010] which can be seen in Figure 7 12. The channels were examined using the program SECTION, which was used to view sections through the unit cell and these sections are shown in Figure 7.13.

The main channels along [010] are located at 0 along [100] and half a unit cell length along [001] and have a maximum cross-section of approximately 12.1 Å x 6.1 Å at

0 Å along [010] (Figure 7.13(a)). Between 5.0 Å and 11.3 Å along [010], these channels meet with smaller undulating channels along [100], which are also located at half a unit cell length along [001] (Figure 7.13(b)). The channels along [010] can be clearly seen in a section through the unit cell at 0 Å along [100] (Figure 7.13(c)).

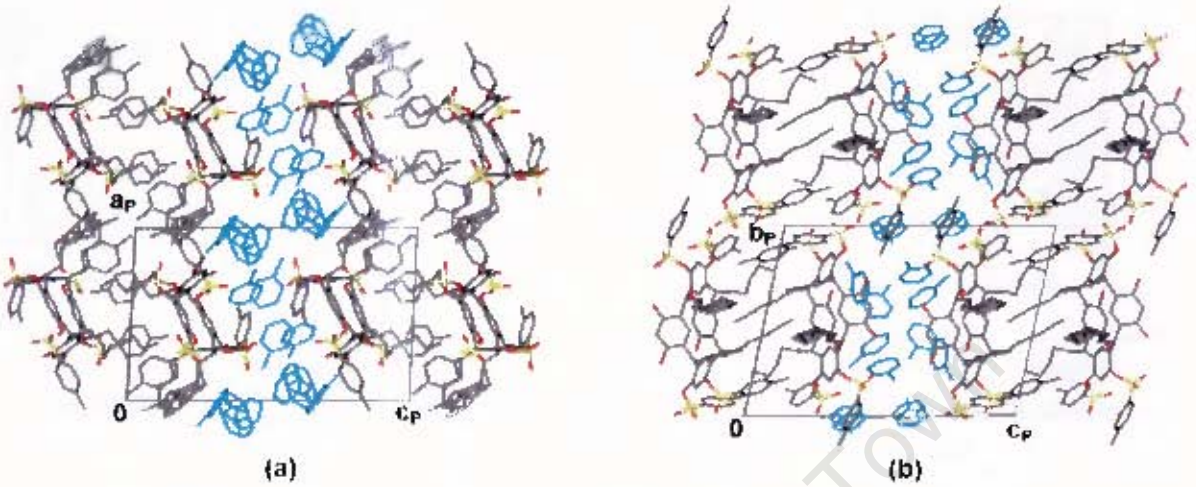

Figure 7.11 Packing diagrams of **TTRSC•5(2PIC)** **(a)** along [010] and **(b)** along [100].

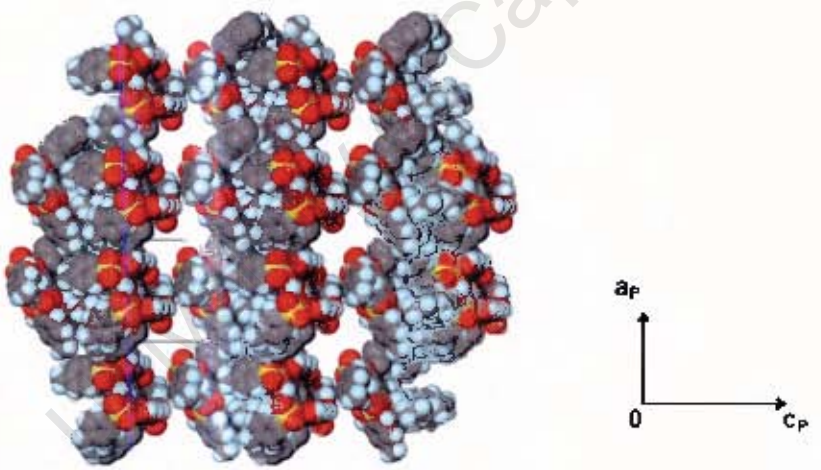

Figure 7.12 Space-filling projection showing channels of **TTRSC•5(2PIC)** along [010] with guest molecules omitted.

Four of the 2-picoline guest molecules are hydrogen bonded to the host molecule via its hydroxyl groups. The fifth 2-picoline guest molecule is not involved in hydrogen bonding. The hydrogen bonding in **TTRSC•5(2PIC)** is depicted in Figure 7.14 and the hydrogen bonding details are given in Table 7.4. The TG trace shows a two step mass loss and we can surmise that the first small mass loss with concomitant

endotherm A in the DSC trace (Figure 7.1(b), page 208) corresponds to the loss of the non-hydrogen bonded 2-picoline guest molecule, while the second larger mass loss and endotherm B in the DSC trace are due to the loss of the hydrogen bonded guests molecules.

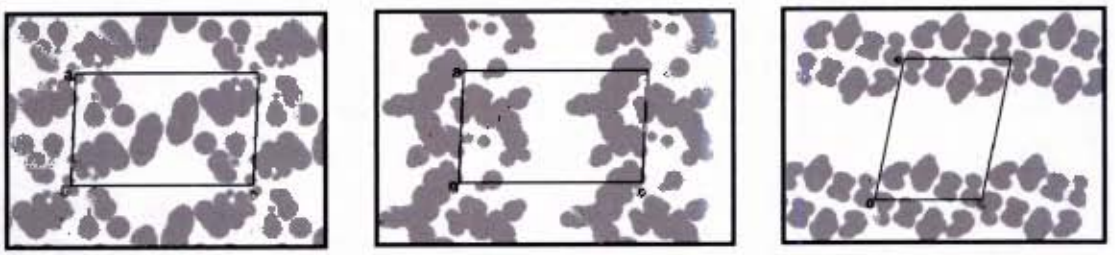

(a) 0 Å along [010] **(b)** 5.1 Å along [010] **(c)** 0 Å along [100]

Figure 7.13 SECTION plots of **TTRSC•5(2PIC)** (with guest molecules omitted and host molecules represented by grey areas) with the unit cell sectioned at **(a)** 0 Å along [010], **(b)** 5.1 Å along [010] and **(c)** 0 Å along [100].

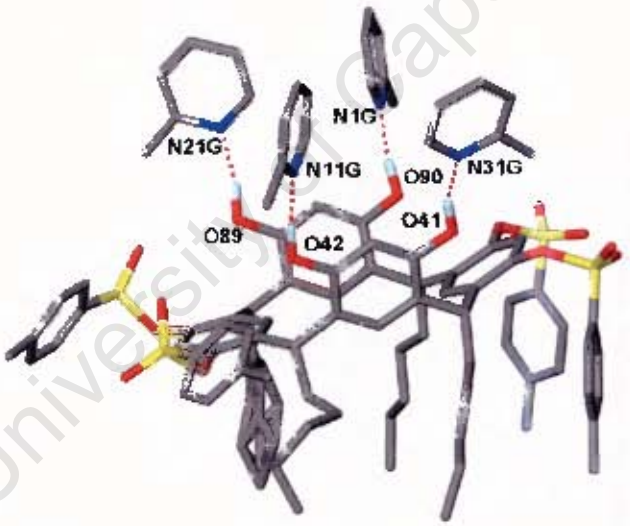

Figure 7.14 Hydrogen bonding interactions in **TTRSC•5(2PIC).**

Table 7.4 Hydrogen bonding details of **TTRSC•5(2PIC)**

Donor (D)	Acceptor (A)	D–H/Å	D···A/Å	D–H···A/°
O41	N31G	0.980(1)	2.694(3)	164(3)
O42	N11G	0.960(1)	2.795(3)	177(3)
O89	N21G	0.970(1)	2.744(3)	169(3)
O90	N1G	0.980(1)	2.698(2)	170(3)

TTRSC•4.5(3PIC)•0.5(H_2O)

$C_{76}H_{88}O_{16}S_4.4.5(C_6H_7N).0.5(H_2O)$
Guests: 3-picoline and water
Space group: C2/c
a = 44.8472(3) Å
b = 20.7901(2) Å β = 117.239(1)°
c = 23.3348(2) Å
V = 19344.1(3) Å^3
Z = 8

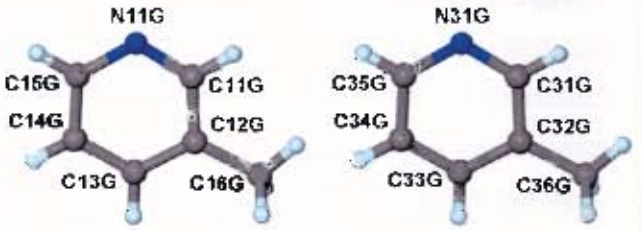

TTRSC•4.5(3PIC)•0.5(H_2O) crystallises in the monoclinic crystal system in the space group C2/c. Direct methods yielded the positions of all non-hydrogen atoms of the host molecule and the positions of non-hydrogen guest atoms were located in difference electron density maps. All non-hydrogen atoms of the host molecule and those of the ordered guest molecules were refined with anisotropic thermal parameters, while all remaining non-hydrogen guest atoms were refined isotropically. The hydroxyl hydrogens on the host molecule were located in difference electron density maps and refined with bond length constraints. All other hydrogen atoms were placed in geometrically constrained positions and assigned isotropic temperature factors of 1.2xU_{eq} of their parent atoms. The structure refined to R_1 = 0.0811.

The structure of **TTRSC•4.5(3PIC)•0.5(H_2O)** has Z = 8 and the asymmetric unit consists of one host molecule and four and a half 3-picoline guest molecules as well as half a water molecule. The host molecules and four 3-picoline guest molecules are located in general positions, while the half 3-picoline guest molecule and the half water molecule are located on a two-fold axis at Wyckoff position *e*.

Two of the complete guest molecules are ordered and the atom labelling of these molecules is given in the guest numbering scheme above. The remaining two complete guest molecules were found to be disordered and this disorder, as well as the guest numbering scheme, is illustrated in Figure 7.15. The molecule containing N1G was found to be disordered over two positions with site occupancy factors of 0.48 (atoms labelled with suffix A) and 0.52 (atoms labelled with suffix B). The molecule containing N21G was also modelled over two positions, but with the two partial molecules sharing a common nitrogen atom as well as two common carbon

atoms (C21G and C25G). The site occupancies of the two partial molecules were 0.51 (atoms C22G, C23G, C24G and C26G) and 0.49 (atoms C27G, C28G, C29G and C30G). The disorder was modelled using the same method described for **TTRSC•5(2PIC)**. The half 3-picoline molecule in the asymmetric unit, which lies on a two-fold axis, was also found to be disordered and was refined with site occupancy factors of 0.5 for each of the atoms, with the exception of C43G which is common to both partial molecules and therefore has a site occupancy of one. This disorder is depicted in Figure 7.16 along with the guest numbering scheme.

There are a number of fairly high electron density peaks which are unaccounted for and this is a result of the disorder in the structure which proved difficult to model.

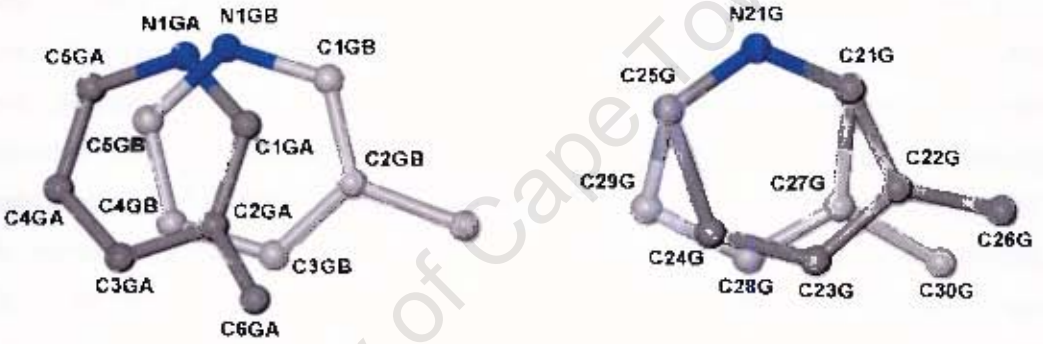

Figure 7.15 Disorder of two 3-picoline guest molecules in **TTRSC•4.5(3PIC)•0.5(H_2O)**.

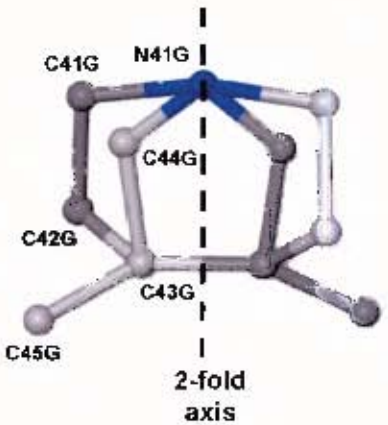

Figure 7.16 Disordered 3-picoline guest molecule located on a 2-fold axis in **TTRSC•4.5(3PIC)•0.5(H_2O)**.

The crystal packing viewed along [010] as well as along [001] is shown in Figure 7.17. The host molecules pack to form layers parallel to the bc plane, with the guest molecules located between these layers. These layers are shown in Figure 7.18.

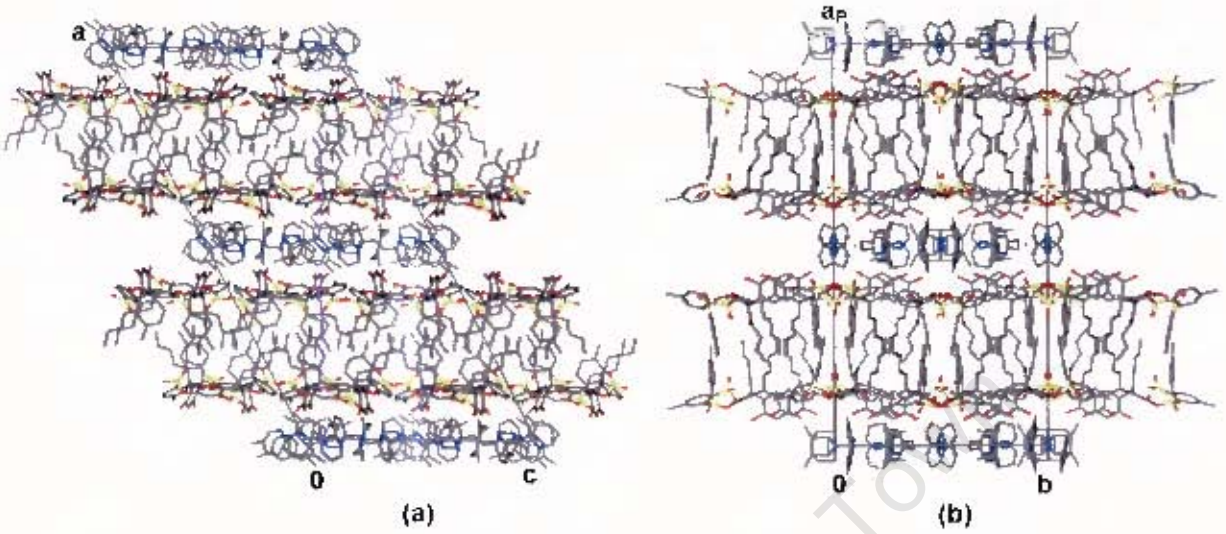

Figure 7.17 Packing diagrams of **TTRSC•4.5(3PIC)•0.5(H_2O)** **(a)** along [010] and **(b)** along [001].

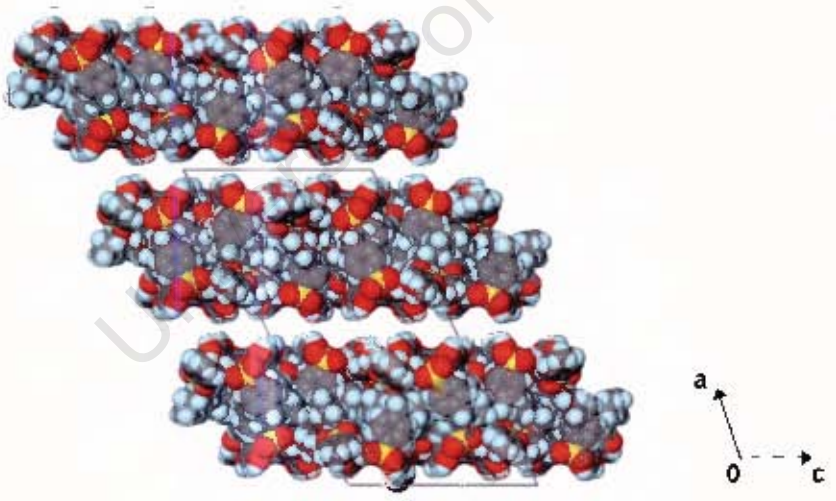

Figure 7.18 Space-filling projection along [010] showing layers of host molecules with guest molecules omitted.

Three of the complete 3-picoline guest molecules are hydrogen bonded to the host molecule via the hydroxyl groups. The fourth host hydroxyl group is hydrogen bonded to a water molecule which is in turn hydrogen bonded to the same hydroxyl

group of a second host molecule. The remaining complete 3-picoline guest and the half 3-picoline guest molecule are not involved in hydrogen bonding. The hydrogen bonding in **TTRSC•4.5(3PIC)•0.5(H_2O)** is depicted in Figure 7.19 and the hydrogen bonding details are given in Table 7.5. The thermal analysis is complex (Figure 7.1(c), page 208) and could not be readily correlated to the structure.

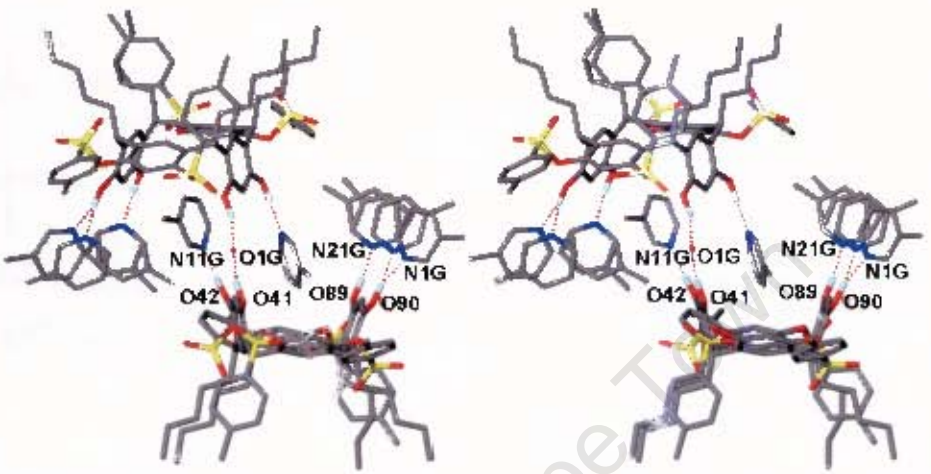

Figure 7.19 Stereoview of hydrogen bonding interactions in **TTRSC•4.5(3PIC)•0.5(H_2O).**

Table 7.5 Hydrogen bonding details of **TTRSC•4.5(3PIC)•0.5(H_2O)**

Donor (D)	Acceptor (A)	D–H/Å	D···A/Å	D–H···A/°
O41	O1G	0.970(1)	2.71(2)	158(4)
O42	N11G	0.970(1)	2.753(4)	174(5)
O89	N21G	0.970(1)	2.737(4)	173(4)
O90	N1GA	0.970(1)	2.801(5)	172(4)
O90	N1GB	0.970(1)	2.748(5)	165(4)

TTRSC•6.5(4PIC)•2(H_2O)

$C_{76}H_{88}O_{16}S_4.6.5(C_6H_7N).2(H_2O)$
Guests: 4-picoline and water
Space group: $P\bar{1}$
a = 16.9366(1) Å α = 104.495(1)°
b = 17.9477(2) Å β = 96.671(1)°
c = 19.4997(2) Å γ = 105.445(1)°
V = 5424.27(9) Å^3
Z = 2

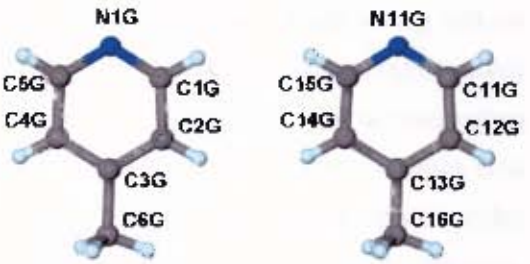

Guest 1 Guest 2

TTRSC•6.5(4PIC)•2(H_2O) crystallises in the triclinic crystal system. The centrosymmetric space group $P\bar{1}$ was chosen based on the $|E^2-1|$ values obtained by direct methods. The positions of all non-hydrogen atoms of the host molecule were obtained by direct methods and the positions of non-hydrogen guest atoms were located in difference electron density maps. All non-hydrogen atoms were refined with anistropic thermal parameters, with the exception of disordered carbon atoms of the host alkyl chains and atoms of the half 4-picoline guest molecule which were refined isotropically.

The hydroxyl hydrogens on the host molecule were located in difference electron density maps and refined with bond length constraints. The rest of the hydrogen atoms were placed with geometric constraints and refined with isotropic temperature factors equal to 1.2xU_{eq} of their parent atoms. No attempt was made to place hydrogen atoms on the half 4-picoline molecule or the water molecules. The structure refined to R_1 = 0.0687.

Three of the alkyl chains of the host molecule were found to be disordered as well as the half 4-picoline guest molecule. Atoms C33, C34, C80, C81, C94 and C96 in the alkyl chains were modelled over two positions and the partial atoms were labelled with suffixes A and B in each case. This disorder is illustrated in Figure 7.20. The disorder was modelled using the same method as described for **TTRSC•6PYR** and the site occupancy factors of the partial atoms are given in Table 7.7 (page 227).

The structure of **TTRSC•6.5(4PIC)•2(H_2O)** has Z = 2 and the asymmetric unit consists of one host molecule, six complete 4-picoline guest molecules and half a 4-picoline guest molecule, as well as two water molecules. The host molecules, the

complete 4-picoline molecules and the water molecules are located in general positions. The half 4-picoline molecule is located on a centre of inversion at (1/2,1/2,0) and was found to be disordered over two positions. This disorder as well as the guest atom numbering is depicted in Figure 7.21. The atoms were refined with site occupancy factors of 0.5, with the exception of atoms shared by both partial molecules which were assigned site occupancies of one. In the case of the nitrogen and methyl carbon which overlap, the atom was assigned as a nitrogen atom and refined with a site occupancy of 0.93. We used this approximation as being the 'average' of the scattering factor of a nitrogen atom (Z = 7) and a carbon atom (Z = 6). The average is 6.5 and the scattering factor is therefore 6.5/7 which is equal to 0.93. The electron density peak of 1.11 e.Å^{-3} which is unaccounted for is once again due to disorder in the structure which proved difficult to model.

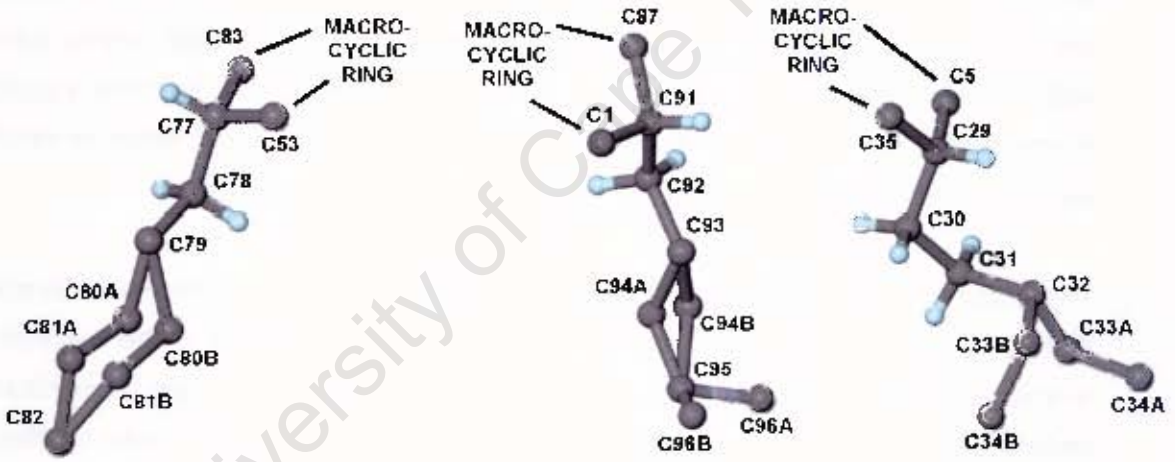

Figure 7.20 Disorder in alkyl chains of host molecule in **TTRSC•6.5(4PIC)•2(H_2O)**.

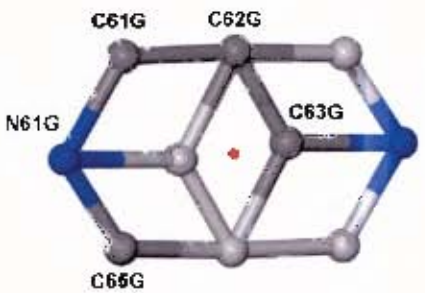

Figure 7.21 Disorder of 4-picoline guest molecule on a centre of inversion in **TTRSC•6.5(4PIC)•2(H_2O)**.

The crystal packing viewed along [010] and [100] is shown in Figure 7.22. The host molecules pack to form restricted channels along [010], as well as along [100] and the guest molecules are located in these channels. The channels along [010] are clearly shown in Figure 7.23. The program SECTION[1] was used to examine the channels by viewing sections through the unit cell along [100] and along [010]. Two of these sections are illustrated in Figure 7.24.

The channels along [010] have a maximum cross-sectional area of approximately 16.8 Å x 11.1 Å at 1.5 Å down [010] and at x = 0.5, z = 0. They have a minimum cross-sectional area of approximately 8.4 Å x 8.4 Å at 5.4 Å along [010] and at x = 0.75, z = 0. The channels along [100] have a maximum cross-sectional area of approximately 14.0 Å x 14.0 Å at 8.2 Å down [100] and at y = 0, z = 0 and a minimum cross-sectional area of approximately 9.5 Å x 8.4 Å at 0.4 Å along [100] and at y = 0.5, z = 0.

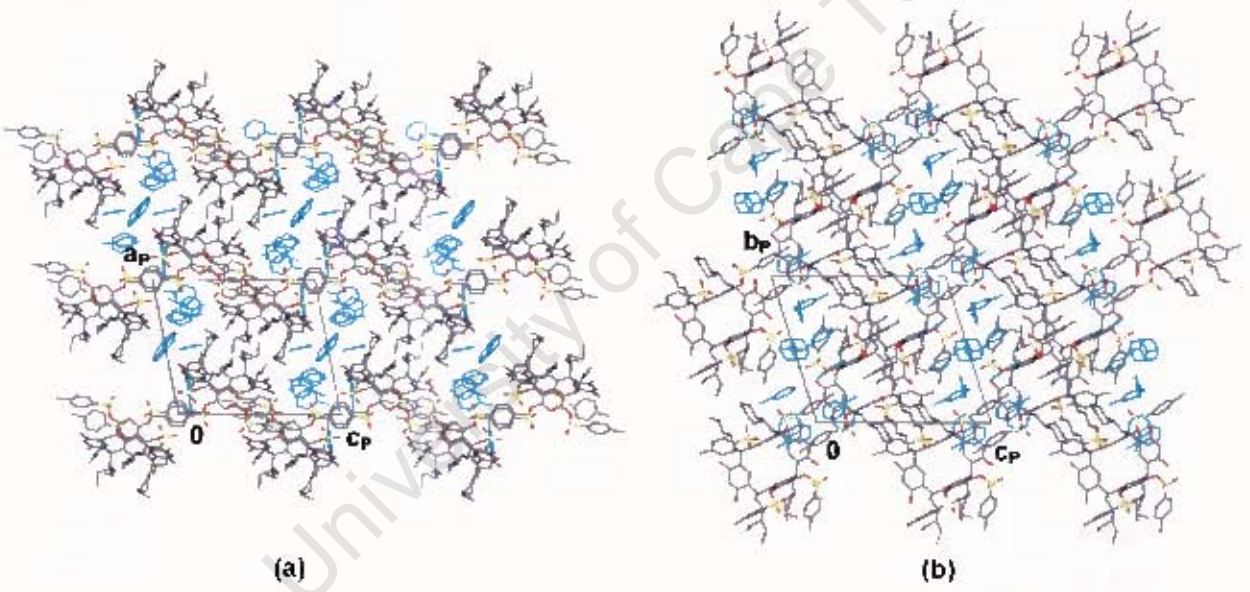

Figure 7.22 Packing diagrams of **TTRSC•6.5(4PIC)•2(H_2O)** viewed **(a)** along [010] and **(b)** along [100].

Four of the 4-picoline guest molecules are hydrogen bonded to the host molecule via its hydroxyl groups. One of the water molecules is hydrogen bonded to a fifth 4-picoline guest molecule, while the other water molecule and remaining complete 4-picoline guest molecule and half 4-picoline molecule are not involved in hydrogen bonding. The hydrogen bonding details are given in Table 7.6 and the hydrogen bonding in **TTRSC•6.5(4PIC)•2(H_2O)** is depicted in Figure 7.25.

The thermal analysis is complex (Figure 7.1(d), page 208) and could not readily be correlated to the structure.

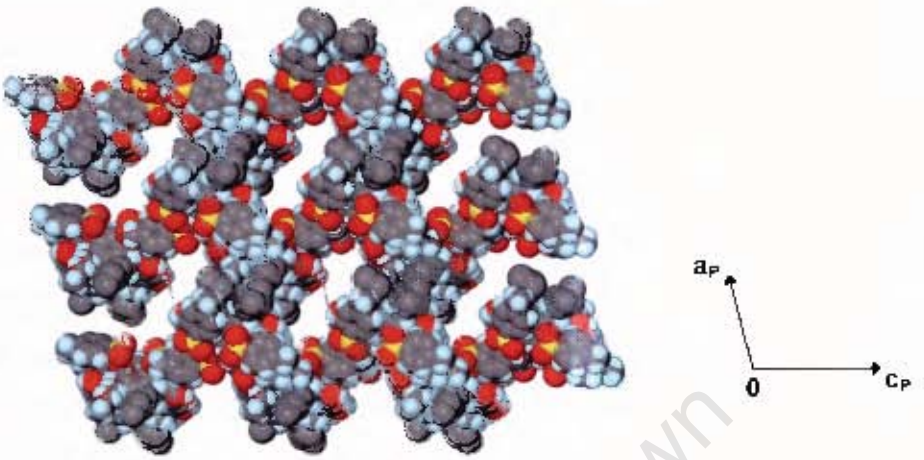

Figure 7.23 Space-filling projection along [010] showing channels of **TTRSC•6.5(4PIC)•2(H_2O)** with guest molecules omitted.

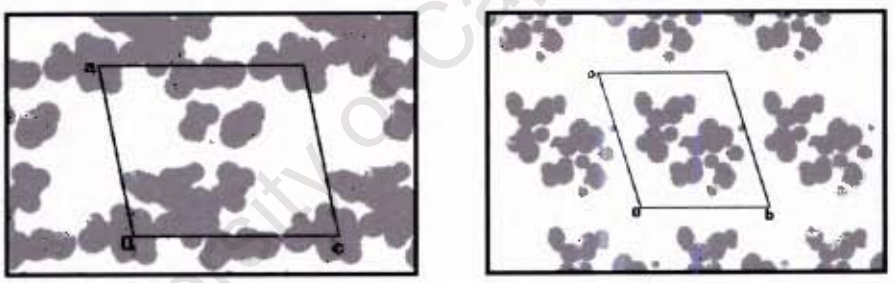

(a) 1.5 Å along [010] **(b)** 8.2 Å along [100]

Figure 7.24 SECTION plots of **TTRSC•6.5(4PIC)•2(H_2O)** (with guest molecules omitted and host molecules represented by grey areas) with the unit cell sectioned at **(a)** 1.5 Å along [010] and **(b)** 8.2 Å along [100].

Table 7.6 Hydrogen bonding details of **TTRSC•6.5(4PIC)•2(H_2O)**

Donor (D)	Acceptor (A)	D–H/Å	D···A/Å	D–H···A/°
O41	N31G	0.960(1)	2.782(3)	175(4)
O42	N11G	0.970(1)	2.760(3)	170(5)
O89	N21G	0.970(1)	2.736(3)	168(4)
O90	N1G	0.980(1)	2.653(3)	169(5)
O1G	N41G		2.707(9)	

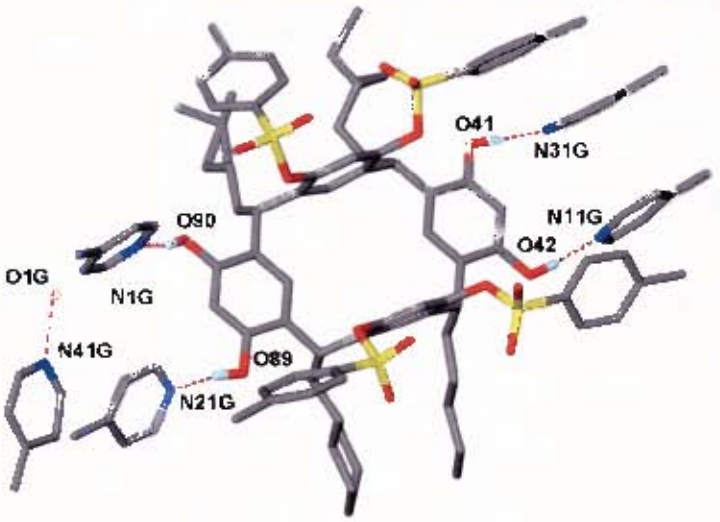

Figure 7.25 Hydrogen bonding interactions in TTRSC•6.5(4PIC)•2(H_2O).

Table 7.7 Site occupancy factors of partial disordered atoms

Inclusion Compound	Partial atom pair		Site occupancy factors	
	Atom 1	Atom 2	Atom 1	Atom 2
TTRSC•6PYR	C33A	C33B	0.70	0.30
	C34A	C34B	0.70	0.30
	C95A	C95B	0.67	0.33
	C96A	C96B	0.48	0.52
TTRSC•5(2PIC)	C79A	C79B	0.70	0.30
	C80A	C80B	0.60	0.20
		C80C		0.20
	C81A	C81B	0.60	0.20
		C81C		0.20
	C82A	C82B	0.60	0.40
TTRSC•6.5(4PIC)•2(H_2O)	C33A	C33B	0.30	0.70
	C34A	C34B	0.30	0.70
	C80A	C80B	0.77	0.33
	C81A	C81B	0.77	0.33
	C94A	C94B	0.75	0.25
	C96A	C96B	0.70	0.30

COMPETITION EXPERIMENTS

Competition experiments between 3-picoline and 4-picoline were carried out to establish whether the host would selectively include either of these isomers. The results are illustrated in Figure 7.26. The graph shows the mole fraction X of 3-picoline in the initial solution versus the mole fraction Z of 3-picoline included by the host. The red diagonal line (x = y) represents zero selectivity and the blue curve represents the experimental results.

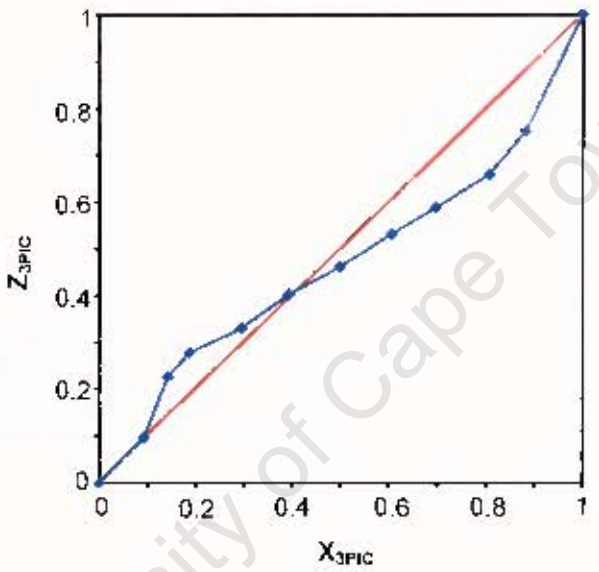

Figure 7.26 Results of the 3-picoline versus 4-picoline competition experiments.

From Figure 7.26, which shows the results of the 3-picoline versus 4-picoline competition experiment, it can be seen that the selectivity of **TTRSC** for these two isomers is concentration dependent, although not in the way which would be expected. When the selectivity of a host is found to be concentration dependent, the typical result obtained is that the host preferentially enclathrates the guest of which there is a greater mole fraction in the solution, as shown in Figure 1.6(c) (page 11). In this case however, the host was found to preferentially enclathrate the guest of which there is a lower mole fraction in the initial solution. This is counterintuitive and certainly unusual.

This selectivity can be explained by the solubilities of the two clathrates in 3- and 4-picoline. If the solubility of the 3-picoline clathrate in 3-picoline is significantly greater than that of the 4-picoline clathrate in 3-picoline, then when there is more 3-picoline in the solution, it will be the 4-picoline clathrate which will crystallise out of solution. Similarly if the 4-picoline clathrate is more soluble than the 3-picoline clathrate in 4-picoline, the 3-picoline clathrate would crystallise out of a solution with a greater mole fraction of 4-picoline.

The solubilities of each of the clathrates in both 3-picoline and 4-picoline were measured and the results corresponded to the above explanation. In 3-picoline it was found that the solubility of the 3-picoline clathrate is 0.513 g/ml, whereas the solubility of the 4-picoline clathrate is 0.252 g/ml. In 4-picoline, the solubility of the 3-picoline clathrate was found to be 0.165 g/ml while that of the 4-picoline clathrate was 0.339 g/ml. This experiment therefore explains the shape of the selectivity curve shown in Figure 7.26.

SUMMARY AND DISCUSSION

The resorcinarene host **TTRSC** was found to form inclusion compounds with pyridine and the three picoline isomers, namely 1-, 2- and 3-picoline. In the case of the inclusion compounds with 3- and 4-picoline, water is also included in the structures of the host-guest compounds. The structures of each of the complexes formed have been elucidated and thermal analysis was carried out including TG, DSC and HSM. The selectivity of the host for 3-picoline versus 4-picoline was examined by performing competition experiments with these two guests.

It was found that **TTRSC•6PYR** (with H:G = 1:6), **TTRSC•5(2PIC)** (with H:G = 1:5) and **TTRSC•6.5(4PIC)•2(H_2O)** (with H:G:H_2O = 1:6.5:2) all crystallise in the triclinic crystal system, in the space group $P\bar{1}$, with $Z = 2$ in each case. All of these structures have one host molecule in the asymmetric unit which is located in a general position in the unit cell. In the **TTRSC•6PYR** and **TTRSC•5(2PIC)** structures the guest molecules are all located in general positions and in the structure of **TTRSC•6.5(4PIC)•2(H_2O)** there are six 4-picoline guest molecules, as well as two water molecules, located in general positions and the remaining half 4-picoline guest molecule in the asymmetric unit is located on a centre of symmetry.

In each of these three structures the guests are located in channels. In **TTRSC•6PYR** the host molecules pack to form channels along [100] in which the guest molecules are located. The host molecules in **TTRSC•5(2PIC)** pack to form channels along [010], with a second set of smaller undulating channels along [100]. In the structure of **TTRSC•6.5(4PIC)•2(H_2O)** the host molecules pack to form restricted channels along [010] as well as along [100] in which the guest molecules are situated.

TTRSC•4.5(3PIC)•0.5(H_2O) (with H:G:H_2O = 1:4.5:0.5) crystallises in the monoclinic crystal system in the space group C2/c with $Z = 8$. The asymmetric unit consists of one host molecule, four and a half 3-picoline guest molecules and half a water molecule. The host molecule and four 3-picoline guest molecules are located in general positions, while the half 3-picoline guest molecule and half water molecule are located on a two-fold axis at Wyckoff position e. The host molecules pack to form layers parallel to the bc plane and the guest molecules are located between these layers.

In all four of the structures there are four guest molecules hydrogen bonded to the host molecule via the hydroxyl groups. In the case of **TTRSC•4.5(3PIC)•0.5(H_2O)**, one of the four hydrogen bonded guests is the water molecule and is hydrogen bonded to two host molecules. In the case of **TTRSC•6.5(4PIC)•2(H_2O)**, there is an additional hydrogen bond between one of the water molecules and one of the 4-picoline guest molecules which is not hydrogen bonded to the host molecule.

In contrast to the hydrogen bonding pattern of the inclusion compounds with the pentanols, there is no hydrogen bonding between host molecules. In each of these structures, the guests are once again captured between the resorcinarene molecules and not within the resorcinarene cavity.

Competition experiments were carried out in order to establish whether the host would preferentially include 3-picoline or 4-picoline. It was found that when **TTRSC** is dissolved in a mixture of 3-picoline and 4-picoline, this host will selectively enclathrate the guest of lower mole fraction in the starting solution. This can be explained by the solubilities of the two clathrates in 3- and 4-picoline, as the 3-picoline clathrate was found to be twice as soluble in 3-picoline as the 4-picoline clathrate, resulting in preferential crystallisation of the 4-picoline clathrate when the solution has a higher mole fraction of 3-picoline. The opposite is true when the solution has a higher mole fraction of 4-picoline, as the 4-picoline clathrate is twice as soluble in 4-picoline as the 3-picoline clathrate. This is an unusual result.

REFERENCES

[1] L.J. Barbour, SECTION, A computer program for the graphic display of cross sections through a unit cell, *J. Appl. Cryst.*, 1999, **32**, 353.

Chapter 8

HOST CONFORMATIONS

*The conformations of the host molecules, namely trans-9,10-dihydroxy-9,10-bis(p-tert-butylphenyl)-9,10-dihydroanthracene (abbreviated **TBDDDA**), 9,9'-(Biphenyl-4,4'-diyl)difluoren-9-ol (abbreviated **WEB24**) and $1^4,1^6,5^4,5^6$-tetrahydroxy-2,4,6,8-tetrapentyl-$3^4,3^6,7^4,7^6$-tetra(p-toluenesulfonyl-oxy)-1,3,5,7(1,3)-tetrabenzenacyclo-octaphane (abbreviated **TTRSC**) are discussed collectively in this chapter. The differences in conformation of each host molecule in the structures of the various inclusion compounds formed are examined.*

The host numbering schemes have been given in the relevant chapters and are also displayed on the bookmark.

TBDDDA CONFORMATION

The host *trans*-9,10-dihydroxy-9,10-bis(p-*tert*-butylphenyl)-9,10-dihydroanthracene is a diol host compound with the two hydroxyl groups in a *trans* conformation. The conformation of the host molecule can be described by one torsion angle and one dihedral angle. The values of these angles for the structures of each of the inclusion compounds formed with this host are given in Table 8.1 and the dihedral angle measured is that between the plane of the tricyclic moiety and the plane of the *tert*-butylphenyl group.

A search of the Cambridge Structural Database[1] revealed three inclusion compounds previously formed with this host and the angles for these structures are given in Table 8.1 for comparison. The values of the dihedral angles lie in the range 86.6°-89.6°, which shows that the *tert*-butylphenyl groups and the hydroxyl groups are at approximately 90 degrees to each other in all cases. The relevant torsion angle along with the different bond types occurring in **TBDDDA** are illustrated in Figure 8.1 and the bond length ranges are summarised in Table 8.2. The bond lengths for all the structures are comparable with the standard values given for these bond types.[2]

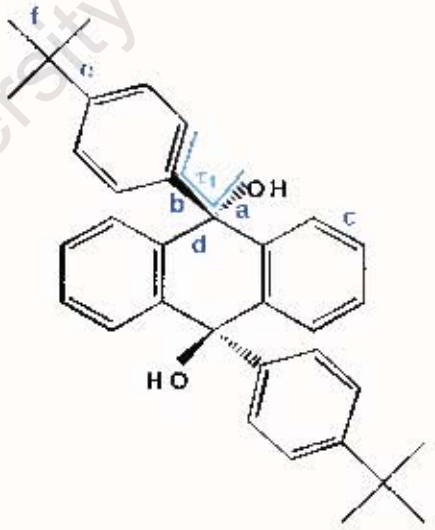

Figure 8.1 Classification of bonds for the host **TBDDDA**, also showing the torsion angle describing the host conformation.

The host molecule has the same general conformation in all of the inclusion compounds and this conformation, taken from the **TBDDDA•4DMF** structure is depicted in Figure 8.2. The tricyclic anthracene moiety, as well as the phenyl rings of the *tert*-butylphenyl substituents, were found to be planar in the structures of all of the inclusion compounds, with the aromatic carbon atoms having a maximum deviation of 0.040(2) Å and 0.010(2) Å respectively from the ring plane.

Table 8.1 Torsion and dihedral angles (°) describing **TBDDDA** conformations

	τ_1*	Dihedral angle
TBDDDA•4DMF	4.5(2)	89.59(7)
TBDDDA•3DMF•1DMSO	4.5(3)	88.25(9)
TBDDDA•2DMF•2DMSO	5.7(3)	86.6(1)
TBDDDA•1DMF•3DMSO	4.6(4)	86.7(1)
TBDDDA•4DMSO	4.9(3)	86.7(1)
TBDDDA•4ACE	3.3(3)	86.83(9)
TBDDDA•2DMF•2ACE	4.3(3)	87.45(9)
TBDDDA•2DMSO•2ACE	3.6(3)	86.87(9)
Methanol clathrate[3] (H:G = 1:1)**	9.9, 5.6	83.30, 88.12
Diethyl ether clathrate[4] (H:G = 1:2)	10.9	86.89
Benzene clathrate[5] (H:G = 1:3)	2.7	85.54

* *τ_1 represents either O1-C1-C8-C9 or O1-C1-C8-C13 in each case (numbering scheme given on the bookmark and in Chapter 3)*

** *This structure has two half host molecules in the asymmetric unit*

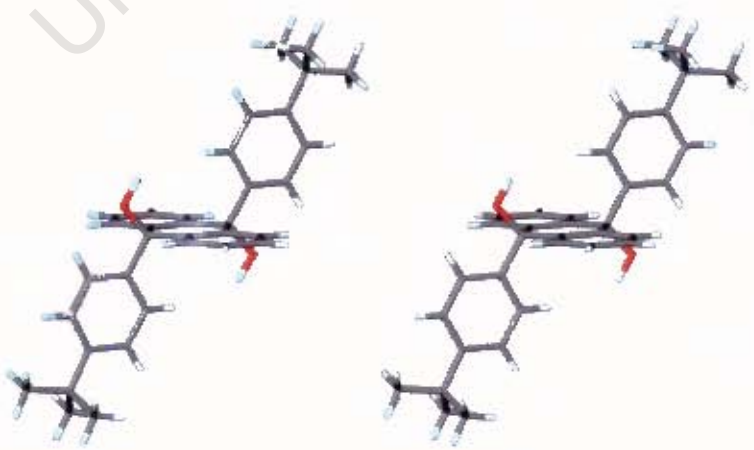

Figure 8.2 Stereoview of general host conformation of **TBDDDA**, extracted from the **TBDDDA•4DMF** structure.

Table 8.2 Bond length ranges observed in the **TBDDDA** structures*

	a = C_{sp3}-O (Å)	b = C_{sp3}-C_{ar} (Å)	c = C_{ar} =C_{ar} (Å)	d = C_{ar}-C_{sp3} (Å)	e = C_{ar}-C_{sp3} (Å)	f = C_{sp3}-C_{sp3} (Å)
TBDDDA	1.439(3) 1.447(3)	1.527(3) 1.536(4)	1.377(4) 1.406(4)	1.521(3) 1.531(3)	1.518(4) 1.535(4)	1.470(8) 1.578(8)
TBDDDA •4DMF	1.429(2)	1.537(2)	1.374(3) 1.410(3)	1.526(3)	1.539(3)	1.521(3) 1.539(3)
TBDDDA •3DMF •1DMSO	1.433(3)	1.525(3)	1.380(3) 1.406(3)	1.517(3)	1.537(4)	1.514(4) 1.537(3)
TBDDDA •2DMF •2DMSO	1.434(3)	1.536(3)	1.378(4) 1.403(3)	1.526(3)	1.533(3)	1.529(4) 1.537(4)
TBDDDA •1DMF •3DMSO	1.437(3)	1.530(4)	1.375(5) 1.406(4)	1.527(4)	1.536(4)	1.516(6) 1.545(6)
TBDDDA •4DMSO	1.429(3)	1.536(3)	1.377(4) 1.410(4)	1.530(3)	1.531(4)	1.524(5) 1.535(5)
TBDDDA •4ACE	1.443(2)	1.533(3)	1.374(3) 1.404(3)	1.528(3)	1.521(3)	1.501(5) 1.64(1)
TBDDDA •2DMF •2ACE	1.432(2)	1.533(3)	1.378(3) 1.410(3)	1.527(3)	1.536(3)	1.46(1) 1.65(1)
TBDDDA •2DMSO •2ACE	1.435(2)	1.530(3)	1.382(3) 1.407(3)	1.370(3) 1.524(3)	1.534(3)	1.512(4) 1.532(5)
Standard values**	1.440 (0.012)	1.527 (0.016)	1.384 (0.013)	1.527 (0.016)	1.527 (0.016)	1.534 (0.011)

** For each structure the first value given is that of the minimum bond length and the second value that of the maximum bond length*

***The standard value given is the unweighted sample mean for that bond type in each case*[2]

In the structure of the apohost, there are two independent host molecules and one of these molecules has a significantly different conformation from that of the host molecules in the inclusion compounds. This structure has one and a half host molecules in the asymmetric unit, with the complete host molecule located in a general position and the half host molecule on a centre of inversion at Wyckoff position *c*.

The 9,10-dihydroanthracene moiety of the molecule located on a centre of inversion must be planar and this molecule was found to have τ_1 = -4.0(3)° and a dihedral angle between the tricyclic moiety and the *tert*-butylphenyl group of 82.8(1)°. This molecule therefore has a very similar conformation to that observed in the structures of the inclusion compounds.

Interestingly however, in the complete host molecule, which lies in a general position, the 9,10-dihydroanthracene moiety is bent away from planarity and in particular the centre ring displays a boat conformation, which is illustrated in Figure 8.3. Another feature of the host conformation in this structure is that the methyl carbons of one of the *tert*-butylphenyl groups are disordered over two positions. This is also seen in the structures of **TBDDDA•4ACE** and **TBDDDA•2DMF•2ACE**.

Figure 8.3 Stereoview of boat conformation of host molecule in **TBDDDA** structure.

For a boat conformation, two mirror plane asymmetry parameters can be calculated. These are shown in Figure 8.4. We have calculated the asymmetry parameters using equations 1 and 2,[5] and obtained values of $\Delta C_s(1)$ = 3.65 and $\Delta C_s(2\text{-}7)$ = 3.96. These values are small, which indicates that the ring deviates very little from the boat conformation.

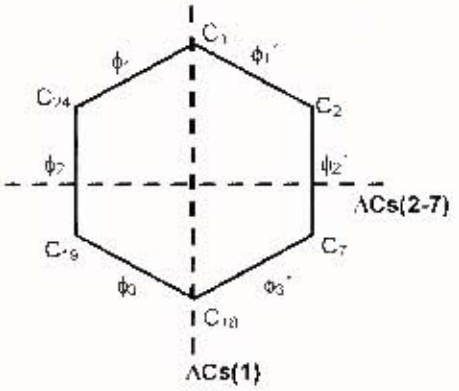

Figure 8.4 Mirror plane asymmetry parameters calculated for the centre ring of the 9,10-dihydroanthracene moiety.

$$\Delta C_s(1) = \sqrt{\frac{\sum_{i=1}^{3} (o_i + o_i')^2}{3}} \quad \text{..... (1)} \qquad \Delta C_s(2\text{-}7) = \sqrt{\frac{(\phi_4 - o_3)^2 + (\phi_1' - o_3')^2}{2}} \quad \text{..... (2)}$$

Table 8.3 Torsion and dihedral angles (°) describing **WEB24** conformation

	τ_1	τ_2	τ_3	Dihedral angle
WEB24	45.3(1)	0	-	68.21(3)
WEB24•4DMA*	23.4(4)	-24.3(4)	-0.8(3)	81.7(1) 85.5(1)
WEB24•2DMA	10.6(4)	0	-	88.2(1)
WEB24•3DIOX	23.5(2)	0	-	85.22(4)
WEB24•2MEK	12.5(2)	0	29.0(2)	81.00(4) 70.12(4)
WEB24•2ETHYL*	17.7(2)	-25.2(2)	18.1(2)	80.57(6) 84.38(6)
WEB24•2PROPYL*	36.7(3)	39.9(3)	14.4(3)	75.74(9) 85.56(9)

* *These structures have a complete host molecule in the asymmetric unit and the two dihedral angles given are between the planes of one of the central phenyl rings and the closest fluorenyl moiety*

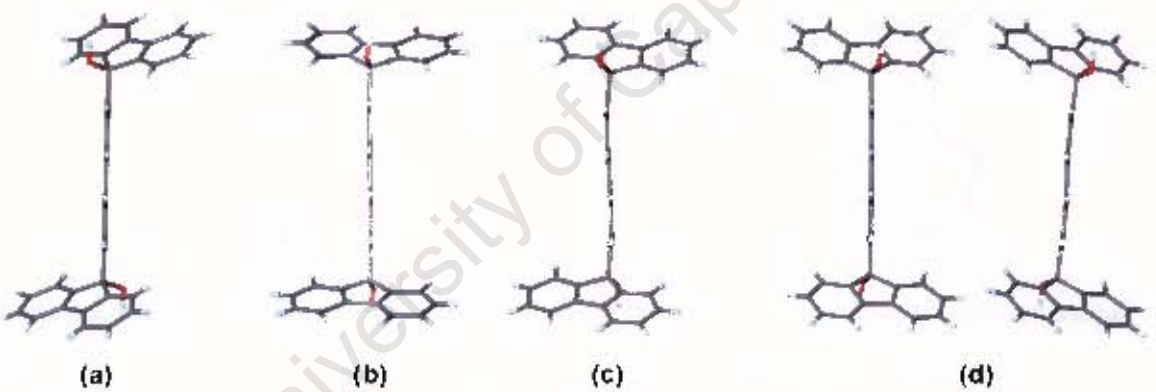

Figure 8.6 Conformation of host molecules viewed along the plane of the central phenyl rings in **(a) WEB24**, **(b) WEB24•2DMA**, **(c) WEB24•3DIOX** and **(d) WEB24•2MEK**.

In the structures of **WEB24•4DMA**, **WEB24•2ETHYL** and **WEB24•2PROPYL** there is a complete host molecule in the asymmetric unit and in these structures the two central phenyl rings do not lie in exactly the same plane. The variation in the angle between these two rings is shown by the torsion angle τ_2 and these variations are illustrated in Figure 8.7, from which it can be seen that the greatest angle between the two central phenyl rings occurs in the structure of **WEB24•2PROPYL**.

WEB24 CONFORMATION

The host 9,9'-(Biphenyl-4,4'-diyl)difluoren-9-ol is a diol host molecule consisting of two fluorenyl moieties separated by two phenyl rings. A search of the Cambridge Structural Database[1] showed no previous structures involving this host.

The host conformation is defined by three torsion angles, τ_1, τ_2 and τ_3, shown in Figure 8.5, and the dihedral angle between the central phenyl groups and the tricyclic fluorenyl moiety. Table 8.3 compares these angles in the structures of each of the inclusion compounds as well as in the structure of the apohost. The different bond types occurring in **WEB24** are shown in Figure 8.5 and the bond length ranges observed in the **WEB24** structures are given in Table 8.4. The bond lengths were all found to be comparable with the standard values.[2]

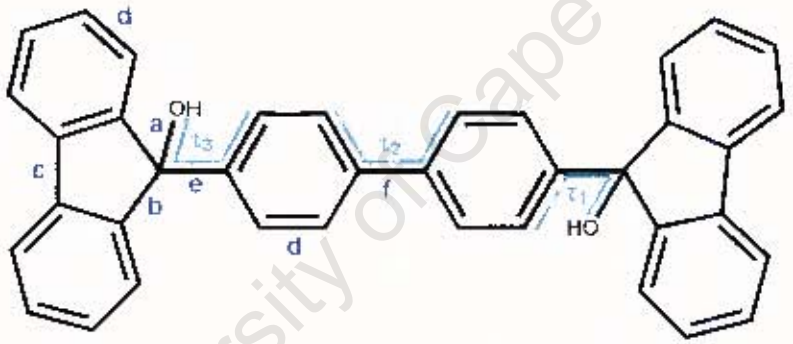

Figure 8.5 Classification of bonds for the host **WEB24** and torsion angles describing the host conformation.

In each of the structures the tricyclic fluorenyl moieties are planar with the maximum deviation of an aromatic carbon atom from the plane of the rings being 0.108(3) Å. The individual central phenyl rings were also found to be planar with the aromatic carbon atoms having a maximum deviation of 0.022(2) Å from the ring plane. In the structures of **WEB24**, **WEB24•2DMA**, **WEB24•3DIOX** and **WEB24•2MEK** there is half a host molecule in the asymmetric unit (in the case of **WEB24•2MEK** there are two half host molecules) with the host molecule located on a centre of symmetry. In these structures the two phenyl groups lie in the same plane and therefore τ_2 is zero and only τ_1 and the dihedral angle mentioned above vary between the structures. These variations are illustrated in Figure 8.6.

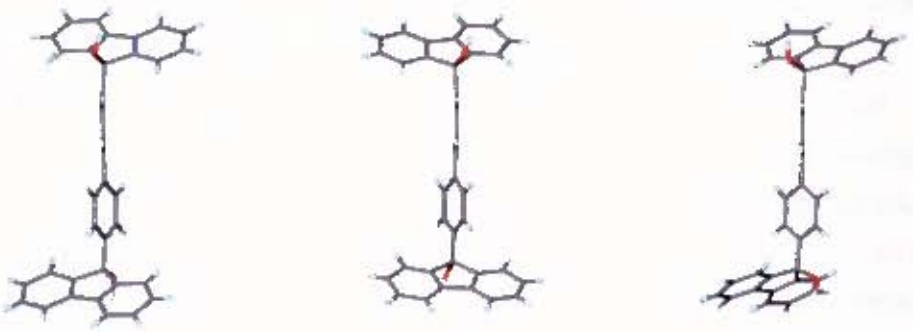

(a) (b) (c)

Figure 8.7 Conformation of host molecules viewed along the plane of one of the central phenyl rings in **(a) WEB24•4DMA**, **(b) WEB24•2ETHYL** and **(c) WEB24•2PROPYL**.

Table 8.4 Bond length ranges observed in the **WEB24** structures*

	a = C_{sp3}-O(Å)	b = C_{ar}-C_{sp3}(Å)	c = C_{ar}-C_{ar}(Å)	d = C_{ar}=C_{ar}(Å)	e = C_{sp3}-C_{ar} (Å)	f = C_{ar}-C_{ar}(Å)
WEB24	1.428(2)	1.526(2) 1.527(2)	1.459(2)	1.371(3) 1.398(2)	1.530(2)	1.493(2)
WEB24 •4DMA	1.423(3) 1.427(3)	1.527(3) 1.535(4)	1.474(4) 1.479(4)	1.362(5) 1.398(3)	1.519(4) 1.522(3)	1.483(4)
WEB24 •2DMA	1.424(3)	1.522(4) 1.525(4)	1.465(5)	1.354(8) 1.406(7)	1.524(4)	1.484(5)
WEB24 •3DIOX	1.431(2)	1.526(2) 1.534(2)	1.473(2)	1.378(2) 1.401(2)	1.525(2)	1.491(3)
WEB24 •2MEK	1.433(2) 1.434(2)	1.522(2) 1.532(2)	1.469(2) 1.475(2)	1.372(2) 1.401(2)	1.527(2) 1.528(2)	1.492(3) 1.497(3)
WEB24 •2ETHYL	1.424(2) 1.426(2)	1.523(2) 1.534(2)	1.471(2) 1.472(2)	1.378(3) 1.404(2)	1.524(2) 1.527(2)	1.485(2)
WEB24•2PROPYL	1.423(3) 1.430(3)	1.520(3) 1.536(3)	1.468(4) 1.469(4)	1.372(4) 1.406(3)	1.527(3) 1.531(3)	1.491(3)
Standard values**	1.440 (0.012)	1.527 (0.016)	1.490 (0.010)	1.384 (0.013)	1.527 (0.016)	1.487 (0.007)

* *For each structure the first value given is that of the minimum bond length and the second value that of the maximum bond length*

***The standard value given is the unweighted sample mean for that bond type in each case*[2]

TTRSC CONFORMATION

The host $1^4,1^6,5^4,5^6$-tetrahydroxy-2,4,6,8-tetrapentyl-$3^4,3^6,7^4,7^6$-tetra(p-toluene sulfonyl-oxy)-1,3,5,7(1,3)-tetrabenzenacyclooctaphane is a resorcinarene host with four substituted tosylate groups on the upper rim and with pentyl groups on the lower rim. The stereochemistry of resorcinarenes can be defined by the conformation of the macrocyclic ring (crown, boat, chair, diamond and saddle) combined with the relative and individual configurations of the substituents at the methylene bridges.[7] In each of the inclusion compounds the resorcinarene host has an all-*cis* and all-*axial* arrangement of the pentyl groups with the macrocyclic ring in a boat-like conformation. The boat conformation occurs when two opposite resorcinol units are coplanar with the main macrocyclic plane and the other two are perpendicular to the plane.

For the pentanol inclusion compounds, the torsion and dihedral angles defining the conformation of the host are given in Table 8.5 and the bond length ranges of the unique bonds in the molecule are given in Table 8.6, along with the standard values for these bond types[2] for comparison. Both the torsion angles defining the host conformation and the bond classification are shown in Figure 8.8.

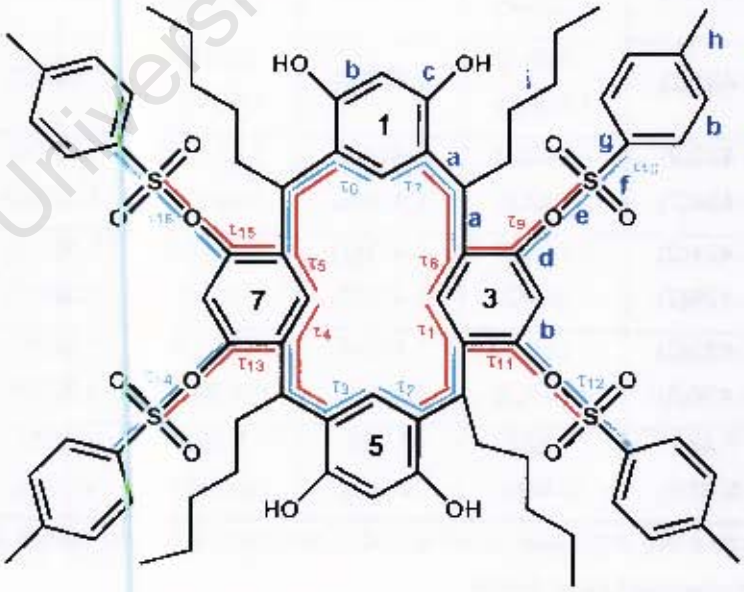

Figure 8.8 Classification of bonds for the host **TTRSC** and torsion angles describing the host conformation.

The conformation of the host molecule in the structures of each of the pentanol inclusion compounds is very similar and the conformation of the host molecule in **TTRSC•2(3M1B)** is shown in Figure 8.9 as an example. In these structures the host conformation is such that the two unsubstituted resorcinol rings are nearly coplanar with the macrocyclic ring, while the tosylated resorcinol units are almost perpendicular to the plane. The tosyl groups are oriented outwards from the centre and bent in a downward direction.

Table 8.5 Torsion and dihedral angles(°) describing **TTRSC** conformation in the pentanol inclusion compounds

	TTRSC• 2(1PENT)	**TTRSC• 2(2PENT)**	**TTRSC• 2(2M1B)**	**TTRSC• 2(3M1B)**	**TTRSC• 2(3PENT)**	**TTRSC• 2(2M2B)**	**TTRSC• 2(3M2B)**
τ_1	-103.0(6)	-102.1(5)	-102.4(6)	-102.9(5)	-101.9(3)	-93.6(3)	-101.6(3)
τ_2	53.5(7)	54.1(6)	53.2(7)	54.4(6)	51.6(4)	52.0(3)	53.4(4)
τ_3	-53.5(8)	-52.5(6)	-52.3(9)	-52.2(7)	-59.3(3)	-54.1(3)	
τ_4	109.3(6)	108.5(5)	108.1(7)	106.6(6)	111.2(3)	112.3(3)	
τ_5	-103.2(6)	-102.7(5)	-102.5(7)	-102.2(5)	-95.7(3)	-101.2(2)	
τ_6	48.5(8)	51.9(6)	48.7(7)	48.8(6)	51.3(4)	50.4(3)	
τ_7	-50.2(7)	-52.7(6)	-49.0(8)	-49.1(6)	-54.9(4)	-57.7(3)	
τ_8	104.2(6)	103.7(5)	105.0(7)	103.1(6)	112.2(3)	106.1(2)	106.1(4)
τ_9	-115.4(5)	-116.1(4)	-117.2(6)	-116.3(4)	-117.7(3)	-114.2(2)	-116.5(3)
τ_{10}	67.5(4)	67.9(3)	66.4(4)	67.1(4)	67.1(2)	60.7(2)	57.8(3)
τ_{11}	112.0(4)	111.6(4)	110.8(5)	111.4(4)	115.4(2)	110.2(2)	114.0(3)
τ_{12}	-67.7(4)	-66.5(3)	-69.5(4)	-67.4(4)	-60.7(2)	-77.4(2)	-80.3(2)
τ_{13}	-116.4(5)	-116.6(4)	-116.1(6)	-114.9(5)	-114.7(3)	-118.2(2)	
τ_{14}	60.3(5)	58.8(4)	59.6(5)	59.6(4)	59.3(2)	67.5(2)	
τ_{15}	113.6(5)	113.8(4)	112.0(6)	112.6(5)	110.0(3)	115.9(2)	
τ_{16}	-77.9(5)	-78.8(4)	-77.5(5)	-77.9(4)	-78.9(2)	-61.1(2)	
Dihedral angle 1*	21.1(2)	23.0(2)	21.0(3)	22.5(2)	21.1(1)	26.3(1)	
Dihedral angle 2*	151.6(3)	149.0(2)	150.7(3)	152.2(3)	144.0(4)	145.6(1)	

** Dihedral angle 1 is the angle between the planes of the rings labelled 3 and 7 in Figure 8.8 and Dihedral angle 2 is the angle between the planes of the rings labelled 1 and 5*

Table 8.6 Bond length ranges observed in the pentanol inclusion compounds of **TTRSC***

	TTRSC• 2(1PENT)	TTRSC• 2(2PENT)	TTRSC• 2(2M1B)	TTRSC• 2(3M1B)	TTRSC• 2(3PENT)	TTRSC• 2(2M2B)	TTRSC• 2(3M2B)	Standard values**
a = C_{sp3}-C_{ar} (Å)	1.496(7) 1.547(8)	1.519(6) 1.531(6)	1.510(7) 1.537(7)	1.513(7) 1.533(7)	1.512(4) 1.533(4)	1.513(3) 1.531(3)	1.512(4) 1.527(4)	1.515 (0.011)
b = C_{ar} ≅C_{ar}(Å)	1.34(1) 1.42(1)	1.351(9) 1.404(6)	1.36(1) 1.424(9)	1.35(1) 1.408(7)	1.367(5) 1.401(4)	1.361(5) 1.409(5)	1.357(6) 1.411(7)	1.384 (0.013)
c = C_{ar}-O (Å)	1.358(7) 1.383(6)	1.367(6) 1.378(5)	1.371(8) 1.380(7)	1.371(6) 1.398(6)	1.363(4) 1.382(4)	1.369(3) 1.373(3)	1.373(4) 1.377(4)	1.362 (0.015)
d = C_{ar}-O (Å)	1.415(6) 1.429(6)	1.421(5) 1.436(5)	1.415(6) 1.431(7)	1.417(5) 1.431(6)	1.415(3) 1.424(3)	1.420(3) 1.425(3)	1.412(3) 1.423(3)	—
e = O-S(Å)	1.592(4) 1.604(4)	1.598(3) 1.610(3)	1.600(4) 1.617(5)	1.601(4) 1.618(4)	1.593(2) 1.610(2)	1.592(2) 1.603(2)	1.592(3) 1.609(2)	1.580 (0.015)
f = S=O (Å)	1.414(5) 1.428(4)	1.417(4) 1.430(4)	1.411(4) 1.431(5)	1.416(4) 1.435(4)	1.416(2) 1.423(2)	1.415(2) 1.426(2)	1.414(3) 1.428(3)	1.423 (0.008)
g = S-C_{ar} (Å)	1.708(7) 1.765(8)	1.733(6) 1.745(5)	1.736(7) 1.752(7)	1.741(7) 1.750(5)	1.739(3) 1.753(4)	1.743(3) 1.750(3)	1.743(5) 1.748(3)	1.752 (0.008)
h = C_{sp3}-C_{ar} (Å)	1.47(1) 1.55(1)	1.503(9) 1.520(9)	1.49(1) 1.510(9)	1.51(1) 1.521(9)	1.501(5) 1.514(5)	1.496(5) 1.513(5)	1.492(8) 1.524(6)	1.506 (0.011)
i = C_{sp3}-C_{sp3} (Å)	1.47(1) 1.62(1)	1.490(8) 1.552(7)	1.45(1) 1.548(8)	1.28(1)*** 1.54(1)	1.484(6) 1.561(5)	1.493(5) 1.60(1)	1.502(7) 1.540(6)	1.524 (0.011)

** For each structure the first value given is that of the minimum bond length and the second value that of the maximum bond length*

*** The standard value given is the unweighted sample mean for that bond type in each case*[2]

**** Disordered moiety*

Figure 8.9 Stereoview of general host conformation of **TTRSC** in structures of pentanol inclusion compounds, extracted from **TTRSC•2(3M1B)** structure.

For the pyridine and picoline inclusion compounds, the torsion and dihedral angles defining the conformation of the host are given in Table 8.7. A search of the Cambridge Structural database[1] revealed the structure of only one additional inclusion compound formed with this host and the torsion angles describing the host conformation in this structure are displayed in Table 8.7 for comparison. The bond length ranges of the unique bonds in the molecule in each of the structures are given in Table 8.8, along with the standard bond length values[2] for comparison.

Table 8.7 Torsion and dihedral angles(°) describing **TTRSC** conformation in the pyridine and picoline inclusion compounds

	TTRSC •6PYR	**TTRSC •5(2PIC)**	**TTRSC •4.5(3PIC) •0.5(H_2O)**	**TTRSC•6.5(4PIC) •2(H_2O)**	**bis (triethylammonium) dichloride clathrate[8]**
τ_1	-102.2(6)	-59.3(3)	-57.0(4)	-102.1(3)	-52.0
τ_2	34.3(7)	104.6(2)	107.1(3)	30.9(4)	107.3
τ_3	-40.7(7)	-100.7(2)	-103.7(3)	-36.4(3)	-106.2
τ_4	106.1(6)	33.9(3)	52.2(4)	103.2(3)	48.3
τ_5	-101.9(6)	-36.7(3)	-53.1(4)	-101.3(3)	-49.2
τ_6	33.8(7)	95.3(3)	102.9(3)	35.0(3)	107.5
τ_7	-34.9(7)	-105.1(2)	-98.8(3)	-33.4(3)	-106.2
τ_8	104.5(6)	61.9(2)	52.1(4)	105.0(3)	54.9
τ_9	-124.9(4)	-120.5(2)	-94.0(3)	-118.5(2)	-124.0
τ_{10}	161.0(4)	69.5(2)	-104.9(2)	48.5(2)	71.5
τ_{11}	124.2(4)	117.4(2)	126.1(3)	115.8(2)	92.8
τ_{12}	-165.5(4)	-70.1(2)	-68.2(3)	-162.0(2)	102.0
τ_{13}	-122.7(4)	122.0(2)	-93.5(3)	-125.3(2)	-125.6
τ_{14}	52.5(4)	-138.7(2)	-98.6(2)	150.6(2)	87.0
τ_{15}	116.4(4)	-108.1(2)	123.4(3)	119.3(2)	96.7
τ_{16}	-160.4(4)	-72.9(2)	-90.1(3)	-164.9(2)	101.2
Dihedral angle 1*	10.9(3)	160.0(1)	140.4(2)	8.2(1)	141.28
Dihedral angle 2*	175.7(3)	34.4(1)	28.6(2)	179.3(1)	16.34

** Dihedral angle 1 is the angle between the planes of the rings labelled 3 and 7 in Figure 8.8 and Dihedral angle 2 is that between the planes of the rings labelled 1 and 5*

Table 8.8 Bond length ranges observed in the pyridine and picoline inclusion compounds*

	TTRSC•6PYR	TTRSC•5(2PIC)	TTRSC•4.5(3PIC)•0.5(H_2O)	TTRSC•6.5(4PIC)•2(H_2O)	Standard values**
a = C_{sp2}-C_{ar}(Å)	1.492(8) 1.539(8)	1.520(3) 1.529(3)	1.516(4) 1.528(4)	1.515(3) 1.524(3)	1.515 (0.011)
b = C_{ar}≅C_{ar} (Å)	1.342(9) 1.412(7)	1.378(4) 1.403(3)	1.376(6) 1.406(4)	1.377(5) 1.405(3)	1.384 (0.013)
c = C_{sp3}-O (Å)	1.377(7) 1.529(7)	1.359(3) 1.366(3)	1.358(4) 1.367(4)	1.364(3) 1.371(3)	1.362 (0.015)
d = C_{sp3}-O (Å)	1.417(6) 1.427(6)	1.414(3) 1.426(3)	1.417(3) 1.421(4)	1.415(3) 1.427(3)	—
e = O-S(Å)	1.593(4) 1.611(4)	1.595(2) 1.609(2)	1.591(2) 1.606(2)	1.602(2) 1.604(2)	1.580 (0.015)
f = S=O (Å)	1.407(5) 1.447(5)	1.420(2) 1.426(2)	1.413(3) 1.428(3)	1.418(3) 1.429(2)	1.423 (0.008)
g = S-C_{ar} (Å)	1.715(6) 1.737(7)	1.749(2) 1.754(3)	1.745(4) 1.753(3)	1.745(3) 1.756(3)	1.752 (0.008)
h = C_{sp3}-C_{ar}(Å)	1.47(1) 1.52(1)	1.498(4) 1.508(4)	1.506(6) 1.511(6)	1.499(5) 1.518(4)	1.506 (0.011)
i = C_{sp}-C_{sp} (Å)	1.47(1) 1.96(6)***	1.514(4) 1.543(3)	1.487(6) 1.536(4)	1.515(5) 1.544(4)	1.524 (0.011)

* *For each structure the first value given is that of the minimum bond length and the second value that of the maximum bond length*

***The standard value given is the unweighted sample mean for that bond type in each case*[2]

*** *Disordered moiety*

The conformations of the host molecule in the structures of the inclusion compounds with pyridine and 4-picoline are very similar and the conformation of the host molecule in **TTRSC•6.5(4PIC)•0.5(H_2O)** is shown in Figure 8.10 as an example. In both cases the resorcinarene molecule is once again in the boat conformation, as in the case of the inclusion compounds of this host with the pentanol isomers. A further similarity with the previous structures is that the resorcinol rings are nearly coplanar with the macrocyclic ring, while the tosylated resorcinol units are perpendicular to the plane.

The only difference lies in the orientation of the tosyl groups. We may regard the resorcinarene molecule as being made up of two 'flat' resorcinol units connected to two others which are 'vertical'. The rectangular 'flat' plane is elongated in the C37-C85 direction, and the tosyl groups lie either in planes parallel to this direction or at right angles to it as shown in Figure 8.10.

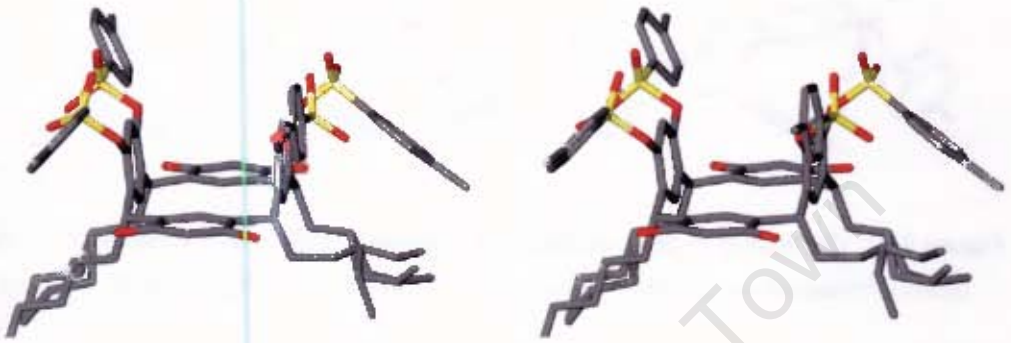

Figure 8.10 Stereoview of general host conformation of **TTRSC** in structures of pyridine and 4-picoline inclusion compounds, extracted from **TTRSC•6.5(4PIC)•2(H_2O)** structure.

The host molecule has a very similar conformation in the structures of the inclusion compounds with 2- and 3-picoline, and in both cases the resorcinarene molecule is once again in the boat conformation. In these two structures, however, the tosylated resorcinol units are nearly coplanar with the macrocyclic ring, while the two unsubstituted resorcinol rings are perpendicular to the plane and almost parallel. The conformation of the host molecule in **TTRSC•4.5(3PIC)•0.5(H_2O)** is shown in Figure 8.11 as an example.

The only differences between the conformations of the host molecule in these structures lie in the orientation of the tosyl groups and this can be seen in the variation of the values of torsion angles τ_9 to τ_{16}. Similar boat-like conformations have been reported for the X-ray crystal structures of bis-benzoxazine derivatives of tetratosylate,[9] the resorcinarene tetratosylate bis(triethylammonium) dichloride clathrate[8] (torsion and dihedral angles given in Table 8.7 for comparison) as well as for a variety of tetrasulfonates.[10]

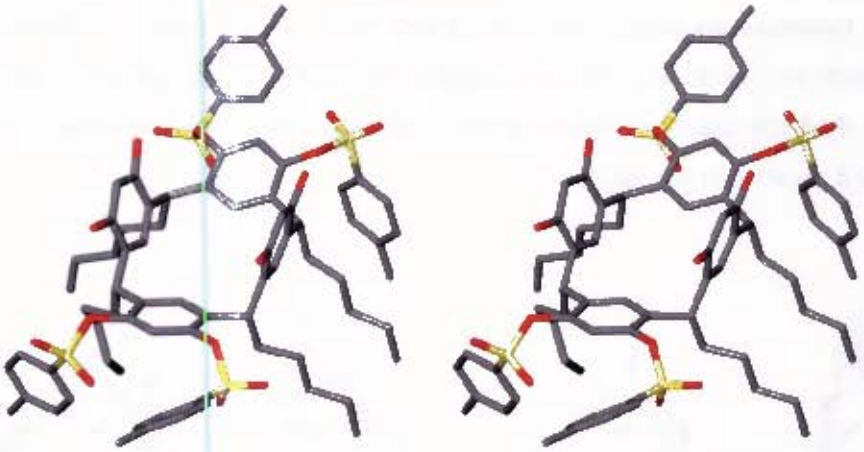

Figure 8.11 Stereoview of general host conformation of **TTRSC** in structures of 2- and 3-picoline inclusion compounds, extracted from **TTRSC•4.5(3PIC)•0.5(H_2O)** structure.

REFERENCES

[1] Cambridge Structural Database and Cambridge Structural Database System, Version 5.23 (April 2002), Cambridge Crystallographic Data Centre, University Chemical Laboratory, Cambridge, England.

[2] F.H. Allen, O. Kennard, D.G. Wayson, L. Brammer, A.G. Orpen and R. Taylor, *International Tables for Crystallography*, Vol. C, ed. A.J.C. Wilson, Kluwer Academic Publishers, Dordrecht, 1992, p 685.

[3] A. Coetzee, *Supramolecular Chemistry*, 1998, **9**, 109.

[4] L.J. Barbour, M.R. Caira and L.R. Nassimbeni, *J. Chem. Soc., Perkin Trans. 2*, 1993, 1413.

[5] L.J. Barbour, M.R. Caira, A. Coetzee and L.R. Nassimbeni, *J. Chem. Soc., Perkin Trans. 2*, 1995, 1345.

[6] *Atlas of steroid structure*, ed. W.L. Duax and D. A. Norton, Plenum Data Company, New York, 1975, p.18.

[7] P. Timmerman, W. Verboom and D.N. Reinhoudt, *Tetrahedron*, 1996, **52**, 2663.

[8] A. Shivanyuk, E.F. Paulus, K. Rissanen, E. Kolehmainen and V. Böhmer, *Chem. Eur. J.*, 2001, **7**, 1944.

[9] A. Shivanyuk, C. Schmidt, V. Böhmer, E.F. Paulus, O. Lukin and W. Vogt, *J. Am. Chem. Soc.*, 1998, **120**, 4319.

[10] O. Lukin, A. Shivanyuk, V.V. Pirozhenko, I.F. Tsymbal and V.I. Kalchenko, *J. Org. Chem.*, 1998, **63**, 9510.

Chapter 9

FINAL REMARKS

"Where nature finishes producing its own species, man begins, using natural things and with the help of this nature, to create an infinity of species."

- Leonardo da Vinci

The field of inclusion phenomena has shown vast expansion in the last twenty years and clathrate compounds are an important aspect of supramolecular chemistry. This study concentrates on understanding the macroproperties of inclusion compounds containing small, volatile organic guests through analysis of their thermal stabilities, selectivity profiles and kinetics of enclathration and desorption. An attempt has been made to relate the macroproperties of the inclusion compounds to their structures.

Of great importance is understanding the details of the packing of the molecules in the solid state and crystal structure determination allows us to determine the strengths and directions of intermolecular interactions which hold the structure together and can help to predict the behaviour of the solid under various thermodynamic conditions. The crystal structures of each of the inclusion compounds obtained were elucidated and selected characteristics of these structures are given in Table 9.1.

The host **TBDDDA**, investigated during this study, was found to form clathrates containing a mixture of two guests, DMF and DMSO, in selected ratios. The compounds in this series were found to be isostructural with respect to the packing of the host molecules, and based on their topological features, can be classified as tubulates according to the classification given by Weber et al.[1] This also applies to the inclusion compound formed with acetone, as well as the inclusion compounds containing mixtures of acetone/DMF and acetone/DMSO, with the latter two being isostructural with the compounds of the DMF/DMSO series with respect to the packing of the host molecules. Each of the inclusion compounds formed with the host **TBDDDA** has H:G=1:4 and exhibits host···guest hydrogen bonding, with two guest molecules hydrogen bonded to each host molecule via the hydroxyl groups.

Inclusion compounds containing more than one kind of guest molecule are well established in the literature and often arise from the use of solvent mixtures in the crystallisation of the desired compound. A survey giving a statistical analysis of the inclusion of solvent molecules in the crystal structures of organic and metalloorganic compounds has appeared[2] and here it is pointed out that water is the most common molecule occurring as a co-solvate, and there are several examples of inclusion compounds which contain three or four different guest molecules, with the structure of zinc(II)tetrakis(pentafluorophenyl)-β-octabromoporphyrin incorporating no fewer than five different solvents.[3]

The field of inclusion compounds with mixed guests is an important one as systematic studies can establish what aspects are important in the selection of different guests, such as steric factors, polarity, guest symmetry and solubility. The occurrence of a host-guest system in which the ratio of mixed guests can be controlled, has implications for crystal engineering and a knowledge of the physical and chemical properties has significance in fields such as chemical sensors, optical and electronic properties of organic crystals as well as their thermal stabilities and kinetics of desorption.[4]

The inclusion compounds formed with **WEB24** display a range of H:G ratios and all have significantly different structures. This host forms two inclusion compounds with DMA with H:G ratios of 1:4 and 1:2. The inclusion compound with H:G=1:4 was formed by crystallisation at a lower temperature and has a more open structure in which the guest molecules are located between layers of host molecules, while the inclusion compound with H:G=1:2 was formed by crystallisation at a higher temperature and the host molecules pack to form channels in which the guests are situated. These findings are in agreement with the rules formulated by Ibragimov[5] which link guest/host ratios with crystallisation temperature and the resulting topologies of the inclusion compounds.

The host-guest compounds formed with the host **TTRSC** and the seven pentanol isomers as guests all have H:G=1:2, and comparison of the structures reveals that these structures can be grouped into three types, with the guests situated in channels in two of these types and in cavities in the third type. The same hydrogen bonding pattern is found in all of these host-guest compounds, which display both host···guest and host···host hydrogen bonding interactions, with both guests hydrogen bonded to the host via two of the hydroxyl groups and with the remaining two hydroxyl groups of the host molecule participating in host···host hydrogen bonding. In addition there are weaker interactions between the guest oxygen atoms and oxygen atoms in the tosylate groups of the host molecule.

The clathrates formed by **TTRSC** with pyridine and the picoline isomers as guests vary in terms of H:G ratios, although in each case the H:G ratio is high, with the $H:G_{TOTAL}$ ratio being at least 1:5. The structures of these compounds display a range of packing patterns and hydrogen bonding motifs, with two of the clathrates also including water molecules as guests. In these structures there are no host···host

hydrogen bonding interactions, but all four of the hydroxyl groups of the host molecule are involved in host···guest hydrogen bonding interactions. In the structures of all of the inclusion compounds with TTRSC, the guests are captured between the molecules of resorcinarene rather than within the cavity of the resorcinarene.

Table 9.1 Summary of selected characteristics of inclusion compound structures investigated

Complex	Guest	H:G ratio	Space group	Hydrogen bonding	Inclusion mode
TBDDDA•4DMF	DMF	1:4	$P\bar{1}$	O-H···O	channels
TBDDDA•3DMF•1DMSO	DMF, DMSO	1:3:1	$P\bar{1}$	O-H···O	channels
TBDDDA•2DMF•2DMSO	DMF, DMSO	1:2:2	$P\bar{1}$	O-H···O	channels
TBDDDA•1DMF•3DMSO	DMF, DMSO	1:1:3	$P\bar{1}$	O-H···O	channels
TBDDDA•4DMSO	DMSO	1:4	$P\bar{1}$	O-H···O	channels
TBDDDA•4ACE	acetone	1:4	$P2_1/c$	O-H···O	intersecting channels
TBDDDA•2DMF•2ACE	DMF, acetone	1:2:2	$P\bar{1}$	O-H···O	channels
TBDDDA•2DMSO•2ACE	DMSO, acetone	1:2:2	$P\bar{1}$	O-H···O	channels
WEB24•4DMA	DMA	1:4	$P\bar{1}$	O-H···O	layers
WEB24•2DMA	DMA	1:2	$P\bar{1}$	O-H···O	channels
WEB24•3DIOX	1,4-dioxane	1:3	$P2_1/c$	O-H···O	channels
WEB24•2MEK	MEK	1:2	$P2_1/n$	O-H···O	channels
WEB24•2ETHYL	ethylamine	1:2	$P\bar{1}$	O-H···N	channels
WEB24•2PROPYL	propylamine	1:2	$Pca2_1$	O-H···N	channels
TTRSC•2(1PENT)	1-pentanol	1:2	Pcca	O-H···O	channels
TTRSC•2(2PENT)	2-pentanol	1:2	Pcca	O-H···O	channels
TTRSC•2(2M1B)	2-methyl-1-butanol	1:2	Pcca	O-H···O	channels
TTRSC•2(3M1B)	3-methyl-1-butanol	1:2	Pcca	O-H···O	channels
TTRSC•2(3PENT)	3-pentanol	1:2	$P2_1/n$	O-H···O	cavities
TTRSC•2(2M2B)	2-methyl-2-butanol	1:2	$P2_1/n$	O-H···O	cavities
TTRSC•2(3M2B)	3-methyl-2-butanol	1:2	P2/n	O-H···O	channels
TTRSC•6PYR	pyridine	1:6	$P\bar{1}$	O-H···N	channels
TTRSC•5(2PIC)	2-picoline	1:5	$P\bar{1}$	O-H···N	intersecting channels
TTRSC•4.5(3PIC)•0.5($H_2$0)	3-picoline, H_2O	1:4.5:0.5	C2/c	O-H···N	layers
TTRSC•6.5(4PIC)•2($H_2$0)	4-picoline, H_2O	1:6.5:2	$P\bar{1}$	O-H···N	intersecting channels

Molecular recognition, which depends on the strength and direction of the intermolecular forces occurring in a host-guest system, is fundamental to supramolecular chemistry and can be exploited to carry out selective enclathration. The possibility of selective enclathration by a particular host can be examined through competition experiments and such experiments were carried out with **TBDDDA** in order to determine the selectivity for DMF versus DMSO and with **TTRSC** to determine the selectivity for three pairs of pentanol isomers as well as for 3-picoline versus 4-picoline.

For the competition experiment carried out between DMF and DMSO with **TBDDDA**, the results presented show that this host-guest system behaves in a completely different manner from typical systems, in that the resulting inclusion compounds represent a completely tuneable system in which any ratio of the two guests can be obtained by adjusting the relative concentrations of the starting solution. Another very interesting result was obtained for the 3-picoline versus 4-picoline competition experiment with **TTRSC**, which displays a concentration dependent selectivity, but instead of selective inclusion of the guest of higher concentration, it was in fact the guest of lower concentration in the solution which was preferentially enclathrated. This unusual result could be explained in terms of solubilities of the clathrates in the two guests.

Competition experiments carried out among three pairs of pentanol isomers with **TTRSC** showed selective enclathration of 3-methyl-1-butanol above either 3-pentanol or 2-pentanol. As previously discussed, it has been suggested[6] that the stability of an inclusion complex can be evaluated by subtracting the normal boiling point of the guest from the onset temperature of guest release, obtained from DSC data, with a more positive value of T_{on}-T_b indicating a more stable complex. These values were calculated for the inclusion compounds which **TTRSC** forms with the pentanol isomers and the results showed that the thermal stabilities of the inclusion compounds could be correlated with the competition experiments as the more stable inclusion compound was preferentially formed in each case.

Thermal analysis is an important tool in inclusion chemistry for investigation of thermal stability and was carried out for each of the inclusion compounds obtained in this study. Values of T_{on}-T_b for the two clathrates of **WEB24** with DMA were calculated, which show that the compound with H:G=1:2 is more stable and it was found that the thermal stabilities of these clathrates are related to the packing of the

host-guest systems. The inclusion compound with a higher H:G ratio has a more open structure and is less stable and should therefore decay more easily to a more stable intermediate with a lower H:G ratio, which in turn should decay less easily to the guest-free host compound. An investigation of the kinetics of desorption of **WEB24•4DMA** proved this to be correct as it was found that desorption takes place in two steps, with the first step, which results in the intermediate **WEB24•2DMA**, having an activation energy of 79.1 $kJ.mol^{-1}$ and the second step, which results in the guest-free apohost, **WEB24**, having a higher activation energy of 115.4 $kJ.mol^{-1}$.

The kinetics of desorption thus yield activation energies which are related to the topologies of the host-guest systems, as well as their stabilities. Solid state NMR was also employed to monitor the desorption of some of the inclusion compounds formed with **WEB24** and has shown that, upon desorption, the inclusion compounds revert to the structure of the apohost. These results display the usefulness of a multiple technique approach to the study of organic inclusion compounds when relating structure to macroproperties.

The kinetics of desorption of a number of other inclusion compounds were investigated in this study and all of the desorption reactions were found to display Arrhenius behaviour. The activation energy for the desorption of **WEB24•3DIOX** was found to be lower than that of **WEB24•4DMA**, but higher than that of **WEB24•2DMA,** which can be explained in terms of the topologies. The structure of **WEB24•3DIOX**, which is an open structure in which the host molecules pack in zigzagged layers forming channels, is more open than that of **WEB24•2DMA**, in which the channels are more restricted, thus allowing easier guest release from **WEB24•3DIOX**. The structure is, however, not as open as that of **WEB24•4DMA,** in which the guest molecules are located between layers of host molecules.

The desorption of both **WEB24•2ETHYL** and **WEB24•ETHYL** was found to take place in a single step and thus, as might be expected, the activation energy of desorption is higher for **WEB24•2ETHYL**. The activation energy of the desorption of **WEB24•2PROPYL** is higher than that of **WEB24•2ETHYL**, although in both of these structures the guests are located in channels. However, the channels in **WEB24•2PROPYL** undulate sharply, which may result in the guest molecules being held more tightly by the structure, resulting in a higher activation energy of desorption.

Molecular recognition in the form of solid-gas enclathration reactions has application in the development of sensing devices; however, kinetic studies of these reactions have not received much attention due to experimental difficulty. In this study, the kinetics of enclathration of **TBDDDA** with acetone vapour and of **WEB24** with ethylamine and propylamine vapour have been investigated and in each case the reaction displays anti-Arrhenius behaviour due to the inclusion compounds having a greater propensity to decompose at higher temperatures. An investigation of the structures of these two host compounds reveals that both have a face from which exposed hydroxyl groups protrude. This suggests a mechanism in which this is the reactive face that presents free OH donors for host···guest hydrogen bonding with incoming gaseous guest molecules.

This study thus makes a contribution to thermodynamic, kinetic and structural studies of host-guest compounds. Such studies are of significance as the structures and topologies of inclusion compounds form the basis of their reactivities and their physico-chemical properties. With this knowledge an understanding of the molecular recognition processes occurring in these compounds can be developed, which forms the basis of predicting their behaviour and has important implications for crystal engineering.

REFERENCES

[1] E. Weber, H.-P. Josel, *Journal of Inclusion Phenomena*, 1983, **1**, 79.

[2] C.H. Gorbitz and H.P. Hersleth, *Acta Crystallogr.*, 2000, B**56**, 526.

[3] R.E. Marsh, W.P. Schaeffer, J.A. Hodge, M.E. Hughes, H.B. Gray, J.E. Lyons and P. Ellis Jr., *Acta Crystallogr.*, 1993, C**49**, 1339.

[4] D.V. Soldatov and J.A. Ripmeester, *Chem. Eur. J.*, 2001, **7**, 2979.

[5] B.T. Ibragimov, *J. Incl. Phenom. Macrocyclic Chem.*, 1999, **34**, 345.

[6] M.R. Caira, L.R. Nassimbeni, M.L. Niven, W.-D. Schubert, E. Weber and N. Dörpinghaus, *J. Chem. Soc., Perkin Trans. 2*, 1990, 2129.

APPENDIX

The supplementary material for all crystal structures elucidated in this study can be found on the attached CD-ROM in the directory 'APPENDIX'. Five files are included for each structure, namely:

Filename.HKL	contains reflection data
Filename.FCF	contains tables of observed and calculated structure factors
Filename.LIS	contains tables of atomic coordinates, bond lengths and angles, torsion angles, isotropic and anisotropic displacement parameters and hydrogen bonding details
Filename.RES	can be used for visualisation of the structures and packing features using an appropriate program such as X-SEED or Platon
Filename.CIF	the Crystallographic Information File

The files for each structure can be found in a directory named after the relevant host compound and in a subdirectory named after the structure code. All files are text files which can be viewed in a text editor such as WORDPAD in Windows98 or any later version thereof.